Characterization of micro liquid chromatography - theoretical performance limits and practical aspects for routine analysis on the example of cytotoxic drugs

Dissertation

zur Erlangung des akademischen Grades eines
Doktors der Naturwissenschaften
– Dr. rer. nat. –

vorgelegt von

Terence Hetzel

geboren in Geldern

Fakultät für Chemie
der
Universität Duisburg-Essen

2017

Die vorliegende Arbeit wurde im Zeitraum von Oktober 2013 bis Dezember 2016 im Arbeitskreis von Prof. Dr. Torsten C. Schmidt in der Fakultät für Chemie im Bereich Instrumentelle Analytische Chemie der Universität Duisburg-Essen durchgeführt.

Tag der Disputation: 02.06.2017

Gutachter:	Prof. Dr. Torsten C. Schmidt
	Prof. Dr. Oliver J. Schmitz
Vorsitzender:	Jun.-Prof. Dr. Michael Giese

„Erst zweifeln, dann untersuchen,

dann entdecken!“

Henry Thomas Buckle

Summary

Miniaturized liquid chromatography (*LC*) is ideally suited to reduce the resource consumption without compromising data quality in the analytical laboratory. However, the applicability and handling of miniaturized LC in routine analysis is often being questioned. In addition, only little information on the theoretical performance limits of this separation technique is available. Therefore, the aim of this study was the characterization of micro-liquid chromatography (*micro-LC*) from the theoretical and practical point of view. For the evaluation the development of a fast method for the analysis of antineoplastic drugs from wipe samples using micro-LC-MS/MS was applied. The investigated analytes comprise polar as well as non-polar compounds. In addition, three critical peak pairs were included that either cannot be differentiated by mass spectrometry or are affected by ion suppression at co-elution. Therefore, a chromatographic separation was mandatory. Micro-LC was used as separation dimension using a column with an inner diameter of 300 µm due to the advantages of reduced resource consumption and high linear velocity leading to increased sample throughput. To achieve a chromatographic separation, a suitable chromatographic phase system was identified by principal component analysis (*PCA*). Afterwards, the column efficiency was investigated using van Deemter and kinetic plot analysis for isocratic and gradient elution. The results indicate a higher packing quality of the sub-2 µm fully porous particle packed column compared to larger particle diameters of various morphology. In addition, similar values for the reduced plate height were found in micro-LC compared to conventional column inner diameters (≥ 2.1 mm). The investigation of peak capacity also demonstrates the benefit of sub-2 µm fully porous particles for gradient times between 5 s and 5 min. Further optimization of the extraction efficiency, ion source parameters and system design was done to establish the method on basis of micro-LC-MS/MS. This hyphenation technique enables to separate the target analytes within 2.5 min at a flow rate of only 25 µL min^{-1}. Thereby the sample throughput can be increased by a factor of 2 reducing the resource consumption by 98% compared to the previously used conventional LC-MS/MS method. Method validation was accomplished to demonstrate that sensitivity and robustness of the developed method is given in a routine environment. Furthermore, it was shown that the method can be used to analyze real samples from hospital pharmacies in order to verify the reference value of 0.1 ng cm^{-2} for workplace contamination of antineoplastic drugs. In summary, it was exemplarily demonstrated that micro-LC can successfully replace conventional LC-MS in targeted ultrasensitive MS analysis.

Zusammenfassung

Verfahren wie die miniaturisierte Hochleistungsflüssigkeitschromatographie (*LC*) sind ideal geeignet, um den Verbrauch an Ressourcen zu verringern ohne dabei die Datenqualität im analytischen Labor negativ zu beeinflussen. Nichtsdestotrotz wird die Anwendbarkeit dieser Technik in der Routineanalytik aufgrund der Handhabbarkeit oftmals kritisch hinterfragt. Des Weiteren sind nur wenige Informationen bezüglich der theoretischen Leistungsfähigkeit dieser Trenndimension verfügbar. Aus diesem Grund ist das Ziel dieser Arbeit die Charakterisierung der Mikro-Flüssigkeitschromatographie (*Mikro-LC*) aus Sicht der Theorie und Praxis. Zur Bewertung wurde die Entwicklung einer schnellen Analysenmethode ausgewählter Zytostatika von Wischproben mittels Mikro-LC-MS/MS verwendet. Die untersuchten Analyten umfassen dabei sowohl polare als auch unpolare Substanzen. Weiterhin sind drei kritische Peakpaare enthalten, bei denen entweder eine Ionensuppression bei Koelution beobachtet wird oder eine Unterscheidung mittels Massenspektrometrie nicht möglich ist. Aus den genannten Gründen ist eine chromatographische Trennung notwendig. Um dies zu erreichen, wurden Mikro-LC-Säulen mit einem Innendurchmesser von 300 µm eingesetzt. Dies bietet neben dem reduzierten Verbrauch von Ressourcen den Vorteil, dass durch hohe lineare Fließgeschwindigkeiten ein erhöhter Probendurchsatz generiert werden kann. Um eine chromatographische Trennung zu erreichen, wurde ein geeignetes Phasensystem durch den Einsatz der Hauptkomponentenanalyse (*PCA*) identifiziert. Anschließend wurde die Effizienz miniaturisierter Trennsäulen mittels van Deemter und Kinetic Plot Analyse sowohl für die isokratische Arbeitsweise als auch für die Gradientenelution untersucht. Dabei stellte sich heraus, dass vollporöse Partikel mit einem Partikeldurchmesser von kleiner 2 µm (*sub-2 µm*) eine verbesserte Packungsqualität gegenüber größeren Partikeln unterschiedlicher Morphologie aufweisen. Weiterhin konnte festgestellt werden, dass im Vergleich zu konventionellen Innendurchmessern vergleichbare Packungsqualitäten erreicht werden können. Die Untersuchung der Peakkapazität für Gradientenlaufzeiten zwischen 5 s und 5 min ergab, dass mit vollporösen sub-2 µm Partikeln eine höhere Peakkapazität pro Zeiteinheit generiert werden konnte. Des Weiteren wurden neben dem Systemaufbau, die Extraktionseffizienz sowie die Ionenquellenparameter optimiert, um die Methode auf Basis der Mikro-LC-MS/MS zu etablieren. Durch diese Kopplung konnten die Komponenten innerhalb von 2.5 min bei einer Flussrate von lediglich 25 µL min^{-1} getrennt werden. Dadurch konnte der Probendurchsatz um den Faktor 2 bei gleichzeitiger Reduzierung der Ressourcen um 98% im Vergleich zur zuvor etablierten konventionellen LC-MS/MS gesteigert werden. Anschließend wurden Validierungsdaten erhoben, um die Sensitivität und Robustheit der entwickelten Methode im

Routineumfeld zu demonstrieren. Anhand von Realproben aus Krankenhausapotheken wurde gezeigt, dass der Referenzwert für die Arbeitsplatzkontamination von Zytostatika von 0,1 ng cm^{-2} mittels der Methode überprüft werden kann. Damit konnte exemplarisch gezeigt werden, dass die Mikro-LC qualifiziert ist, die konventionelle LC-MS im Bereich der ultra-sensitiven Targetanalytik zu ersetzen.

Table of Content

Chapter 1 Introduction and theoretical background

1.1 Introduction

Every year, the Global Footprint Network calculates the so-called Earth Overshoot Day on the basis of the world biocapacity and ecological footprint [1]. This day specifies the date on which the naturally resources of one year are exhausted. Whereas the Earth Overshoot Day was on the 19th of December in 1987, the date continuously moves forward to the 8th of August in 2016 demonstrating that the exploitation of natural resources has increased drastically. Therefore, sustainable processes are needed to ensure the ecological health of the earth in the future. Of course this development also comprises the analytical laboratory. Beside the reduction of energy consumption, the more efficient use of resources is one of the main objectives.

Liquid chromatography (*LC*) is nowadays one of the most important separation technique. Its fundamentals were first discovered by Michail Semjonowitsch Tswett in 1903 [2-4]. Almost 50 years later, Martin and Synge were awarded the Nobel Prize for their work on partition chromatography [5, 6]. The first commercially available liquid chromatography system was developed by Jim Waters in 1964 [7]. Until today, the system design has been further developed and improved several times. Today, LC systems are capable of 1,500 bar system pressure using reduced column inner diameters (*i.d.*, 0.075 - 2.1 mm) packed with small particles (d_p, 1.3 – 3.0 µm) of various morphology [8-11]. Today it is also known as ultra-high performance liquid chromatography (*UHPLC*) [12-14]. The design of a liquid chromatography system is schematically depicted in Figure 1.1.

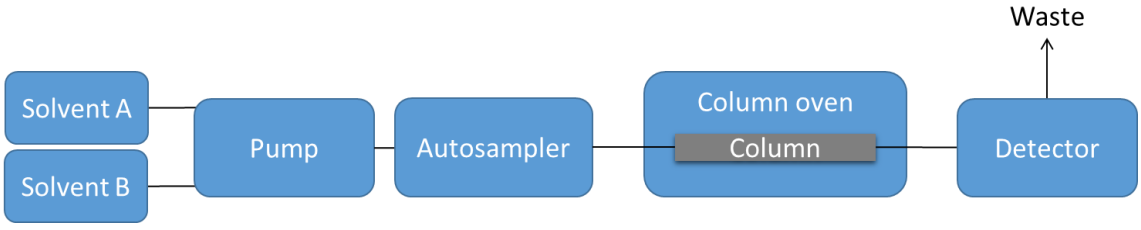

Figure 1.1: Illustration of the general system design of a liquid chromatography system.

One fundamental desire in liquid chromatography is to achieve more efficient separations in faster analysis time [15-17]. To that end, the development of miniaturized column inner diameters was identified as the most promising approach. It was early recognized that small *i.d.* columns have several advantages like reduced solvent consumption as well as improved compatibility to mass spectrometry [18]. Further advantages are discussed in more detail in the following. Depending on the column *i.d.*, liquid chromatography can be divided into different categories as illustrated in Table 1.1.

Table 1.1: Classification of liquid chromatography depending on the column inner diameter and resulting flow rate range. It must be noted, that the specified flow rate ranges are only a rough classification.

Analytical LC		
Category	**Column i.d. / mm**	**Flow rate range / µL min^{-1}**
(U)HPLC	4.6	1000 - 2000
	3.0	500 - 1000
UHPLC	2.1	300 - 500
	1.0	100 - 300
Miniaturized LC		
Category	**Column i.d. / mm**	**Flow rate range / µL min^{-1}**
Micro-LC	0.5	20 - 100
	0.3	5 - 50
Nano-LC	0.1	0.5 - 2
	0.075	0.1 - 0.5

Whereas at the beginning of HPLC, column *i.d.*s of 4.6 mm were used, there has been a subsequent reduction of the inner diameter up to today. Nevertheless, this dimension is still standard in many laboratories. However, with introduction of UHPLC and mass spectrometry, the column inner diameter decreases to 1.0 - 2.1 mm due to the improved flow rate compatibility with common ion sources. This trend continues to even smaller column *i.d.*s depending on the field of application. Nowadays, miniaturized LC systems that can be used with column inner diameters between 0.075 - 0.5 mm are available. In addition, the miniaturization is accompanied with a consequent reduction of the flow rate in the nL min^{-1} - µL min^{-1} range. The usage of miniaturized LC was early discussed in the literature [19-21]. Tsuda and Novotny were among the first pioneers using microbore liquid chromatography columns with an *i.d.* of 50 µm to 200 µm [22]. Scott and Kucera demonstrated the potential of miniaturized separation techniques in a series of impressive contributions [23-27]. For example, the authors investigated the performance of 1 m long columns of various *i.d.* between 1 mm and 500 µm packed with particle diameters between 5 µm – 35 µm using a

specially designed UV detection with a cell volume of only 1-3 µL. Impressively, they reported reduced plate heights of almost 2 for 20 µm particles at a retention factor of 1.8 which represents a good column packing quality as will be discussed below. In addition, they mentioned the advantage of increased heat dissipation of miniaturized columns, which is nowadays known as frictional heating [26]. However, the corresponding chromatograms were either characterized by long analysis times or decreased resolution when applying shorter columns. In general, the system designs of former times were not suitable to successfully apply small *i.d.* columns for several reasons.

At the beginning of using miniaturized column *i.d.* conventional HPLC systems were applied using flow splitters to reduce the flow rate [22]. This approach has several disadvantages because flow splitting can affect system robustness since the resulting flow rate can be influenced by temperature changes as well as clogging. Therefore, specially designed miniaturized LC systems were developed. Renewed interest in the field of miniaturized separation technique was given by the inspiring work of Joergensen et al. in 1999 [28-30]. The group developed a miniaturized LC system on the basis of syringe pumps capable of 9,000 bar maximum pressure using a column *i.d.* of only 33 µm packed with 1.0 µm non-porous particles demonstrating the potential of miniaturized LC with improved equipment [29].

Nowadays, most of the commercially available miniaturized liquid chromatography systems are based on flow meters using pneumatic syringe pumps controlled by the so-called microfluidic flow control (*MFC*) or automatic flow control (*AFC*) depending on the manufacturer instead of conventional piston pumps to ensure flow rate accuracy and to minimize the influence of pulsation which is of utmost importance when utilizing small flow rates. When using pneumatic syringe pumps, a flow calibration of the flow meters depending on the mobile phase viscosity and temperature needs to be done. During operation, the flow meter monitors the pressure drop of the individual solvent channel and sends a signal to the controller that is connected to the pressure source. The main task of the controller is the adjustment of the pressure source to regulate the flow rate. By changing the pressure, the flow rate is automatically adjusted according to the flow calibration. The pressure is established by a connected gas stream like nitrogen. Dedicated miniaturized systems are characterized by low gradient delay volumes (V_{dwell}). The gradient delay volume includes the volume from the point of mixing of the mobile phases to the head of the column. This volume is responsible for the involuntary isocratic step at the beginning of every solvent gradient and leads to a temporal offset of the separation. Moreover, analytes eluting within this time-frame cannot be affected by the gradient. Figure 1.2 shows a schematic representation of the gradient delay volume.

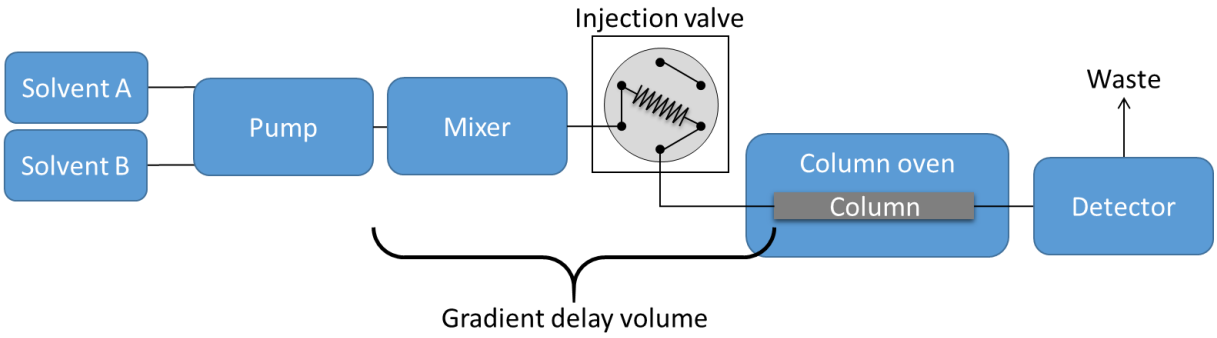

Figure 1.2: Illustration of the gradient delay volume for binary mixing LC systems.

Figure 1.3 demonstrates the influence of the gradient delay volume for different V_{dwell} at a flow rate of 40 µL min^{-1} which is a standard flow rate for 0.3 mm - 0.5 mm *i.d.* columns. A delay volume of 500 µL represents a typical value for a conventional HPLC system, whereas using a fully optimized UHPLC system, a gradient delay volume of 50 µL can be achieved. In contrast, specially designed miniaturized LC systems are characterized by a V_{delay} in the range of only 1 µL.

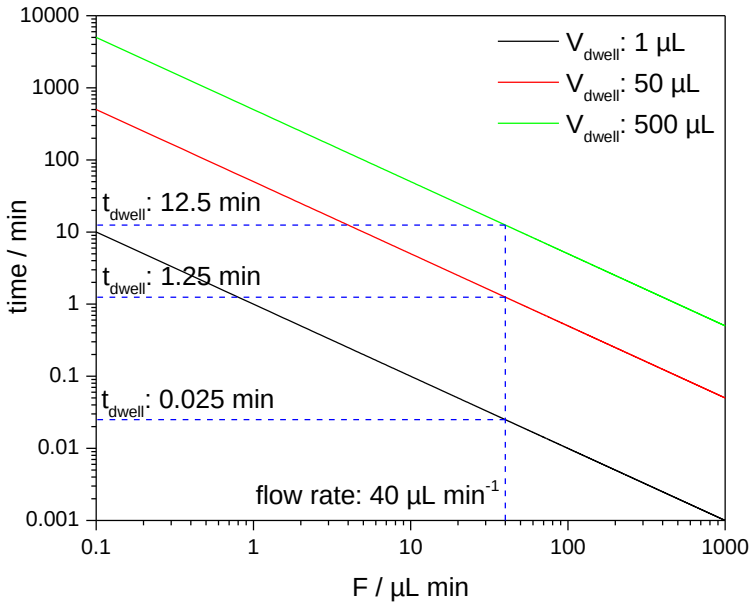

Figure 1.3: Illustration of the influence of the applied flow rate and gradient delay volume on the gradient delay time.

As can be identified from the double logarithmic plot, it takes 12.5 min until the gradient reaches the column at a flow rate of 40 µL min^{-1} using a HPLC system having a delay volume of 500 µL. Reducing V_{dwell} to 50 µL leads to a gradient delay time (t_{dwell}) of 1.25 min for an optimized UHPLC system. These values clearly demonstrate the necessity of decreasing the gradient delay volume when using low flow rates and miniaturized column i.d to achieve fast separations. For a gradient delay volume of 1 µL in a dedicated miniaturized LC system t_{dwell} is only 0.025 min and thereby an immediate effectiveness of the gradient can be ensured. Another

important characteristic of miniaturized LC system is the reduced extra-column volume which is a decisive parameter when using small *i.d.* columns to utilize the separation performance of the column. The influence of the extra-column volume on column performance was already discussed in the 1970's by Kirkland [26, 31] and is still one of the most important parameters when designing new LC instrumentation [32]. In general, this volume is responsible for extra-column band broadening and all components of a LC system are contributors. In general, a measure for band broadening in the chromatographic system is the peak variance (σ^2) of a Gaussian elution profile [29, 33, 34]. According to the Equation 1.1, the number of theoretical plates can be calculated by the square of the ratio of the retention time (t_R) and the standard deviation (σ) of the Gaussian peak.

$$N = \left(\frac{t_R}{\sigma}\right)^2 \qquad \textbf{Equation 1.1}$$

The total system variance ($\sigma^2_{v,total}$) is defined as the sum of the variances of the different LC system components as shown in Equation 1.2.

$$\sigma^2_{v,total} = \sigma^2_{v,inj} + \sigma^2_{v,cap} + \sigma^2_{v,col} + \sigma^2_{v,det} \qquad \textbf{Equation 1.2}$$

where $\sigma^2_{v,inj}$ is the variance caused by the injector, $\sigma^2_{v,cap}$ the variance of the connection capillaries, $\sigma^2_{v,col}$ the column variance and $\sigma^2_{v,det}$ the contribution of the detector. In general, the extra-column variance (σ^2_{ec}) including $\sigma^2_{v,inj}$, $\sigma^2_{v,cap}$ and $\sigma^2_{v,det}$ should be at least a factor of 4-10 smaller than the column variance to avoid excessive loss of separation performance [35]. It is therefore an important aim to minimize the contribution of extra-column system components to achieve a more favourable ratio between the column and extra-column variance in order to utilize the full performance of miniaturized columns. When an LC system with unfavourable extra-column variance is used for small *i.d.* columns, the extra column band broadening significantly affects the separation performance because the small peak volumes achieved on the chromatographic column gets broadened leading to decreased separation power. The variance caused by the connection capillaries typically contributes strongly to the overall extra-column variance. It can be reduced by decreasing the inner diameter of the connection capillaries. For analytical LC columns, the inner diameter of the capillaries is typically in the range of 100 µm - 250 µm. In contrast, for miniaturized LC columns a further reduction of the capillary *i.d.* to 25 µm - 75 µm is mandatory to avoid a pronounced loss of separation efficiency. To identify the appropriate capillary inner diameter for miniaturized LC, Figure 1.4 demonstrates the influence of the capillary *i.d.* on the resulting separation using a common LC performance mix on a 50 x 0.3 mm micro-LC column as defined in Table 1.1.

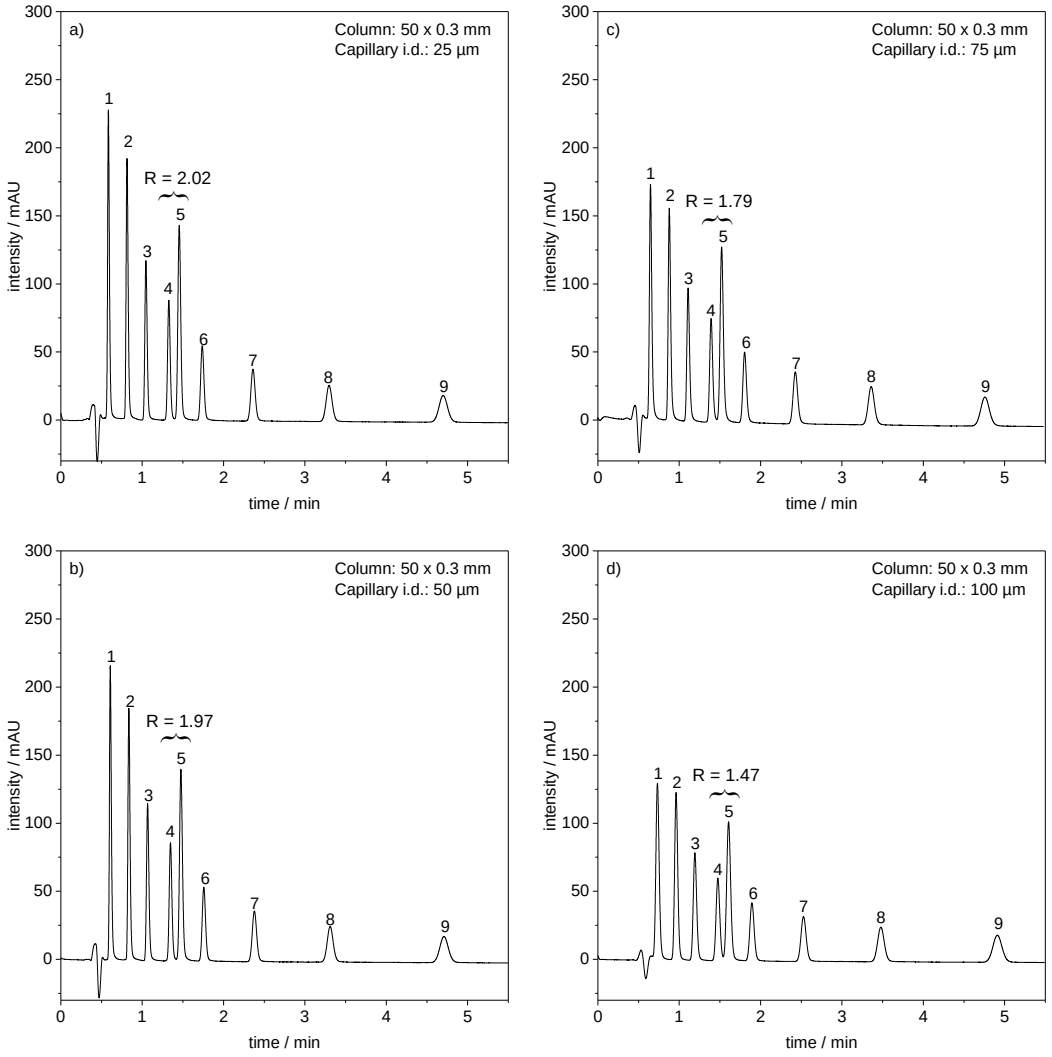

Figure 1.4: Resulting chromatograms for the separation of a common performance mix on a 50 x 0.3 mm column using different outlet capillary inner diameters. a) 25 µm, b) 50 µm, c) 75 µm and d) 100 µm.

It can be seen from Figure 1.4 a) and b) that the inner diameter of the connection capillary should be between 25 µm - 50 µm because no significant performance differences between the obtained chromatograms can be identified. A further increase of the *i.d.* to 75 µm or 100 µm leads to a decrease in sensitivity as well as to a loss of separation efficiency as can be seen for the resolution between the compounds 4 and 5 in Figure 1.4 c) and d) which continuously decreases from 2.02 for the 25 µm *i.d.* capillary to 1.47 for the 100 µm connection tubing. Since no significant differences between Figure 1.4 a) and b) are observed, an inner diameter of 50 µm should be used for a 0.3 mm *i.d.* column due to the reduced back pressure.

To further emphasize the importance of the extra-column variance, the variance of a chromatographic peak obtained on the column can be calculated for the example of a 50 x 0.3 mm micro-LC column, a porosity (ε) of 0.7, a number of theoretical plates (N) of 10,000 and a retention factor (k) of 2 using Equation 1.3.

$$\sigma^2_{v,column} = \frac{\varepsilon^2 \cdot \pi^2 \cdot r_c^4 \cdot L^2}{N}(1+k)^2$$ **Equation 1.3**

According to Equation 1.3, the column variance is only 5.5 x 10^{-3} µL^2. Based on the requirement of at least a factor 4 smaller extra-column variance compared to the column variance, σ^2_{ec} has to be in the order of 1.4 x 10^{-3} µL^2. Whereas fully optimized conventional LC systems have a σ^2_{ec} of 2.4 µL² [32], miniaturized LC systems are characterized by an extra-column variance in the order of 10^{-2} µL^2 demonstrating the need of further minimization [35]. This could be one reason why earlier the applicability of small *i.d.* columns was not successful although the theoretical background and advantages of micro-LC were already well known [19-21].

As indicated in Equation 1.2, the variances and therefore the *i.d.* of the connection tubings need to be considered for reduced inner diameter columns. In general, when a liquid flows through a capillary a laminar flow profile forms, which is illustrated in Figure 1.5.

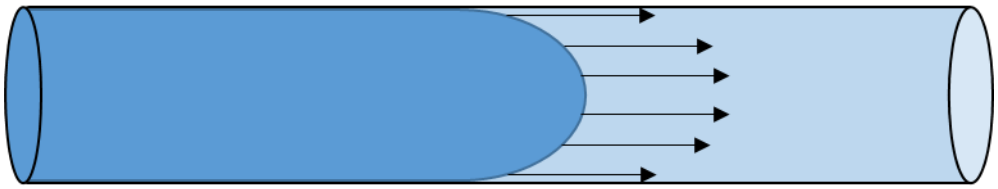

Figure 1.5: Illustration of the formed laminar flow profile and resulting velocity flow paths in a capillary.

Because of the resulting flow profile there are regions with different flow velocities as indicated by the arrows. The flow velocity continuously decreases from the center to the capillary wall and is zero at the wall due to friction [36]. As a consequence, the migration for each analyte molecule is different depending on the current position in the tubing and resulting velocity. Therefore, it is important that the molecules are able to cross the different velocity regions by diffusion to experience different flow velocities in order to obtain a sharp analyte band. Figure 1.6 shows a computational fluid dynamic (*CFD*) simulation of the resulting peak profiles in a capillary assuming enabled and disabled analyte diffusion [37].

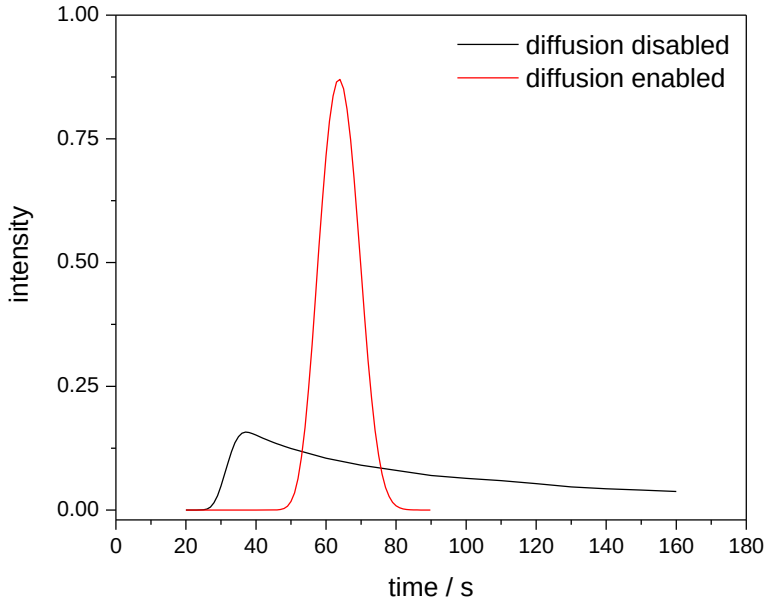

Figure 1.6: Illustration of the resulting peak profile simulated for enabled and disabled analyte diffusion in an unfilled capillary [37]. Parameter: capillary length: 30 cm, inner diameter: 50 µm, flow rate: 1 µL min^{-1}, mobile phase: methanol, analyte: toluene. The diffusion coefficient was calculated according to the Wilke-Chang equation (see Chapter 5.3.1).

As can be seen it is of utmost importance that the analytes diffuse into different regions where the flow velocities are different. Otherwise, a pronounced peak tailing can be observed. However, these diffusion processes are time-dependent and therefore controlled by the analyte diffusion coefficient. The smaller the analyte the higher the diffusion coefficient which leads to faster migration between the flow paths. In addition to the capillary inner diameter, the column cross section is also an important parameter that affects the time an analyte molecule needs to diffuse from the column wall to the center of the column and therefore from a region with low flow velocity to the faster velocity section to obtain a small peak width on the chromatographic column. The time the analyte needs to diffuse from the column wall to the center of the column is also known as critical diffusion time (t_D) which is shown in Equation 1.4 [30].

$$t_D = \frac{r^2}{2 \cdot \gamma \cdot D_m} \qquad \textbf{Equation 1.4}$$

where r is the column radius, γ the tortuosity factor and D_m the molecular diffusion coefficient. Decreasing the column *i.d.* consequently leads to a reduction of t_D and a faster radial diffusion of the analyte is possible. Thereby, the analyte band is compressed and sharper peak profiles are obtained. Figure 1.7 illustrates the resulting t_D for different column *i.d.* and molecular diffusion coefficients.

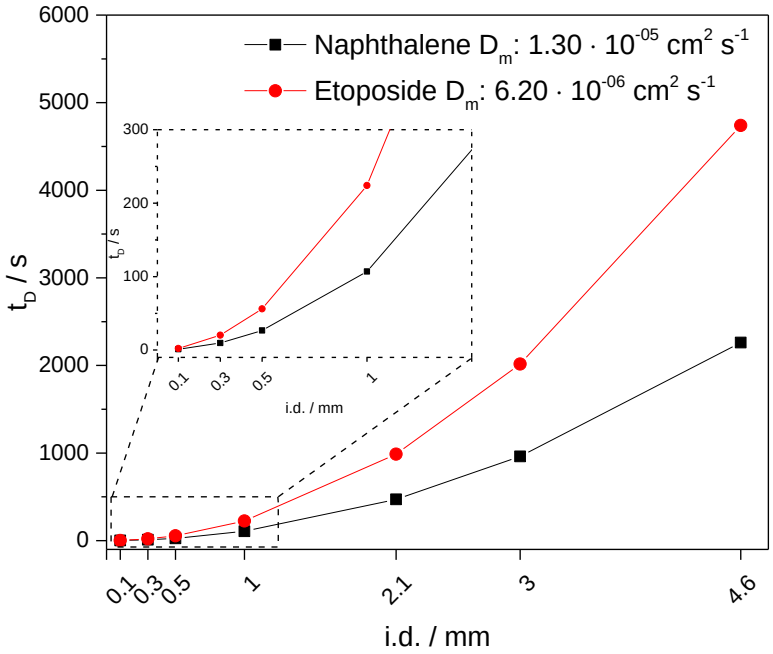

Figure 1.7: Illustration of the resulting critical diffusion time (t_D) depending on the column inner diameter and analyte diffusion coefficient for the lower molecular weight compound naphthalene and higher mass substance etoposide. The diffusion coefficients were calculated according to the Wilke-Chang equation (see Chapter 5.3.1).

As becomes clear, decreasing the column *i.d.* from e.g. 4.6 mm to 0.3 mm reduces t_D from 2260 s to 9.6 s for the lower molecular weight compound naphthalene, whereas for the lower diffusion coefficient analyte etoposide t_D decreases from 4740 s to 20 s demonstrating the benefit of miniaturized column *i.d.* By decreasing the column *i.d.*, t_D is reduced by the factor of 236 independently of the molecular diffusion coefficient. Reducing the tubing and column *i.d.* has another important advantage regarding the linear velocity (u_0). According to the continuity equation shown in Equation 1.5, the linear velocity increases for incompressible fluids when the radius is decreased [38].

$$Q = A_1 \cdot v_1 = A_2 \cdot v_2 \qquad \textbf{Equation 1.5}$$

where A_1 and A_2 are the cross-sectional areas of a column or tubing, v_1 and v_2 are the flow velocities and Q the volume based velocity. For a given Q obtained for a defined cross-sectional area A_1 and a velocity v_1, the velocity v_2 increases when the cross-sectional area A_2 decreases to obtain a constant volume based velocity. As a consequence, the separation speed in liquid chromatography increases with decreasing inner diameter when a constant flow rate is used. This property is demonstrated in Figure 1.8 where the u_0 is plotted versus the column *i.d.* assuming a flow rate of 40 µL min^{-1}, a column length (L) of 50 mm and a porosity of 0.7.

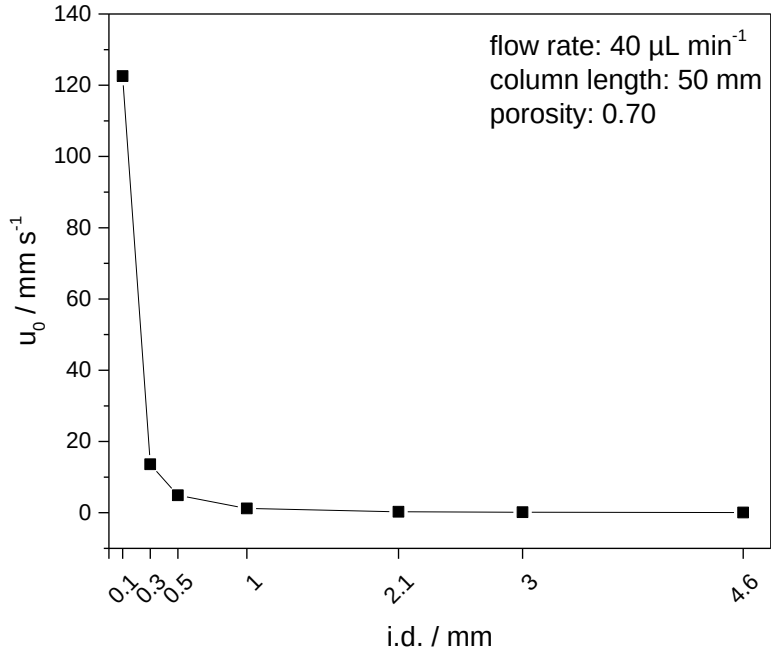

Figure 1.8: Illustration of the resulting linear velocity depending on the column inner diameter for a flow rate of 40 µL min^{-1}.

As becomes clear, at a constant flow rate of e.g. 40 µL min^{-1} a significant increase of the linear velocity can be observed when the column *i.d.* is reduced below 1.0 mm. An even more pronounced shift of u_0 can be observed when changing the column *i.d.* from 0.5 mm to 0.3 mm demonstrating the benefit of 0.3 mm *i.d.* columns and smaller. This property directly leads to increased separation speed. For example, u_0 is 0.28 mm s^{-1} for a 2.1 mm *i.d.* column which is the standard dimension for LC-MS whereas a linear velocity of 13.6 mm s^{-1} can be achieved at the same flow rate and column length using a column inner diameter of 0.3 mm. On the other hand, to achieve similar separation speed the flow rate needs to be increased for an enlarged inner diameter. This dependency is illustrated in Figure 1.9 under consideration of a u_0 of 13.6 mm s^{-1}.

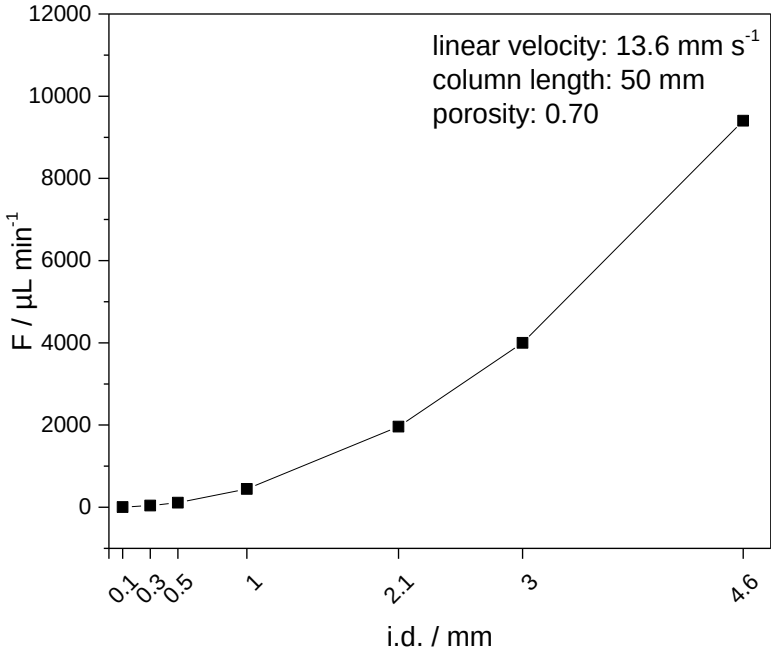

Figure 1.9: Illustration of the resulting flow rate depending on the column inner diameter to achieve a linear velocity of 13.6 mm s^{-1}.

It can be identified that e.g. a flow rate of approximately 4 mL min^{-1} is necessary to obtain a similar separation speed for a 3.0 mm *i.d.* column compared to only 40 µL min^{-1} using a column inner diameter of 0.3 mm. This is an undisputed benefit of miniaturized separation techniques because a lower flow rate leads to faster separations with decreased solvent consumption reducing the cost for purchase and disposal of organic solvents at the same time in terms of green analytical chemistry [18, 39-41]. However, the influence on column performance at increased linear velocities must be considered as shown below. The flow rate reduction is consequently advantageous when certain detection techniques are coupled to liquid chromatography. Especially aerosol based detectors benefit from low flow rates due to the smaller volume of organic solvent that needs to be evaporated and removed [18]. In particular the hyphenation to mass spectrometry (*MS*) is favoured by decreased flow rates due to the increased ionization efficiency as was demonstrated by Shen et al [42]. However, the common ion sources are developed to handle high flow rates up to several millilitres per minute.

The miniaturization of liquid chromatography has not only advantages. Considering the loading capacity of small *i.d.* columns, the injection volume needs to be decreased to avoid both mass and volume column overloading. Mass overloading occurs due to the high amount of analytes injected onto the column. The number of analyte molecules is too high compared to the capacity of the stationary phase resulting in triangular peak shapes. In contrast, volume column overloading is caused by unusual high injection volumes which leads to broad but symmetrical peak shapes sometimes associated with a formation of a plateau. For an ideal chromatography,

the injection volume should be chosen to be around less than 10% of the column void volume ($V_{col,eff}$) [43]. The column void volume can be calculated according to Equation 1.6.

$$V_{col,eff} = \left(\frac{d_c}{2}\right)^2 \cdot \pi \cdot L \cdot \epsilon \qquad \textbf{Equation 1.6}$$

As can be seen, the effective column volume depends on the column inner diameter, column length and porosity. Therefore, a drastic reduction of the injection volume is necessary to ensure optimum chromatographic conditions when small *i.d.* columns are used. The relation between the column *i.d.* and optimum injection volume is depicted in Figure 1.10.

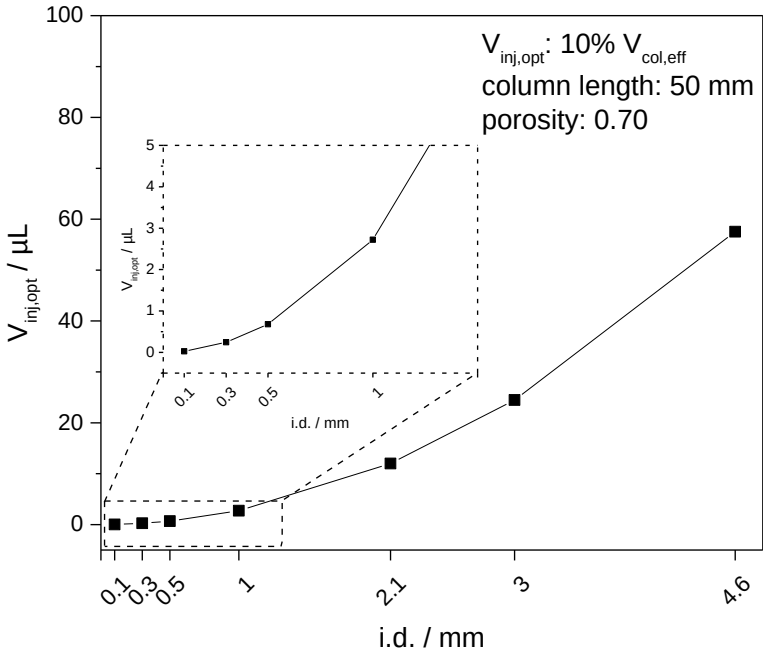

Figure 1.10: Illustration of the optimum injection volume depending on the column inner diameter.

The optimum injection volume decreases from 58 µL for a standard 4.6 mm column to 12 µL for the preferred conventional LC-MS 2.1 mm *i.d.* column whereas for miniaturized column inner diameters such as 0.3 mm a decreased injection of only 0.25 µL should be used. As a consequence, the injected mass is dramatically decreased for small *i.d.* columns. This seems disadvantageously for mass-dependent detection techniques like mass spectrometry and it is often being stated that miniaturized column *i.d.* is only advantageously when the sample volume is limited [18]. However, the reduced injected mass has two further advantages. First, the chromatographic band gets less diluted by the column volume. Therefore, small *i.d.* columns will always lead to higher sensitivity at constant injection volumes no matter if concentration- or mass-dependent detectors are used as shown in Figure 1.11 [39, 44].

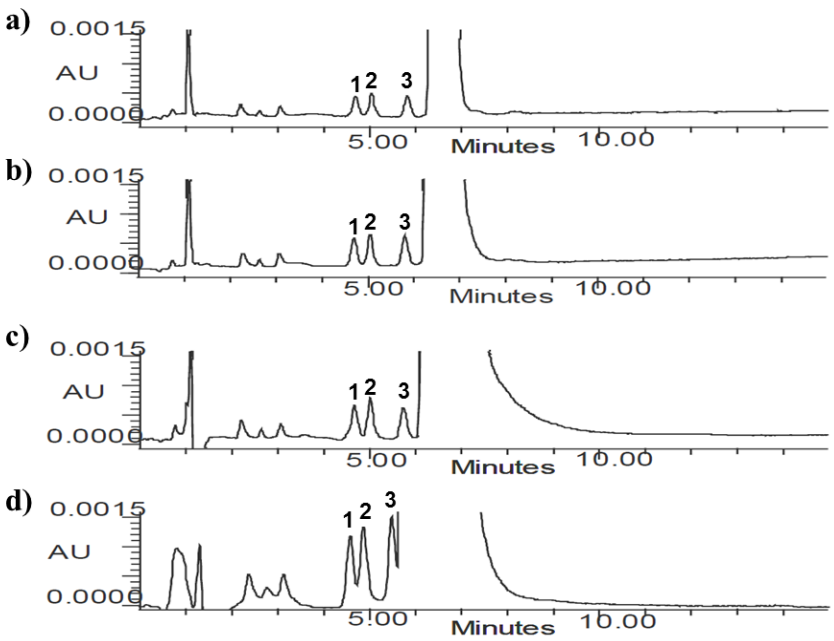

Figure 1.11: Illustration of the resulting sensitivity at a constant injection volume of 7 µL for a column *i.d.* and flow rate of a) 4.6 mm at 1.4 mL min^{-1}, b) 3.9 mm at 1.0 mL min^{-1}, c) 3.0 mm at 0.6 mL min^{-1} and d) 2.1 mm at 0.29 mL min^{-1} [44].

Secondly, due to the reduction of injected mass, the amount of matrix ingredients is reduced leading to smaller amount of dirt that is introduced into highly sensitive detectors and consequently to extended cleaning intervals. That is an important characteristic because the absolute sensitivity or analyte response is not the decisive parameter. The parameter of interest for routine application is the signal-to-noise (S/N) ratio, which decreases with more contaminated equipment. To summarize, both the advantages as well as disadvantages regarding miniaturized column *i.d.* are illustrated in Figure 1.12.

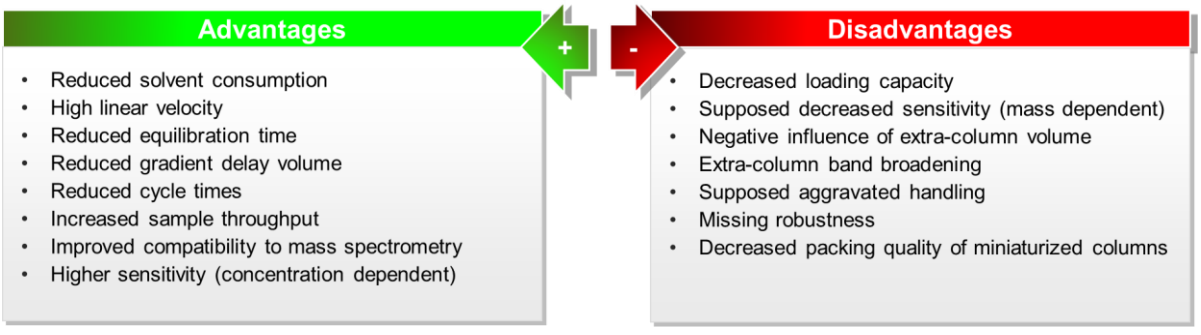

Figure 1.12: Illustration of both advantages and disadvantages of miniaturized LC.

The chromatographic column is the heart of every separation. It is often being questioned whether small *i.d.* columns can provide the same separation efficiency like their conventional counterparts [18, 35, 45]. In the past, the packing quality of miniaturized columns seems to have been an issue why this separation dimension was not successfully applied. In addition, the commercial availability was limited. However, over the last years a development of stationary

phases with inner diameters below 1 mm has occurred and new generations of small *i.d.* columns became commercially available from several manufacturers like YMC or Waters [46, 47]. Different chromatographic supports such as fully porous and core-shell particles with varying particle diameter were also introduced for miniaturized LC. In addition, monolithic columns synthesized in fused silica capillaries were developed [48].

To evaluate the separation efficiency of chromatographic columns, different approaches were developed over the last 50 years. The most familiar one is the van Deemter analysis describing the column performance depending on the linear velocity and peak broadening effects [49, 50]. The van Deemter equation is shown in Equation 1.7 whereas the van Deemter plot is illustrated in Figure 1.13.

$$H(u_0) = A \cdot d_p + \frac{B \cdot D_m}{u_0} + C \cdot \frac{d_p^2}{D_m} \qquad \textbf{Equation 1.7}$$

where H is the plate height, A the Eddy diffusion, d_p the particle diameter, B the longitudinal diffusion and C the mass transfer.

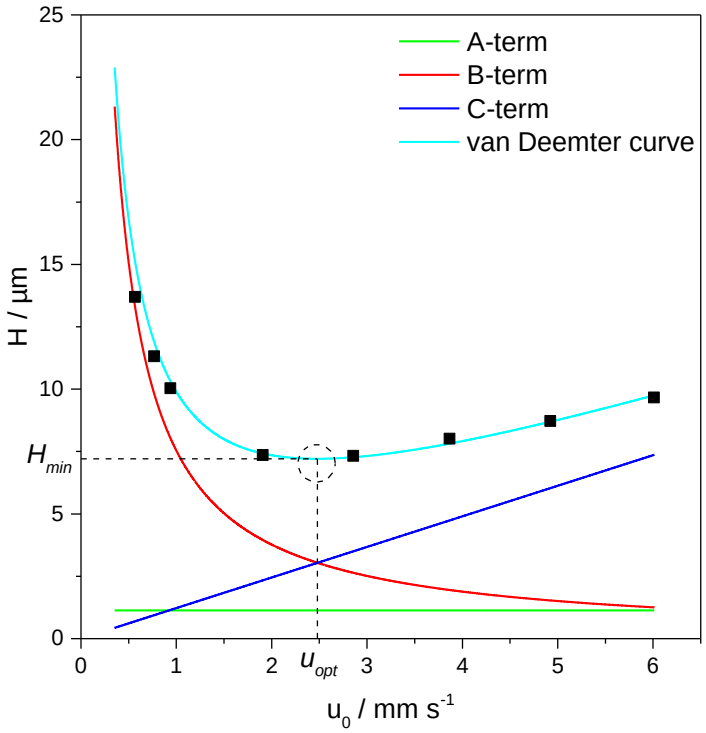

Figure 1.13: Illustration of the van Deemter plot including the Eddy diffusion (*A*), longitudinal diffusion (*B*) and the mass transfer (*C*).

Considering the van Deemter equation, the plate height depends on the packing quality (*A*-term), diffusion in longitudinal direction (*B*-term) and the mass transfer (*C*-term) of the analyte between the stationary phase and mobile phase. All parameters depend on the linear velocity. At the optimum linear velocity (u_{opt}), the plate height is minimal (H_{min}) as indicated by the

dashed circle. However, the efficiency depends on the particle diameter and molecular diffusion coefficient as shown in Equation 1.7 [51, 52]. Therefore, Giddings proposed the use of reduced parameters to achieve a fair comparison between various stationary phases of different particle diameter or morphology to evaluate the columns in terms of the packing quality using the reduced plate height (*h*) and reduced velocity (*v*) as shown in Equation 1.8 and Equation 1.9. [53, 54].

$$h = \frac{H}{d_p}$$ **Equation 1.8**

$$v = \frac{u_0 \cdot d_p}{D_m}$$ **Equation 1.9**

where *h* is the reduced plate height and *v* the reduced linear velocity. For well packed columns the minimum reduced plate height (h_{min}) should be 2-2.5 [8]. This equation directly enables to compare different stationary phases with varying particle diameter. In addition, differences in analyte diffusion coefficients are considered. Subsequently, Knox developed the Knox equation on the basis of reduced parameters to take these dependencies into consideration as illustrated in Equation 1.10 [54, 55].

$$h(v) = a \cdot v^{1/3} + \frac{b}{v} + c \cdot v$$ **Equation 1.10**

where *a*, *b* and *c* are dimensionless coefficients. To emphasize the difference of the van Deemter and the Knox equation, Figure 1.14 shows the obtained plots for two different columns packed with 1.9 µm fully porous particles and 2.7 core-shell particles.

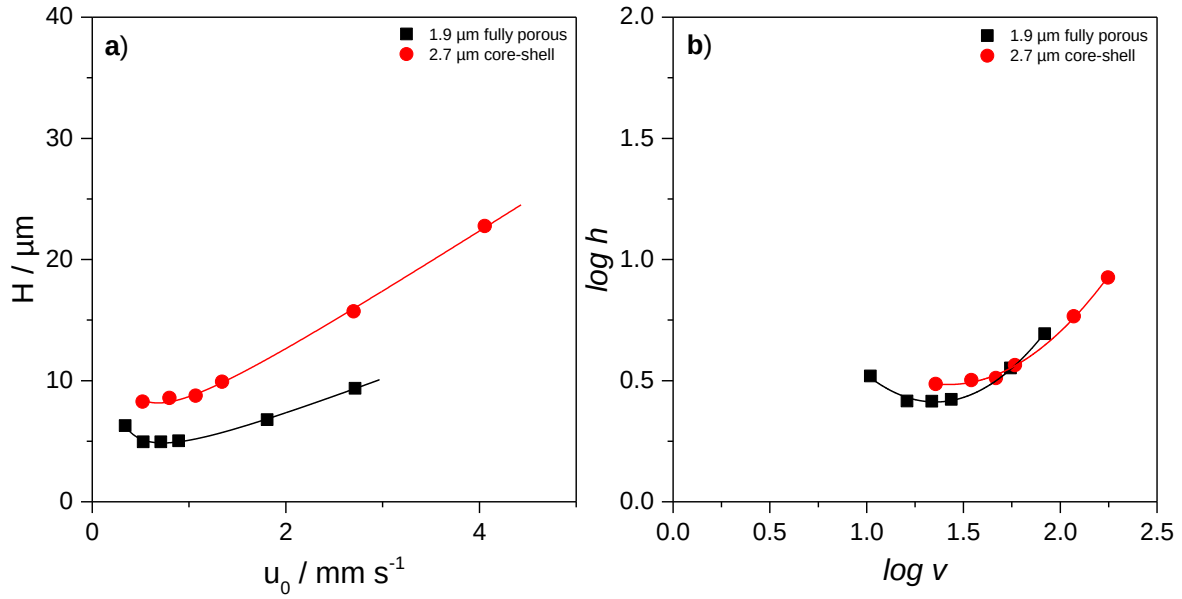

Figure 1.14: Comparison of a) the van Deemter and b) the Knox plot for 1.9 µm fully porous and 2.7 µm core-shell particle packed columns.

According to Equation 1.7, pronounced differences of the minimum plate height (H_{min}) between the two different columns can be observed as expected for the van Deemter plot in Figure 1.14 a) due to the varying particle diameter. Considering the Knox plot in Figure 1.14 b), it can be demonstrated that the columns show a similar reduced plate height and therefore a comparable packing quality. This conclusion cannot be drawn from the van Deemter analysis. However, both equations include no information about the back pressure characteristic of a column which depends on mobile phase viscosity (η) and permeability (K_{v0}) [56, 57]. These parameters are especially important when trying to accelerate the separation. In addition, column efficiency can easily be improved by using a lower mobile phase viscosity or longer columns. To address this issue, Bristow and Knox introduced the theory of column separation impedance (E_0) as illustrated in Equation 1.11 [55].

$$E_0 = \frac{t_0}{N^2} \cdot \frac{\Delta P}{\eta} = \frac{H^2}{K_{v0}} = h^2 \cdot \Phi \qquad \textbf{Equation 1.11}$$

$$K_{v0} = \frac{u_0 \cdot \eta \cdot L}{\left(\Delta P_{total} - \Delta P_{system}\right)} \qquad \textbf{Equation 1.12}$$

$$\phi = \frac{d_p^2}{K_{v0}} \qquad \textbf{Equation 1.13}$$

where ϕ is the flow resistance, ΔP_{total} the total backpressure and ΔP_{system} the pressure drop only caused by the LC system. The column permeability can be calculated according to Equation 1.12 whereas the flow resistance is shown in Equation 1.13.

The separation impedance is ideally suited to compare the performance of columns packed with different particles sizes and morphology [58]. However, as a dimensionless parameter, no direct information in terms of practical purposes can be obtained. Therefore, Giddings was the first who pointed out that the more straightforward way to compare different columns for practical applications is the time dependent ability to create separation performance [59]. Hans Poppe introduced plots of the so-called plate time as the ratio of the column void time (t_0) and plate number (N) versus N (the so-called Poppe plots) as shown in Figure 1.15 [60].

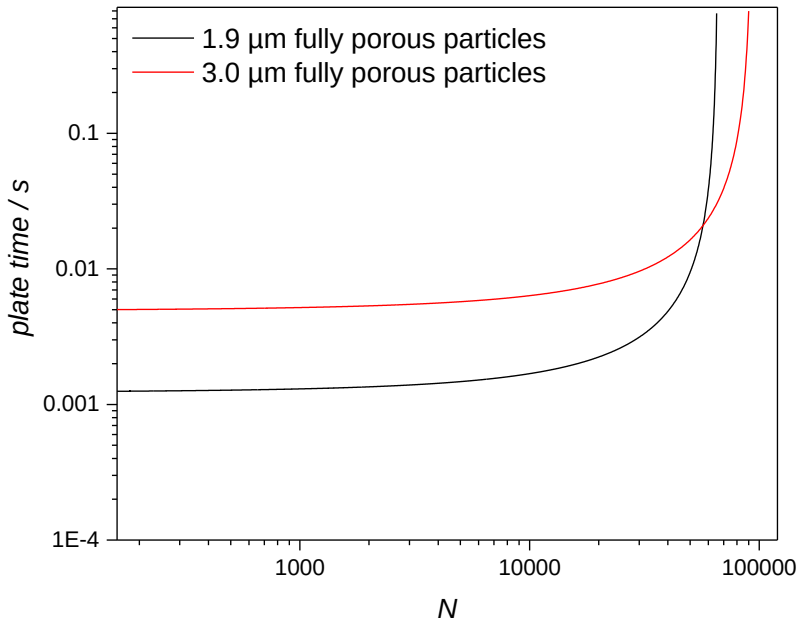

Figure 1.15: Illustration of a Poppe plot for 1.9 µm and 3.0 µm fully porous particles.

Thereby, it can be directly identified how long it takes to create a theoretical plate depending on the applied particle diameter [60]. In 2005, Desmet and co-workers established transformation equations to obtain several versions of the so-called kinetic plot limits [56, 61]. These types of plots directly enable to compare columns at maximum pressure and therefore at maximum efficiency and to visualize which length it takes to create a certain efficiency. The comparison at maximum pressure is useful due to the proportionality of efficiency, column length and back pressure as illustrated in Equation 1.14 and Equation 1.15. Higher pressure capabilities enable to use longer columns to achieve higher efficiency. Therefore, it is straightforward to compare different columns at maximum pressure.

Until today, the kinetic plot theory has been expanded to gradient elution and is the ideal tool to design a chromatographic system on the basis of the underlying requirements [61-63]. In the following, the theoretical derivation of the kinetic plot theory is shown for an isocratic transformation. Equation 1.14 illustrates the calculation of the back pressure (ΔP) depending on the mobile phase viscosity (η), column length (L), linear velocity (u_0) and column permeability (K_{v0}).

$$\Delta P = \frac{\eta \cdot u_0 \cdot L}{K_{vo}} \qquad \textbf{Equation 1.14}$$

The column length can be replaced by Equation 1.15.

$$L = N \cdot H \qquad \textbf{Equation 1.15}$$

The obtained equation can be transformed leading to Equation 1.16.

$$N = \left(\frac{\Delta P}{\eta}\right) \cdot \left[\frac{K_{v0}}{H \cdot u_0}\right]_{exp}$$ **Equation 1.16**

This equation can be transformed to calculate the column void time (t_0) by introducing Equation 1.17.

$$t_0 = \frac{L}{u_0} = \frac{N \cdot H}{u_0}$$ **Equation 1.17**

Inserting Equation 1.16 into Equation 1.17 leads to Equation 1.18.

$$t_0 = \left(\frac{\Delta P}{\eta}\right) \cdot \left[\frac{K_{v0}}{u_0^2}\right]_{exp}$$ **Equation 1.18**

Since all parameter are linked to the van Deemter analysis, all experimentally obtained van Deemter data can be transferred into a couple of N and t_0 data to illustrate the time needed to achieve a certain number of theoretical plates. The transformation is shown in Figure 1.16.

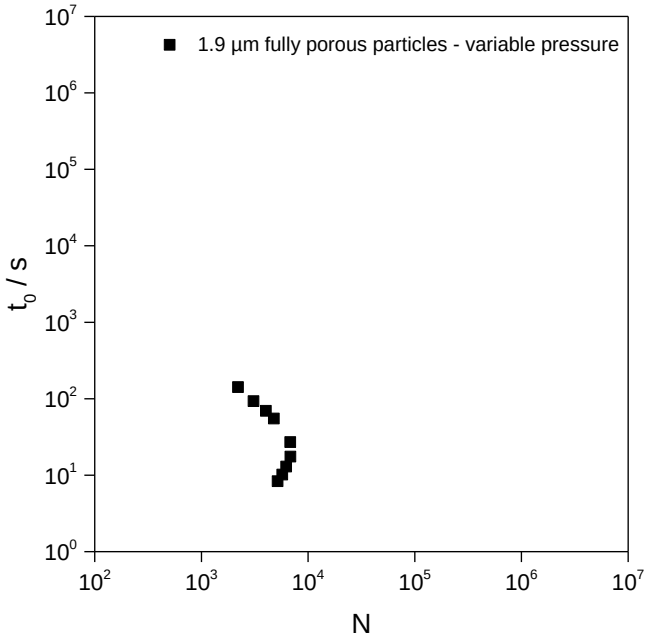

Figure 1.16: Transformation of experimentally obtained $H(u_0)$ data to the more practical relevant plot of t_0 versus N.

This type of plot can be used to identify a column void time which depends on the applied flow rate to obtain a certain number of theoretical plates. As mentioned above, the kinetic plot theory directly enables to compare columns at maximum pressure (ΔP_{max}) by replacing the experimental ΔP with ΔP_{max} of the column or applied LC system leading to Equation 1.19 and Equation 1.20.

$$N = \left(\frac{\Delta P_{max}}{\eta}\right) \cdot \left[\frac{K_{v0}}{H \cdot u_0}\right]_{exp} \qquad \textbf{Equation 1.19}$$

$$t_0 = \left(\frac{\Delta P_{max}}{\eta}\right) \cdot \left[\frac{K_{v0}}{u_0^2}\right]_{exp} \qquad \textbf{Equation 1.20}$$

The resulting transformation is depicted in Figure 1.17.

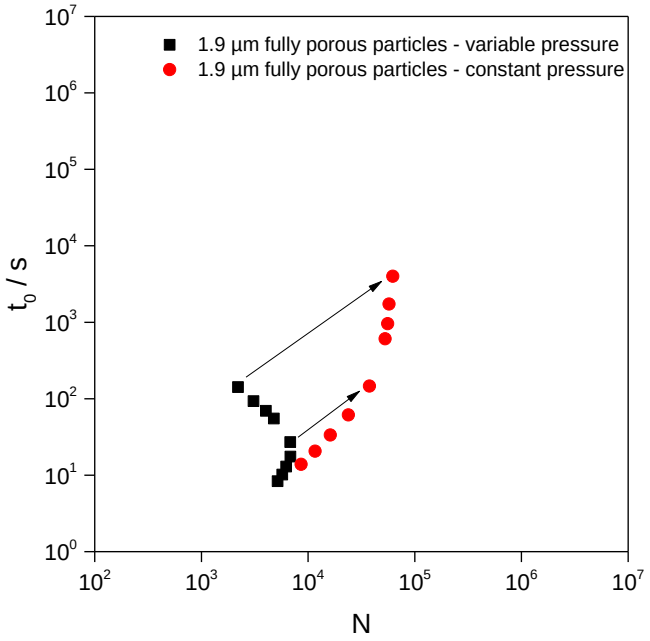

Figure 1.17: Illustration of the transformation of experimentally obtained *N* and t_0 data to the kinetic plot limit at maximum pressure.

Now the experimentally obtained *N* and t_0 data are transformed to the maximum pressure as indicated by the full line arrows, illustrating the maximum performance that can be achieved using this chromatographic support. This type of plot allows for the fairest comparison between different stationary phases since the performance is compared at maximum efficiency.

Despite all described advantages, the acceptance of miniaturized separation techniques is still limited preventing the extension of this technique. The usage is often restricted to certain fields of applications as e.g. bioanalysis, where the sample volume is limited [18]. Small *i.d.* columns are favourable due to the decreased dilution by the column and commonly nano-LC with an *i.d.* of 0.1 mm and less are used [39]. However, the question arises how the applicability of miniaturized LC systems can be extended to different fields of application where the sample volume is not a limiting factor. Especially the robustness and handling is often being questioned [64] when small *i.d.* columns are applied compared to conventional inner diameters (≥ 2.1 mm). Due to the small resulting column volumes, decreased column *i.d.* are more vulnerable to extra-column band broadening as discussed above. This becomes even more pronounced for nano-LC or chip-LC compared to micro-LC due to the further reduction of the column *i.d.* from 300 µm for micro-LC to 100 µm and less for nano-LC or chip-LC. In addition, when using nano-LC or chip-LC often dedicated detection capabilities are necessary leading to additional cost for the purchase of specialized equipment. For example, dedicated nano-LC ion sources are needed for the hyphenation to mass spectrometry which are often characterized by complicated handling. In general, mass spectrometry is nowadays the detection of choice due

to the possibility of separating compounds by their mass-to-charge (*m/z*) ratio. Several manufacturers responded to this issue by introducing specialized systems to simplify the usage. One example is the so-called IonKey introduced by Waters in 2014 [65]. However, it would be much more straightforward to use already existing equipment without the need of additional high investments and to increase sample throughput at the same time. In addition, the advantages of high linear velocity at low flow rates and decreased critical diffusion times should be maintained. Especially, the high linear velocity is of interest to achieve fast separations and decreased analysis cycle times. Thereby, the sample throughput can be significantly increased leading to a high return of invest for routine laboratories applying LC-MS. This can be achieved by using column inner diameters of 0.3 µm as shown in Figure 1.6 - Figure 1.9 using dedicated micro-LC systems. These systems can be used with column *i.d.* between 0.1-1.0 mm and are cheaper to purchase than an additional mass spectrometer to handle a higher number of samples. Moreover, the increase of column *i.d.* to 0.3 mm compared to 0.1 mm leads to increased loading capacity by a factor of approximately 10. In addition, already established mass spectrometers can be used without the need of dedicated ion sources. The only necessary modification is the change of the inner diameter of the emitter tip to reduce extra-column band broadening. Therefore, micro-LC used with a column *i.d.* of 0.3 mm is ideally suited and represents the most promising approach to combine the properties of high linear velocities, decreased analysis cycle times and sufficient loading capacity at reduced flow rates with conventional detection techniques. In addition, the influence of the extra-column volume is less pronounced for 0.3 mm *i.d.* columns compared to even smaller inner diameters. However, only a few reports about the performance of micro-LC columns as well as the applicability in high throughput analysis in routine environments are available.

When developing an LC method, there is one equation that illustrates the influence parameter of resolution (*R*) in liquid chromatography. This equation is also known as Purnell equation [66, 67] and is shown in Equation 1.21 and Equation 1.22 both for isocratic and gradient elution.

$$R = \frac{1}{4} \cdot \sqrt{N} \cdot (\alpha - 1) \cdot \frac{k}{k+1} \qquad \textbf{Equation 1.21}$$

$$R = \frac{1}{4} \cdot \sqrt{N^*} \cdot (\alpha^* - 1) \cdot \frac{k^*}{k^* + 1} \qquad \textbf{Equation 1.22}$$

where N is the number of theoretical plates, α the selectivity and k the retention factor, N^*, α^*, k^* are the corresponding values in gradient elution. As can be seen, there are three parameters affecting the chromatographic resolution with different impact as shown in Figure 1.18.

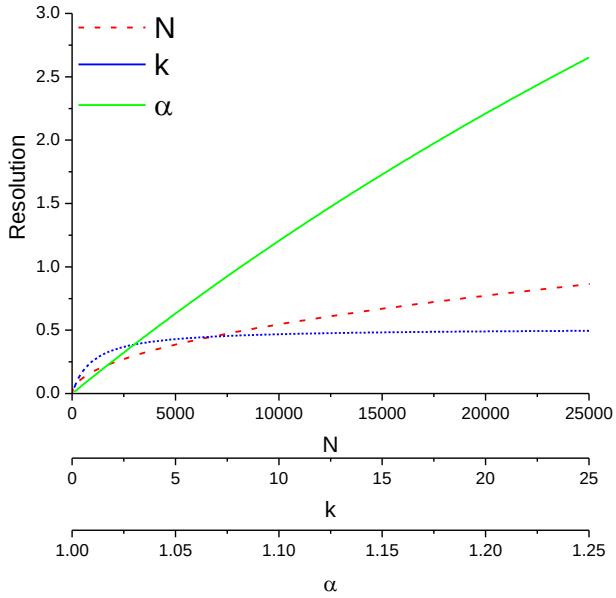

Figure 1.18: Illustration of the resulting chromatographic resolution depending on column efficiency (*N*), analyte retention (*k*) and selectivity (*α*). For the calculation an *α* of 1.03, a *k* of 3 and an *N* of 5,000 was used.

The lowest impact on resolution can be achieved by increased retention. However, retention is necessary otherwise no resolution is obtained. Although the efficiency of the chromatography shows a medium influence on resolution, chromatographic separations are often achieved by increased efficiency when using for example longer columns or smaller particle diameter as shown in Chapter 7. However, large changes in efficiency have only a limited influence on resolution, whereas the selectivity (*α*) is of utmost importance to be able to resolve compounds during chromatography. Small changes of α lead to a significant increase in resolution which is especially important when isobaric compounds are included that need to be resolved by chromatography.

1.2 Scope of the thesis

The aim of this work was the characterization of micro-LC systems from theoretical and practical points of view. Moreover, method development and implementation of a robust and reliable method for the analysis of antineoplastic drugs from wipe samples is performed to replace conventional LC-MS and to demonstrate the potential of this separation dimension. Antineoplastic drugs are applied during cancer therapy and are differentiated by their mechanism of action [68]. In general, this class of compounds is of high interest due to the possibility of occupational exposure for healthcare workers [69]. The selected range of analytes comprises the most frequently used pharmaceuticals and include polar as well as non-polar compounds. In addition, isobaric compounds are included that cannot be differentiated by MS. Therefore, a chromatographic separation is mandatory and challenging. Figure 1.19 illustrates

the different parts of the investigation to characterize the micro-LC dimension to establish a method on the basis of micro-LC-MS/MS.

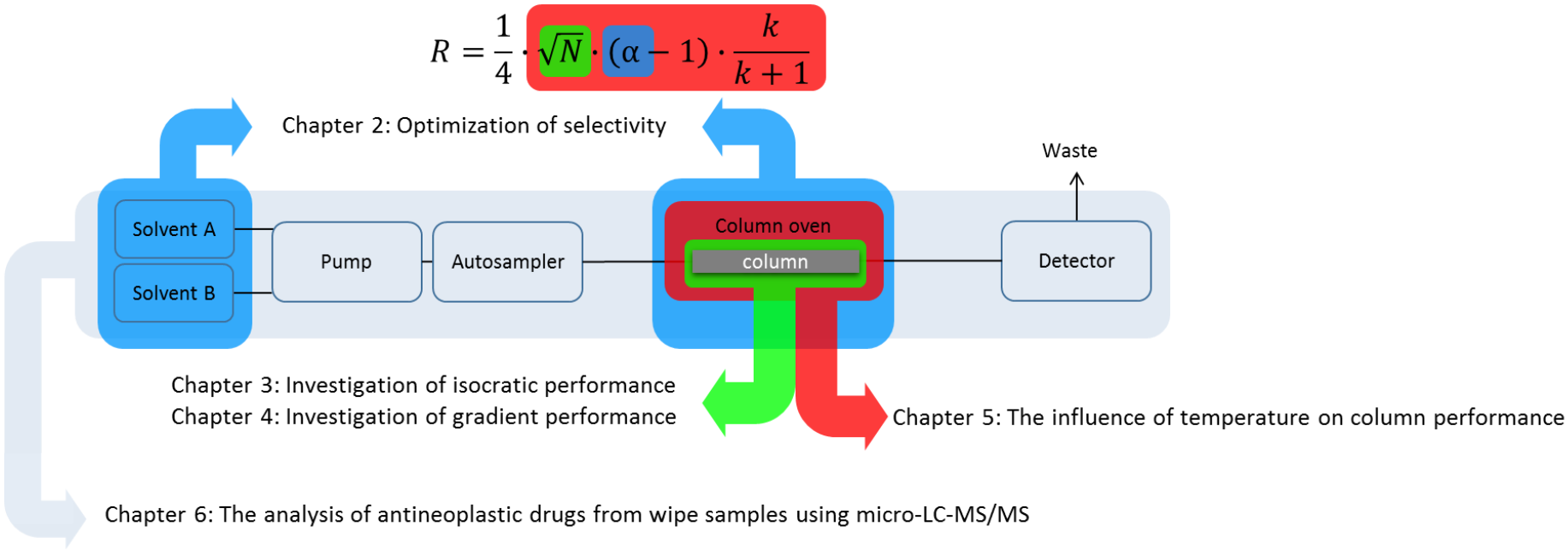

Figure 1.19: Graphical overview of the thesis scope.

During this work the influence of selectivity is characterized by a column screening and subsequent data analysis by principal component analysis (*PCA*, see Chapter 2) whereas the efficiency is evaluated by van Deemter and kinetic plot theory (see Chapter 3 - Chapter 5) to demonstrate the benefit of such theoretical approaches for the real analytical world. All aspects and conclusions of these theoretical investigations are being used for the development of the final method (see Chapter 6) before analytical performance parameters are determined to evaluate the robustness of micro-LC-MS/MS for routine application.

1.3 References

[1] Global Footprint Network, http://www.footprintnetwork.org/, 2003, (accessed 03.02.2017)
[2] L.S. Ettre, Chromatography: The separation technique of the 20th century, Chromatographia, 51 (2000) 7.
[3] L.S. Ettre, K.I. Sakodynskii, Tswett, M.S. and the discovery of chromatography - 2. Completion of the development of chromatography (1903-1910), Chromatographia, 35 (1993) 329-338.
[4] L.S. Ettre, K.I. Sakodynskii, M. S. Tswett and the discovery of chromatography I: Early work (1899–1903), Chromatographia, 35 (1993) 223-231.
[5] A.J.P. Martin, R.L.M. Synge, A new form of chromatogram employing two liquid phases, A theory of chromatography. 2. Application to the micro-determination of the higher monoamino-acids in proteins, 35 (1941) 1358-1368.
[6] A.J.P. Martin, The development of partition chromatography, Nobel Lecture, (1952).
[7] L.S. Ettre, Jim Waters: The Development of GPC and the First HPLC Instruments, LCGC North America, 23 (2005) 752-761.
[8] S. Fekete, K. Ganzler, J. Fekete, Efficiency of the new sub-2 μm core–shell (Kinetex™) column in practice, applied for small and large molecule separation, J. Pharm. Biomed. Anal., 54 (2011) 482-490.
[9] R.W. Brice, X. Zhang, L.A. Colon, Fused-core, sub-2 μm packings, and monolithic HPLC columns: a comparative evaluation, J. Sep. Sci., 32 (2009) 2723-2731.
[10] J. De Vos, M. De Pra, G. Desmet, R. Swart, T. Edge, F. Steiner, S. Eeltink, High-speed isocratic and gradient liquid-chromatography separations at 1500 bar, J. Chromatogr. A, 1409 (2015) 138-145.
[11] V. Gonzalez-Ruiz, A.I. Olives, M.A. Martin, Core-shell particles lead the way to renewing high-performance liquid chromatography, Trac-Trends in Analytical Chemistry, 64 (2015) 17-28.
[12] M.E. Swartz, UPLC™: An Introduction and Review, Journal of Liquid Chromatography & Related Technologies, 28 (2005) 1253-1263.
[13] J.M. Cunliffe, S.B. Adams-Hall, T.D. Maloney, Evaluation and comparison of very high pressure liquid chromatography systems for the separation and validation of pharmaceutical compounds, J. Sep. Sci., 30 (2007) 1214-1223.
[14] D.T.T. Nguyen, D. Guillarme, S. Rudaz, J.-L. Veuthey, Fast analysis in liquid chromatography using small particle size and high pressure, J. Sep. Sci., 29 (2006) 1836-1848.
[15] S. Fekete, I. Kohler, S. Rudaz, D. Guillarme, Importance of instrumentation for fast liquid chromatography in pharmaceutical analysis, J. Pharm. Biomed. Anal., 87 (2014) 105-119.
[16] S. Fekete, J. Schappler, J.L. Veuthey, D. Guillarme, Current and future trends in UHPLC, Trac-Trends in Analytical Chemistry, 63 (2014) 2-13.

[17] D. Guillarme, J. Ruta, S. Rudaz, J.L. Veuthey, New trends in fast and high-resolution liquid chromatography: a critical comparison of existing approaches, Analytical and Bioanalytical Chemistry, 397 (2010) 1069-1082.
[18] G. Desmet, S. Eeltink, Fundamentals for LC Miniaturization, Anal. Chem., 85 (2013) 543-556.
[19] J.H. Knox, Theoretical Aspects of LC with Packed and Open Small-Bore Columns J Chromatogr Sci, 19 (1980) 453-461.
[20] C.E. Reese, R.P.W. Scott, Microbore columns – design, construction, and operation, J Chromatogr Sci 18 (1980) 479-486.
[21] J.P.C. Vissers, H.A. Claessens, C.A. Cramers, Microcolumn liquid chromatography: instrumentation, detection and applications, J. Chromatogr. A, 779 (1997) 1-28.
[22] T. Tsuda, M. Novotny, Packed microcapillary columns in high performance liquid chromatography, Anal. Chem., 50 (1978) 271-275.
[23] P. Kucera, Design and use of short microbore columns in liquid-chromatography, Journal of Chromatography, 198 (1980) 93-109.
[24] R.P.W. Scott, Microbore columns in liquid-chromatography, J. Chromatogr. Sci., 18 (1980) 49-54.
[25] R.P.W. Scott, P. Kucera, Use of microbore columns for the separation of substances of biological origin, Journal of Chromatography, 185 (1979) 27-41.
[26] R.P.W. Scott, P. Kucera, Mode of operation and performance-characteristics of microbore columns for use in liquid-chromatography, Journal of Chromatography, 169 (1979) 51-72.
[27] R.P.W. Scott, P. Kucera, M. Munroe, Use of microbore columns for rapid liquid-chromatographic separations, Journal of Chromatography, 186 (1979) 475-487.
[28] R.T. Kennedy, J.W. Jorgenson, Preparation and evaluation of packed capillary liquid chromatography columns with inner diameters from 20 to 50 micrometers, Anal. Chem., 61 (1989) 1128-1135.
[29] J.E. MacNair, K.D. Patel, J.W. Jorgenson, Ultrahigh pressure reversed-phase capillary liquid chromatography: Isocratic and gradient elution using columns packed with 1.0-mu m particles, Anal. Chem., 71 (1999) 700-708.
[30] K.D. Patel, A.D. Jerkovich, J.C. Link, J.W. Jorgenson, In-depth characterization of slurry packed capillary columns with 1.0-mu m nonporous particles using reversed-phase isocratic ultrahigh-pressure liquid chromatography, Anal. Chem., 76 (2004) 5777-5786.
[31] J.J. Kirkland, W.W. Yau, H.J. Stoklosa, C.H. Dilks, Sampling and extra-column effects in high-performance liquid chromatography - influence of the peak skew on plate count calculations, J. Chromatogr. Sci., 15 (1977) 303-316.
[32] J. De Vos, K. Broeckhoven, S. Eeltink, Advances in ultrahigh-pressure liquid chromatography technology and system design, Anal. Chem., 88 (2016) 262-278.
[33] S. Buckenmaier, C.A. Miller, T. van de Goor, M.M. Dittmann, Instrument contributions to resolution and sensitivity in ultra high performance liquid chromatography using small bore columns: Comparison of diode array and triple quadrupole mass spectrometry detection, J. Chromatogr. A, 1377 (2015) 64-74.
[34] S. Fekete, J. Fekete, The impact of extra-column band broadening on the chromatographic efficiency of 5 cm long narrow-bore very efficient columns, J. Chromatogr. A, 1218 (2011) 5286-5291.
[35] F. Gritti, G. Guiochon, Kinetic performance of narrow-bore columns on a micro-system for high performance liquid chromatography, J. Chromatogr. A, 1236 (2012) 105-114.
[36] J.H. Knox, I.H. Grant, Miniaturisation in pressure and electroendosmotically driven liquid chromatography: Some theoretical considerations, Chromatographia, 24 (1987) 135-143.

[37] DECHEMA - Gesellschaft für Chemische Technik und Biotechnologie e. V. - Entwicklung eines Chips zur Kopplung der nano-Flüssigkeitschromatografie mit der Massenspektrometrie unter besonderer Berücksichtigung von Druck- und Temperatureffekten (LC-Chip), http://dechema.de/392+ZBG.html, 2013, (accessed 02.02.2017)
[38] ASM International, Casting Design and Performance, ASM International, 2009, pp 74.
[39] M. Hilhorst, C. Briscoe, N. van de Merbel, Sense and nonsense of miniaturized LC-MS/MS for bioanalysis, Bioanalysis, 6 (2014) 3263-3265.
[40] H. Shaaban, New insights into liquid chromatography for more eco-friendly analysis of pharmaceuticals, Analytical and Bioanalytical Chemistry, (2016) 1-16.
[41] D.W. Arnold, S.R. Needham, Micro-LC-MS/MS: the future of bioanalysis, Bioanalysis, 5 (2013) 1329-1331.
[42] Y.F. Shen, R. Zhao, S.J. Berger, G.A. Anderson, N. Rodriguez, R.D. Smith, High-efficiency nanoscale liquid chromatography coupled on-line with mass spectrometry using nanoelectrospray ionization for proteomics, Anal. Chem., 74 (2002) 4235-4249.
[43] F. Busetti, W.J. Backe, N. Bendixen, U. Maier, B. Place, W. Giger, J.A. Field, Trace analysis of environmental matrices by large-volume injection and liquid chromatography–mass spectrometry, Analytical and Bioanalytical Chemistry, 402 (2012) 175-186.
[44] U.D. Neue, HPLC Columns - Theory, Technology, and Practice, Wiley-VCH, 1997, pp 52.
[45] W. De Malsche, S. De Bruyne, J.O. De Beek, P. Sandra, H. Gardeniers, G. Desmet, F. Lynen, Capillary liquid chromatography separations using non-porous pillar array columns, J. Chromatogr. A, 1230 (2012) 41-47.
[46] Waters Corporation - Nano and Micro LC Columns, http://www.waters.com/waters/de_DE/nano-and-micro-LC-columns/nav.htm?cid=134808909&locale=de_DE, (accessed 02.02.2017)
[47] YMC Europe GmbH - YMC-Triart, http://ymc.de/ymc-triart.html, (accessed 02.02.2017)
[48] Merck KGaA - Chromolith® CapRod® HPLC Columns, http://www.merckmillipore.com/DE/de/products/analytics-sample-prep/chromatography-for-analysis/analytical-hplc/chromolith-hplc-columns/chromolith-caprod-capillary-columns/6DKb.qB.QfYAAAE_0Px3.Lxi,nav?ReferrerURL=https%3A%2F%2Fwww.google.de%2F, (accessed 02.02.2017)
[49] J.J. van Deemter, F.J. Zuiderweg, A. Klinkenberg, Longitudinal diffusion and resistance to mass transfer as causes of nonideality in chromatography, Chemical Engineering Science, 5 (1956) 271-289.
[50] J.J. van Deemter, F.J. Zuiderweg, A. Klinkenberg, Longitudinal diffusion and resistance to mass transfer as causes of nonideality in chromatography, Chemical Engineering Science, 50 (1995) 3869-3882.
[51] D. Cabooter, J. Billen, H. Terryn, F. Lynen, P. Sandra, G. Desmet, Detailed characterisation of the flow resistance of commercial sub-2 μm reversed-phase columns, J. Chromatogr. A, 1178 (2008) 108-117.
[52] D. Cabooter, S. Heinisch, J.L. Rocca, D. Clicq, G. Desmet, Use of the kinetic plot method to analyze commercial high-temperature liquid chromatography systems: I: Intrinsic performance comparison, J. Chromatogr. A, 1143 (2007) 121-133.
[53] J.C. Giddings, Reduced plate height equation - a common link between chromatographic methods, Journal of Chromatography, 13 (1964) 301-304.
[54] J.C. Giddings, Unified Separation Science, Wiley, 1991, pp 269-278.
[55] P.A. Bristow, J.H. Knox, Standardization of test conditions for high performance liquid chromatography columns, Chromatographia, 10 (1977) 279-289.

[56] G. Desmet, D. Clicq, P. Gzil, Geometry-independent plate height representation methods for the direct comparison of the kinetic performance of LC supports with a different size or morphology, Anal Chem, 77 (2005) 4058-4070.
[57] S. Fekete, K. Ganzler, J. Fekete, Facts and myths about columns packed with sub-3 μm and sub-2 μm particles, J. Pharm. Biomed. Anal., 51 (2010) 56-64.
[58] Y. Vanderheyden, D. Cabooter, G. Desmet, K. Broeckhoven, Isocratic and gradient impedance plot analysis and comparison of some recently introduced large size core-shell and fully porous particles, J. Chromatogr. A, 1312 (2013) 80-86.
[59] J.C. Giddings, Comparison of Theoretical Limit of Separating Speed in Gas and Liquid Chromatography, Anal. Chem., 37 (1965) 60-63.
[60] H. Poppe, Some reflections on speed and efficiency of modern chromatographic methods, J. Chromatogr. A, 778 (1997) 3-21.
[61] G. Desmet, D. Cabooter, K. Broeckhoven, Graphical data representation methods to assess the quality of LC columns, Anal. Chem., 87 (2015) 8593-8602.
[62] K. Broeckhoven, D. Cabooter, S. Eeltink, G. Desmet, Kinetic plot based comparison of the efficiency and peak capacity of high-performance liquid chromatography columns: Theoretical background and selected examples, J. Chromatogr. A, 1228 (2012) 20-30.
[63] K. Broeckhoven, D. Cabooter, F. Lynen, P. Sandra, G. Desmet, The kinetic plot method applied to gradient chromatography: Theoretical framework and experimental validation, J. Chromatogr. A, 1217 (2010) 2787-2795.
[64] S.R. Needham, G.A. Valaskovic, Microspray and microflow LC-MS/MS: the perfect fit for bioanalysis, Bioanalysis, 7 (2015) 1061-1064.
[65] J. P. Murphy, J. Johnson, P. D. Rainville - Enhancing mass spectrometry sensitivity by reducing chromatographic flow rates with IonKey/MS, http://www.waters.com/webassets/cms/library/docs/720004967en.pdf, 2014, (accessed 03.02.2017)
[66] J.H. Purnell, Comparison of efficiency and separating power of packed and capillary gas chromatographic columns, Nature, 184 (1959) 2009-2009.
[67] J.H. Purnell, The correlation of separating power and efficiency of gas-chromatographic columns, Journal of the Chemical Society, (1960) 1268-1274.
[68] S. Nussbaumer, P. Bonnabry, J.-L. Veuthey, S. Fleury-Souverain, Analysis of anticancer drugs: A review, Talanta, 85 (2011) 2265-2289.
[69] T.H. Connor, M.D. Zock, A.H. Snow, Surface wipe sampling for antineoplastic (chemotherapy) and other hazardous drug residue in healthcare settings: Methodology and recommendations, Journal of Occupational and Environmental Hygiene, 13 (2016) 658-667.

Chapter 2 Selectivity screening and subsequent data evaluation strategies in liquid chromatography: the example of twelve antineoplastic drugs

Redrafted from "Hetzel, T., Teutenberg, T., Schmidt, T.C., Selectivity screening and subsequent data evaluation strategies in liquid chromatography: the example of 12 antineoplastic drugs, Analytical and Bioanalytical Chemistry, 407 (2015) 8475–8485."

Abstract

Optimization of the chromatographic selectivity is the most important parameter if a separation is needed for the hyphenation of liquid chromatography with mass spectrometry. In mass spectrometry this is necessary if the investigated analytes have identical mass transitions, like isomers or epimers. For the separation of the twelve most important antineoplastic drugs, a selectivity screening was performed using 20 columns, two organic modifiers and temperatures to find a suitable phase system in order to separate critical peak pairs. Therefore, an evaluation strategy was applied in form of a principal component analysis (*PCA*), selectivity factor and overall selectivity comparison to find a suitable phase system. Some boundary conditions were defined to consider the specific requirements of tandem mass spectrometry. The results clearly indicated that the selectivity factor of the critical peak pairs is increased using methanol at higher temperature.

2.1 Introduction

With the introduction of powerful mass spectrometers (*MS*), multi-component analysis comes into focus to save time and resources by including many target analytes into one method. For target analysis, triple quadrupole mass spectrometers are used for quantification using the multiple reaction monitoring (*MRM*) mode. Usually, two mass transitions are selected to identify and quantify the target compounds. The fast cycle times enable recording a high number of mass transitions in a short time. Therefore, a chromatographic separation of all analytes is often not deemed necessary if the analytes can be distinguished by their specific mass transitions. However, sometimes even the mass spectrometer reaches a limit. This especially occurs if the target components have identical mass transitions like isomers or epimers. At this point, the optimization of the chromatographic phase system, which is defined in this manuscript as combination of stationary phase, mobile phase and temperature, is mandatory to achieve a separation for an unequivocal identification and quantification. Besides that, the quality of mass spectrometric detection will increase when target compounds are well separated.

However, the systematic evaluation of a suitable phase system can be time consuming and complex, if the procedure is governed by trial and error. In the pharmaceutical industry, method development is a crucial step. Once a method has been validated, a change in the separation conditions that leads to a revalidation is associated with high costs. Although there exist many approaches based on systematic method development, the explanation why a specific phase system has been chosen is usually not based on a statistical data evaluation.

In the literature, many column tests are described to characterize the different retention mechanisms of the stationary phase to represent selectivity differences [1-5]. Usually, model components are used to determine specific parameters like hydrophobicity or silanol activity. Unfortunately, such tests only reveal which column chemistries provide the highest selectivity differences on the basis of the selected model compounds. For a specific separation problem, these tests can only hint at a possibly suitable column. Many different impact factors for selectivity changes are described. It is known that the type of the organic co-solvent as well as the column surface modification have a significant influence on separation selectivity [6-9]. Most studies revealed that methanol has a positive effect on separation selectivity due to its protic nature and lower elution strength [10]. Other influence factors are the column temperature [9, 11, 12] and mobile phase pH [7, 8].

Several automated method scouting systems are available which offer the possibility to optimize the chromatographic resolution but not the selectivity of the phase system. Therefore, this study is focused on the question whether statistical methods like e. g. principal component analysis (*PCA*) can be used to unambiguously identify the best phase system which corresponds to the highest selectivity for a specific separation problem. This is demonstrated for a separation of the twelve most important cytotoxic drugs as part of a study of the European Society of Oncology Pharmacy (*ESOP*) [13]. These substances are applied during cancer therapy and are divided into several groups depending on their mode of action. The analyte spectrum includes polar and non-polar substances as well as acidic and basic compounds. Furthermore, three critical peak pairs can be identified that have to be resolved chromatographically. Additionally, for the polar compounds a retention factor higher than two is desirable to reduce ion suppression and matrix effects [14-16]. The selectivity screening was performed using 20 columns, two organic modifiers and two temperatures.

2.2 Material and methods

All measurements were performed on an Agilent 1200 system (Agilent Technologies, Waldbronn, Germany). In front of the pump a vacuum degasser is used. The binary pump offers the possibility to select four different mobile phases up to 600 bar with a gradient delay volume of 400 µL. The sample injection is done by a flow through autosampler with a loop volume of 100 µL. Furthermore, a column oven with an integrated switching valve is used for temperature control of the stationary phase to ensure reproducible chromatographic conditions. For data acquisition, a diode array detector (*DAD*) is employed with a cell volume of 1.7 µL. The tubing in front of the column is made of stainless steel (*SS*) with an inner diameter (*ID*) of 125 µm. In the low pressure range, polyetheretherketone (*PEEK*) capillaries are used with the same inner diameter for the connection of the column to the *DAD*. For data acquisition and analysis the Chemstation for LC 3D Systems (Rev. B. 04.02 (96)) was used. Further data processing was done using Origin Lab v. 9.1 and Microsoft Excel 2010.

Table 2.1 presents an overview of the investigated columns. Because of varying column dimensions, the flow rate as well as the injection volume had to be adapted [17]. In this way the results are directly comparable. The flow rate was adjusted to 350 µL min^{-1} and the injection volume was set to 2 µL for 2.1 mm ID columns. Due to the generic approach, a linear gradient was used with a gradient slope of 9.8% B min^{-1}. Further adjustments of the gradient slope were not necessary because all investigated columns have identical column length. The column oven

temperature is varied between 30 and 50 °C. A lower temperature limit of 30 °C was chosen in order to avoid high back pressure for mobile phases containing methanol. An upper temperature limit of 50 °C was defined because of limited temperature stability of some of the selected columns. For data acquisition the UV-spectra between 190 - 800 nm are recorded.

Table 2.1: List of the investigated columns.

description	surface modification	particle	end capping	particle size / µm	pore diameter / Å
Agilent Zorbax SB	C18	fully porous	sterically protected	1.8	80
ChromaNik Sunshell RP-Aqua	C28	core-shell	multistage	2.6	160
Macherey Nagel Nucleoshell RP 18plus	C18	core-shell	multistage	2.7	90
Merck Chromolith FastGradient RP 18e	C18	monolithic	fully endcapped	macro pores 1.5	meso pores 130
Phenomenex Kinetex	C18	core-shell	trimethyl silane	2.6	100
Phenomenex Synergi RP polar	ether-linked phenyl phase	fully porous	polar endcapped	2.5	100
Restek Raptor ARC 18	C18	core-shell	sterically protected	2.7	90
Restek Raptor	Biphenyl		fully endcapped		
Supelco Ascentis Express	C18 C8 CN ES C18 EPG [a] Amide Phenyl-Hexyl	core-shell	trimethyl silane	2.7	90
TCI Kaseisorb LC ODS-SAX Super	C18 + Anion-Exchange	fully porous	fully endcapped	3	120
Thermo HypersilGold	PFP	fully porous	fully endcapped	1.9	175
Waters Acquity BEH	C18			1.7	130
Waters HSS T3	C18	fully porous	fully endcapped	1.8	100
Waters XBridge	C18			2.5	130
YMC Triart	C18	fully porous	multistage	1.9	120

[a] EPG = embedded polar group

Water, acetonitrile and methanol were used as mobile phase constituents. All solvents were purchased from Th. Geyer-Chemsolute (Renningen, Germany) with purity for LC-MS. Formic

acid (*FA*), purchased from Sigma-Aldrich (Seelze, Germany) was used as solvent additive to adjust the pH of the mobile phase. A content of 0.1% FA was added to the mobile phases and analyte mixture, because it is more favorable for MS analysis of the selected antineoplastic drugs [18-21].

Table-S 2.1 shows a list of the selected substances including the provider of the drugs as well as important physico-chemical properties, while the structural formulas are compiled in Figure 2.1. Stock solutions were prepared using dimethyl sulfoxide (*DMSO*) from Sigma Aldrich. This solvent was used to ensure high solubility of all substances in a sufficient concentration. For HPLC analysis the multicomponent standard was diluted with acidified water (0.1% FA) in the ratio of 1 to 10. The final concentration of all analytes was 0.1 mg mL^{-1} with a composition of 90/10 (v/v) H_2O/DMSO + 0.1% FA.

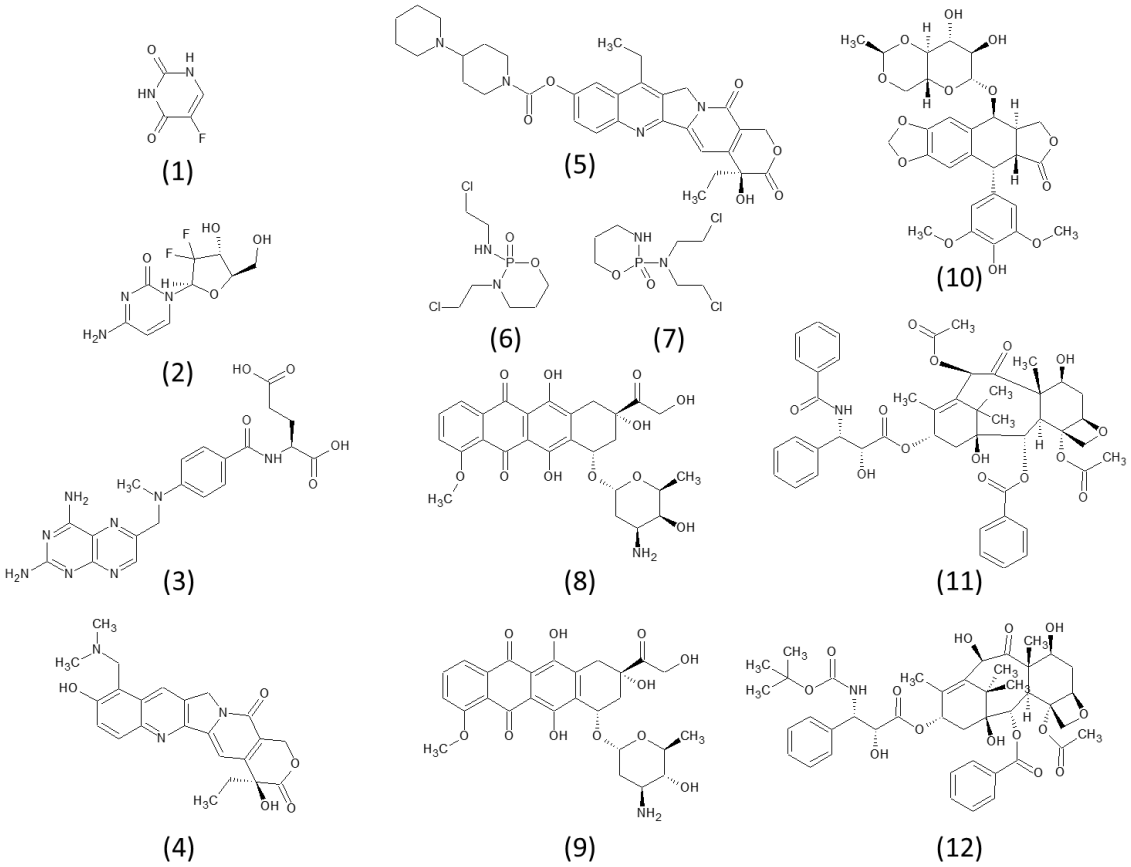

Figure 2.1: Structures of the investigated compounds: (1) 5-fluorouracil, (2) gemcitabine, (3) methotrexate, (4) topotecan, (5) irinotecan, (6) ifosfamide, (7) cyclophosphamide, (8) doxorubicin, (9) epirubicin, (10) etoposide, (11) paclitaxel, (12) docetaxel [22]. Note: Only the neutral species are shown which are not necessarily present at the applied pH.

2.3 Results and discussion

In order to compare different phase systems, Neue et al. choose a very illustrative way to express column differences [7, 23]. They plotted the retention factors of each investigated substance on two columns under certain analysis conditions against each other to compare the selectivity of different stationary phases. Afterwards, the correlation and the resulting variance were taken to quantify differences in selectivity. This kind of representation was also applied in this study to express the overall selectivity differences for the whole range of analytes depending on the applied separation conditions. To evaluate the selectivity change of the different columns in terms of the three critical pairs (ifosfamide/cyclophosphamide, doxorubicin/epirubicin, docetaxel/paclitaxel) the selectivity factor (α) can be calculated to express selectivity differences independent of the particle diameter of the stationary phase.

The above-mentioned kind of representation was done for every column-, organic modifier- and temperature-combination for all investigated substances. For calculation of the retention factor (k, Equation-S 2.1) the injection signal, which is represented by the first distortion of the UV baseline, was used as column void time. Figure 2.2 shows an exemplary plot of the retention factors obtained on the Restek Raptor ARC-18 and YMC Triart C18 column. Because of the same surface modification a similar overall selectivity can be expected.

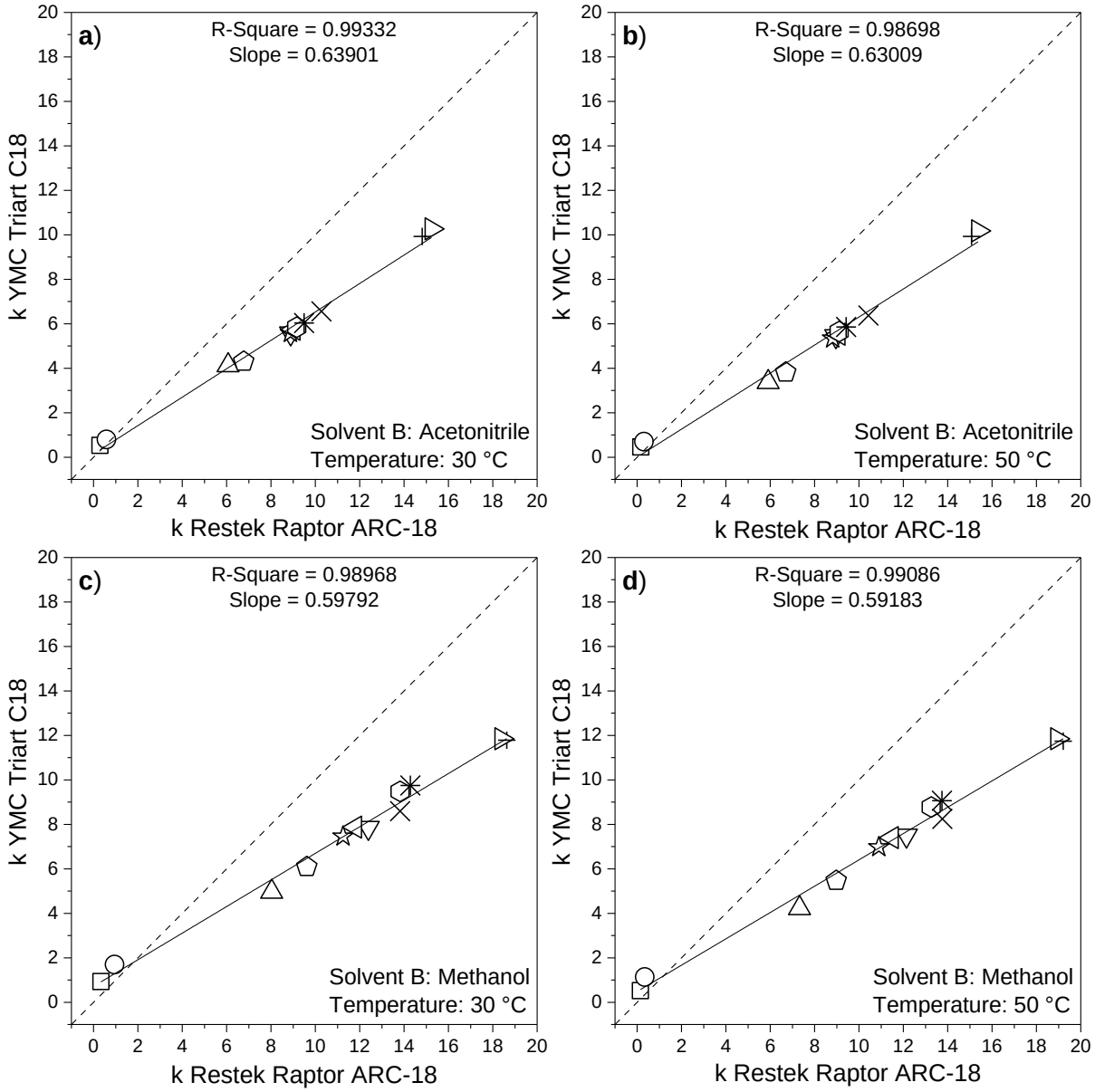

Figure 2.2: Overall selectivity comparison of the columns Restek Raptor ARC-18 and YMC Triart C18 under the following conditions. a) Mobile phase: H_2O - ACN, column temperature: 30 °C; b) mobile phase: H_2O - ACN, column temperature: 50 °C; c) mobile phase: H_2O - MeOH, column temperature: 30 °C; mobile phase: H_2O - MeOH, column temperature: 50 °C. Target compounds: (□) 5-fluorouracil, (○) gemcitabine, (△) methotrexat, (⬟) topotecan, (▽) irinotecan, (★) ifosfamide, (◁) cyclophosphamide, (⬢) doxorubicin, (✳) epirubicin, (×) etoposide, (+) paclitaxel, (▷) docetaxel. The dashed line represents the bisecting line.

As can be seen, the retention is always higher for the Restek Raptor ARC-18 than for the YMC Triart C18 except for the polar compounds 5-fluorouracil and gemcitabine (Figure 2.2 a-d). In addition, methanol provides higher retention than acetonitrile due to its lower elution strength. Moreover, a better band spacing of all target compounds is obtained for methanol instead of acetonitrile. To prove this assumption, the separation of the coeluting compounds (irinotecan(▽), ifosfamide(★), cyclophosphamide(◁), doxorubicin(⬢), epirubicin(✳),

etoposide(×)) for every phase system can be compared. To that end, the ratio of the difference of the retention factor between the first and last eluting compound of this cluster $\Delta(k_{last}-k_{first})$ to the actually available chromatographic space Δk_{total} was calculated as shown in Table 2.2.

Table 2.2: Comparison of the utilization of the chromatographic space using acetonitrile and methanol at 30 °C and 50 °C.

column	Restek Raptor ARC-18				YMC Triart C18				Restek Raptor Biphenyl			
separation condition	ACN		MeOH		ACN		MeOH		ACN		MeOH	
	30 °C	50 °C	30 °C	50 °C	30 °C	50 °C	30 °C	50 °C	30 °C	50 °C	30 °C	50 °C
$\Delta(k_{last}-k_{first})$	1.40	1.61	3.03	2.87	0.98	1.03	2.30	2.09	1.67	1.91	2.86	3.04
Δk_{total}	14.94	15.21	18.30	19.06	9.74	9.72	10.92	11.33	13.00	13.54	17.93	18.38
$\Delta(k_{last}-k_{first})/\Delta k_{total}$ / %	9.34	10.59	16.56	15.06	10.09	10.60	21.03	18.44	12.82	14.14	15.93	16.56

The results clearly show that the use of methanol leads to a higher utilization of the available chromatographic space. For the YMC Triart C18, the distribution of the selected compounds is better when methanol is used compared to acetonitrile because 21% instead of 10% of the available retention space is covered at 30 °C. In general, the requirement for $k \approx 2$ for polar compounds can be obtained for gemcitabine using methanol at 30 °C. At this point it should be stressed that the higher retention of the polar compounds can be explained by the lower elution strength of a mobile phase containing methanol instead of acetonitrile. In contrast, the higher coverage of the retention space when using methanol is based on the specific interactions. This leads to a more even distribution of all analytes across the gradient window which is not correlated with the lower elution strength of methanol when compared to acetonitrile.

As depicted in Figure 2.2 d), increasing the temperature from 30 °C to 50 °C reduces the retention factor of the first eluting compounds due to the increasing elution strength of the mobile phase. This also applies to acetonitrile as co-solvent (Figure 2.2 b). For all other target compounds besides the polar analytes, the retention factors obtained on the Restek Raptor ARC-18 column show always higher values. One possible explanation for this phenomenon could be the surface coverage of the particles which is different for both stationary phases. High surface coverage could lead to a hindrance for bulky target compounds to migrate between the chains of the stationary phase and therefore to lower retention, which is known as shape selectivity [3]. Wise et. al. found that shape selectivity is influenced by the chain length, organic solvent, ligand density and temperature. In addition the separation of structurally similar compounds is favored by lower temperature and increased shape recognition [24-26]. This could explain why

the small polar analytes are retarded well on the YMC Triart C18 whereas bulky molecules show lower retention factors despite the high carbon load (20%) of the YMC Triart C18 phase. At a first glance, this result is unexpected and seems to contradict the findings by Haun et al. [27]. The authors of that study obtained very high retention factors for acenaphthene. However, the planar structure of this molecule favors a migration into the alkyl chains and therefore a high interaction with the stationary phase, whereas the compounds used in this study are sterically hindered to migrate deep into the C18 moieties.

Unfortunately, the high carbon content of 20% for the YMC Triart C18 column neither provides information about the exact amount of carbon which actually offers the possibility for interactions nor about the hydrophobicity of the stationary phase. It might be possible that a high content of the carbon is part of the particle backbone and therefore not accessible to the analytes. Because of the use of multiple endcapping procedures in the preparation of the YMC Triart phase, a large part of the carbon content could result from the endcapping reagents. As a consequence, the hydrophobicity of the stationary phase is not as high as suspected. This could also explain why the non-polar compounds are less retarded on the YMC Triart C18 phase.

Nevertheless, both columns show almost the same overall selectivity behavior confirmed by R^2 close to one (R^2 = 0.987-0.993, s^2 = 0.007-0.013). However, the resulting α-values for the three critical pairs are different as shown in Table 2.3. Comparing the three different columns, using acetonitrile as organic co-solvent, the resulting α-values for ifosfamide/cyclophosphamide and paclitaxel/docetaxel are higher independent of the column temperature for the YMC Triart C18 phase. In contrast, the use of methanol as organic modifier results in a higher selectivity for doxorubicin/epirubicin as well as for paclitaxel/docetaxel for the Restek Raptor ARC-18 phase.

Table 2.3: Resulting selectivity factor for the three critical peak pairs using acetonitrile and methanol at 30 °C and 50 °C. Critical peak pairs (1: ifosfamide/cyclophosphamide; 2: doxorubicin/epirubicin; 3: docetaxel/paclitaxel).

Column	selectivity factor α											
	Acetonitrile						Methanol					
	30 °C			50 °C			30 °C			50 °C		
	critical pair			critical pair			critical pair			critical pair		
	1	2	3	1	2	3	1	2	3	1	2	3
Restek Raptor ARC-18	1.016	1.036	1.028	1.030	1.035	1.019	1.048	1.033	1.013	1.055	1.036	1.014
Restek Raptor Biphenyl	1.011	1.028	1.054	1.014	1.025	1.049	1.010	1.025	1.030	1.014	1.019	1.031
YMC Triart C18	1.030	1.032	1.034	1.034	1.035	1.025	1.056	1.028	1.005	1.062	1.032	1.009

Figure 2.3 shows a plot of the retention factors obtained on the Restek Raptor Biphenyl and YMC Triart C18 column. Because of the different bonding, different retention and selectivity could be expected.

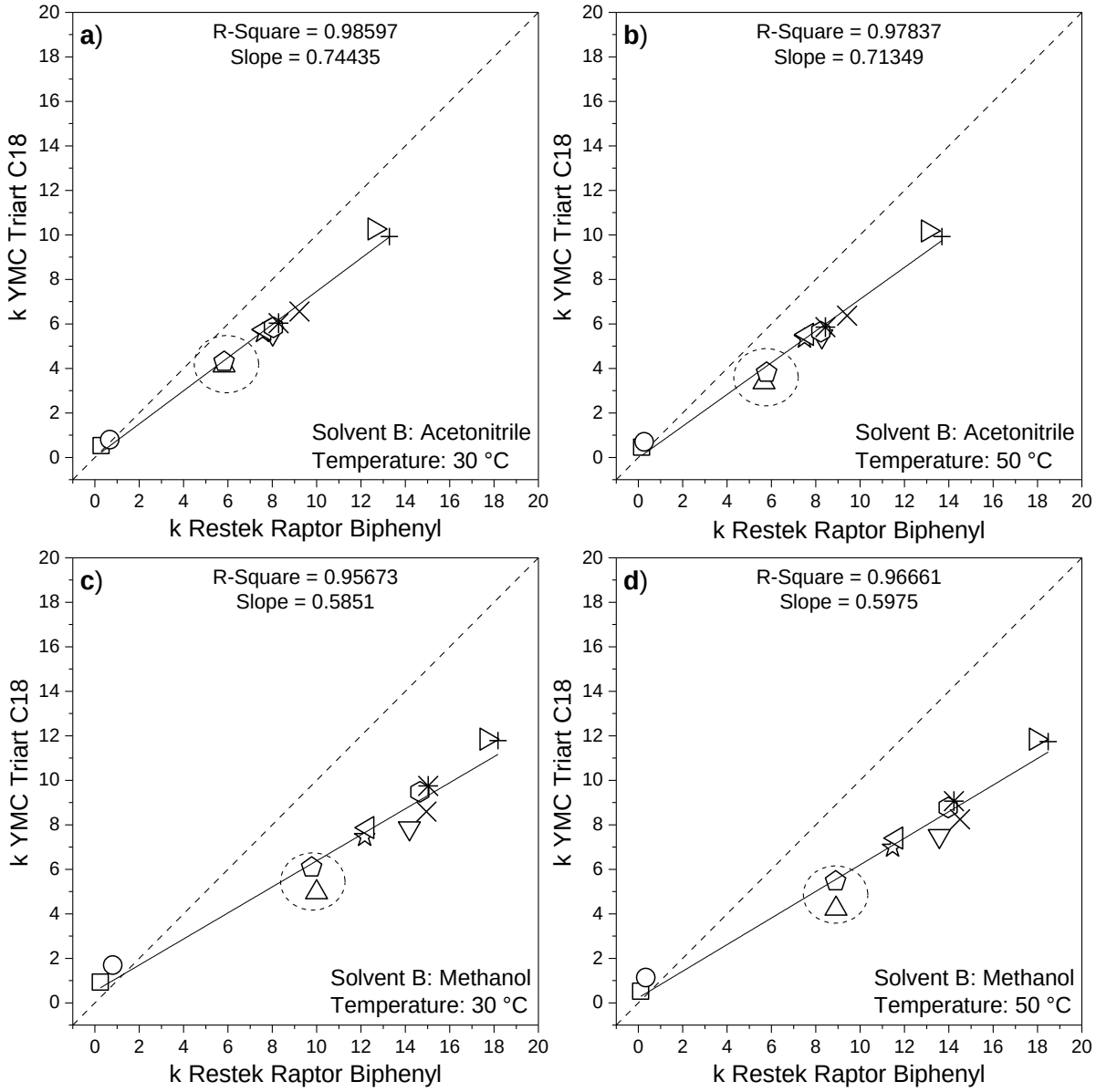

Figure 2.3: Overall selectivity comparison of the column Restek Raptor Biphenyl and YMC Triart C18 under the following conditions. a) Mobile phase: H_2O - ACN, column temperature: 30 °C; b) mobile phase: H_2O - ACN, column temperature: 50 °C; c) mobile phase: H_2O - MeOH, column temperature: 30 °C; mobile phase: H_2O - MeOH, column temperature: 50 °C. Target compounds: (□) 5-fluorouracil, (○) gemcitabine, (△) methotrexat, (⬟) topotecan, (▽) irinotecan, (★) ifosfamide, (◁) cyclophosphamide, (⬢) doxorubicin, (✳) epirubicin, (×) etoposide, (+) paclitaxel, (▷) docetaxel. The dashed line represents the bisecting line.

In principle, all previous statements regarding the retention characteristic are also valid for this example. As depicted in Figure 2.3 a) and b), the retention factors for the compounds methotrexate (△) and topotecan (⬟) show a co-elution on the Restek Raptor Biphenyl whereas

the YMC Triart C18 column is able to separate these substances at least at 50 °C. In Figure 2.3 c), the Biphenyl column shows a change in the retention order for these substances. Increasing the temperature leads to a co-elution for the Restek Raptor Biphenyl as shown in Figure 2.3 d). This co-elution presents no problem because these substances can be separated by mass spectrometry due to their specific mass transitions, but it clearly shows the influence of the organic modifier and temperature on the chromatographic selectivity. In general, considering the correlation values and resulting variances (R^2 = 0.957-0.986; s^2 = 0.014-0.043), a large difference between the two stationary phases can be observed. As for the example depicted in Figure 2.2, the distribution of the target compounds across the chromatogram is higher using methanol (Table 2.2). In addition, the Restek Raptor Biphenyl column provides a good separation for the critical pair paclitaxel and docetaxel. This can be shown by α listed in Table 2.3. In general, the α-values for the Restek Raptor Biphenyl indicate higher selectivity using acetonitrile instead of methanol for the three critical peak pairs in this case. Figure 2.2 and Figure 2.3 reveal that different selectivity does not automatically provide a better chromatographic separation. In addition, the same surface modification does not lead to the same selectivity as can be seen in Table 2.3 for the different C18 columns. More detailed background of the calculations as well as all other resulting variance values of the investigated columns can be found in the supplementary material (Chapter 2.7.1.1 - 2.7.1.2, Table-S 2.2 - Table-S 2.5). The drawback of this approach is that a graphical comparison can only be made of two columns. If a high number of columns have to be compared, an alternative strategy on the basis of multivariate data analysis should be attempted.

The calculated α enables to classify similarities and differences in selectivity performing a principal component analysis (*PCA*) over all α-values of the critical peak pairs including all separation conditions [10, 28-31]. The used data for the *PCA* as well as some background information on *PCA* can be found in supplementary material (Table-S 2.6, Chapter 2.7.1.3). Figure 2.4 shows the result of the *PCA* for the principal component 1 (*PC1*) and 2 (*PC2*).

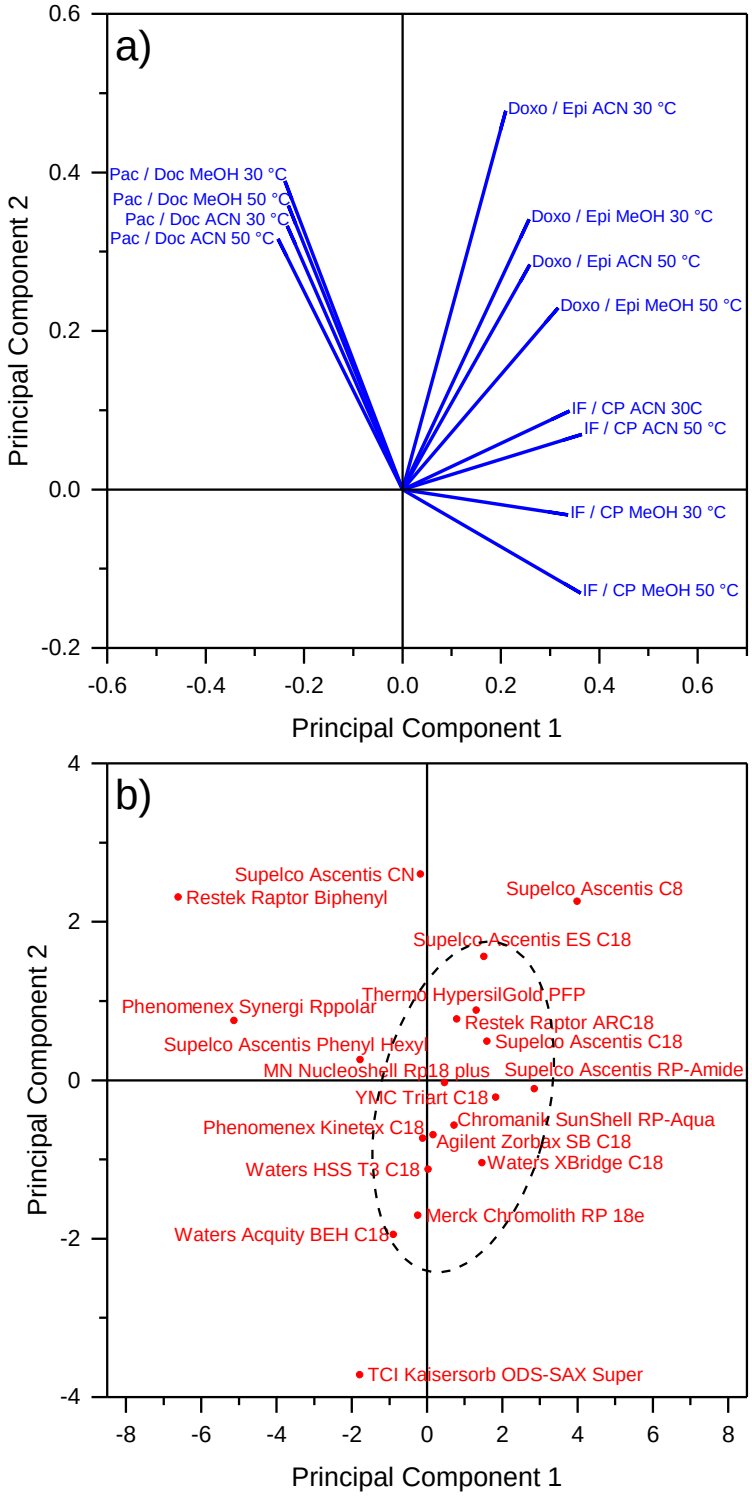

Figure 2.4: Principal component analysis over all estimated selectivity factors for all columns and operation conditions showing principal component 1 (PC1: 50.3%) and principal component 2 (PC2: 20.3%). a) loading plot; b) score plot; IF/CP: ifosfamide/cyclophosphamide, Doxo/Epi: doxorubicin/epirubicin, Pac/Doc: paclitaxel/docetaxel. Note: All investigated Supelco columns belong to the Ascentis Express series.

The presented loadings in Figure 2.4 a) show where the initial variables (combination of critical peak pair, temperature and organic co-solvent) are located with respect to the shown *PC1* and

PC2. It can be seen that the change in selectivity for paclitaxel and docetaxel is almost independent of the applied separation conditions due to the small splitting of the loadings. In contrast, for the critical peak pairs doxorubicin/epirubicin and ifosfamide/cyclophosphamide a higher influence of the separation conditions can be observed because of the larger distribution of the loadings. Therefore, changing the separation conditions can improve the selectivity for these pairs. The difference in selectivity between paclitaxel/docetaxel and doxorubicin/epirubicin can be explained by a low and high contribution of the *PC1*, respectively. In contrast, the selectivity for ifosfamide/cyclophosphamide is almost independent of the *PC1* and varies only in *PC2*.

Looking now at the *PCA* score plot (Figure 2.4 b) of the columns it can be deduced which stationary phase is suitable for the individual critical peak pair from its position within the score plot compared to the loading plot (Figure 2.4 a). For example, the selectivity for paclitaxel/docetaxel is increased for columns that provide the possibility for π-π interactions [32, 33] because their scores are located nearby the loadings for this critical peak pair. This is consistent with the results shown in Table 2.3 and Figure 2.3 for the Restek Raptor Biphenyl column. The difference between biphenyl and phenyl hexyl is a result of the greater aromatic selectivity for the biphenyl column [30]. In contrast, the selectivity for doxorubicin/epirubicin can be increased using shorter alkyl chain length of the stationary phase. For ifosfamide/cyclophosphamide, the amide surface modification as well as longer alkyl chains yield a better selectivity.

As highlighted by the dashed circle in Figure 2.4 b), most columns show almost the same selectivity. This could be expected because most of the columns have the same surface modification. Nevertheless, there are still selectivity differences although it is always C18 moieties which are bonded on the silica surface. The resulting hydrophobicity depends on the carbon load of the stationary phase, which in turn depends on the packing density, pore size, ligand length and type of endcapping. These factors have an impact on the capability of the solutes to migrate between the chains of the stationary phase. This effect is known as shape selectivity or steric resistance depending on the type of bonding technology (monomeric, polymeric) [3, 24-26]. The varying sterical orientation and hydrodynamic diameter of the analytes could lead to a changed retention behavior and therefore to different separation results. In addition, other types of endcapping can result in different retention behavior for the target compounds. Especially, basic components are affected by free silanol groups at acidic pH, due to secondary interactions [1].

Comparing the results of Figure 2.2 and Figure 2.3 with Figure 2.4, some similarities in terms of the selectivity can be observed. In Figure 2.2 and Figure 2.3, the correlations and resulting variances are a measure for the differences between the columns. Looking at the correlations, a higher similarity of the Restek Raptor ARC-18 and YMC Triart C18 could be found than for the Triart C18 and Restek Raptor Biphenyl. This statement is also confirmed by the *PCA* for the critical peak pairs. Therefore, this kind of representation (Figure 2.4) can also be applied to express selectivity differences with the additional advantage of all necessary information of all combinations in one plot, which allows for a targeted evaluation.

There is also one column which shows a totally different selectivity for the critical peak pairs. The TCI Kaseisorb LC ODS-SAX Super column is a mixed-mode stationary phase with an anion exchange group in addition to the C18 chain. This column is the only one which provides a change in the retention order of the polar compounds 5-fluorouracil and gemcitabine, but is not suitable for the separation of the three critical peak pairs. Exemplarily, for gemcitabine it can be assumed that this analyte is positively charged at the applied pH, which causes a lower retention. The use of an anion exchange is unfavorable for this compound. In contrast to other target analytes both retention mechanisms cannot be exploited. As a consequence, the retention order of the polar compounds 5-fluorouracil and gemcitabine is reversed compared to classic C18 moieties.

In order to substantiate the results of the *PCA*, the average α-values for the three critical pairs were calculated. The higher the average value, the greater the chance to achieve a separation for all critical peak pairs under the specific separation condition. Table-S 2.7 shows the calculated values for all investigated columns including all separation conditions.

In order to determine the specific differences between particular stationary phases in combination with the applied mobile phase and temperature, the results of Table-S 2.6 and Table-S 2.7 as well as Figure 2.4 contain all necessary information. It can be concluded that for example the Supelco Ascentis Express C18 column is superior for the critical peak pairs 1 and 2. In contrast, the Supelco Ascentis Express Phenyl-Hexyl phase is more suitable for the critical peak pair 3. The positioning of the column within the *PCA* score plot visualizes this result. The loading plot in Figure 2.4 a) shows that the selectivity using methanol as co-solvent leads to a decreased selectivity for paclitaxel/docetaxel on the phenyl hexyl stationary phase.

Considering Table-S 2.7, the influence of the applied separation conditions on the selectivity can be evaluated. The impact of higher temperatures using acetonitrile seems to have a limited

effect on the average selectivity for these examples. The α-values comprises improvements as well as aggravations for the individual critical pairs because of the higher elution strength. In contrast, using methanol and elevated temperatures causes higher α-values for almost every column due to its protic character, specific interactions and lower elution strength. In terms of the α-values for the critical peak pairs, this separation condition seems to have the highest benefit. In general, the use of elevated temperatures has several advantages which can be exploited if α is constant. This concerns the acceleration of the analysis and the resulting backpressure which decreases when the temperature is increased [11].

At this point it should be mentioned that the evaluation of the common average calculation of α could lead to wrong conclusions, because the impact of one high value for one α of one critical peak pair influences the average to a great extent. For this reason a weighting system on the basis of the importance to obtain a separation is applied. The separation of docetaxel and paclitaxel was deemed necessary because of ion suppression, although the mass spectrometer is able to differentiate between these substances. Therefore, α is multiplied with the factor of one. Ifosfamide and cyclophosphamide have one identical mass transition. The verification could be influenced at co-elution but the second mass transition still enables to separate these compounds using mass spectrometry. Therefore, the α-value is weighted by the factor of two. Doxorubicin and epirubicin are epimers, which differ only in the steric orientation of one hydroxyl group. An identification without a chromatographic separation is not possible because all mass transitions are equal. A chromatographic separation of this critical pair is mandatory, which is why the α-value is multiplied by three. The weighted average values are given in Table-S 2.7. The influence of the applied weighting system can be seen for the Restek Raptor Biphenyl column. Whereas the non-weighted average value implies a better α for the three critical peak pairs, the weighted approach clearly shows that the average selectivity is influenced by a higher value for the peak pair docetaxel and paclitaxel, of which chromatographic separation was defined as less important.

In order to obtain a general statement about the influence of the applied separation conditions on the selectivity of the investigated critical peak pairs, the weighted average α-values over all columns can be calculated as shown in Table-S 2.7. Methanol leads to higher values than acetonitrile no matter which temperature is applied. For both organic modifiers, α can be improved by higher temperatures. This corroborates previous findings [10].

To carry out a final evaluation which phase system provides the best results in terms of retention for the polar target compounds and the highest weighted average selectivity factor using a generic gradient, the resulting chromatograms for three different columns are shown in Figure 2.5. The chromatograms are selected on the basis of the results of the retention factors for the polar compounds, *PCA* and weighted average α-values. As shown in Table-S 2.7, using methanol at 50 °C provides the highest weighted average α. Therefore, the separation conditions were kept constant for all shown chromatograms.

Figure 2.5 a) depicts the separation for the twelve cytotoxic drugs on the Waters HSS T3 column. This phase system was selected primarily because it provides an acceptable retention for the polar compounds under the selected separation conditions. This can be seen by the retention factor for 5-fluorouracil (k_1=0.40) and gemcitabine (k_2=1.35). In addition, the resulting separation for the three critical peak pairs is sufficient.

Figure 2.5 b) represents the analysis on the Supelco Ascentis Express C8 column. The results of the *PCA* and average α indicate a suitable selectivity for all critical peak pairs. Looking at the score plot of the *PCA* in Figure 2.4 b), it can clearly be seen that the Ascentis Express C8 column is characterized by a high *PC1* and *PC2*. The comparison of the score plot (Figure 2.4 b) and the loading plot (Figure 2.4 a) reveals that these properties are useful in order to separate all critical peak pairs. This can exactly be found in the shown chromatogram. As depicted, the separation of the three critical peak pairs (5/6 ifosfamide/cyclophosphamide, 9/10 doxorubicin/epirubicin and 11/12 docetaxel/paclitaxel) is sufficient for a clear differentiation by mass spectrometry. However, the polar target compounds experience no retention due to the lower hydrophobicity of the stationary phase and elute with the column void volume.

Figure 2.5 c) shows the separation on the YMC Triart C18 column. With respect to the *PCA*, it can be seen that this column is suitable for the separation of ifosfamide and cyclophosphamide as well as for doxorubicin and epirubicin, due to the contribution of *PC1*. The applied phase system also provides an acceptable compromise between retention for the polar compounds (k_1=0.52, k_2=1.14) and weighted average α for the critical peak pairs. Unfortunately, the separation for docetaxel/paclitaxel (compound 11/12) shows a partial co-elution, which can be expected due to the positioning of the column within the *PCA*.

An additional criterion to evaluate the separation in terms of the application for routine operation is the analysis time. Higher run-times lead to a decreased sample throughput. For the shown examples, the run-time is decreased from 9.36 min to 8.04 min from Figure 2.5 a) to c).

This should also be considered for a final decision which phase system is finally selected, if a choice between two equally suitable phase systems has to be made.

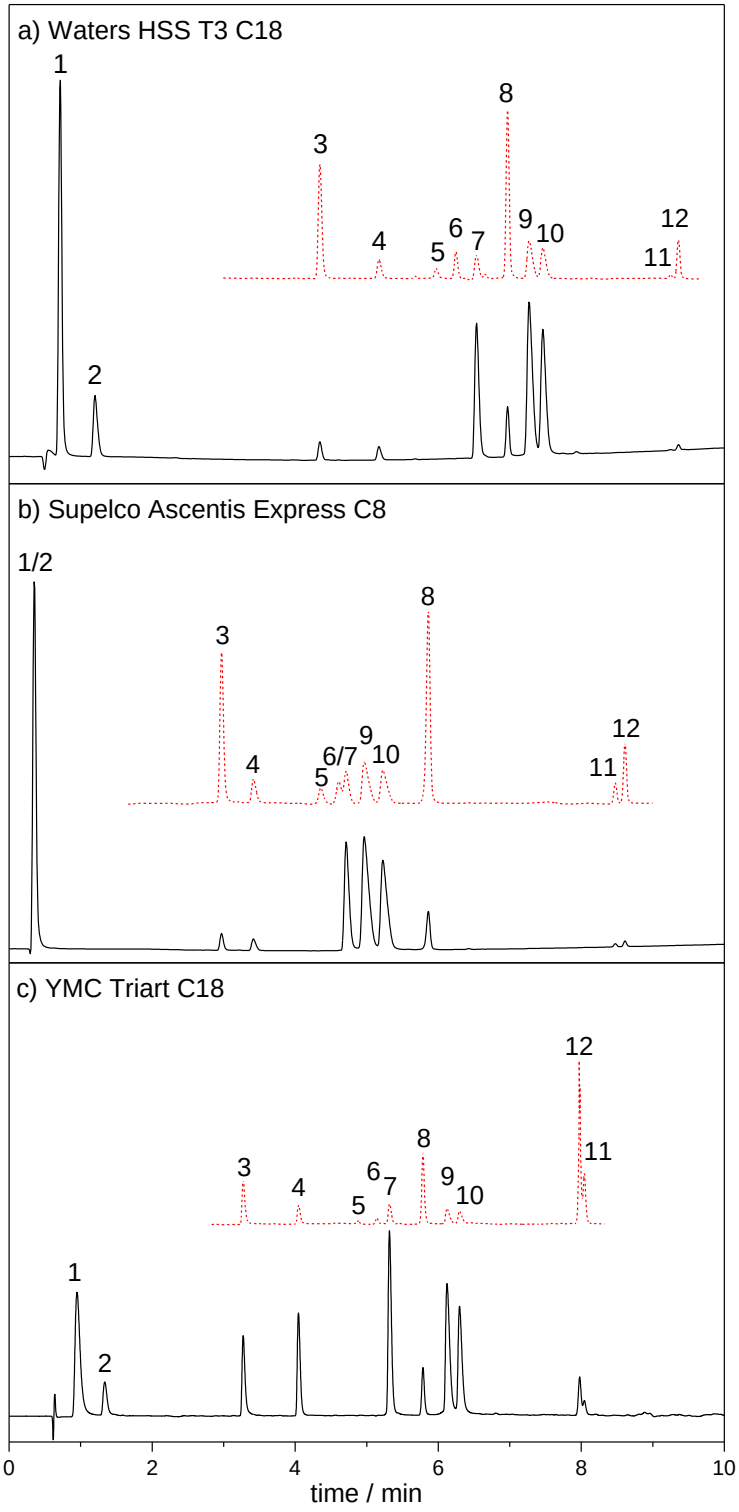

Figure 2.5: Resulting chromatograms for the analysis of the twelve cytotoxic drugs on a) Waters HSS T3 C18; b) Ascentis Express C8 and c) YMC Triart C18. Organic modifier: methanol; Temperature: 50 °C; Wavelength: (-) 254 nm; (---) 200 nm; Target compounds: (1) 5-fluorouracil, (2) gemcitabine, (3) methotrexat, (4) topotecan, (5) ifosfamide, (6) cyclophosphamide, (7) irinotecan, (8) etoposide, (9) doxorubicin, (10) epirubicin, (11) docetaxel, (12) paclitaxel.

2.4 Conclusion

The applicability of the *PCA* to express selectivity differences in order to find a suitable phase system for the separation of critical peak pairs of twelve most important antineoplastic drugs could be shown. One advantage of this kind of data analysis is the availability and visualization of information about columns with similar selectivity, which can be applied as backup column for the analysis if needed. If the developed method should be applied over years the results of the *PCA* serve as an appropriate basis for the decision why a certain phase system has been chosen. In addition, it is a good starting point for future method development to choose a different selectivity. The introduction of the weighted average α calculation can be used to further validate the results. The definition of desired requirements is the key aspect and the first thing to do before a final phase system can be selected. The shown examples clearly show that several phase systems have benefits in dependence of the defined requirements which have to be achieved. After the final selection is made, the optimization of the column efficiency by variation of the particle diameter should be investigated in order to accomplish further improvements of the chromatographic separation.

2.5 Acknowledgements

The authors would like to thank all column manufacturers for the donation of information and columns. We would like to especially thank Dr. Frank Michel and Dr. Paul Rodwell (Sigma-Aldrich) as well as Dr. Friederike Becker (YMC Europe GmbH) and Dr. Hansjörg Majer (Restek Corporation). Furthermore, the authors would like to thank Dr. Jürgen Maier-Rosenkranz (Dr. Maisch HPLC GmbH) for the critical discussion of data. In addition, the authors would like to thank for financial support from the German Federal Ministry of Economic Affairs and Energy based on a decision of the German Bundestag (KF2025428ZG2).

2.6 References

[1] H.A. Claessens, M.A. van Straten, C.A. Cramers, M. Jezierska, B. Buszewski, Comparative study of test methods for reversed-phase columns for high-performance liquid chromatography, J. Chromatogr. A, 826 (1998) 135-156.

[2] K. Kimata, K. Iwaguchi, S. Onishi, K. Jinno, R. Eksteen, K. Hosoya, M. Araki, N. Tanaka, Chromatographic characterization of silica C18 packing materials. Correlation between a preparation method and retention behavior of stationary phase, J. Chromatogr. Sci., 27 (1989) 721-728.

[3] U.D. Neue, Stationary phase characterization and method development, J. Sep. Sci., 30 (2007) 1611-1627.

[4] U.D. Neue, E. Serowik, P. Iraneta, B.A. Alden, T.H. Walter, Universal procedure for the assessment of the reproducibility and the classification of silica-based reversed-phase

packings - I. Assessment of the reproducibility of reversed-phase packings, J. Chromatogr. A, 849 (1999) 87-100.
[5] L.R. Snyder, J.W. Dolan, P.W. Carr, The hydrophobic-subtraction model of reversed-phase column selectivity, J. Chromatogr. A, 1060 (2004) 77-116.
[6] M. Gilar, A. Jaworski, T.S. McDonald, Solvent selectivity and strength in reversed-phase liquid chromatography separation of peptides, J. Chromatogr. A, 1337 (2014) 140-146.
[7] U.D. Neue, J.E. O'Gara, A. Mendez, Selectivity in reversed-phase separations - Influence of the stationary phase, J. Chromatogr. A, 1127 (2006) 161-174.
[8] L.R. Snyder, J.W. Dolan, Optimizing selectivity during reversed-phase high performance liquid chromatography method development: Prioritizing experimental conditions, J. Chromatogr. A, 1302 (2013) 45-54.
[9] P.L. Zhu, J.W. Dolan, L.R. Snyder, Combined use of temperature and solvent strength in reversed-phase gradient elution .2. Comparing selectivity for different samples and systems, J. Chromatogr. A, 756 (1996) 41-50.
[10] M.R. Euerby, M. James, B.O. Axelsson, O. Rosen, P. Petersson, Validation of the extended Tanaka column characterization protocol by multivariate analysis of chromatographic retention of low-molecular-weight analytes on reversed phase columns using methanol and acetonitrile as organic modifiers, J. Sep. Sci., 35 (2012) 2592-2598.
[11] D. Guillarme, S. Heinisch, J.L. Rocca, Effect of temperature in reversed phase liquid chromatography, J. Chromatogr. A, 1052 (2004) 39-51.
[12] J.W. Li, Effect of temperature on selectivity in reversed-phase liquid chromatography, a thermodynamic analysis, Anal Chim Acta, 369 (1998) 21-37.
[13] European Society of Oncology Pharmacy http://www.esop.li/, (accessed 25.01.2015)
[14] J.P. Antignac, K. de Wasch, F. Monteau, H. De Brabander, F. Andre, B. Le Bizec, The ion suppression phenomenon in liquid chromatography-mass spectrometry and its consequences in the field of residue, Anal Chim Acta, 529 (2005) 129-136.
[15] P.J. Larger, M. Breda, D. Fraier, H. Hughes, C.A. James, Ion-suppression effects in liquid chromatography-tandem mass spectrometry due to a formulation agent, a case study in drug discovery bioanalysis, J. Pharm. Biomed. Anal., 39 (2005) 206-216.
[16] H. Trufelli, P. Palma, G. Famiglini, A. Cappiello, An overview of matrix effects in liquid chromatography–mass spectrometry, Mass Spectrom. Rev., 30 (2011) 491-509.
[17] D. Guillarme, D.T.T. Nguyen, S. Rudaz, J.L. Veuthey, Method transfer for fast liquid chromatography in pharmaceutical analysis: Application to short columns packed with small particle. Part II: Gradient experiments, Eur. J. Pharm. Biopharm., 68 (2008) 430-440.
[18] N. Negreira, M.L. de Alda, D. Barcelo, On-line solid phase extraction-liquid chromatography-tandem mass spectrometry for the determination of 17 cytostatics and metabolites in waste, surface and ground water samples, J. Chromatogr. A, 1280 (2013) 64-74.
[19] N. Negreira, N. Mastroianni, M.L. de Alda, D. Barcelo, Multianalyte determination of 24 cytostatics and metabolites by liquid chromatography-electrospray-tandem mass spectrometry and study of their stability and optimum storage conditions in aqueous solution, Talanta, 116 (2013) 290-299.
[20] S. Nussbaumer, S. Fleury-Souverain, P. Antinori, F. Sadeghipour, D.F. Hochstrasser, P. Bonnabry, J.-L. Veuthey, L. Geiser, Simultaneous quantification of ten cytotoxic drugs by a validated LC-ESI-MS/MS method, Analytical and Bioanalytical Chemistry, 398 (2010) 3033-3042.
[21] S. Nussbaumer, L. Geiser, F. Sadeghipour, D. Hochstrasser, P. Bonnabry, J.-L. Veuthey, S. Fleury-Souverain, Wipe sampling procedure coupled to LC-MS/MS analysis for the

simultaneous determination of 10 cytotoxic drugs on different surfaces, Analytical and Bioanalytical Chemistry, 402 (2012) 2499-2509.
[22] Scifinder, https://www.scifinder.cas.org, (accessed 26.01.2015)
[23] U.D. Neue, Grumbach, E. S., Mazzeo, J. R., Tran, K., Wagrowski-, D.M. Diehl, Method development in reversed phase chromatography, Handbook of Analytical Separations, 4 (2003) 185 – 214.
[24] L.C. Sander, M. Pursch, S.A. Wise, Shape selectivity for constrained solutes in reversed-phase liquid chromatography, Anal. Chem., 71 (1999) 4821-4830.
[25] L.C. Sander, S.A. Wise, Shape Selectivity in Reversed-Phase Liquid-Chromtaography for the Separation of planar and nonplanar Solutes, J. Chromatogr. A, 656 (1993) 335-351.
[26] L.C. Sander, S.A. Wise, The influence of column temperature on selectivity in reversed-phase liquid chromatography for shape-constrained solutes, J. Sep. Sci., 24 (2001) 910-920.
[27] J. Haun, T. Teutenberg, T.C. Schmidt, Long-term high-temperature and pH stability assessment of modern commercially available stationary phases by using retention factor analysis, J. Chromatogr. A, submitted (2012).
[28] M. Euerby, P. Petersson, Chromatographic classification and comparison of commercially available reversed-phase liquid chromatographic columns using principal component analysis, J. Chromatogr. A, 994 (2003) 13-36.
[29] M.R. Euerby, P. Petersson, Chromatographic classification and comparison of commercially available reversed-phase liquid chromatographic columns containing polar embedded groups/amino endcappings using principal component analysis, J. Chromatogr. A, 1088 (2005) 1-15.
[30] M.R. Euerby, P. Petersson, W. Campbell, W. Roe, Chromatographic classification and comparison of commercially available reversed-phase liquid chromatographic columns containing phenyl moieties using principal component analysis, J. Chromatogr. A, 1154 (2007) 138-151.
[31] P. Petersson, M.R. Euerby, An evaluation of the robustness of the Tanaka characterization protocol for reversed-phase liquid chromatography columns, J Sep Sci, 28 (2005) 2120-2129.
[32] K. Croes, A. Steffens, D.H. Marchand, L.R. Snyder, Relevance of pi-pi and dipole-dipole interactions for retention on cyano and phenyl columns in reversed-phase liquid chromatography, J. Chromatogr. A, 1098 (2005) 123-130.
[33] D.H. Marchand, K. Croes, J.W. Dolan, L.R. Snyder, R.A. Henry, K.M.R. Kallury, S. Waite, P.W. Carr, Column selectivity in reversed-phase liquid chromatography - VIII. Phenylalkyl and fluoro-substituted columns, J. Chromatogr. A, 1062 (2005) 65-78.

2.7 Chapter appendix

2.7.1 Mathematical Background for the calculations

2.7.1.1 Neue et al. approach

In order to accomplish the Neue et al. approach the retention factor must be calculated for each compound using Equation-S 2.1.

$$k = \frac{t_R - t_0}{t_0}$$ **Equation-S 2.1**

where t_R is the retention time and t_0 the column void time. The obtained retention factor can be plotted as shown in Figure 2.2 and Figure 2.3. Afterwards, the correlation coefficient can be estimated using Equation-S 2.2.

$$R = \frac{s_{xy}}{s_x \cdot s_y}$$ **Equation-S 2.2**

where s_{xy} is the covariance, s_x and s_y are the variances of the x and y data, respectively. The Neue et al. approach uses the squared R value because this is a characteristic for the explained variances of the data. The higher R^2, the higher is the similarity of the compared stationary phases. Now, the unexplained variances as a quantitative measure of column differences can be calculated using Equation-S 2.3.

$$s^2 = 1 - R^2$$ **Equation-S 2.3**

where s^2 is the unexplained variances of the data due to the column differences. The higher the s^2 value, the higher the differences of the compared stationary phases.

2.7.1.2 Selectivity Factor

For the calculation of the selectivity factor (α) for the critical peak pairs the ratio between the retention factors is estimated using Equation-S 2.4.

$$\alpha = \frac{k_2}{k_1}$$ **Equation-S 2.4**

where k_1 is the retention factor of the earlier eluting compound and k_2 of the later eluting compound. Therefore, the selectivity factor is always higher than one. This value can be used to compare the selectivity of different stationary phases independently of the particle diameter.

2.7.1.3 Principal component analysis (*PCA*)

The principal component analysis (*PCA*) is used to simplify large data sets without losing the most important information. Therefore, the original data matrix is transformed into a new coordinate system by data axis transformation showing the calculated principal components on the x- and y-axis, respectively, assuming a two-dimensional illustration. The first principal component (*PC1*) is calculated in order to illustrate the highest variance of the data. The second principal component (*PC2*) is arranged in an orthogonal direction to the *PC1* displaying the next highest possible variance. All succeeding principal components are calculated in the same way. The strength of the *PCA* is as mentioned above the data reduction. This is possible because correlated data are condensed and principal components of higher order, which describe only a small portion of the variance, are not necessarily considered. As a consequence, the number of considered variables is often smaller than the number of initial variables. During *PCA* creation two characteristic values are calculated for each variable and data point. The loadings describe the direction of the initial variables with respect to the principal components. The scores are the values of the initial data points transformed into the new coordinate system. Besides the data reduction, the main intention of *PCA* is the illustration of correlations between the data which cannot be seen directly in classic data analysis. Nevertheless, in order to successfully apply the *PCA* some background knowledge about the data is desirable. In addition, *PCA* is sensitive with respect to the scaling of the data. Due to the reason that the *PCA* is a non-parametric approach, the results are independent of the data source and user [1, 2]. Further information about the *PCA* can be found in [3, 4].

2.7.2 Additional tables

A list of the investigated compounds is shown in Table-S 2.1.

Table-S 2.1: List of the investigated compounds, including CAS number, sum formula, pKa and log D [5-7].

number	compound	CAS	sum formula	Purity / %	provider	pK_a (T=25 °C)	log D (T=25 °C, pH=3)
(1)	5-fluorouracil	51-21-8	$C_4H_3FN_2O_2$	≥ 99	Fluka	7.76 / 8.02	-0.65
(2)	gemcitabine	95058-81-4	$C_9H_{11}F_2N_3O_4$	≥ 98	Sigma	3.60 / 11.52	-3.34
(3)	methotrexate	59-05-2	$C_{20}H_{22}N_8O_5$	≥ 98	Fluka	3.41 / 4.70	-2.95
(4)	topotecan	123948-87-8	$C_{23}H_{23}N_3O_5$	≥ 98	Sigma	8.00	-3.36
(5)	irinotecan	97682-44-5	$C_{33}H_{38}N_4O_6$	≥ 97	Sigma	11.71	-0.34
(6)	ifosfamide	3778-73-2	$C_7H_{15}Cl_2N_2O_2P$	≥ 98	Sigma	13.24	0.75
(7)	cyclophosphamide	50-18-0	$C_7H_{15}Cl_2N_2O_2P$	≥97	Sigma	12.78	0.50
(8)	doxorubicin	23214-92-8	$C_{27}H_{29}NO_{11}$	≥ 98	Sigma	9.53	-2.86
(9)	epirubicin	56420-45-2	$C_{27}H_{29}NO_{11}$	≥ 90	Sigma	9.53	-2.86
(10)	etoposide	33419-42-0	$C_{29}H_{32}O_{13}$	≥ 98	Sigma	9.33	0.28
(11)	paclitaxel	33069-62-4	$C_{47}H_{51}NO_{14}$	≥ 95	Sigma	10.36	3.95
(12)	docetaxel	114977-28-5	$C_{43}H_{53}NO_{14}$	≥ 97	Sigma	10.96	2.46

Table-S 2.2 - Table-S 2.5 illustrates the calculated variances for all column combinations, organic modifier and temperatures whereas the selectivitiy factors for all critical peak pairs are shown in Table-S 2.6. The resulting average and weighted average selectivity factors for all columns, organic modifier and temperatures for the critical peak pairs are given in Table-S 2.7.

Table-S 2.2: Calculated variances for all column combinations using acetonitrile at 30 °C. Note: All investigated Supelco columns belong to the Ascentis Express series.

s^2 ACN 30 °C	Supelco Ascentis C8	Supelco Ascentis C18	Supelco Ascentis CN	Supelco Ascentis ES C18	Supelco Ascentis RP-Amide	Supelco Ascentis Phenyl Hexyl	ChromaNik SunShell RP-Aqua	Phenomenex Kinetex C18	Restek Raptor ARC-18	Thermo Hypersil PFP	Waters BEH C18	Waters HSS T3 C18	Waters Xbridge C18	MN Nucleoshell Rp18 plus	Phenomenex Synergi Rppolar	TCI Kaisersorb ODA-SAX Super	Merck Chromolith RP18e	Agilent Zorbax SB C18	Restek Raptor Biphenyl	YMC Triart C18
Supelco Ascentis C8	0	0.032	0.043	0.027	0.011	0.036	0.036	0.045	0.009	0.114	0.027	0.012	0.017	0.013	0.045	0.046	0.056	0.017	0.017	0.008
Supelco Ascentis C18	0.032	0	0.005	0.002	0.011	0.010	0.002	0.007	0.008	0.029	0.014	0.010	0.007	0.012	0.009	0.052	0.024	0.013	0.009	0.020
Supelco Ascentis CN	0.043	0.005	0	0.008	0.017	0.005	0.003	0.003	0.015	0.024	0.012	0.022	0.011	0.024	0.005	0.040	0.016	0.024	0.014	0.034
Supelco Ascentis ES C18	0.027	0.002	0.008	0	0.010	0.009	0.003	0.008	0.007	0.036	0.010	0.007	0.004	0.007	0.007	0.046	0.023	0.009	0.005	0.018
Supelco Ascentis RP-Amide	0.011	0.011	0.017	0.010	0	0.019	0.014	0.022	0.004	0.064	0.018	0.008	0.008	0.007	0.022	0.051	0.042	0.011	0.008	0.005
Supelco Ascentis Phenyl Hexyl	0.036	0.010	0.005	0.009	0.019	0	0.004	0.002	0.013	0.042	0.003	0.018	0.006	0.021	0.006	0.021	0.006	0.021	0.014	0.034
ChromaNik SunShell RP-Aqua	0.036	0.002	0.003	0.003	0.014	0.004	0	0.002	0.010	0.030	0.007	0.013	0.005	0.014	0.005	0.038	0.014	0.015	0.011	0.026
Phenomenex Kinetex C18	0.045	0.007	0.003	0.008	0.022	0.002	0.002	0	0.017	0.029	0.006	0.022	0.009	0.022	0.003	0.031	0.008	0.021	0.016	0.039
Restek Raptor ARC-18	0.009	0.008	0.015	0.007	0.004	0.013	0.010	0.017	0	0.065	0.011	0.003	0.003	0.005	0.019	0.038	0.029	0.008	0.006	0.007
Thermo Hypersil PFP	0.114	0.029	0.024	0.036	0.064	0.042	0.030	0.029	0.065	0	0.059	0.069	0.056	0.069	0.025	0.107	0.053	0.069	0.051	0.088
Waters BEH C18	0.027	0.014	0.012	0.010	0.018	0.003	0.007	0.006	0.011	0.059	0	0.015	0.004	0.015	0.010	0.015	0.007	0.015	0.013	0.029
Waters HSS T3 C18	0.012	0.010	0.022	0.007	0.008	0.018	0.013	0.022	0.003	0.069	0.015	0	0.004	0.004	0.023	0.048	0.035	0.007	0.009	0.008
Waters Xbridge C18	0.017	0.007	0.011	0.004	0.008	0.006	0.005	0.009	0.003	0.056	0.004	0.004	0	0.006	0.011	0.029	0.018	0.007	0.006	0.014
MN Nucleoshell Rp18 plus	0.013	0.012	0.024	0.007	0.007	0.021	0.014	0.022	0.005	0.069	0.015	0.004	0.006	0	0.021	0.051	0.038	0.001	0.008	0.008
Phenomenex Synergi Rppolar	0.045	0.009	0.005	0.007	0.022	0.006	0.005	0.003	0.019	0.025	0.010	0.023	0.011	0.021	0	0.036	0.013	0.020	0.011	0.040
TCI Kaisersorb ODA-SAX Super	0.046	0.052	0.040	0.046	0.051	0.021	0.038	0.031	0.038	0.107	0.015	0.048	0.029	0.051	0.036	0	0.014	0.049	0.042	0.066
Merck Chromolith RP18e	0.056	0.024	0.016	0.023	0.042	0.006	0.014	0.008	0.029	0.053	0.007	0.035	0.018	0.038	0.013	0.014	0	0.034	0.031	0.061
Agilent Zorbax SB C18	0.017	0.013	0.024	0.009	0.011	0.021	0.015	0.021	0.008	0.069	0.015	0.007	0.007	0.001	0.020	0.049	0.034	0	0.012	0.014
Restek Raptor Biphenyl	0.017	0.009	0.014	0.005	0.008	0.014	0.011	0.016	0.006	0.051	0.013	0.009	0.006	0.008	0.011	0.042	0.031	0.012	0	0.014
YMC Triart C18	0.008	0.020	0.034	0.018	0.005	0.034	0.026	0.039	0.007	0.088	0.029	0.008	0.014	0.008	0.040	0.066	0.061	0.014	0.014	0

Table-S 2.3: Calculated variances for all column combinations using acetonitrile at 50 °C. Note: All investigated Supelco columns belong to the Ascentis Express series.

s^2 ACN 50 °C	Supelco Ascentis C8	Supelco Ascentis C18	Supelco Ascentis CN	Supelco Ascentis ES C18	Supelco Ascentis RP-Amide	Supelco Ascentis Phenyl Hexyl	ChromaNik SunShell RP-Aqua	Phenomenex Kinetex C18	Restek Raptor ARC-18	Thermo Hypersil PFP	Waters BEH C18	Waters HSS T3 C18	Waters Xbridge C18	MN Nucleoshell Rp18 plus	Phenomenex Synergi Rppolar	TCI Kaisersorb ODA-SAX Super	Merck Chromolith RP18e	Agilent Zorbax SB C18	Restek Raptor Biphenyl	YMC Triart C18
Supelco Ascentis C8	0	0.025	0.023	0.018	0.004	0.007	0.015	0.035	0.006	0.103	0.004	0.011	0.007	0.007	0.036	0.039	0.043	0.007	0.012	0.008
Supelco Ascentis C18	0.025	0	0.007	0.001	0.011	0.010	0.002	0.005	0.010	0.032	0.012	0.008	0.008	0.010	0.006	0.048	0.017	0.011	0.008	0.029
Supelco Ascentis CN	0.023	0.007	0	0.006	0.009	0.014	0.005	0.020	0.016	0.039	0.018	0.016	0.013	0.016	0.016	0.070	0.038	0.018	0.012	0.023
Supelco Ascentis ES C18	0.018	0.001	0.006	0	0.007	0.006	0.000	0.008	0.006	0.040	0.008	0.005	0.004	0.007	0.008	0.044	0.019	0.008	0.006	0.021
Supelco Ascentis RP-Amide	0.004	0.011	0.009	0.007	0	0.003	0.005	0.021	0.004	0.070	0.004	0.007	0.004	0.004	0.022	0.044	0.033	0.006	0.007	0.011
Supelco Ascentis Phenyl Hexyl	0.007	0.010	0.014	0.006	0.003	0	0.006	0.015	0.001	0.070	0.002	0.004	0.002	0.005	0.017	0.025	0.019	0.005	0.006	0.015
ChromaNik SunShell RP-Aqua	0.015	0.002	0.005	0.000	0.005	0.006	0	0.011	0.005	0.046	0.006	0.004	0.003	0.005	0.011	0.046	0.022	0.006	0.005	0.017
Phenomenex Kinetex C18	0.035	0.005	0.020	0.008	0.021	0.015	0.011	0	0.015	0.030	0.020	0.015	0.016	0.018	0.004	0.036	0.006	0.019	0.013	0.050
Restek Raptor ARC-18	0.006	0.010	0.016	0.006	0.004	0.001	0.005	0.015	0	0.073	0.000	0.002	0.001	0.003	0.018	0.026	0.020	0.002	0.006	0.013
Thermo Hypersil PFP	0.103	0.032	0.039	0.040	0.070	0.070	0.046	0.030	0.073	0	0.080	0.067	0.069	0.074	0.028	0.120	0.052	0.079	0.056	0.109
Waters BEH C18	0.004	0.012	0.018	0.008	0.004	0.002	0.006	0.020	0.000	0.080	0	0.002	0.001	0.002	0.021	0.028	0.024	0.002	0.006	0.010
Waters HSS T3 C18	0.011	0.008	0.016	0.005	0.007	0.004	0.004	0.015	0.002	0.067	0.002	0	0.002	0.004	0.017	0.032	0.020	0.003	0.007	0.014
Waters Xbridge C18	0.007	0.008	0.013	0.004	0.004	0.002	0.003	0.016	0.001	0.069	0.001	0.002	0	0.002	0.016	0.032	0.022	0.002	0.004	0.011
MN Nucleoshell Rp18 plus	0.007	0.010	0.016	0.007	0.004	0.005	0.005	0.018	0.003	0.074	0.002	0.004	0.002	0	0.021	0.039	0.026	0.000	0.007	0.013
Phenomenex Synergi Rppolar	0.036	0.006	0.016	0.008	0.022	0.017	0.011	0.004	0.018	0.028	0.021	0.017	0.016	0.021	0	0.042	0.011	0.021	0.008	0.048
TCI Kaisersorb ODA-SAX Super	0.039	0.048	0.070	0.044	0.044	0.025	0.046	0.036	0.026	0.120	0.028	0.032	0.032	0.039	0.042	0	0.019	0.035	0.036	0.064
Merck Chromolith RP18e	0.043	0.017	0.038	0.019	0.033	0.019	0.022	0.006	0.020	0.052	0.024	0.020	0.022	0.026	0.011	0.019	0	0.025	0.022	0.062
Agilent Zorbax SB C18	0.007	0.011	0.018	0.008	0.006	0.005	0.006	0.019	0.002	0.079	0.002	0.003	0.002	0.000	0.021	0.035	0.025	0	0.008	0.012
Restek Raptor Biphenyl	0.012	0.008	0.012	0.006	0.007	0.006	0.005	0.013	0.006	0.056	0.006	0.007	0.004	0.007	0.008	0.036	0.022	0.008	0	0.022
YMC Triart C18	0.008	0.029	0.023	0.021	0.011	0.015	0.017	0.050	0.013	0.109	0.010	0.014	0.011	0.013	0.048	0.064	0.062	0.012	0.022	0

Table-S 2.4: Calculated variances for all column combinations using methanol at 30 °C. Note: All investigated Supelco columns belong to the Ascentis Express series.

s^2 MeOH 30 °C	Supelco Ascentis C8	Supelco Ascentis C18	Supelco Ascentis CN	Supelco Ascentis ES C18	Supelco Ascentis RP-Amide	Supelco Ascentis Phenyl Hexyl	Chroma Nik SunShell RP-Aqua	Phenomenex Kinetex C18	Restek Raptor ARC-18	Thermo Hypersil PFP	Waters BEH C18	Waters HSS T3 C18	Waters Xbridge C18	MN Nucleoshell Rp18 plus	Phenomenex Synergi Rppolar	TCI Kaisersorb ODA-SAX Super	Merck Chromolith RP18e	Agilent Zorbax SB C18	Restek Raptor Biphenyl	YMC Triart C18
Supelco Ascentis C8	0	0.045	0.061	0.041	0.029	0.029	0.046	0.046	0.011	0.188	0.021	0.039	0.018	0.017	0.109	0.022	0.019	0.019	0.045	0.026
Supelco Ascentis C18	0.045	0	0.008	0.002	0.004	0.015	0.001	0.005	0.012	0.059	0.015	0.015	0.009	0.010	0.031	0.090	0.013	0.012	0.024	0.018
Supelco Ascentis CN	0.061	0.008	0	0.013	0.011	0.028	0.010	0.014	0.026	0.048	0.033	0.039	0.027	0.027	0.039	0.115	0.030	0.031	0.035	0.035
Supelco Ascentis ES C18	0.041	0.002	0.013	0	0.003	0.010	0.001	0.002	0.010	0.063	0.008	0.009	0.006	0.009	0.026	0.076	0.008	0.008	0.016	0.021
Supelco Ascentis RP-Amide	0.029	0.004	0.011	0.003	0	0.013	0.004	0.005	0.007	0.079	0.007	0.017	0.006	0.007	0.040	0.064	0.006	0.009	0.020	0.020
Supelco Ascentis Phenyl Hexyl	0.029	0.015	0.028	0.010	0.013	0	0.014	0.010	0.008	0.093	0.007	0.009	0.007	0.011	0.036	0.049	0.007	0.006	0.007	0.022
ChromaNik SunShell RP-Aqua	0.046	0.001	0.010	0.001	0.004	0.014	0	0.004	0.013	0.059	0.013	0.012	0.009	0.010	0.029	0.089	0.013	0.011	0.022	0.020
Phenomenex Kinetex C18	0.046	0.005	0.014	0.002	0.005	0.010	0.004	0	0.014	0.058	0.008	0.012	0.009	0.013	0.020	0.074	0.008	0.011	0.013	0.030
Restek Raptor ARC-18	0.011	0.012	0.026	0.010	0.007	0.008	0.013	0.014	0	0.117	0.005	0.013	0.002	0.002	0.058	0.043	0.004	0.003	0.021	0.010
Thermo Hypersil PFP	0.188	0.059	0.048	0.063	0.079	0.093	0.059	0.058	0.117	0	0.106	0.096	0.104	0.111	0.034	0.238	0.107	0.109	0.084	0.126
Waters BEH C18	0.021	0.015	0.033	0.008	0.007	0.007	0.013	0.008	0.005	0.106	0	0.009	0.003	0.006	0.043	0.036	0.001	0.004	0.012	0.024
Waters HSS T3 C18	0.039	0.015	0.039	0.009	0.017	0.009	0.012	0.012	0.013	0.096	0.009	0	0.006	0.010	0.040	0.063	0.010	0.005	0.017	0.019
Waters Xbridge C18	0.018	0.009	0.027	0.006	0.006	0.007	0.009	0.009	0.002	0.104	0.003	0.006	0	0.002	0.048	0.047	0.002	0.001	0.017	0.011
MN Nucleoshell Rp18 plus	0.017	0.010	0.027	0.009	0.007	0.011	0.010	0.013	0.002	0.111	0.006	0.010	0.002	0	0.055	0.051	0.004	0.001	0.027	0.009
Phenomenex Synergi Rppolar	0.109	0.031	0.039	0.026	0.040	0.036	0.029	0.020	0.058	0.034	0.043	0.040	0.048	0.055	0	0.128	0.045	0.048	0.032	0.082
TCI Kaisersorb ODA-SAX Super	0.022	0.090	0.115	0.076	0.064	0.049	0.089	0.074	0.043	0.238	0.036	0.063	0.047	0.051	0.128	0	0.038	0.046	0.055	0.076
Merck Chromolith RP18e	0.019	0.013	0.030	0.008	0.006	0.007	0.013	0.008	0.004	0.107	0.001	0.010	0.002	0.004	0.045	0.038	0	0.003	0.016	0.020
Agilent Zorbax SB C18	0.019	0.012	0.031	0.008	0.009	0.006	0.011	0.011	0.003	0.109	0.004	0.005	0.001	0.001	0.048	0.046	0.003	0	0.020	0.011
Restek Raptor Biphenyl	0.045	0.024	0.035	0.016	0.020	0.007	0.022	0.013	0.021	0.084	0.012	0.017	0.017	0.027	0.032	0.055	0.016	0.020	0	0.043
YMC Triart C18	0.026	0.018	0.035	0.021	0.020	0.022	0.020	0.030	0.010	0.126	0.024	0.019	0.011	0.009	0.082	0.076	0.020	0.011	0.043	0

Table-S 2.5: Calculated variances for all column combinations using methanol at 50 °C. Note: All investigated Supelco columns belong to the Ascentis Express series.

s^2 MeOH 50 °C	Supelco Ascentis C8	Supelco Ascentis C18	Supelco Ascentis CN	Supelco Ascentis ES C18	Supelco Ascentis RP-Amide	Supelco Ascentis Phenyl Hexyl	ChromaNik SunShell RP-Aqua	Phenomenex Kinetex C18	Restek Raptor ARC-18	Thermo Hypersil PFP	Waters BEH C18	Waters HSS T3 C18	Waters Xbridge C18	MN Nucleoshell Rp18 plus	Phenomenex Synergi Rppolar	TCI Kaisersorb ODA-SAX Super	Merck Chromolith RP18e	Agilent Zorbax SB C18	Restek Raptor Biphenyl	YMC Triart C18
Supelco Ascentis C8	0	0.056	0.065	0.063	0.029	0.049	0.057	0.068	0.023	0.221	0.040	0.051	0.037	0.047	0.127	0.039	0.040	0.033	0.064	0.036
Supelco Ascentis C18	0.056	0	0.011	0.003	0.006	0.013	0.000	0.006	0.013	0.068	0.018	0.009	0.009	0.013	0.024	0.086	0.012	0.013	0.019	0.019
Supelco Ascentis CN	0.065	0.011	0	0.022	0.013	0.032	0.013	0.027	0.033	0.061	0.049	0.035	0.033	0.036	0.041	0.124	0.037	0.036	0.041	0.035
Supelco Ascentis ES C18	0.063	0.003	0.022	0	0.011	0.010	0.002	0.001	0.014	0.071	0.012	0.006	0.006	0.013	0.017	0.076	0.007	0.011	0.012	0.023
Supelco Ascentis RP-Amide	0.029	0.006	0.013	0.011	0	0.014	0.006	0.014	0.007	0.102	0.016	0.013	0.008	0.013	0.045	0.065	0.010	0.010	0.023	0.015
Supelco Ascentis Phenyl Hexyl	0.049	0.013	0.032	0.010	0.014	0	0.012	0.011	0.006	0.108	0.008	0.005	0.005	0.019	0.032	0.048	0.006	0.005	0.006	0.015
ChromaNik SunShell RP-Aqua	0.057	0.000	0.013	0.002	0.006	0.012	0	0.005	0.013	0.069	0.017	0.008	0.008	0.012	0.022	0.084	0.010	0.012	0.018	0.019
Phenomenex Kinetex C18	0.068	0.006	0.027	0.001	0.014	0.011	0.005	0	0.017	0.071	0.012	0.009	0.009	0.013	0.015	0.073	0.007	0.014	0.012	0.031
Restek Raptor ARC-18	0.023	0.013	0.033	0.014	0.007	0.006	0.013	0.017	0	0.134	0.005	0.007	0.002	0.013	0.051	0.037	0.005	0.002	0.016	0.009
Thermo Hypersil PFP	0.221	0.068	0.061	0.071	0.102	0.108	0.069	0.071	0.134	0	0.133	0.106	0.115	0.115	0.042	0.261	0.116	0.128	0.099	0.137
Waters BEH C18	0.040	0.018	0.049	0.012	0.016	0.008	0.017	0.012	0.005	0.133	0	0.006	0.003	0.013	0.043	0.030	0.002	0.004	0.012	0.021
Waters HSS T3 C18	0.051	0.009	0.035	0.006	0.013	0.005	0.008	0.009	0.007	0.106	0.006	0	0.002	0.013	0.034	0.055	0.005	0.003	0.012	0.010
Waters Xbridge C18	0.037	0.009	0.033	0.006	0.008	0.005	0.008	0.009	0.002	0.115	0.003	0.002	0	0.010	0.039	0.045	0.002	0.002	0.012	0.011
MN Nucleoshell Rp18 plus	0.047	0.013	0.036	0.013	0.013	0.019	0.012	0.013	0.013	0.115	0.013	0.013	0.010	0	0.037	0.064	0.008	0.009	0.034	0.023
Phenomenex Synergi Rppolar	0.127	0.024	0.041	0.017	0.045	0.032	0.022	0.015	0.051	0.042	0.043	0.034	0.039	0.037	0	0.127	0.036	0.045	0.029	0.068
TCI Kaisersorb ODA-SAX Super	0.039	0.086	0.124	0.076	0.065	0.048	0.084	0.073	0.037	0.261	0.030	0.055	0.045	0.064	0.127	0	0.040	0.040	0.052	0.064
Merck Chromolith RP18e	0.040	0.012	0.037	0.007	0.010	0.006	0.010	0.007	0.005	0.116	0.002	0.005	0.002	0.008	0.036	0.040	0	0.003	0.013	0.018
Agilent Zorbax SB C18	0.033	0.013	0.036	0.011	0.010	0.005	0.012	0.014	0.002	0.128	0.004	0.003	0.002	0.009	0.045	0.040	0.003	0	0.017	0.008
Restek Raptor Biphenyl	0.064	0.019	0.041	0.012	0.023	0.006	0.018	0.012	0.016	0.099	0.012	0.012	0.012	0.034	0.029	0.052	0.013	0.017	0	0.033
YMC Triart C18	0.036	0.019	0.035	0.023	0.015	0.015	0.019	0.031	0.009	0.137	0.021	0.010	0.011	0.023	0.068	0.064	0.018	0.008	0.033	0

Table-S 2.6: Calculated selectivity factors for all columns, organic modifiers and separation temperatures that were used for the principal component analysis. IF / CP: ifosfamide / cyclophosphamide, Doxo / Epi: doxorubicin / epirubicin, Pac / Doc: paclitaxel / docetaxel.

Columns	Acetonitrile 30 °C			Acetonitrile 50 °C			Methanol 30 °C			Methanol 50 °C		
	IF / CP	Doxo / Epi	Pac / Doc	IF / CP	Doxo / Epi	Pac / Doc	IF / CP	Doxo / Epi	Pac / Doc	IF / CP	Doxo / Epi	Pac / Doc
Agilent Zorbax SB C18	1.023	1.026	1.028	1.029	1.027	1.020	1.047	1.027	1.013	1.056	1.035	1.013
Chromanik SunShell RP-Aqua	1.024	1.028	1.018	1.031	1.034	1.015	1.047	1.027	1.012	1.052	1.032	1.014
Merck Chromolith RP18e	1.023	1.017	1.014	1.031	1.020	1.006	1.045	1.029	1.016	1.050	1.031	1.018
MN Nucleoshell Rp18 plus	1.023	1.027	1.026	1.029	1.032	1.018	1.047	1.031	1.015	1.059	1.032	1.017
Phenomenex Kinetex C18	1.022	1.029	1.024	1.031	1.030	1.018	1.038	1.027	1.009	1.041	1.031	1.012
Phenomenex Synergi Rppolar	1.015	1.024	1.048	1.018	1.016	1.044	1.025	1.023	1.025	1.030	1.023	1.027
Restek Raptor Biphenyl	1.011	1.028	1.054	1.014	1.025	1.049	1.010	1.025	1.030	1.014	1.019	1.031
Restek Raptor ARC-18	1.016	1.036	1.028	1.030	1.035	1.019	1.048	1.033	1.013	1.055	1.036	1.014
Supelco Ascentis Express C18	1.028	1.034	1.019	1.032	1.035	1.011	1.052	1.031	1.016	1.056	1.035	1.018
Supelco AscentisExpress C8	1.033	1.046	1.019	1.033	1.031	1.009	1.059	1.042	1.015	1.062	1.056	1.017
Supelco Ascentis Express CN	1.024	1.030	1.039	1.032	1.038	1.036	1.031	1.037	1.019	1.037	1.042	1.019
Supelco Ascentis Express ES C18	1.026	1.044	1.022	1.033	1.040	1.016	1.044	1.033	1.014	1.046	1.036	1.016
Supelco Ascentis Express RP-Amide	1.032	1.033	1.040	1.038	1.038	1.031	1.052	1.031	1.000	1.066	1.036	1.000
Supelco Ascentis Express Phenyl Hexyl	1.018	1.029	1.039	1.027	1.026	1.038	1.043	1.024	1.017	1.047	1.028	1.018
TCI Kaisersorb ODS-SAX Super	1.013	1.013	1.023	1.017	1.015	1.018	1.035	1.027	1.000	1.041	1.030	1.000
Thermo Hypersil PFP	1.035	1.034	1.031	1.033	1.027	1.027	1.035	1.035	1.011	1.048	1.041	1.010
Waters Acquity BEH C18	1.019	1.020	1.014	1.030	1.029	1.007	1.017	1.026	1.011	1.047	1.028	1.014
Waters HSS T3 C18	1.027	1.030	1.021	1.026	1.031	1.014	1.041	1.023	1.010	1.050	1.028	1.012
Waters XBridge C18	1.031	1.026	1.015	1.033	1.031	1.000	1.051	1.028	1.014	1.056	1.031	1.017
YMC Triart C18	1.030	1.032	1.034	1.034	1.035	1.025	1.056	1.028	1.005	1.062	1.032	1.009

Table-S 2.7: Resulting average and weighted average selectivity factors for all columns, organic modifier and separation temperatures for the three critical peak pairs ifosfamide/cyclophosphamide, doxorubicin/epirubicin and paclitaxel/docetaxel. Weighting factor: IF/CP:Doxo/Epi:Pac/Doc 2:3:1.

Column	Acetonitrile				Methanol			
	average α (30 °C)	*weighted average α (30 °C)*	average α (50 °C)	*weighted average α (50 °C)*	average α (30 °C)	*weighted average α (30 °C)*	average α (50 °C)	*weighted average α (50 °C)*
Agilent Zorbax SB C18	1.025	*1.025*	1.025	*1.026*	1.029	*1.031*	1.035	*1.038*
ChromaNik Sunshell RP-Aqua	1.024	*1.025*	1.027	*1.030*	1.029	*1.031*	1.033	*1.036*
Macherey Nagel Nucleoshell RP 18plus	1.025	*1.025*	1.027	*1.029*	1.031	*1.033*	1.036	*1.038*
Merck Chromolith FastGradient RP 18e	1.018	*1.018*	1.019	*1.021*	1.030	*1.032*	1.033	*1.035*
Phenomenex Kinetex C18	1.025	*1.026*	1.026	*1.028*	1.025	*1.028*	1.028	*1.031*
Phenomenex Synergi RP polar	1.029	*1.025*	1.026	*1.021*	1.024	*1.024*	1.027	*1.026*
Restek Raptor ARC-18	1.027	*1.028*	1.028	*1.031*	1.032	*1.035*	1.035	*1.038*
Restek Raptor Biphenyl	1.031	*1.027*	1.030	*1.025*	1.022	*1.021*	1.021	*1.019*
Supelco Ascentis Express C18	1.027	*1.030*	1.026	*1.030*	1.033	*1.035*	1.036	*1.039*
Supelco Ascentis Express C8	1.033	*1.037*	1.024	*1.028*	1.039	*1.043*	1.045	*1.052*
Supelco Ascentis Express CN	1.031	*1.029*	1.035	*1.036*	1.029	*1.032*	1.033	*1.036*
Supelco Ascentis Express ES C18	1.031	*1.034*	1.030	*1.033*	1.030	*1.033*	1.033	*1.036*
Supelco Ascentis Express RP-Amide	1.035	*1.034*	1.035	*1.037*	1.028	*1.033*	1.034	*1.040*
Supelco Ascentis Express Phenyl-Hexyl	1.029	*1.027*	1.030	*1.028*	1.028	*1.029*	1.031	*1.033*
TCI Kaseisorb LC ODS-SAX Super	1.016	*1.014*	1.017	*1.016*	1.021	*1.025*	1.024	*1.029*
Thermo HypersilGold PFP	1.033	*1.034*	1.029	*1.029*	1.027	*1.031*	1.033	*1.038*
Waters Acquity BEH C18	1.018	*1.019*	1.022	*1.025*	1.018	*1.020*	1.030	*1.032*
Waters HSS T3 C18	1.026	*1.028*	1.024	*1.026*	1.025	*1.027*	1.030	*1.033*
Waters Xbridge C18	1.024	*1.026*	1.021	*1.027*	1.031	*1.033*	1.034	*1.037*
YMC Triart C18	1.032	*1.032*	1.031	*1.033*	1.030	*1.034*	1.034	*1.038*
	weighted average α (30 °C)		*weighted average α (50 °C)*		*weighted average α (30 °C)*		*weighted average α (50 °C)*	
All columns (n=20)	*1.027*		*1.029*		*1.031*		*1.035*	

2.7.3 References

[1] R. Bro, A.K. Smilde, Principal component analysis, Anal. Methods, 6 (2014) 2812-2831.
[2] J. Shlens, A tutorial on principal component analysis, arXiv preprint arXiv:1404.1100, (2014).
[3] M. Mellinger, Multivariate Data Analysis - Its Methods, Chemometrics Intell. Lab. Syst., 2 (1987) 29-36.
[4] S. Wold, K. Esbensen, P. Geladi, Principal Component Analysis, Chemometrics Intell. Lab. Syst., 2 (1987) 37-52.
[5] ChemSpider, http://www.chemspider.com, (accessed 25.01.2015)
[6] DrugBank, http://www.drugbank.ca/, (accessed 26.01.2015)
[7] Scifinder, https://www.scifinder.cas.org, (accessed 26.01.2015)

Chapter 3 Characterization of efficiency of microbore liquid chromatography columns by van Deemter and kinetic plot analysis

Redrafted from "Hetzel, T., Loeker, D., Teutenberg, T., Schmidt, T.C., Characterization of efficiency of micro liquid chromatography columns by van Deemter and kinetic plot analysis, Journal of Separation Science, 39 (2016) 3889–3897."

Abstract

The efficiency of miniaturized liquid chromatography columns with inner diameters between 200 and 300 µm has been investigated using a dedicated micro-LC system. Fully porous, core-shell and monolithic commercially available stationary phases were compared applying van Deemter as well as kinetic plot analysis. It was found that the sub-2 µm fully porous as well as the 2.7 µm core-shell particle packed columns showed superior efficiency and similar values for the minimum reduced plate heights (2.56-2.69) before correction for extra-column contribution compared to normal bore columns. Moreover, the influence of extra-column contribution was investigated to demonstrate the difference between apparent and intrinsic efficiency by replacing the column by a zero dead volume union to determine the band spreading caused by the system. It was demonstrated that 72% of the intrinsic efficiency could be reached. The results of the kinetic plot analysis indicate the superior performance of the sub-2 µm fully porous particle packed column for ultra-fast liquid chromatography.

3.1 Introduction

Currently, there is a renewed interest in miniaturized liquid chromatography [1]. Several groups and vendors are working on new developments and improvements in the field of micro-LC, nano-LC, and chip-LC [2, 3]. In particular, the advantages of increased separation speed at reduced solvent consumption as well as reduced cycle times are the main motivation for miniaturization. Regarding the separation speed, miniaturized separation techniques allow to use high linear velocities at low flow rates in the nL-µL min^{-1} range. In order to achieve similar linear velocities using conventional HPLC columns with an inner diameter (*i.d.*) between 2.1 mm and 4.6 mm, flow rates in the mL min^{-1} range must be applied. This is an undisputed benefit of miniaturized LC columns with an *i.d.* between 50 µm and 300 µm. Furthermore, the need for increased detection sensitivity in combination with mass spectrometry (*MS*) favors miniaturized separation techniques because lower flow rates improve the ionization and ion desorption process [4-6].

In general, miniaturized columns are limited in terms of the injection volume. With decreasing *i.d.* of the column the maximum injection volume also decreases because of the reduced column volume. Therefore, nano-LC is mainly used in the field of proteomics and bioanalysis because the limited sample volume is less diluted by the column volume [1, 7]. While nano-LC requires dedicated detection capabilities like e.g. a nano-ESI source, micro-LC is compatible without a significant modification of conventional ion sources. Thus, micro-LC can also be used in other fields of application such as environmental and pharmaceutical analysis where the sample volume is not a limiting factor. It could be a suitable alternative to the established LC methods because micro-LC combines the advantages of increased separation speed with decreased resource consumption and sufficient sensitivity due to the decreased dilution by the column volume and higher loading capacity compared to nano-LC. Furthermore, in the field of multi-dimensional LC separations, micro-LC can be used in the second dimension in order to accomplish very fast cycle times as has recently been demonstrated by Haun et al. (≤ 60 s) [8].

However, the prerequisite for the use of micro-LC in routine analysis are robust, reliable, and efficient LC columns. The common opinion is that such miniaturized columns cannot be packed adequately due to the decreased *i.d.* [1, 2, 9]. In addition, the negative influence of the extra-column volume on the chromatographic efficiency is given as a reason why the intrinsic column efficiency cannot be utilized and therefore the obtained efficiencies are significantly lower compared to columns with an *i.d.* above 2.1 mm [10, 11]. This argument is also underlined by

Gritti et al. who characterized the efficiency of 500 µm *i.d.* columns packed with 3 µm fully porous and 2.7 µm core-shell particles [9]. It was found that the obtained plate heights are significantly higher compared to normal bore columns due to the extra-column volume contribution of the micro-LC system.

Meanwhile, columns packed with fully porous and core-shell particles as well as monolithic columns are commercially available for an *i.d.* between 200 and 300 µm. Core-shell particle packed columns are increasingly being used instead of fully porous particle packed columns due to their reduced back pressure at a given flow rate [12]. Especially, monolithic columns are characterized by a very high permeability and recently published work by Hara et al. showed an increased pressure stability up to 800 bar [13, 14].

Therefore, this investigation focused on the question which efficiencies can be obtained with commercially available 200-300 µm *i.d.* micro-LC columns on a dedicated micro-LC system. For data evaluation, the van Deemter analysis as well as the kinetic plot method were applied [15]. Moreover, the influence of the extra-column volume on the performance of micro-LC columns was investigated by varying the *i.d.* of the connection tubings. Furthermore, the obtained apparent efficiencies were also compared to the intrinsic column efficiencies by correcting for the contribution of the extra-column volume.

3.2 Materials and methods

All measurements were performed on an Eksigent ExpressLC Ultra system (Sciex, Dublin, CA) with a standard micro-LC flow module (flow rate range: 1-10 µL min^{-1}). The pneumatic pump offers the possibility to select six different mobile phases up to 690 bar for each solvent channel. The sample loop filling was done by an HTS PAL autosampler (CTC Analytics, Zwingen, Switzerland). The installed loop, made of fused-silica surrounded by polyetheretherketone (PEEKSil), has an inner diameter of 75 µm and a length of 10 cm and represents the standard configuration. The corresponding loop volume was 442 nL. The sample injection was done by a built-in six-port valve using the full loop injection mode of the software. The integrated static air column oven was used for temperature control of the stationary phase. For data acquisition, a built-in diode array detector (*DAD*) was employed with a cell volume of 100 nL. Chromatograms were recorded at 254 nm with a data acquisition rate of 10 Hz.

All tubings prior to and after the column were made of 360 µm outer diameter (*o.d.*) fused-silica capillaries with an *i.d.* of 25 µm and 50 µm with a length of 10 and 13 cm, respectively. Using sleeves, the *o.d.* was expanded to 1/32” for the connection to the columns and detector.

The lengths of the individual connections were adjusted using a diamond cutter. For data acquisition and analysis the Eksigent control software (Version 4.1 Patch for ekspert nanoLC 400 and batch acquisition control) was used. Further data processing was done using Origin Lab v. 9.1 and Microsoft Office Excel 2010. Data fitting was done via least square method. For the measurement of the van Deemter curves, the flow rate was varied in a range between 2 and 15 µL min^{-1}. All measurements were done in triplicate.

Table 3.1 presents an overview of the investigated columns. The column oven temperature was set to 30 °C. The retention factor *k* was calculated according to Equation 3.1 using the retention time of an unretained marker as column void time (t_0).

$$k = \frac{t_R - t_0}{t_0} \qquad \textbf{Equation 3.1}$$

In order to obtain constant retention factors, the mobile phase composition was adjusted for every column. An overview can be found in the supporting information (Table-S 3.1).

Table 3.1: List of the investigated columns.

Description	surface modification	chromatographic support	end capping	L / mm	i.d. / mm	d_p / µm	pore diameter / Å	ΔP_{max}/ bar
Eksigent HALO	C18	core-shell	fully endcapped	50	0.3	2.7	90	690
Merck Chromolith CapRod	C18	monolithic	fully endcapped	150	0.2	macro pores 2.0	meso pores130	218
YMC Triart	C18	fully porous	Multistage endcapped	50	0.3	1.9	120	600
YMC Triart	C18			50	0.3	3.0	120	550

i.d.: column inner diameter, L: column length, d_p: particle diameter, ΔP_{max}: maximum backpressure

Water (H_2O) and acetonitrile (ACN) were used as mobile phase constituents. All solvents were purchased from Th. Geyer-Chemsolute (Renningen, Germany) with purity for LC-MS. Formic acid (FA), purchased from Sigma-Aldrich (Seelze, Germany), was used at 0.1% (v/v) as solvent additive to adjust the pH of the mobile phase and analyte mixture.

Table 3.2 shows the selected substances including important physico-chemical properties, while the structural formulas are compiled in Figure-S 3.1. Naphthalene has been selected because there are numerous studies using this model compound [9, 16]. Due to its low molecular weight it has a high diffusion coefficient (D_m). Furthermore, its retention is not influenced by the mobile phase pH and exhibits only hydrophobic interactions with the

stationary phase. In contrast, etoposide has a higher molecular weight and thus lower diffusion coefficient. Moreover, etoposide is a pharmaceutical of interest in terms of routine analysis and was also part of a previous study we performed to investigate the selectivity of different stationary phases [17].

Table 3.2: List of the investigated compounds including CAS number, sum formula, molar mass and D_m calculated according to Wilke-Chang equation for a mobile phase composition of H_2O/ACN 50/50 (v/v) and a temperature of 30 °C [18-21]. The viscosity was calculated according to [22].

number	Compound	CAS	sum formula	purity / %	provider	M / g mol^{-1}	D_m / cm^2 s^{-1}
(1)	Etoposide	33419-42-0	$C_{29}H_{32}O_{13}$	≥ 98	Sigma	588.57	6.2 x 10^{-6}
(2)	Naphthalene	91-20-3	$C_{10}H_8$	≥ 98	Fluka	128.17	1.3 x 10^{-5}

The stock solution for the analyte etoposide was prepared using a mixture of 50/50 H_2O/ACN (v/v). In contrast, naphthalene was dissolved in 100% ACN. For the micro-LC analysis the single standards were diluted with acidified water in the ratio of 1 to 10. The final concentration for etoposide and naphthalene was 0.1 mg mL^{-1} and 0.05 mg mL^{-1} with a composition of 95/5 and 90/10 H_2O/ACN + 0.1% FA (v/v), respectively.

3.3 Results and discussion

3.3.1 Determination of efficiency by van Deemter analysis

The easiest and commonly used way to evaluate the column efficiency in isocratic separation is done by van Deemter analysis which is illustrated in Equation 3.2 [15, 23].

$$H = A + \frac{B}{u_0} + C \cdot u_0 \qquad \textbf{Equation 3.2}$$

where *A* is the eddy diffusion, *B* the longitudinal diffusion, *C* the mass transfer and u_0 the linear velocity. For the determination of efficiency by van Deemter analysis the retention factor should be constant for all investigated columns. Thereby, the results are directly comparable because the influence of *k* on *N* can be neglected [24]. This is especially important for small *i.d.* columns. Figure 3.1 shows the comparison of the van Deemter curves for the different chromatographic supports at 30 °C for etoposide and naphthalene.

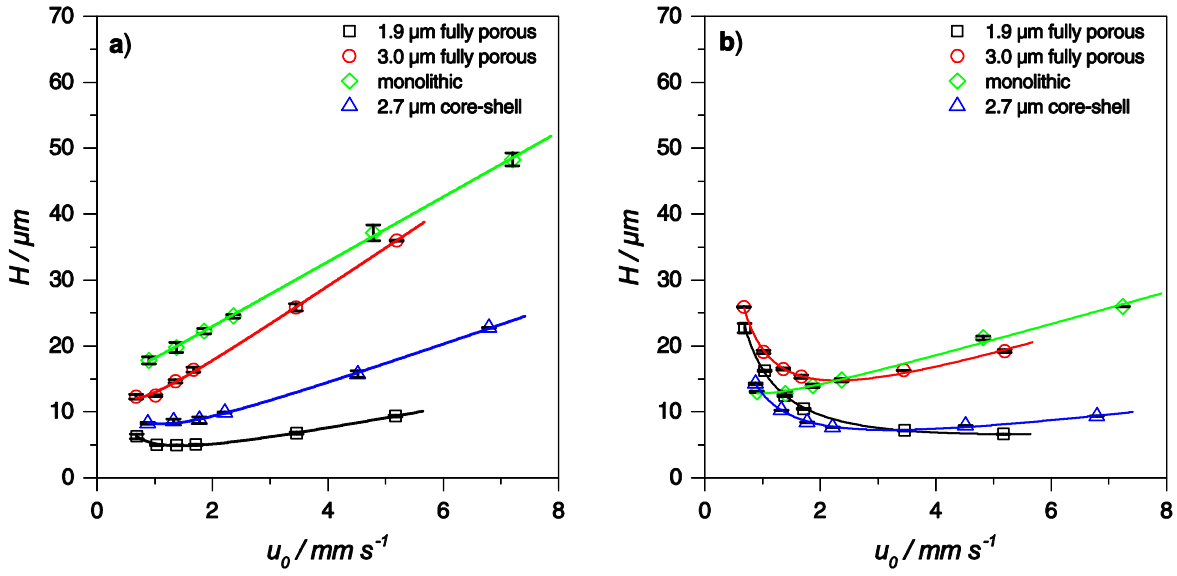

Figure 3.1: Van Deemter plots for a) etoposide and b) naphthalene at 30 °C. For mobile phase compositions, please refer to Table-S 3.1.

Comparing the obtained van Deemter curves for etoposide and naphthalene on the columns packed with 1.9 µm and 3.0 µm fully porous particles it can be seen that decreasing the particle diameter leads to smaller values for *H* due to the decreased *A*-term. In addition, the slope in the *C*-term region of the van Deemter curve is much smaller because of the improved mass transfer for sub-2 µm particles. Decreasing the particle diameter from 3.0 µm to 1.9 µm improves the value of H_{min} from 12.0 µm to 4.9 µm for etoposide and from 14.8 µm to 6.6 µm for naphthalene. This corresponds to a factor of 2.5 and 2.3 showing the poor packing of the 3.0 µm particle packed column because an improvement by a factor of 1.6 was expected.

Considering Figure 3.1 a) it can be seen that the *B*-term region cannot be represented adequately for etoposide due to its higher molecular weight and decreased diffusion coefficient. However, the column packed with 1.9 µm fully porous particles shows superior efficiency over the entire flow rate range with H_{min} of 4.9 µm when compared to all other columns. The column packed with 2.7 µm core-shell particles has a slightly higher H_{min} compared to the 1.9 µm fully porous particle packed column for etoposide. The slope in the *C*-term region is comparable for the core-shell and the monolithic stationary phase. For the monolithic column it can be assumed that the minimum plate height is comparable to the column packed with 3.0 µm fully porous particles which has a larger H_{min} due to the increased particle diameter, which is consistent with literature data [25]. In addition, the slope of the *C*-term for the column packed with 3.0 µm fully porous particles is much higher than for every other column due to a slower mass transfer and poor packing quality.

For the small molecule naphthalene in Figure 3.1 b), the core-shell as well as the column packed with 1.9 µm fully porous particles show comparable efficiencies. Again, the monolithic column and the column packed with 3.0 µm fully porous particles have an increased H_{min} compared to the core-shell and sub-2 µm particle packed column. In general, the slope of the *C*-term is reduced for all columns because of the higher diffusion coefficient of the low molecular weight compound naphthalene.

An overview about the minimum reduced plate heights h_{min} is given in Table 3.3 for the apparent efficiency of the investigated columns in order to compare the different particle diameters and chromatographic supports in terms of the packing quality using Equation 3.3 [26].

$$h = \frac{H}{d_p} \; or \; \frac{H}{d_d} \qquad \textbf{Equation 3.3}$$

For the calculation of h_{min} for monolithic columns the domain size (d_d) is used instead of the particle diameter [25, 27].

Table 3.3: Comparison of the minimum reduced plate height h_{min} for etoposide (k=4) and naphthalene (k=11) for all investigated columns as well as the ratio between the column *i.d.* and particle diameter.

chromatographic support	Minimum reduced plate height h_{min}		Aspect ratio
	Etoposide (k=4)	Naphthalene (k=11)	d_c/d_p
fully porous, 3.0 µm	3.99	4.92	100
fully porous, 1.9 µm	2.56	3.48	158
monolithic[a)]	4.49*	3.79	-
core-shell, 2.7 µm	3.02	2.69	111

[a)] domain size: 3.38 µm [25, 27]

*H_{min} not reached

In Table 3.3 it can be seen that the obtained values for h_{min} strongly depend on the selected compound [26]. Comparing the minimum reduced plate height for the columns packed with 1.9 µm and 3.0 µm fully porous particles, significant differences for h_{min} are observed. Due to its lower h_{min}, it can be assumed that sub-2 µm particles can be packed more efficiently in 300 µm *i.d.* columns than the 3.0 µm particles. This seems surprising because the common opinion is that sub-2 µm particles are difficult to pack homogeneously [1]. One possible explanation for our results could be the aspect ratio between column *i.d.* and particle diameter

as shown in Table 3.3 which is more favorable for the 1.9 µm particles. In literature different results can be found for the influence of the aspect ratio on the reduced plate height when the column diameter is reduced at constant particle diameter. Whereas Eeltink et al. [28] found no influence of the aspect ratio for 75 - 150 µm columns, Kennedy et al. [29] and Patel et al. [3] found decreasing efficiency with increasing column diameter from 25 to 150 µm due to the increased radial diffusion time. To that end, decreasing the *i.d.* of the column to 300 µm has a negative influence on the achievable h_{min} when the particle diameter is constant compared to even smaller *i.d.* columns [11, 25]. However, the influence of the extra-column volume needs to be considered when different *i.d.* columns are compared on identical LC systems. Furthermore, the particle size distribution (*psd*) is a key parameter for the packing quality [6, 30]. Considering the data included in Table 3.3, pronounced differences for h_{min} between the column packed with 3.0 µm fully porous particles and the 2.7 µm core-shell particle packed column can be observed although the aspect ratio is almost constant. Since the *psd* is higher for 3.0 µm particles (d_{90}/d_{10} = 1.54), the obtained packing quality could be negatively influenced compared to the 2.7 µm core-shell particles (d_{90}/d_{10} = 1.16) [25]. Whereas Gritti et al. reported minor effects of *psd* for 4.6 mm i.d columns [31], Cabooter et al. found a clear relation between *psd* and column efficiency [32]. In general, the impact of large *psd* for decreased column *i.d.* could be more pronounced due to wall effects during the packing procedure. Commonly, a smaller *psd* is given as a reason why the packing of core-shell stationary phases is more uniform compared to fully porous particles leading to a reduced *A*-term contribution [6, 25, 33]. The efficiency of the monolithic column is comparable to 3.0 µm fully porous particles, which was also found by Olah et al. [25].

For well packed columns, the minimum reduced plate height should be between 2.0 and 2.5 [34]. Fekete et al. reported h_{min} values between 2.2 - 3.1 for various fully porous particle diameters between 1.5 - 3.0 µm packed into 2 - 2.1 mm *i.d.* columns [26]. Diószegi et al. investigated the column performance of 300 µm *i.d.* columns packed with 2.7 µm core-shell particles. The obtained h_{min} was 6.69 [35]. This value is much higher compared to other reported values below 2 for conventional column *i.d.* for the same stationary phase material. Gritti et al reported an h_{min} of 6.5 for a 500 µm i.d column packed with 2.7 µm core-shell particles [9].

In general, the column packed with 1.9 µm fully porous particles (h_{min} = 2.56) as well as the column packed with 2.7 µm core-shell particles (h_{min} = 2.69) are close to the optimal range for h_{min} considering the apparent efficiency. In addition, the h_{min} values obtained in our study are comparable to or even lower than the values reported by Fekete et al. for conventional column

i.d. packed with fully porous particles and Gritti et al. for the 500 µm *i.d.* column packed with 2.7 µm core-shell particles [9, 26]. Assuming a lower extra-column volume for the system used in our study, the apparent efficiency could be improved and therefore the value of h_{min} could be decreased. The influence of the extra-column volume will be discussed in more detail in the following section. Due to the superior performance (h_{min} = 2.56) of the column packed with fully porous 1.9 µm particles, the following investigations are focused on this column.

3.3.2 Extra-column contribution of chromatographic system

Over the last years, the influence of the extra-column volume in liquid chromatography on the obtained chromatographic efficiency has been extensively discussed in the literature when small *i.d.* columns became commercially available [5, 9, 36-39]. In general, the apparent column efficiency is always negatively affected by the total system variance ($\sigma^2_{v,ec}$) of the LC system including tubings ($\sigma^2_{v,ec,cap}$), injection valve and injection volume ($\sigma^2_{v,ec,inj}$) as well as the detector cell ($\sigma^2_{v,ec,det}$) and becomes more crucial when the peak volumes decrease [5]. The total band spreading due to the system volumes can be estimated using Equation 3.4.

$$\sigma^2_{v,ec} = \sigma^2_{v,ec,inj} + \sigma^2_{v,ec,cap} + \sigma^2_{v,ec,det} = \frac{V^2_{inj}}{12} + \sigma^2_{v,ec,cap} + \sigma^2_{v,ec,det} \qquad \textbf{Equation 3.4}$$

In order to determine the intrinsic efficiency the obtained efficiency values can be corrected for extra-column volume [38, 40]. This can be done by replacing the column by a zero dead volume (ZDV) union [36]. After this replacement, the flow-dependent experiments are repeated in order to determine the band spreading which is caused by the micro-LC system. The experimental extra-column volume, as depicted in Figure-S 3.3, was 0.0406 µL² at 15 µL min^{-1} without correcting for the injection plug.

Figure 3.2 shows the comparison of the apparent and intrinsic efficiency for naphthalene on the column packed with 1.9 µm particles at 30 °C. The intrinsic efficiency ($N_{intrinsic}$) was calculated according to Equation 3.5 [38].

$$N_{intrinsic} = 16 \cdot \frac{\left[t_{R,obs} - t_{0,ec}\right]^2}{w^2_{4\sigma,obs} - w^2_{4\sigma,ec}} \qquad \textbf{Equation 3.5}$$

where $t_{R,\mathrm{obs}}$ is the observed retention time, $t_{0,ec}$ the system void time, $w_{4\sigma,obs}$ the observed base peak width and $w_{4\sigma,ec}$ the observed extra-column peak width.

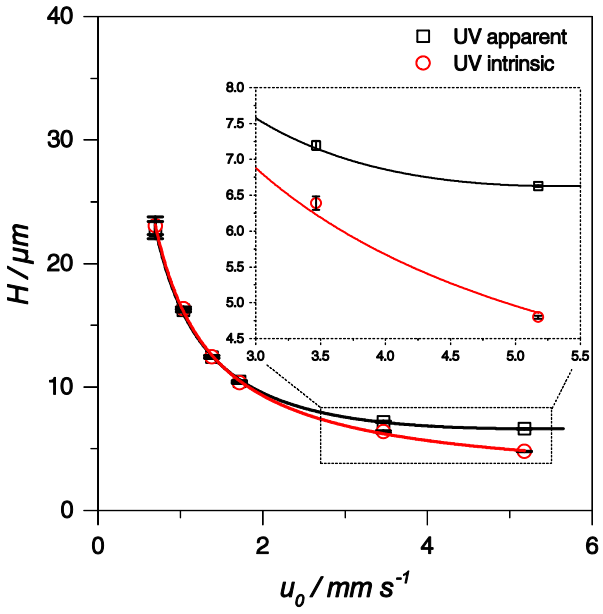

Figure 3.2: Comparison of the apparent and intrinsic van Deemter plots for naphthalene on the column packed with 1.9 µm fully porous particles. For mobile phase compositions, please refer to Table-S 3.1.

Figure 3.2 demonstrates that the negative influence of the extra-column volume causes a substantial loss in efficiency when the linear velocity is higher than 2.25 mm s^{-1} even for a *k* of 11. Comparing the values for *H* at 5.18 mm s^{-1} it can be calculated that only 72% of the intrinsic efficiency is achieved.

To improve the apparent efficiency, the *i.d.* of the connection tubings was decreased from 50 µm to 25 µm before and after the column. As can be seen from Figure-S 3.4, the influence of the tubing *i.d.* is negligible. One possible explanation could be the contribution of the injection valve and especially the influence of the injection volume. Considering Equation 3.4, the band broadening caused by the injection plug can be calculated. For an injection volume of 442 nL the resulting $\sigma^2_{v,ec,inj}$ is 1.63 10^{-2} µL² and therefore 40% of the total system variance. Consequently, the contribution of the injection volume is much more pronounced. Therefore, the injection volume should be decreased in order to represent the influence of the detection cell. Assuming an injection volume of 0.02 µL, the contribution of the injection plug can be reduced to $\sigma^2_{v,ec,inj}$ = 3.3 10^{-5} µL² to achieve larger apparent efficiencies.

3.3.3 Characterization of efficiency by kinetic plot analysis

The fundamentals for the kinetic plot theory were first developed by Giddings et al. [41] and Poppe et al. [42], before Desmet et al. established several versions of the kinetic plot data evaluation strategy for isocratic separations [15]. Using this kind of data analysis allows for a

fair comparison of efficiency for different chromatographic supports. In addition, practical information about the achievable efficiency in a given time can be obtained. To that end, the van Deemter data are transformed into so-called fixed length kinetic plots. By replacing the actual pressure drop of the analysis by a defined maximum pressure (ΔP_{max}), the fixed length kinetic plot can be transformed into a variable length kinetic plot using Equation 3.6 and Equation 3.7 in order to create the kinetic plot limit (*KPL*) curve [43, 44]. The permeability (K_{v0}) was calculated according to Equation 3.8.

$$t_0 = \frac{\Delta P_{max}}{\eta} \cdot \left[\frac{K_{v0}}{u_0^2}\right]_{exp} \quad \textbf{Equation 3.6}$$

$$N = \frac{\Delta P_{max}}{\eta} \cdot \left[\frac{K_{v0}}{u_0 \cdot H}\right]_{exp} \quad \textbf{Equation 3.7}$$

$$K_{v0} = \frac{u_0 \cdot \eta \cdot L}{\left(\Delta P_{total} - \Delta P_{system}\right)} \quad \textbf{Equation 3.8}$$

where η is the mobile phase viscosity. This curve illustrates the maximum achievable efficiency which can be reached for each stationary phase material in a given time at ΔP_{max} [45]. The comparison of the *KPL* curves allows for conclusions about the most efficient column and gives information about the corresponding column length. Figure 3.3 illustrates the resulting KPL curves for etoposide and naphthalene for a ΔP_{max} of 600 bar which corresponds to the maximum pressure of the column packed with 1.9 µm fully porous particles as specified by the manufacturer. In addition, Hara et al. very recently showed increased pressure capabilities for monolithic columns in capillary column formats up to 800 bar [14]. Furthermore, this ΔP_{max} is an appropriate assumption for a practically applied pressure drop.

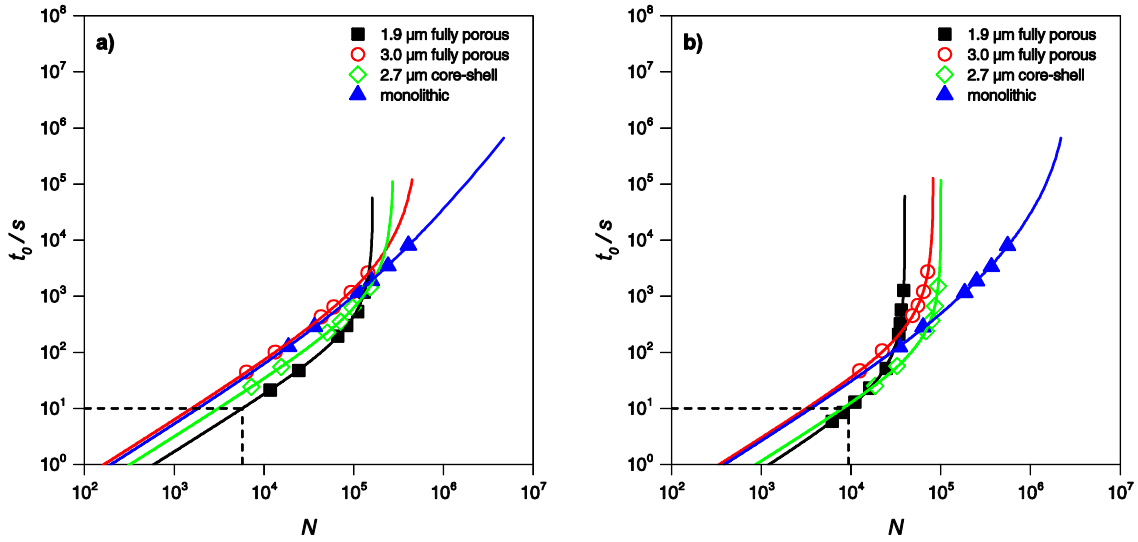

Figure 3.3: Kinetic plot for a) etoposide (k=4) and b) naphthalene (k=11) assuming a ΔP_{max} of 600 bar. The viscosity was calculated according to [22]. For mobile phase compositions, please refer to Table-S 3.1.

In the context of ultra-fast liquid chromatography, a column void time of 10 s maximum, which is highlighted by the dashed lines in Figure 3.3 a) and b), should be achieved. Within this region, the column packed with 1.9 µm fully porous particles shows superior efficiency compared to all other columns for etoposide and naphthalene. Even at a column void time of 1 s, the value of *N* is 1231 using a column length of 2.47 cm for naphthalene. All other columns have smaller values of *N* despite the longer corresponding column length. These results clearly show that sub-2 µm particles should be used for ultra-fast liquid chromatography. The first alternative for such applications is the column packed with 2.7 µm core-shell particles. At a column void time of 20 s, higher efficiency can be obtained using this stationary phase material for naphthalene. At this point it must be noted that these are extrapolated data and therefore should be interpreted with care. In addition, within this region the column length becomes very short, therefore extra-column contribution must be considered. In contrast, for ultra-high efficiency, the monolithic column exhibits superior performance. However, the consequence is increased analysis times. For a *k* of approximately 4, all columns show similar maximum efficiencies. Only at a t_0 larger than 10^4 s, the monolithic column outperforms all other stationary phases.

In Table 3.4, the values of *N* and corresponding column length (*L*) are calculated for a t_0 of 1 s and 10 s assuming three different scenarios for ΔP_{max}. A ΔP_{max} of 200 bar was chosen because it represents the maximum pressure of the monolithic column as specified by the manufacturer. In addition to the practical applied maximum pressure of 600 bar, a ΔP_{max} of 1,000 bar has been chosen because most UHPLC systems can be used at this pressure drop.

Table 3.4: Comparison of the maximum achievable efficiency at 200, 600 and 1,000 bar and a column void time of 10^0 s and 10^1 s for etoposide (k=4) and naphthalene (k=11). The viscosity was calculated according to [22].

t_0 / s	chromatographic support	compound etoposide k = 4						
		200 bar		600 bar		1,000 bar		efficiency gain
		N	L / cm	N	L / cm	N	L / cm	1,000 : 200 bar / %
10^0	1.9 µm [a]	591	1.38	596	2.39	597	3.08	0.90
	3.0 µm [a]	163	2.00	165	3.46	166	4.46	2.35
	monolithic	193	4.62	198	8.00	199	10.33	3.15
	2.7 µm [b]	319	1.93	322	3.33	323	4.30	1.38
10^1	1.9 µm [a]	5383	4.37	5760	7.55	5842	9.75	8.53
	3.0 µm [a]	1485	6.31	1571	10.93	1599	14.12	7.68
	monolithic	1723	14.60	1845	25.30	1887	32.66	9.52
	2.7 µm [b]	2971	6.09	3110	10.54	3150	13.61	6.05
t_0 / s	chromatographic support	compound naphthalene k = 11						
		200 bar		600 bar		1,000 bar		efficiency gain
		N	L / cm	N	L / cm	N	L / cm	1,000 : 200 bar / %
10^0	1.9 µm [a]	1147	1.43	1231	2.47	1250	3.19	9.03
	3.0 µm [a]	336	2.05	342	3.54	344	4.58	2.50
	monolithic	379	4.67	390	8.08	394	10.43	3.85
	2.7 µm [b]	859	1.97	873	3.42	876	4.41	2.02
10^1	1.9 µm [a]	6273	4.52	9393	7.82	10458	10.10	66.72
	3.0 µm [a]	2877	6.47	3197	11.21	3280	14.47	14.00
	monolithic	3303	14.76	3588	25.55	3687	33.00	11.63
	2.7 µm [b]	6988	6.24	8107	10.81	8377	13.96	19.88

a) fully porous particles, b) core-shell particles

Considering the data included in Table 3.4 it can be seen that for a t_0 of 1 s an increased ΔP_{max} results in almost no benefit on the achievable efficiency for etoposide with a k of approximately 4. This observation is not valid for naphthalene. For a k of 11, the efficiency of the column packed with 1.9 µm fully porous particles can be increased by 9%. One possible explanation

for the almost constant efficiency for all applied ΔP_{max} at a t_0 of 1 s could be the influence of the extra-column volume [36]. However, assuming a t_0 of 10 s, the increased ΔP_{max} leads to higher efficiency for all columns. This is more pronounced for naphthalene due to the higher retention factor. Nevertheless, for all applied pressure drops the column packed with 1.9 µm fully porous particles outperforms all other columns regardless which k and ΔP_{max} is adjusted. Therefore, the data contained in Table 3.4 support the results which can be derived from Figure 3.3 that the sub-2 µm particle packed column should be used for ultra-fast liquid chromatography in isocratic elution. However, for ultra-high efficiencies, the monolithic column provides the highest number of theoretical plates.

3.4 Conclusion

The results of the van Deemter analysis clearly show the superior performance of 1.9 µm fully porous particles. The calculated h_{min} is comparable or even decreased compared to conventional normal bore columns packed with sub-2 µm fully porous particles and definitely lower compared to all other reported values for micro-LC columns despite the higher extra column volume compared to Gritti et. al. An increased h_{min} was found for the 3.0 µm fully porous particle packed column as well as for the column packed with 2.7 µm core-shell particles compared to literature data for normal bore *i.d.* columns. One possible explanation could be the aspect ratio between the column *i.d.* and particle diameter. Nevertheless, the packing quality of 2.7 µm core-shell particles seems to be higher due to the narrower particle size distribution compared to 3.0 µm fully porous particles. Eliminating the extra-column band spreading and calculating the intrinsic efficiency, h_{min} is 2.1 for the 2.7 µm core-shell particle packed column which is within the optimum range as shown in Figure-S 3.5.

Kinetic plot studies were done to evaluate the performance for ultra-fast liquid chromatography. The results indicate that a higher pressure has a limited benefit for the achievable efficiency at a t_0 of 1 s especially when ΔP_{max} is increased from 600 to 1,000 bar. In following studies the system design will be optimized by reducing the injection volume and decreasing the detector cell contribution in order to achieve higher apparent efficiencies. In addition, the investigations will be expanded to gradient elution experiments.

3.5 Acknowledgements

The authors would like to thank all column manufacturers for the donation of information and columns. We would like to especially thank Dr. Friederike Becker (YMC Europe GmbH), Dr. Stephan Altmaier (Merck KGaA), Eike Logé and Dr. Peter Fischer (AB Sciex Deutschland

GmbH). Moreover, we would like to thank Dr. Steffen Wiese (Roche Diagnostics GmbH) as well as Prof. Deirdre Cabooter (KU Leuven) for the helpful comments and the fruitful discussion of the data.

3.6 References

[1] G. Desmet, S. Eeltink, Fundamentals for LC Miniaturization, Anal. Chem., 85 (2013) 543-556.
[2] W. De Malsche, S. De Bruyne, J.O. De Beek, P. Sandra, H. Gardeniers, G. Desmet, F. Lynen, Capillary liquid chromatography separations using non-porous pillar array columns, J. Chromatogr. A, 1230 (2012) 41-47.
[3] K.D. Patel, A.D. Jerkovich, J.C. Link, J.W. Jorgenson, In-depth characterization of slurry packed capillary columns with 1.0-mu m nonporous particles using reversed-phase isocratic ultrahigh-pressure liquid chromatography, Anal. Chem., 76 (2004) 5777-5786.
[4] Y.F. Shen, R. Zhao, S.J. Berger, G.A. Anderson, N. Rodriguez, R.D. Smith, High-efficiency nanoscale liquid chromatography coupled on-line with mass spectrometry using nanoelectrospray ionization for proteomics, Anal. Chem., 74 (2002) 4235-4249.
[5] S. Buckenmaier, C.A. Miller, T. van de Goor, M.M. Dittmann, Instrument contributions to resolution and sensitivity in ultra high performance liquid chromatography using small bore columns: Comparison of diode array and triple quadrupole mass spectrometry detection, J. Chromatogr. A, 1377 (2015) 64-74.
[6] N. Tanaka, D.V. McCalley, Core–Shell, Ultrasmall Particles, Monoliths, and Other Support Materials in High-Performance Liquid Chromatography, Anal. Chem., 88 (2016) 279-298.
[7] L. Novakova, A. Vaast, C. Stassen, K. Broeckhoven, M. De Pra, R. Swart, G. Desmet, S. Eeltink, High-resolution peptide separations using nano-LC at ultra-high pressure, J. Sep. Sci., 36 (2013) 1192-1199.
[8] J. Haun, J. Leonhardt, C. Portner, T. Hetzel, J. Tuerk, T. Teutenberg, T.C. Schmidt, Online and splitless nanoLC x capillaryLC with quadrupole/time-of-flight mass spectrometric detection for comprehensive screening analysis of complex samples, Anal. Chem., 85 (2013) 10083-10090.
[9] F. Gritti, G. Guiochon, Kinetic performance of narrow-bore columns on a micro-system for high performance liquid chromatography, J. Chromatogr. A, 1236 (2012) 105-114.
[10] S. Heinisch, G. Desmet, D. Clicq, J.L. Rocca, Kinetic plot equations for evaluating the real performance of the combined use of high temperature and ultra-high pressure in liquid chromatography - Application to commercial instruments and 2.1 and 1 mm ID columns, J. Chromatogr. A, 1203 (2008) 124-136.
[11] N.J. Wu, A.C. Bradley, Effect of column dimension on observed column efficiency in very high pressure liquid chromatography, J. Chromatogr. A, 1261 (2012) 113-120.
[12] D.S. Bell, R.E. Majors, Current state of superficially porous particle technology in liquid chromatography, Lc Gc N. Am., 33 (2015) 386.
[13] D. Cabooter, J. Billen, H. Terryn, F. Lynen, P. Sandra, G. Desmet, Detailed characterisation of the flow resistance of commercial sub-2 µm reversed-phase columns, J. Chromatogr. A, 1178 (2008) 108-117.
[14] T. Hara, S. Eeltink, G. Desmet, Exploring the pressure resistance limits of monolithic silica capillary columns, J. Chromatogr. A, 1446 (2016) 164-169.
[15] G. Desmet, D. Cabooter, K. Broeckhoven, Graphical data representation methods to assess the quality of LC columns, Anal. Chem., 87 (2015) 8593-8602.

[16] R.W. Brice, X. Zhang, L.A. Colon, Fused-core, sub-2 μm packings, and monolithic HPLC columns: a comparative evaluation, J. Sep. Sci., 32 (2009) 2723-2731.
[17] T. Hetzel, T. Teutenberg, T.C. Schmidt, Selectivity screening and subsequent data evaluation strategies in liquid chromatography: the example of 12 antineoplastic drugs, Analytical and Bioanalytical Chemistry, 407 (2015) 8475–8485.
[18] ChemSpider, http://www.chemspider.com, (accessed 09.06.2016)
[19] DrugBank, http://www.drugbank.ca/, (accessed 07.08.2016)
[20] D. Guillarme, S. Heinisch, J.L. Rocca, Effect of temperature in reversed phase liquid chromatography, J. Chromatogr. A, 1052 (2004) 39-51.
[21] Scifinder, https://www.scifinder.cas.org, (accessed 07.08.2016)
[22] C.V. McNeff, B. Yan, D.R. Stoll, R.A. Henry, Practice and theory of high temperature liquid chromatography, J. Sep. Sci., 30 (2007) 1672-1685.
[23] A. Vaast, K. Broeckhoven, S. Dolman, G. Desmet, S. Eeltink, Comparison of the gradient kinetic performance of silica monolithic capillary columns with columns packed with 3 μm porous and 2.7 μm fused-core silica particles, J. Chromatogr. A, 1228 (2012) 270-275.
[24] R. Russo, D. Guillarme, S. Rudaz, C. Bicchi, J.L. Veuthey, Evaluation of the coupling between ultra performance liquid chromatography and evaporative light scattering detector for selected phytochemical applications, J. Sep. Sci., 31 (2008) 2377-2387.
[25] E. Oláh, S. Fekete, J. Fekete, K. Ganzler, Comparative study of new shell-type, sub-2 μm fully porous and monolith stationary phases, focusing on mass-transfer resistance, J. Chromatogr. A, 1217 (2010) 3642-3653.
[26] S. Fekete, K. Ganzler, J. Fekete, Facts and myths about columns packed with sub-3 μm and sub-2 μm particles, J. Pharm. Biomed. Anal., 51 (2010) 56-64.
[27] S. Fekete, J. Fekete, K. Ganzler, Characterization of new types of stationary phases for fast liquid chromatographic applications, J. Pharm. Biomed. Anal., 50 (2009) 703-709.
[28] S. Eeltink, G.P. Rozing, P.J. Schoenmakers, W.T. Kok, Study of the influence of the aspect ratio on efficiency, flow resistance and retention factors of packed capillary columns in pressure- and electrically-driven liquid chromatography, J. Chromatogr. A, 1044 (2004) 311-316.
[29] R.T. Kennedy, J.W. Jorgenson, Preparation and evaluation of packed capillary liquid chromatography columns with inner diameters from 20 to 50 micrometers, Anal. Chem., 61 (1989) 1128-1135.
[30] K. Horvath, D. Lukacs, A. Sepsey, A. Felinger, Effect of particle size distribution on the separation efficiency in liquid chromatography, J. Chromatogr. A, 1361 (2014) 203-208.
[31] F. Gritti, T. Farkas, J. Heng, G. Guiochon, On the relationship between band broadening and the particle-size distribution of the packing material in liquid chromatography: Theory and practice, J. Chromatogr. A, 1218 (2011) 8209-8221.
[32] D. Cabooter, A. Fanigliulo, G. Bellazzi, B. Allieri, A. Rottigni, G. Desmet, Relationship between the particle size distribution of commercial fully porous and superficially porous high-performance liquid chromatography column packings and their chromatographic performance, J. Chromatogr. A, 1217 (2010) 7074-7081.
[33] J.J. DeStefano, S.A. Schuster, J.M. Lawhorn, J.J. Kirkland, Performance characteristics of new superficially porous particles, J. Chromatogr. A, 1258 (2012) 76-83.
[34] S. Fekete, K. Ganzler, J. Fekete, Efficiency of the new sub-2 μm core–shell (Kinetex™) column in practice, applied for small and large molecule separation, J. Pharm. Biomed. Anal., 54 (2011) 482-490.
[35] T.A. Diószegi, D.E. Raynie, Kinetic performance comparison of a capillary monolithic and a fused-core column in micro-scale liquid chromatography, J. Chromatogr. A, 1261 (2012) 107-112.

[36] S. Fekete, J. Fekete, The impact of extra-column band broadening on the chromatographic efficiency of 5 cm long narrow-bore very efficient columns, J. Chromatogr. A, 1218 (2011) 5286-5291.
[37] A. Prüß, C. Kempter, J. Gysler, T. Jira, Extracolumn band broadening in capillary liquid chromatography, J. Chromatogr. A, 1016 (2003) 129-141.
[38] N. Wu, A.C. Bradley, C.J. Welch, L. Zhang, Effect of extra-column volume on practical chromatographic parameters of sub-2-mum particle-packed columns in ultra-high pressure liquid chromatography, J Sep Sci, 35 (2012) 2018-2025.
[39] J. De Vos, K. Broeckhoven, S. Eeltink, Advances in ultrahigh-pressure liquid chromatography technology and system design, Anal. Chem., 88 (2016) 262-278.
[40] F. Gritti, G. Guiochon, Accurate measurements of the true column efficiency and of the instrument band broadening contributions in the presence of a chromatographic column, J. Chromatogr. A, 1327 (2014) 49-56.
[41] J.C. Giddings, Comparison of theoretical limit of separating speed in gas and liquid Chromatography, Anal. Chem., 37 (1965) 60-63.
[42] H. Poppe, Some reflections on speed and efficiency of modern chromatographic methods, J. Chromatogr. A, 778 (1997) 3-21.
[43] K. Broeckhoven, D. Cabooter, S. Eeltink, G. Desmet, Kinetic plot based comparison of the efficiency and peak capacity of high-performance liquid chromatography columns: Theoretical background and selected examples, J. Chromatogr. A, 1228 (2012) 20-30.
[44] A. Kurganov, A. Kanateva, E. Yakubenko, Application of kinetic plots in gas and liquid chromatography for the optimization of separation conditions, J. Sep. Sci., 39 (2016) 162-176.
[45] G. Desmet, D. Clicq, P. Gzil, Geometry-independent plate height representation methods for the direct comparison of the kinetic performance of LC supports with a different size or morphology, Anal Chem, 77 (2005) 4058-4070.

3.7 Chapter appendix

3.7.1 Analyte structure

Figure-S 3.1 shows the structural formulas of the investigated compounds.

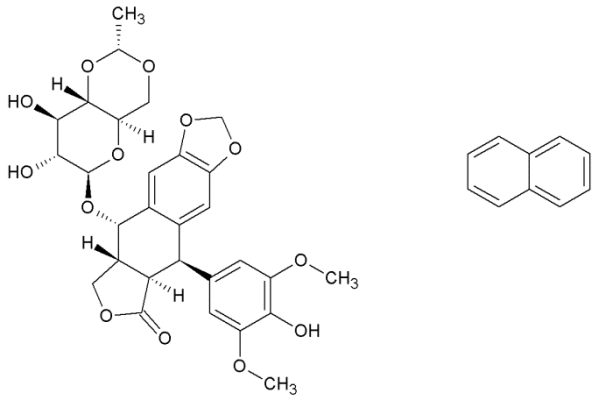

Figure-S 3.1: Structures of the investigated compounds: (1) etoposide and (2) naphthalene [1].

3.7.2 Mobile phase compositions

For the adjustment of the retention factor (*k*), the mobile phase composition was varied for every column according to Table-S 3.1.

Table-S 3.1: Overview of the mobile phase composition to adjust the retention factor for every column.

column	Mobile phase composition: water / acetonitrile (v/v) 30 °C	
	etoposide	naphthalene
Fully porous (50 x 0.3 mm, 1.9 µm)	72.2 / 27.8	58.2 / 41.8
Fully porous (50 x 0.3 mm, 3.0 µm)	72.2 / 27.8	57.4 / 42.6
Core-shell (50 x 0.3 mm, 2.7 µm)	75.0 / 25.0	59.8 / 40.2
Monolith (150 x 0.2 mm)	78.5 / 21.5	68.8 / 31.2

3.7.3 Peak shape study

In general, the peak shape is crucial for the investigation of column efficiency. Therefore, an optimization and critical evaluation of the peak shape is necessary. In particular, the

connections between the different parts of the micro-LC system are decisive. Different fitting and capillary technology was tested to improve the peak shape. Figure-S 3.2 illustrates two different peak profiles for naphthalene before and after optimization.

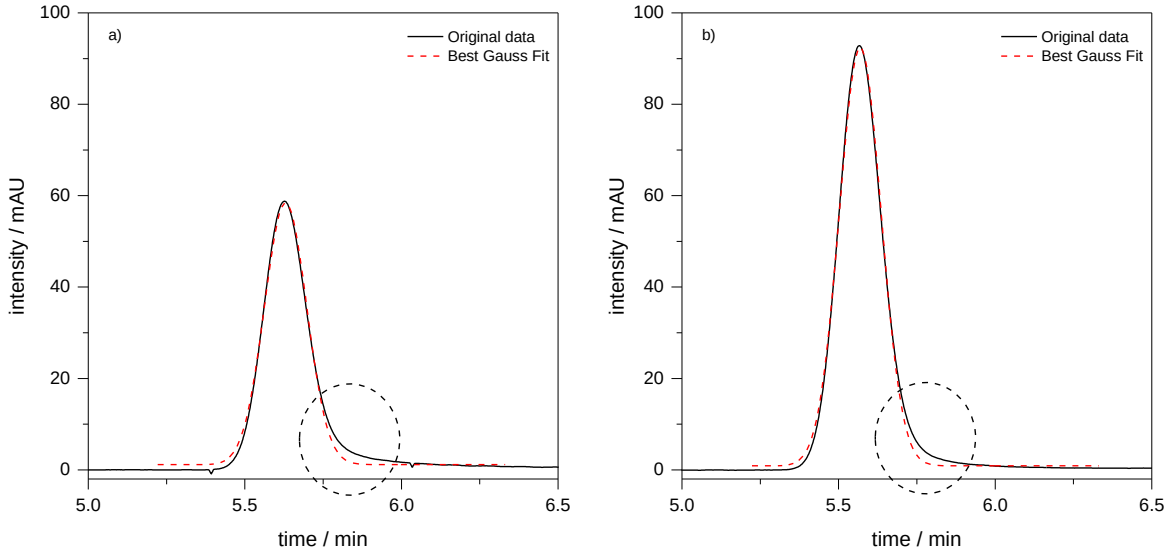

Figure-S 3.2: Comparison of a) the initial peak shape and b) optimized peak shape of naphthalene for a flow rate of 10 µL min^{-1}. Both peak profiles were measured on the column packed with 1.9 µm fully porous particles using the same injection volume.

Although the peak shape in Figure-S 3.2 a) is acceptable, a slight tailing can be observed as highlighted by the dashed circle. In contrast, the peak shape in Figure-S 3.2 b) shows almost a symmetric peak profile when compared to the best Gaussian fit using optimized connections. This optimization allows for a determination of column efficiency at peak base width.

3.7.4 Extra-column variance

Figure-S 3.3 shows the experimentally determined system extra column volume ($\sigma^2_{v,ec}$) for a flow rate range between 10 to 50 µL min^{-1}. For a flow rate of 15 µL min^{-1}, $\sigma^2_{v,ec}$ is 0.0406 µL^2.

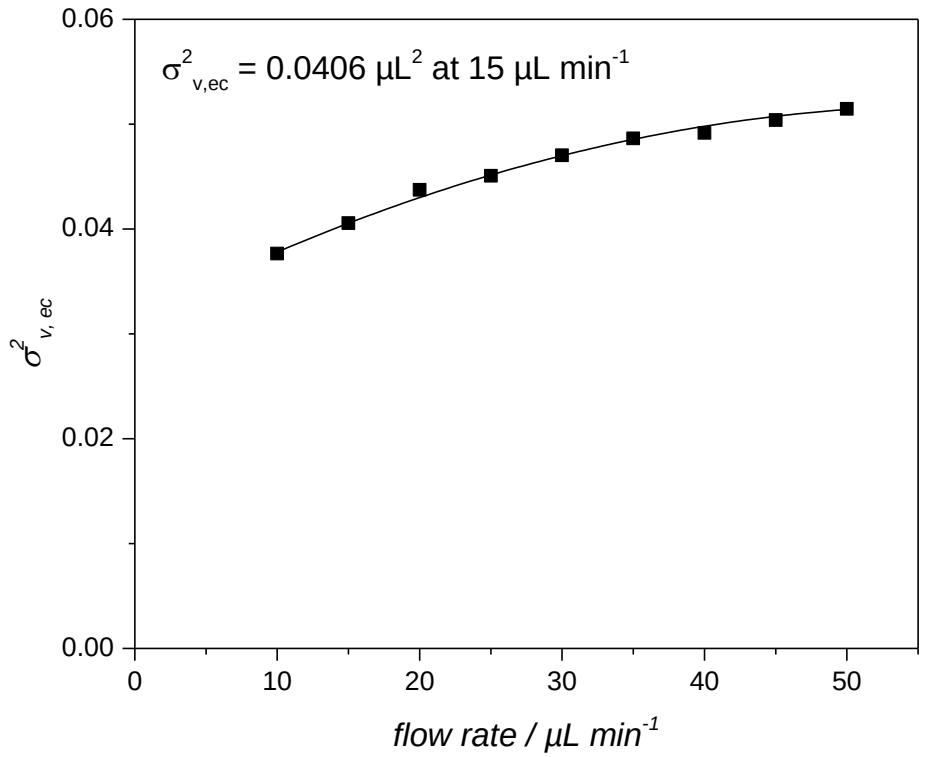

Figure-S 3.3: Experimentally determined system extra column volume ($\sigma^2_{v,ec}$) for a flow rate range between 10 to 50 µL min^{-1}.

3.7.5 Influence of the inner diameter of the connection tubing

To improve the apparent efficiency, the *i.d.* of the connection tubings was decreased from 50 µm to 25 µm before and after the column. Thereby, the extra-column volume contribution of the connection tubings was decreased by a factor of four. Figure-S 3.4 illustrates the comparison between the different tubing *i.d.* for naphthalene and etoposide at 30 °C.

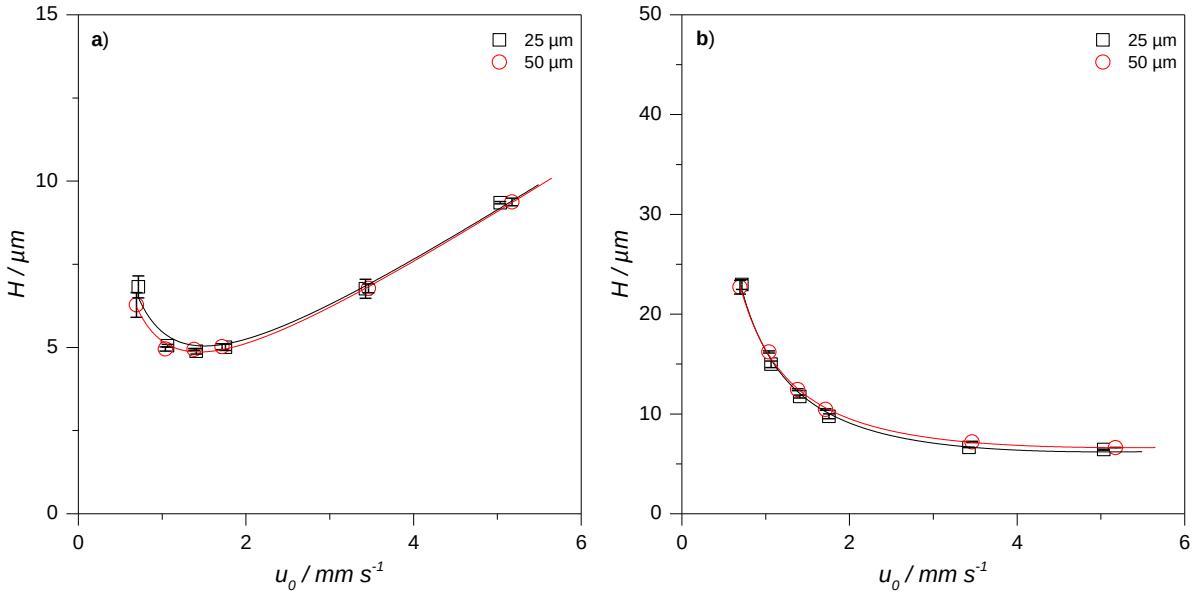

Figure-S 3.4: Comparison of the van Deemter curves for a) etoposide and b) naphthalene at 30 °C on the column packed with 1.9 µm fully porous particles using 25 µm and 50 µm *i.d.* connection tubings. For mobile phase compositions, please refer to Table-S 3.1.

As can be seen, varying the *i.d.* of the connection tubings has only a minor effect on the obtained efficiencies. Apparently, a slight loss of efficiency is only obtained if the flow rate is increased beyond the optimal linear velocity for the higher molecular weight compound. If the column is operated near u_{opt}, the *i.d.* of the connection tubing does not have a negative influence on the band spreading.

3.7.6 Intrinsic efficiency for 2.7 µm core-shell packed column

Figure-S 3.5 illustrates the comparison between the apparent and intrinsic efficiency for naphthalene on the column packed with 2.7 µm core-shell particles.

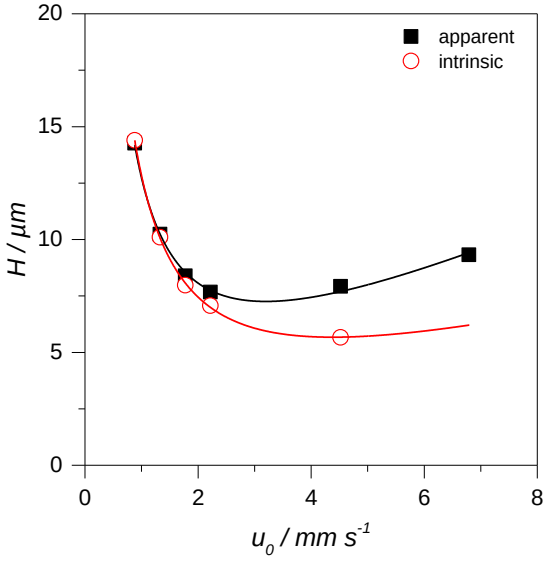

Figure-S 3.5: Comparison of the apparent and intrinsic efficiency for naphthalene on the column packed with 2.7 µm core-shell particles at 30 °C. For mobile phase compositions, please refer to Table-S 3.1.

By eliminating the influence of the extra-column volume contribution, the minimum reduced plate height (h_{min}) can be reduced from 2.69 to 2.10.

3.7.7 References

[1] ChemSpider, http://www.chemspider.com, (accessed 09.06.2016)

Chapter 4 Characterization of peak capacity of microbore liquid chromatography columns using gradient kinetic plots

Redrafted from "Hetzel, T., Blaesing, C., Jaeger, M., Teutenberg, T., Schmidt, T.C., Characterization of peak capacity of microbore liquid chromatography columns using gradient kinetic plots, Journal of Chromatography A, 1485 (2017) 62–69."

Abstract

The performance of micro-liquid chromatography columns with an inner diameter of 0.3 mm was investigated on a dedicated micro-LC system for gradient elution. Core-shell as well as fully porous particle packed columns were compared on the basis of peak capacity and gradient kinetic plot limits. The results for peak capacity showed the superior performance of columns packed with sub-2 µm fully porous particles compared to 3.0 µm fully porous and 2.7 µm core-shell particles within a range of different gradient time to column void time ratios. For ultra-fast chromatography a maximum peak capacity of 16 can be obtained using a 30 s gradient for the sub-2 µm fully porous particle packed column. A maximum peak capacity of 121 can be achieved using a 5 min gradient. In addition, the influence of an alternative detector cell on the basis of optical waveguide technology and contributing less to system variance was investigated showing an increased peak capacity for all applied gradient time / column void time ratios. Finally, the influence of pressure was evaluated indicating increased peak capacity for maximum performance whereas a limited benefit for ultra-fast chromatography with gradient times below 30 s was observed.

4.1 Introduction

Gradient elution in high performance liquid chromatography is nowadays the predominant separation mode [1]. The possibility to separate compounds with different physico-chemical properties in a single chromatographic run within a reasonable time frame favors its application in reversed liquid chromatography. Especially, the advantage of peak focusing related to peak compression in gradient elution methods is considered advantageous compared to isocratic separations [2]. During the last decade, the development of both instrument and column technology offered the opportunity to achieve fast and highly efficient separations due to increasing pressure capabilities of the chromatographic system including the stationary phase up to 1,500 bar [3]. To achieve even faster separations at lower flow rates, which is a prerequisite for coupling with mass spectrometry (*MS*), the column inner diameter (*i.d.*) was subsequently decreased from 4.6 mm to 2.0 mm. Currently, this trend continues to even smaller column *i.d.*s of 1.0 mm to 0.3 mm [4]. At the same time stationary phase materials, such as sub-2 µm fully porous particles with a minimum particle diameter (d_p) of 1.5 µm as well as core-shell particle packed columns with a d_p of 1.3 µm, were introduced to accomplish highly efficient separations and attain increased peak capacities in shorter analysis times when using decreased column *i.d.* and length [5-7]. To take full advantage of such small *i.d.* columns and subsequently small peak volumes, the system contribution to extra-column band broadening needs to be further minimized [8-12]. Especially, for miniaturized columns with an *i.d.* of 0.3 mm dedicated micro-LC systems have been developed. In particular, micro-LC systems are characterized by low gradient delay volumes allowing the use of fast cycle times of 30 s and smaller because of the immediate effectiveness of the solvent gradient. Due to the high linear velocities and decreased gradient delay volumes, fast separations and column re-equilibration can be achieved leading to reduced analysis cycle times, which is of utmost importance for routine analysis [7, 13]. These properties are also favorable for the applicability of micro-LC as a second dimension of an online comprehensive two-dimensional chromatography (LCxLC) system as has been recently shown by Haun and Leonhardt [14, 15]. In general, these benefits have been a major driver for implementing capillary columns - especially in combination with mass spectrometry - in different application areas [13, 16-18]. To circumvent possible column overloading, several investigations have explored means to overcome the limited loadability of small *i.d.* columns by temperature focusing, online solid phase extraction or direct large volume injection, illustrating the effort of optimizing this separation dimension [17, 19, 20].

However, only little information about systematic efficiency characterization in gradient elution is available for miniaturized columns packed with commercially available state-of-the-art particles [21]. Therefore, this contribution focuses on the question, which peak capacity can be obtained using 300 µm *i.d.* micro-LC columns packed with various chromatographic supports on a dedicated micro-LC system. Furthermore, the influence of different chromatographic supports varying in d_p is investigated with respect to applications requiring high peak capacities and therefore decreased gradient slopes. In addition, the range of ultra-fast chromatography with a maximum gradient time of 30 s for the applicability of online LCxLC and high throughput analysis is evaluated. Moreover, an alternative miniaturized detector cell based on optical waveguide technology was evaluated with respect to its influence on peak capacity to demonstrate the impact of reduced extra-column volume. For data evaluation, the peak capacity was determined and subsequently transformed into gradient kinetic plot limits.

4.2 Materials and methods

All experiments were performed on an Eksigent ExpressLC Ultra system (Sciex, Dublin, CA) with a micro-LC flow module (flow rate range: 5-50 µL min^{-1}). The pneumatic pump was capable of 690 bar maximum pressure. Flow calibration was carried out at a flow rate of 25 µL min^{-1}. The sample was loaded by an HTS PAL autosampler (CTC Analytics, Zwingen, Switzerland). The installed fused-silica, surrounded by a polyetheretherketone (PEEKSil) sample loop, had an inner diameter of 75 µm and a length of 10 cm. The sample was injected through a built-in six-port valve using the full loop injection mode of the software injecting 442 nL. An integrated static air column oven was used for temperature control of the stationary phase. For data acquisition, a built-in diode array detector (*DAD*) was employed with a cell volume of 100 nL as well as an alternative detector cell on the basis of optical waveguide technology with a cell volume of 6 nL (KNAUER, Berlin, Germany). Chromatograms were recorded at 272 nm with a data acquisition rate of 40 Hz and 50 Hz depending on the applied detector.

Fused-silica capillaries with an outer diameter (*o.d.*) of 360 µm and an inner diameter (*i.d.*) of 50 µm were used for the connection prior to and after the column with a length of 10 cm and 13 cm. Using sleeves, the *o.d.* was expanded to 1/32” for the connection to the columns and detectors. For data acquisition and analysis the Eksigent control software (Version 4.2 Patch for ekspert nanoLC 400 and batch acquisition control) and ClarityChrom (V. 6.1.0) were used.

Further data processing was performed using Origin Lab V. 9.3 and Microsoft Office Excel 2013. Table 4.1 presents an overview of the investigated columns.

Table 4.1: List of the investigated columns.

Description	surface modification	chromatographic support	end capping	L / mm	i. d. / mm	d_p / µm	pore diameter / Å	ΔP_{max}/ bar
Eksigent HALO	C18	core-shell	fully endcapped	50	0.3	2.7	90	690
YMC Triart	C18	fully porous	Multistage endcapped	50	0.3	1.9	120	600
YMC Triart	C18	fully porous	Multistage endcapped	50	0.3	3.0	120	550

i.d.: column inner diameter, L: column length, d_p: particle diameter, ΔP_{max}: maximum backpressure

Water and acetonitrile (ACN) were used as mobile phase constituents. In addition, acetone was used for the determination of the gradient delay volume. All solvents were purchased from Th. Geyer-Chemsolute (Renningen, Germany) with purity for LC-MS. Formic acid (*FA*), purchased from Sigma-Aldrich (Seelze, Germany), was used at 0.1% (v/v) as solvent additive to adjust the pH of the mobile phase and analyte mixture.

Table 4.2 contains the selected compounds including important physico-chemical properties, while the structural formulas are compiled in Figure-S 4.1. All compounds except uracil are pharmaceuticals and have different log P values and thus different polarity to obtain a uniform distribution over the entire gradient window, which is of utmost importance for an appropriate determination of peak capacity [21].

Table 4.2: List of the investigated compounds including CAS number, sum formula, molar mass and log P [22].

number	Compound	CAS	sum formula	purity / %	provider	M / g mol^{-1}	Log P	c / µg mL^{-1}
(1)	5-Fluorouracil	51-21-8	$C_4H_3FN_2O_2$	≥ 99	Fluka	130.08	0.86	5
(2)	Uracil	66-22-8	$C_4H_4N_2O_2$	≥ 99	Fluka	112.09	0.72	10
(3)	Methotrexate	59-05-2	$C_{20}H_{22}N_8O_5$	≥ 98	Fluka	454.44	-0.24	20
(4)	Etoposide	33419-42-0	$C_{29}H_{32}O_{13}$	≥ 98	Sigma	588.56	1.16	50
(5)	Diclofenac	15307-86-5	$C_{14}H_{11}Cl_2NO_2$	≥ 98.5	Sigma	296.15	4.26	10

The stock solutions for all analytes were prepared using a mixture of 50/50 H_2O/ACN (v/v) at a concentration of 1 mg mL^{-1}. For the analysis the single standards were merged before dilution with acidified water. The final concentrations are given in Table 4.2 with a composition of 96/4 H_2O/ACN + 0.1% FA (v/v).

For the determination of peak capacity, the flow rate was varied between 10 and 50 µL min^{-1} in 5-µL steps using a linear gradient from 5% to 95% B. The influence of the gradient slope was analyzed using four different gradient times (t_G). At a flow rate of 10 µL min^{-1}, t_G was set to 0.5, 1.0, 3.0 and 5.0 min. The first two gradient times were chosen to mimic ultra-fast chromatography whereas the latter two represent applications requiring high peak capacity. In order to ensure the same mobile phase history, the ratio between t_G and the column void time (t_0) needed to be kept constant. Therefore, the t_0 values were determined using uracil as column void marker at a mobile phase composition of 10/90 H_2O/ACN + 0.1% FA (v/v). Afterwards, the obtained t_0 times were corrected for the system void time ($t_{0,sys}$) by replacing the column by a zero-dead volume (*ZDV*) union. The gradient time was adjusted to ensure constant elution volumes resulting in gradient times between 5 s and 5 min depending on the column t_0 and flow rate (see Table-S 4.1 - Table-S 4.4). In addition, the ratio between the delay time (t_d) and t_0 had to be kept constant to obtain comparable results. Consequently, the gradient delay volume had to be determined. Therefore, the column was replaced by a *ZDV* union using water as mobile phase for both solvent channels. In order to illustrate the gradient profile, 0.1% acetone was added to the water of solvent channel B. The use of acetone was not considered critical because no on-line degasser was used. The gradient delay volume was determined at three different flow rates (10, 20 and 40 µL min^{-1}) using a plateau of 0.5 min followed by a 1.0 min linear gradient from 5% to 95% B. Afterwards, the gradient delay volume was corrected for the volumes of

the connection capillary after the column (V_{cap} = 255 nL) as well as for the detector cell volume (V_{det} = 100 nL). Since t_0 differed for all columns, an additional isocratic plateau (t_p) was added at the beginning of the analysis to obtain a constant ratio of t_d to t_0 of 2. In the following, t_d will be used as the sum of the gradient delay time (t_{dwell}) and t_p. All measurements were performed in triplicate at a column temperature of 30 °C.

4.3 Results and discussion

4.3.1 Determination of the gradient delay volume and retention factor

Since the ratio of t_d/t_0 had to be kept constant in order to provide comparable results, the gradient delay volume needed to be determined. This was achieved according to the procedure described in Chapter 4.2. Figure-S 4.2 shows the resulting gradient profile including the determination of the gradient delay volume for a flow rate of 40 µL min^{-1}. In order to characterize t_{dwell}, several determination strategies can be applied [23]. As can be identified in Figure-S 4.2, the point of intersection between the linear regressions of the isocratic plateau and linear gradient was used. Thereby, t_{dwell} is estimated to 0.06 min. After multiplication by the flow rate, the experimentally determined gradient delay volume ($V_{d,exp}$) needs to be corrected for the corresponding volumes of the capillary after the column (V_{cap}) as well as the detector cell volume (V_{det}) according to Equation 4.1 to obtain the corrected gradient delay volume ($V_{d,cor}$). Compared to conventional HPLC systems, this correction is mandatory due to the higher influence of these additional volumes.

$$V_{d,cor} = V_{d,exp} - V_{cap} - V_{det} \qquad \textbf{Equation 4.1}$$

After this correction, the final gradient delay volume amounted to 2 µL ± 4.3%, which is far below the gradient delay volume of conventional HPLC and UHPLC systems [24].

Another important parameter to ensure comparable results is the retention factor (k) of the first and last eluting compound. Broeckhoven et al. underlined the necessity of keeping these k values constant [25, 26]. Therefore, the retention factor at the point of elution (k_e) was calculated according to Equation 4.2 [27].

$$k_e = \frac{t_R - t_0}{t_0} \qquad \textbf{Equation 4.2}$$

Although Equation 4.2 is usually applied for isocratic elution, it can be used to verify if the adjustments of the gradient time depending on the column void time is appropriate. Further

explanations can be found in Chapter 4.7.2. When k_e is not constant for the analytes on different columns, the gradient profile can be modified to obtain similar values for k_e. Figure-S 4.3 exemplarily shows the k_e values obtained for the different columns, analytes and detector cells. As can be seen, no adjustment of the gradient slope is necessary since all analytes show similar retention behavior.

4.3.2 Determination of peak capacity

For the determination of peak capacity the compounds methotrexate, etoposide and diclofenac were used. The peak capacity ($n_{p,exp}$) was calculated according to the well-established Equation 4.3, using the gradient time (t_G) and the average peak width ($\overline{w}$) at the base [28, 29].

$$n_{p,exp} = 1 + \frac{t_G}{\overline{w}} \qquad \textbf{Equation 4.3}$$

After the determination of peak capacity, the obtained $n_{p,exp}$ can be plotted versus gradient time to evaluate the performance in gradient elution for the chromatographic support. Figure 4.1 a) shows the resulting plot of n_p versus t_G for the column packed with 3 µm fully porous particles using a t_G/t_0 ratio of 12 as illustrated by the squares.

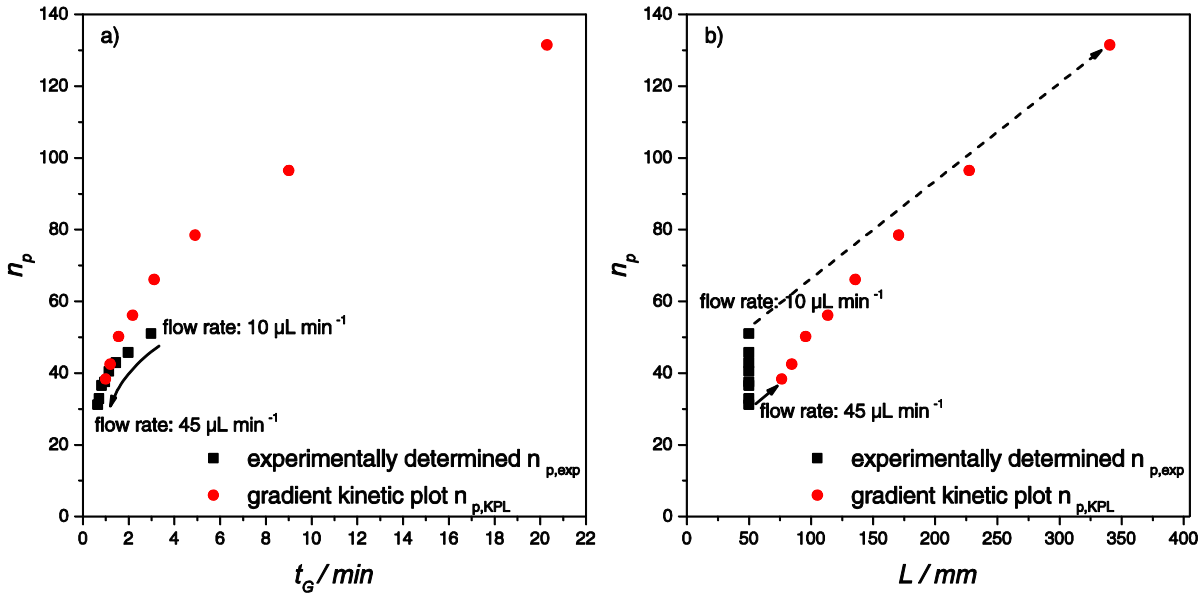

Figure 4.1: Comparison of the experimentally determined peak capacity and gradient kinetic plot limits for a maximum pressure of 600 bar for the column packed with 3 µm fully porous particles using a t_G/t_0 ratio of 12. a) experimentally obtained peak capacity (squares) and gradient kinetic plot limits (circles) versus the gradient time, the curved arrow illustrates the increase in flow rate, b) experimentally obtained peak capacity (squares) and gradient kinetic plot limits (circles) versus the column length, whereas the dashed arrow represents the corresponding column length for a flow rate of 10 µL min^{-1}, the full line arrow demonstrates the length elongation at a flow rate of 45 µL min^{-1} (n=3).

At a flow rate of 10 µL min^{-1} and a t_G of 2.98 min a peak capacity of 51 can be experimentally achieved. With increasing flow rate and thus decreasing t_G, the value for $n_{p,exp}$ decreases to 31 at a t_G of 0.65 min and a flow rate of 45 µL min^{-1} resulting in a ΔP_{max} of 469 bar as indicated by the arrow.

4.3.3 Transformation of peak capacity into gradient kinetic plots

In order to apply the kinetic plot analysis to gradient elution, the analytes have to experience the same relative mobile phase history [28, 29]. Therefore, the ratios between t_G/t_0 as well as t_d/t_0 must be kept constant. To demonstrate that the gradient kinetic plot method can also be applied to miniaturized columns, the transformation of $n_{p,exp}$ values into gradient kinetic plots limits ($n_{p,KPL}$) is shown in Figure 4.1 a) for the column packed with 3.0 µm fully porous particles for a t_G/t_0 ratio of 12 at a maximum backpressure (ΔP_{max}) of 600 bar as illustrated by the circles. The transformation was computed according to the Equation 4.4 - Equation 4.7 [28] introducing the length-elongation factor (λ).

$$\lambda = \frac{\Delta P_{max}}{\Delta P_{exp} - \Delta P_{ec}} \qquad \textbf{Equation 4.4}$$

$$n_{p,KPL} = 1 + \sqrt{\lambda} \cdot \left(n_{p,exp} - 1\right) \qquad \textbf{Equation 4.5}$$

$$t_{G,KPL} = \lambda \cdot t_{G,exp}$$ **Equation 4.6**

$$L_{KPL} = \lambda \cdot L_{exp}$$ **Equation 4.7**

where ΔP_{exp} is the experimental pressure drop, ΔP_{ec} the extra-column backpressure both at maximum viscosity, $t_{G,exp}$ and L_{exp} the experimental gradient time and column length, $t_{G,KPL}$ and L_{KPL} the corresponding gradient time and column length of the gradient kinetic plot. As can be seen from Figure 4.1 a), the maximum peak capacity $n_{p,KPL}$ can be increased to 130 using a gradient time of approximately 20 min but at the same time the column length needs to be increased to 34 cm as indicated by the dashed arrow in Figure 4.1 b) where the peak capacity is plotted against the column length. The peak capacity can thus be increased by a factor of 2.6 by maximizing the column length until the maximum pressure is obtained. At the same time, the gradient time increases by a factor of 6.8, which reduces sample throughput. On the other hand for an increased flow rate of 45 µL min^{-1}, $n_{p,KPL}$ is 38 and thus 20% higher compared to $n_{p,exp}$ as demonstrated by the full line arrow because the maximum pressure of 550 bar is not achieved during the experiments at the applied flow rate as shown above. At this point, it must be noted that the packing of such columns length is challenging. However it would be possible to couple already available column lengths like three times 10 cm and one 5 cm long column in order to obtain a column length of 35 cm.

4.3.4 Comparison of chromatographic supports for maximum peak capacity

For the investigation of maximum peak capacity depending on the applied chromatographic support, the results for the flattest gradient slope of 18% B min^{-1} resulting in a t_G/t_0 ratio of 20 are evaluated. Figure 4.2 shows the peak capacities $n_{p,exp}$ and $n_{p,KPL}$ obtained for a ΔP_{max} of 600 bar. The results for all remaining t_G/t_0 ratios are given in the supplementary material (Figure-S 4.4 - Figure-S 4.6).

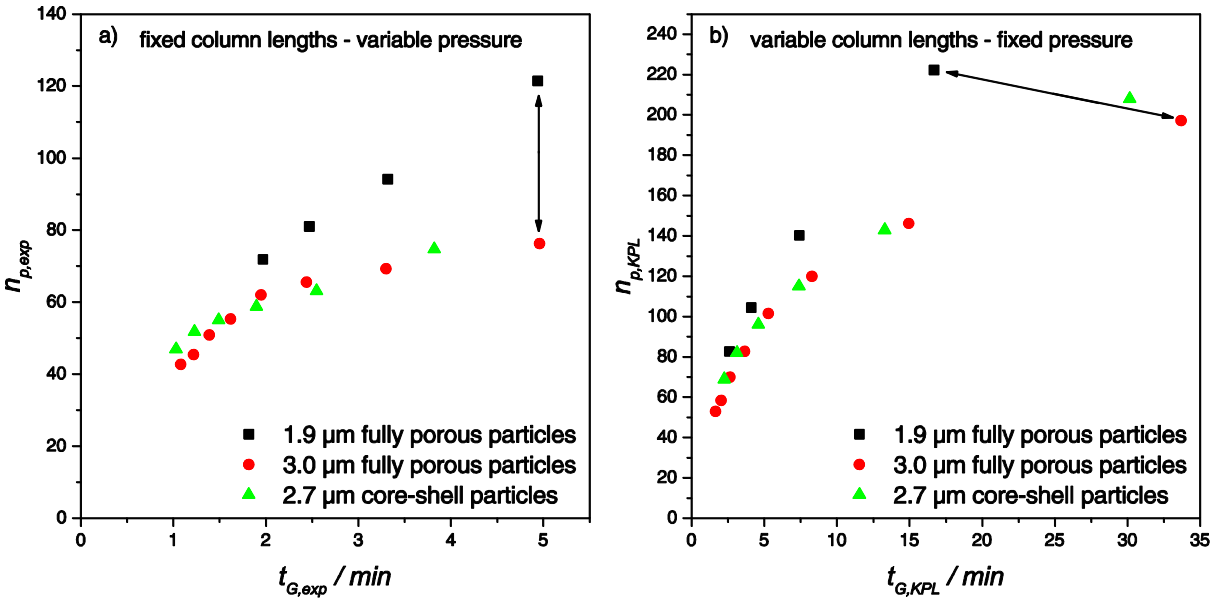

Figure 4.2: Comparison of peak capacity for the different chromatographic supports at t_G/t_0 of 20. a) experimentally obtained peak capacities and b) gradient kinetic plot limits for a maximum pressure of 600 bar. The full line arrows are used for the comparison of the peak capacity achieved for the 1.9 µm and 3.0 µm fully porous particle packed column (n=3).

It can be recognized from Figure 4.2 a) that the column packed with 1.9 µm fully porous particles is superior to the other stationary phase materials over the gradient time between 2 min to 5 min with a maximum pressure of 472 bar at 25 µL min^{-1}. By changing the particle diameter from 3.0 µm to 1.9 µm, the maximum peak capacity $n_{p,exp}$ can be increased from 76 to 121, thus by 59%, in the same t_G as indicated by the arrows. The result is different when considering $n_{p,KPL}$ in Figure 4.2 b). By maximizing the column length until the maximum pressure is obtained, the increase in peak capacity when using the 1.9 µm instead of the 3.0 µm fully porous particles is only 12.7%. In order to obtain such a high peak capacity for the 3.0 µm fully porous particles, the gradient time needs to be increased by a factor of 2 indicating a higher peak capacity production rate for the 1.9 µm fully porous particle packed column which is specified in Equation 4.8. Therefore, sub-2 µm particles should be chosen for the applied t_G/t_0 ratio. The column packed with 2.7 µm core-shell particles shows similar values for $n_{p.exp}$ as well as for $n_{p,KPL}$ compared to the 3.0 µm fully porous particle packed column. This is rather unexpected, since several studies showed similar performance of 2.7 µm core-shell particles to sub-2 µm fully porous particle and superior efficiency compared to 3.0 µm fully porous particle packed columns under gradient elution conditions for normal bore inner diameter columns [30, 31]. In addition, the performance and packing quality was investigated for isocratic elution in a previous study, indicating a more homogenous packing quality of the core-shell column compared to the 3.0 µm fully porous particle packed column [32]. One possible reason could

be the influence of the extra-column volume due to the reduced internal volume of 1.84 µL for the 2.7 µm core-shell particle packed column compared to 2.43 µL for the 3.0 µm fully porous particle packed column indicating a more favourable extra-column to column volume ratio for the fully porous particle packed column. However, Vaast et al. also found comparable peak capacities for 2.7 µm core-shell and 3.0 µm fully porous particle packed columns with an *i.d.* of 0.1 mm using the same t_G/t_0 ratio [21]. In addition, the peak capacity obtained in that study is comparable to the 3.0 µm fully porous particles for a t_G/t_0 of 20 of our study. Furthermore, the obtained peak capacity can be compared to conventional column *i.d.* to evaluate the performance of already established column dimensions. As a tool for better comparison, the peak capacity production rate (ξ) is calculated according to Equation 4.8 [21].

$$\xi = \frac{n_p}{t_G} \qquad \textbf{Equation 4.8}$$

Zhang et al. reached a ξ of 0.42 s^{-1} and 0.58 s^{-1} for a 50 x 2.1 mm column packed with 1.7 µm fully porous and 2.7 µm core-shell particles [33]. The peak capacity production rate for the miniaturized column packed with 1.9 µm fully porous particles amounts to 0.41 s^{-1} and becomes therefore very close to the even smaller fully porous particles of 1.7 µm used in that study. In contrast, the 0.3 mm *i.d.* column packed with 2.7 µm core-shell particles shows a ξ of only 0.33 s^{-1} and therefore less efficiency compared to the normal bore *i.d.* column underlining the above statement of poor performance in gradient elution.

Due to the superior peak capacity of the column packed with 1.9 µm fully porous particles, this column was selected for the following investigations. In particular, the influence of the gradient slope was a goal of the analyses to demonstrate the potential for faster analysis times, which is of utmost importance for routine analysis to increase sample throughput as well as for online comprehensive two-dimensional chromatography.

4.3.5 Influence of the gradient slope

For the evaluation of the influence of the gradient slope on peak capacity, the results for the different t_G/t_0 ratios are shown in Figure 4.3 for the column packed with 1.9 µm fully porous particles, whereas the results for all other chromatographic supports can be found in the supplementary material (Figure-S 4.7 - Figure-S 4.8). A t_G/t_0 of 12 and 20 was assumed for high peak capacity requiring applications whereas the range of ultra-fast chromatography is represented by a t_G/t_0 of 2 and 4.

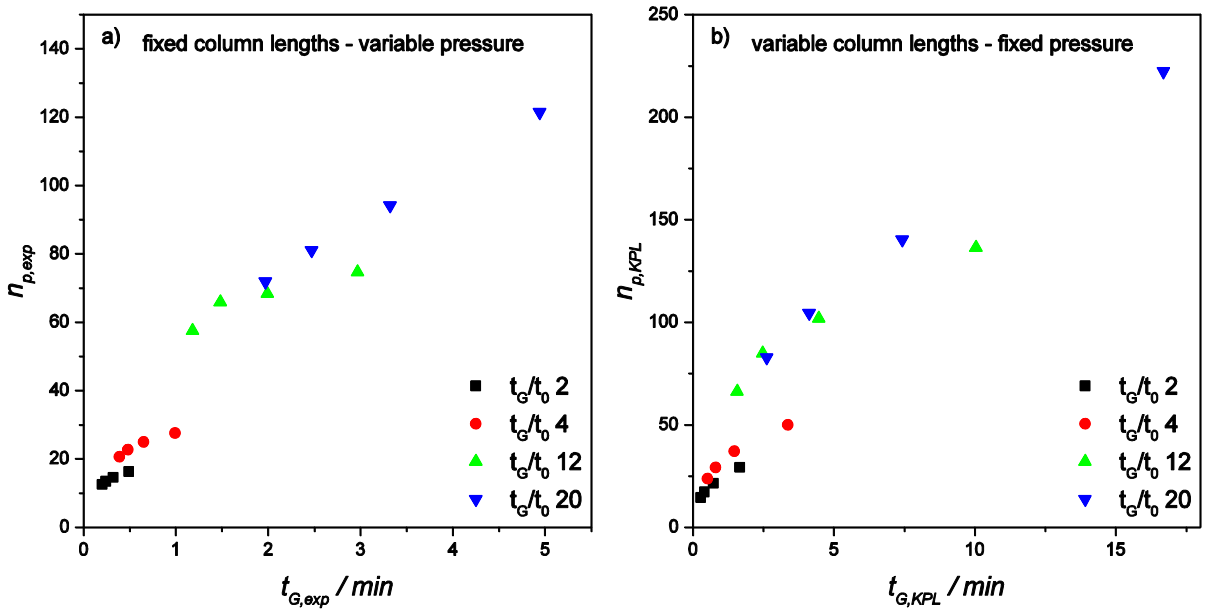

Figure 4.3: Influence of the gradient slope on peak capacity for four different t_G/t_0 ratios a) experimentally obtained peak capacities and b) gradient kinetic plot limits for a maximum pressure of 600 bar for the column packed with 1.9 µm fully porous particles.

Figure 4.3 a) shows the resulting $n_{p,exp}$ values for t_G/t_0 ratios of 2, 4, 12 and 20. As expected, higher peak capacities can be achieved with decreasing gradient slope. Within a 5 min gradient a peak capacity of 121 can be obtained at the lowest flow rate. The value of $n_{p,exp}$ decreases subsequently to 27 using a 1 min gradient time at the same flow rate. However, even at a t_G of 30 s, a peak capacity of 16 can still be achieved at a flow rate of 10 µL min^{-1}. Considering the gradient kinetic plot in Figure 4.3 b) for a ΔP_{max} of 600 bar, the maximum peak capacity can be increased to 225, whereas the value of $n_{p,KPL}$ can be raised to almost 30 compared to an $n_{p,exp}$ of 16 for a t_G/t_0 of 2 by maximizing the column length until the maximum pressure is obtained.

In particular, the t_G/t_0 ratio of 2 is of interest for ultra-fast chromatography and high throughput analysis as well as for online LCxLC. Therefore, one opportunity to increase peak capacity is evaluated by reducing the extra-column volume after the column, since the performance in gradient elution is mainly affected by this dispersion assuming sufficient retention for the investigated analytes. This was investigated using an alternative detector cell with less contribution to system variance.

4.3.6 Influence of the detector cell contribution

As mentioned above, micro-LC can be used as the second dimension of online LCxLC systems [14]. One prerequisite is a very fast cycle time in the second dimension. To achieve such fast cycle times, a maximum gradient time of 30 s is required which is represented by a t_G/t_0 ratio

of 2 at a flow rate of 10 µL min^{-1}. For such steep gradients with a gradient slope of 3.0% B s^{-1} at 10 µL min^{-1} to 7.6% B s^{-1} at 25 µL min^{-1}, the optimization of the extra-column band broadening is mandatory due to the small resulting peak volumes and peak widths to ensure highly efficient separations. The built-in UV detector with a volume of 100 nL was hence replaced by an alternative UV detector on the basis of an optical waveguide with an *i.d.* of 50 µm and a cell volume of only 6 nL. Thereby the extra-column contribution can be significantly reduced but at the same time the signal-to-noise ratio decreases by the factor approximately 130. Figure 4.4 shows the resulting peak capacities for a t_G/t_0 ratio of 2 whereas all other ratios can be found in the supplementary material (Chapter 4.7.5).

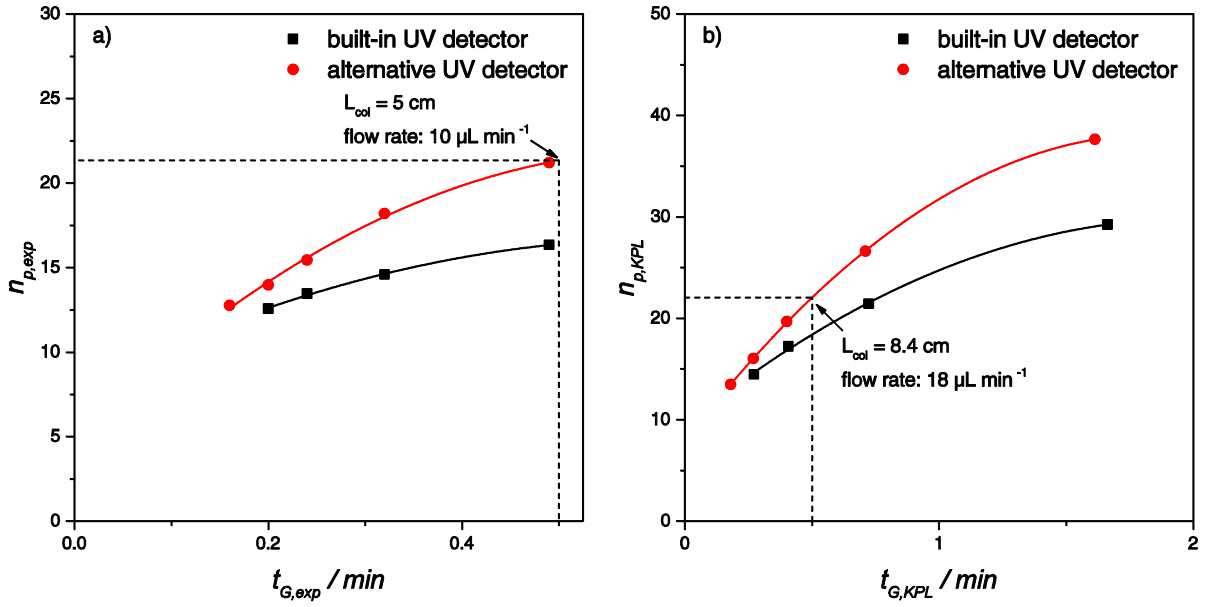

Figure 4.4: Comparison of peak capacity for the built-in and alternative UV detector for the column packed with 1.9 µm fully porous particles at a t_G/t_0 of 2. a) experimentally obtained peak capacity, b) gradient kinetic plot limits (n=3). Best fit lines are displayed as well.

As can be seen, the use of the alternative detector cell has a positive effect on the experimentally obtained peak capacity for all investigated t_G/t_0 ratios (see also Figure-S 4.9 - Figure-S 4.11 a). In addition, the influence is more pronounced for t_G/t_0 2 and 4 as the peak width for the increased gradient slopes is smaller and the generated bands are thus more vulnerable to extra-column band broadening compared to the bands generated at flatter gradient slopes. Moreover, it can be noted that the increase in $n_{p,exp}$ decreases at elevated flow rates. This is attributed to the fact that the band broadening in the connection tubing depends on the flow rate [9]. When comparing the maximum peak capacities for the different gradient slopes, an increase of 30% can be achieved for the highest gradient slope (Figure 4.4 a), whereas for the flatter slope (Figure-S 4.11 a) only an improvement of 21% can be obtained. For the different flow rates

within the t_G/t_0 2 ratio, the improvement in peak capacity decreased from 30% to 11%. For the flatter slope, the increase is only 6% at the highest flow rate (Figure-S 4.11 a). However, it can be clearly demonstrated that a minimization of the extra-column volume is also necessary for gradient elution, especially when steep gradient slopes are applied. The same result was also observed by Vanderlinden et al. for a 2.1 mm i.d column packed with 1.3 µm core-shell particles [9].

Finally, the experimentally obtained peak capacities of Figure 4.4 a) are transformed into $n_{p,KPL}$ at a maximum pressure of 600 bar to demonstrate the potential of the chromatographic support at ΔP_{max} illustrated in Figure 4.4 b). The same trends can be identified for the gradient kinetic plots. At a ΔP_{max} of 600 bar, the maximum achievable peak capacity is 263 for a t_G/t_0 ratio of 20 using the alternative detector cell (Figure-S 4.11 b). For the highest gradient slope in Figure 4.4 b), a maximum $n_{p,KPL}$ of 37 can be obtained for the detector cell based on optical waveguide technology and a column length of 16.4 cm. Yet, the resulting t_G is 1.6 min and thus three times larger than specified for the maximum gradient time in the second dimension for online LCxLC. Considering a maximum t_G of 30 s, the comparison between Figure 4.4 a) and b) clearly shows that no benefit on peak capacity can be achieved at a ΔP_{max} of 600 bar despite the longer column length of 8.4 cm compared to the 5 cm column as indicated by the dashed lines and full lined arrows. However, the same peak capacity can be achieved at a higher flow rate and thus at a higher linear velocity. Whereas the flow rate is 10 µL min^{-1} for the 5 cm column, the flow rate can be increased to 18 µL min^{-1} for a 8.4 cm column. Although no benefit can be obtained with respect to the efficiency, the increased flow rate leads to a decreased gradient delay and column equilibration time, which is favourable for faster analysis cycle times. As a consequence, the sample throughput can be increased. At last, the influence of pressure on $n_{p,KPL}$ will be investigated for the t_G/t_0 2 using the alternative detector cell.

4.3.7 Investigation of pressure for ultra-fast chromatography

Another approach to increase the maximum peak capacity is the increase of ΔP_{max} [8]. Therefore, the influence of an increased ΔP_{max} is evaluated. In Figure 4.5 the resulting $n_{p,KPL}$ are depicted for a ΔP_{max} of 600, 1,000 and 1,500 bar using the alternative UV detector cell. A ΔP_{max} of 600 bar represents the maximum backpressure of the column packed with 1.9 µm fully porous particles as specified by the manufacturer. Increased pressure limits, i.e. 1,000 and 1,500 bar were used, since several UHPLC systems allow the use of such high pressures [3].

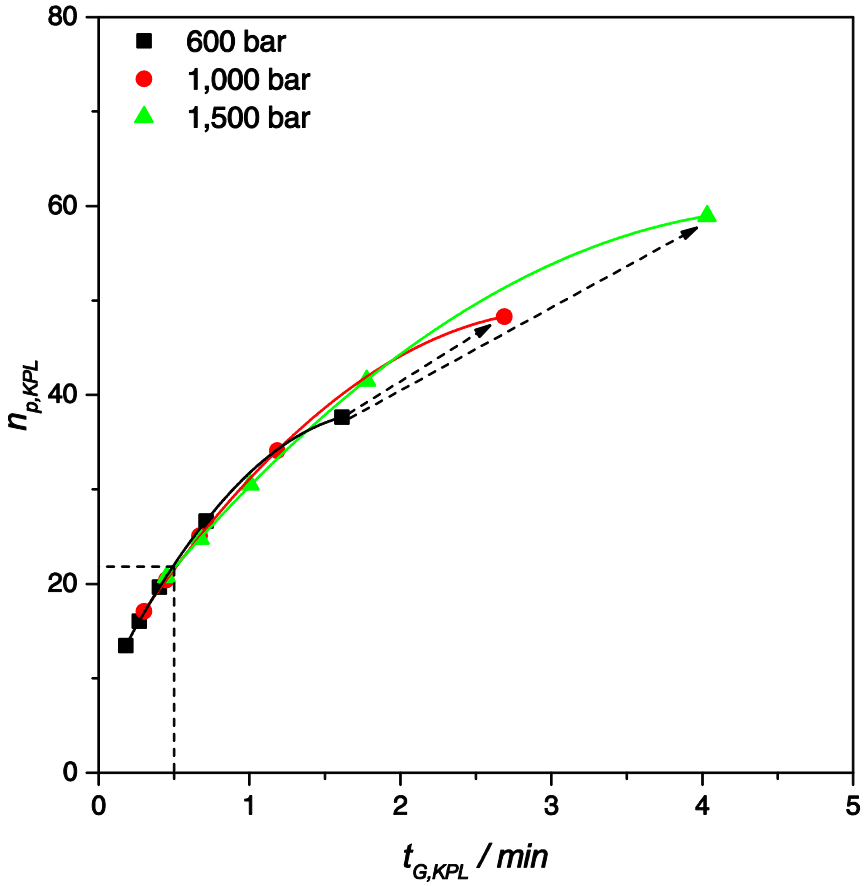

Figure 4.5: Comparison of the resulting gradient kinetic plot limits for a t_G/t_0 of 2 and a maximum pressure of 600, 1,000 and 1,500 bar on the column packed with 1.9 µm fully porous particles using the alternative detector cell. Best fit lines are displayed as well.

As can be recognized from Figure 4.5, the maximum $n_{p,KPL}$ can be increased due to the larger t_G and column length as indicated by the dashed arrows. Identical results were found by De Vos et al. [3, 8]. At a $t_{G,KPL}$ of 30 s, the influence is limited despite the longer column, which increases from 8.4 cm for a ΔP_{max} of 600 bar to 11.8 cm for a maximum pressure of 1000 bar and 14.5 cm for a ΔP_{max} of 1500 bar, as highlighted by the dashed lines. The only advantage is attributed to the higher linear velocity as already discussed above. At this point it should be noted that temperature effects due to frictional heating should be taken into account [34]. While the influence of frictional heating is reduced for miniaturized columns due to increased heat dissipation [4, 18, 35], the influence needs to be further analyzed. Nevertheless, it can be demonstrated that the influence of a very high inlet pressure for ultra-fast chromatography is limited for gradient times below 1.5 min. The same result was also obtained for the efficiency of isocratic separations at a column void time of 1 s [32].

4.4 Conclusion

The peak capacity as well as the results of the gradient kinetic plot limits indicate the superior performance of sub-2 µm fully porous particles for all applied t_G/t_0 ratios compared to all other chromatographic supports. In general, flatter gradient slopes in combination with low flow rates lead to increased peak capacity. Compared to normal bore *i.d.* columns, similar peak capacity production rates can be obtained for sub-2 µm fully porous particles. However, the performance of 2.7 µm core-shell particles is comparable to 3.0 µm fully porous particles and is therefore decreased when compared to conventional column *i.d.* For the range of ultra-fast chromatography with a t_G of 30 s, the sub-2 µm fully porous particle packed column provides a peak capacity of 16. When reducing the extra-column volume by decreasing the detector cell volume, an increase of 30% can be achieved. In general, the influence of the extra-column volume contribution can also be demonstrated for gradient elution, especially when sharp peak profiles with peak widths below 2 s are obtained due to increased gradient slopes. The results of the gradient kinetic plot limits clearly demonstrate that increased pressure capabilities are beneficial for the increase in maximum peak capacity due to the longer column length for all t_G/t_0 ratios. However, the gain in peak capacity is limited for the range of ultra-fast chromatography (t_G below 30 s). In future studies, the system design will be optimized and expanded to temperature depending gradient kinetic plots to further improve peak capacity. Thereby, the pressure drop can be significantly reduced allowing the use of longer columns at the maximum pressure [36].

4.5 Acknowledgements

The authors would like to thank all column manufacturers for the donation of information and columns. We would like to especially thank Dr. Friederike Becker (YMC Europe GmbH), Eike Logé and Dr. Peter Fischer (AB Sciex Deutschland GmbH) as well as Dr. Kate Monks (KNAUER Wissenschaftliche Geräte GmbH).

4.6 References

[1] V. Gonzalez-Ruiz, A.I. Olives, M.A. Martin, Core-shell particles lead the way to renewing high-performance liquid chromatography, Trac-Trends in Analytical Chemistry, 64 (2015) 17-28.

[2] A.P. Schellinger, P.W. Carr, Isocratic and gradient elution chromatography: A comparison in terms of speed, retention reproducibility and quantitation, J. Chromatogr. A, 1109 (2006) 253-266.

[3] J. De Vos, M. De Pra, G. Desmet, R. Swart, T. Edge, F. Steiner, S. Eeltink, High-speed isocratic and gradient liquid-chromatography separations at 1500 bar, J. Chromatogr. A, 1409 (2015) 138-145.
[4] F. Gritti, T. McDonald, M. Gilar, Intrinsic advantages of packed capillaries over narrow-bore columns in very high-pressure gradient liquid chromatography, J. Chromatogr. A, 1451 (2016) 107-119.
[5] S. Fekete, D. Guillarme, Possibilities of new generation columns packed with 1.3 μm core–shell particles in gradient elution mode, J. Chromatogr. A, 1320 (2013) 86-95.
[6] S. Fekete, D. Guillarme, Kinetic evaluation of new generation of column packed with 1.3 μm core–shell particles, J. Chromatogr. A, 1308 (2013) 104-113.
[7] D. Guillarme, J. Ruta, S. Rudaz, J.L. Veuthey, New trends in fast and high-resolution liquid chromatography: a critical comparison of existing approaches, Analytical and Bioanalytical Chemistry, 397 (2010) 1069-1082.
[8] K. Broeckhoven, G. Desmet, The future of UHPLC: Towards higher pressure and/or smaller particles?, Trac-Trends in Analytical Chemistry, 63 (2014) 65-75.
[9] K. Vanderlinden, K. Broeckhoven, Y. Vanderheyden, G. Desmet, Effect of pre- and post-column band broadening on the performance of high-speed chromatography columns under isocratic and gradient conditions, J. Chromatogr. A, 1442 (2016) 73-82.
[10] S. Buckenmaier, C.A. Miller, T. van de Goor, M.M. Dittmann, Instrument contributions to resolution and sensitivity in ultra high performance liquid chromatography using small bore columns: Comparison of diode array and triple quadrupole mass spectrometry detection, J. Chromatogr. A, 1377 (2015) 64-74.
[11] S. Fekete, J. Fekete, The impact of extra-column band broadening on the chromatographic efficiency of 5 cm long narrow-bore very efficient columns, J. Chromatogr. A, 1218 (2011) 5286-5291.
[12] F. Gritti, G. Guiochon, Kinetic performance of narrow-bore columns on a micro-system for high performance liquid chromatography, J. Chromatogr. A, 1236 (2012) 105-114.
[13] T. Hetzel, C. vom Eyser, J. Tuerk, T. Teutenberg, T.C. Schmidt, Micro-liquid chromatography mass spectrometry for the analysis of antineoplastic drugs from wipe samples, Analytical and Bioanalytical Chemistry, 408 (2016) 8221–8229.
[14] J. Haun, J. Leonhardt, C. Portner, T. Hetzel, J. Tuerk, T. Teutenberg, T.C. Schmidt, Online and splitless nanoLC x capillaryLC with quadrupole/time-of-flight mass spectrometric detection for comprehensive screening analysis of complex samples, Anal. Chem., 85 (2013) 10083-10090.
[15] J. Leonhardt, T. Teutenberg, G. Buschmann, O. Gassner, T.C. Schmidt, A new method for the determination of peak distribution across a two-dimensional separation space for the identification of optimal column combinations, Analytical and Bioanalytical Chemistry, 408 (2016) 8079–8088.
[16] S.R. Needham, G.A. Valaskovic, Microspray and microflow LC-MS/MS: the perfect fit for bioanalysis, Bioanalysis, 7 (2015) 1061-1064.
[17] R.E. Wilson, S.R. Groskreutz, S.G. Weber, Improving the Sensitivity, Resolution, and Peak Capacity of Gradient Elution in Capillary Liquid Chromatography with Large-Volume Injections by Using Temperature-Assisted On-Column Solute Focusing, Anal. Chem., 88 (2016) 5112-5121.
[18] G. Desmet, S. Eeltink, Fundamentals for LC Miniaturization, Anal. Chem., 85 (2013) 543-556.
[19] J. Leonhardt, T. Hetzel, T. Teutenberg, T.C. Schmidt, Large Volume Injection of Aqueous Samples in Nano Liquid Chromatography Using Serially Coupled Columns, Chromatographia, 78 (2015) 31-38.

[20] M.A. Stravs, J. Mechelke, P.L. Ferguson, H. Singer, J. Hollender, Microvolume trace environmental analysis using peak-focusing online solid-phase extraction-nano-liquid chromatography-high-resolution mass spectrometry, Analytical and Bioanalytical Chemistry, 408 (2016) 1879-1890.
[21] A. Vaast, K. Broeckhoven, S. Dolman, G. Desmet, S. Eeltink, Comparison of the gradient kinetic performance of silica monolithic capillary columns with columns packed with 3 µm porous and 2.7 µm fused-core silica particles, J. Chromatogr. A, 1228 (2012) 270-275.
[22] ChemSpider, http://www.chemspider.com, (accessed 07.08.2016)
[23] S. Fekete, I. Kohler, S. Rudaz, D. Guillarme, Importance of instrumentation for fast liquid chromatography in pharmaceutical analysis, J. Pharm. Biomed. Anal., 87 (2014) 105-119.
[24] S. Fekete, J. Schappler, J.L. Veuthey, D. Guillarme, Current and future trends in UHPLC, Trac-Trends in Analytical Chemistry, 63 (2014) 2-13.
[25] K. Broeckhoven, D. Cabooter, S. Eeltink, G. Desmet, Kinetic plot based comparison of the efficiency and peak capacity of high-performance liquid chromatography columns: Theoretical background and selected examples, J. Chromatogr. A, 1228 (2012) 20-30.
[26] Y. Vanderheyden, D. Cabooter, G. Desmet, K. Broeckhoven, Isocratic and gradient impedance plot analysis and comparison of some recently introduced large size core-shell and fully porous particles, J. Chromatogr. A, 1312 (2013) 80-86.
[27] U.D. Neue, Theory of peak capacity in gradient elution, J. Chromatogr. A, 1079 (2005) 153-161.
[28] G. Desmet, D. Cabooter, K. Broeckhoven, Graphical data representation methods to assess the quality of LC columns, Anal. Chem., 87 (2015) 8593-8602.
[29] K. Broeckhoven, D. Cabooter, F. Lynen, P. Sandra, G. Desmet, The kinetic plot method applied to gradient chromatography: Theoretical framework and experimental validation, J. Chromatogr. A, 1217 (2010) 2787-2795.
[30] S. Fekete, J. Fekete, K. Ganzler, Characterization of new types of stationary phases for fast liquid chromatographic applications, J. Pharm. Biomed. Anal., 50 (2009) 703-709.
[31] P. Petersson, A. Frank, J. Heaton, M.R. Euerby, Maximizing peak capacity and separation speed in liquid chromatography, J. Sep. Sci., 31 (2008) 2346-2357.
[32] T. Hetzel, D. Loeker, T. Teutenberg, T.C. Schmidt, Characterization of the efficiency of microbore liquid chromatography columns by van Deemter and kinetic plot analysis, J. Sep. Sci., 39 (2016) 3889–3897.
[33] Y. Zhang, X. Wang, P. Mukherjee, P. Petersson, Critical comparison of performances of superficially porous particles and sub-2 µm particles under optimized ultra-high pressure conditions, J. Chromatogr. A, 1216 (2009) 4597-4605.
[34] J.E. MacNair, K.C. Lewis, J.W. Jorgenson, Ultrahigh-Pressure Reversed-Phase Liquid Chromatography in Packed Capillary Columns, Anal. Chem., 69 (1997) 983-989.
[35] J.E. MacNair, K.D. Patel, J.W. Jorgenson, Ultrahigh pressure reversed-phase capillary liquid chromatography: Isocratic and gradient elution using columns packed with 1.0-µm particles, Anal. Chem., 71 (1999) 700-708.
[36] D.T.T. Nguyen, D. Guillarme, S. Heinisch, M.P. Barrioulet, J.L. Rocca, S. Rudaz, J.L. Veuthey, High throughput liquid chromatography with sub-2 µm particles at high pressure and high temperature, J. Chromatogr. A, 1167 (2007) 76-84.

4.7 Chapter appendix

4.7.1 Structural formula of the investigated analytes

The chemical structures of the analytes are depicted in Figure-S 4.1.

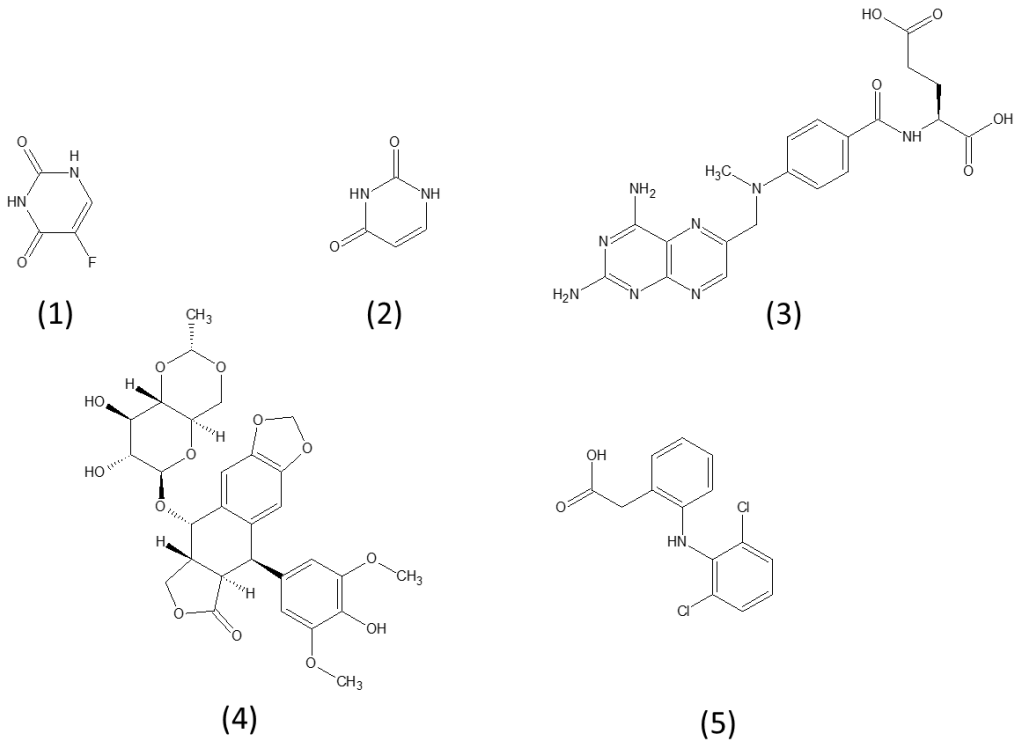

Figure-S 4.1: Chemical structures of the investigated analytes. (1) 5-fluorouracil, (2) uracil, (3) methotrexate, (4) etoposide and (5) diclofenac [1].

Whereas uracil is often used as column void marker in reversed liquid chromatography, the remaining compounds are pharmaceuticals analyzed within our routine analysis. All analytes differ in polarity which is of utmost importance for the characterization of peak capacity to obtain a uniform distribution across the gradient window.

4.7.2 Determination of the gradient times, gradient delay volume and retention factor

Table-S 4.1 - Table-S 4.4 show the resulting gradient times (t_G) depending on the flow rate and column.

Table-S 4.1: Resulting gradient times depending on the flow rate and column for a t_G/t_0 of 2.

t_G/t_0 = 2	Gradient times (t_G) / min		
Flow rate / µL min^{-1}	1.9 µm fully porous	3.0 µm fully porous	2.7 µm core-shell
10	0.49	0.49	0.38
15	0.32	0.32	0.25
20	0.24	0.24	0.18
25	0.20	0.20	0.15
30		0.16	0.12
35		0.14	0.10
40		0.12	0.09
45		0.11	

Table-S 4.2: Resulting gradient times depending on the flow rate and column for a t_G/t_0 of 4.

t_G/t_0 = 4	Gradient times (t_G) / min		
Flow rate / µL min^{-1}	1.9 µm fully porous	3.0 µm fully porous	2.7 µm core-shell
10	0.99	0.99	0.75
15	0.65	0.65	0.50
20	0.48	0.48	0.37
25	0.39	0.39	0.29
30		0.32	0.24
35		0.28	0.21
40		0.24	0.18
45		0.22	

Table-S 4.3: Resulting gradient times depending on the flow rate and column for a t_G/t_0 of 12.

t_G/t_0 = 12	Gradient times (t_G) / min		
Flow rate / µL min^{-1}	1.9 µm fully porous	3.0 µm fully porous	2.7 µm core-shell
10	2.97	2.98	2.29
15	1.99	1.98	1.53
20	1.48	1.44	1.14
25	1.18	1.15	0.89
30		0.96	0.74
35		0.82	0.62
40		0.71	0.54
45		0.65	

Table-S 4.4: Resulting gradient times depending on the flow rate and column for a t_G/t_0 of 20.

t_G/t_0 = 20	Gradient times (t_G) / min		
Flow rate / µL min^{-1}	1.9 µm fully porous	3.0 µm fully porous	2.7 µm core-shell
10	4.94	4.96	3.82
15	3.32	3.30	2.55
20	2.47	2.44	1.90
25	1.97	1.95	1.49
30		1.62	1.23
35		1.39	1.03
40		1.22	0.90
45		1.08	

Figure-S 4.2 exemplarily illustrates the obtained gradient profile at a flow rate of 40 µL min^{-1} including the determination of the gradient delay volume. For the determination, the intersection between the linear regressions are used as illustrated by the dashed lines.

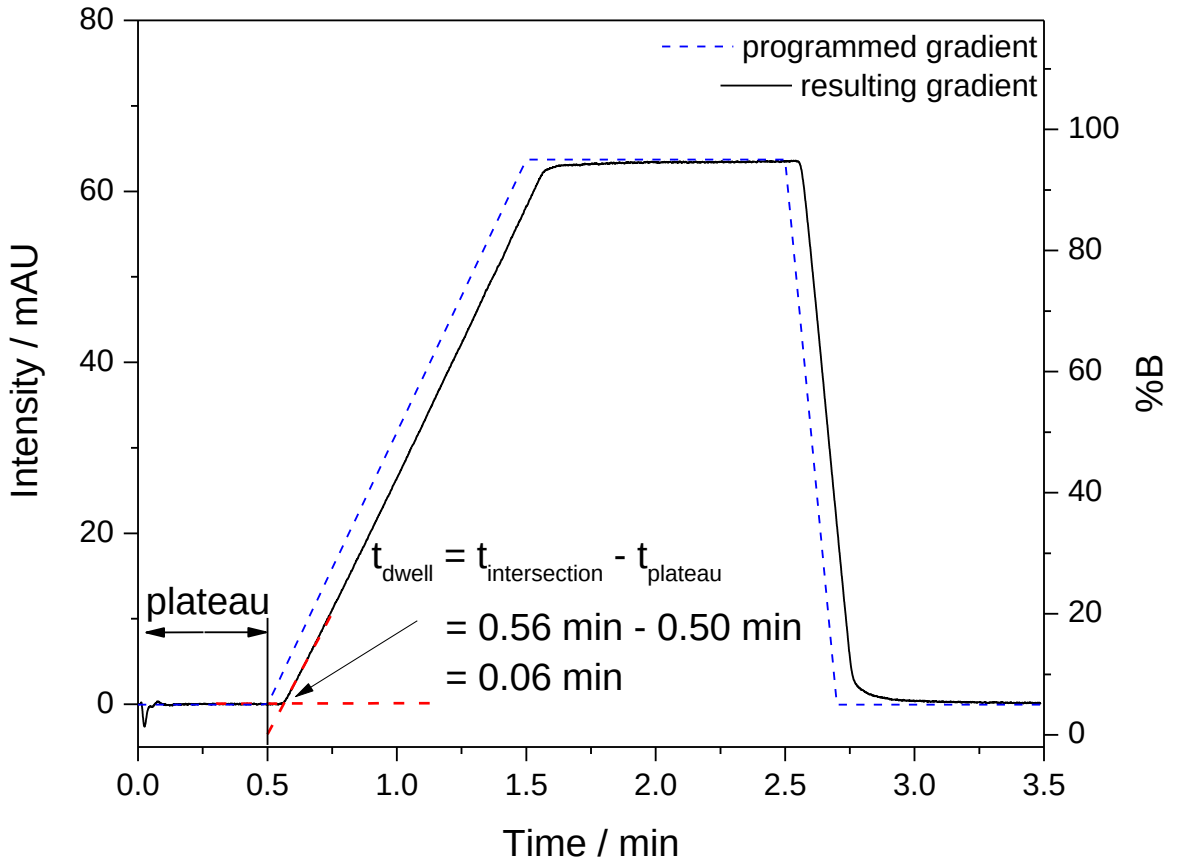

Figure-S 4.2: Illustration for the determination of the gradient delay volume at a flow rate of 40 µL min^{-1}.

The gradient retention factor (k^*) should be constant for the first and last eluting compound in order to obtain comparable results. For an appropriate adjustment of the gradient retention factor, Snyder'definition of k^* can be used which is shown in Equation 4.1.

$$k^* = \frac{0.87 \cdot t_G \cdot F}{V_m \cdot \Delta\Phi \cdot S} \qquad \textbf{Equation-S 4.1}$$

The gradient retention factor depends on the gradient time, flow rate, column volume, gradient range and the slope within the linear solvent strength theory (S). By replacing the column volume by Equation-S 4.2, Equation 4.3 can be obtained.

$$V_m = F \cdot t_0 \qquad \textbf{Equation-S 4.2}$$

$$k^* = \frac{0.87 \cdot t_G}{t_0 \cdot \Delta\Phi \cdot S} \qquad \textbf{Equation-S 4.3}$$

Now the gradient retention factor only depends on the gradient time and column void time since the gradient range as well as S are constant for a given solute. Because the column void time depends on the column, an adjustment of the gradient time needs to be done to achieve a constant ratio for t_G/t_0 and consequently k*. By calculating the retention factor at the time of

elution (k_e), it can be verified whether the adjustment of the gradient time depending on the column void time was appropriate [2]. One example of the obtained retention factors at time of elution is depicted in Figure-S 4.3 for a t_G/t_0 ratio of 20 at a flow rate of 20 µL min^{-1} for all columns, analytes and detector cells.

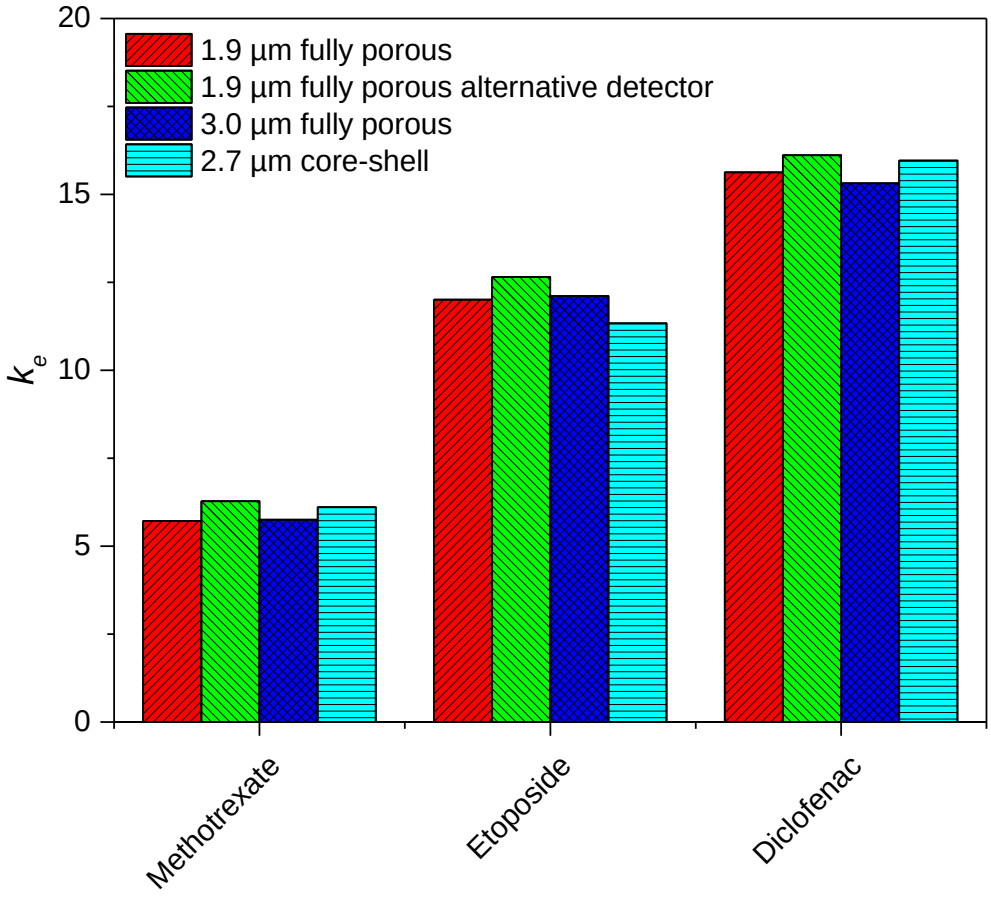

Figure-S 4.3: Comparison of the resulting retention factors for all analytes and detector cells on the different stationary phases at a flow rate of 20 µL min^{-1} (n=3).

4.7.3 Comparison of chromatographic support

Figure-S 4.4 shows the resulting experimentally obtained peak capacities ($n_{p,exp}$) as well as the gradient kinetic plot ($n_{p,KPL}$) for a ratio of the gradient time (t_G) to the column void time (t_0) of 2 obtained on the three different chromatographic supports. For $n_{p,KPL}$ a maximum pressure of 600 bar was used.

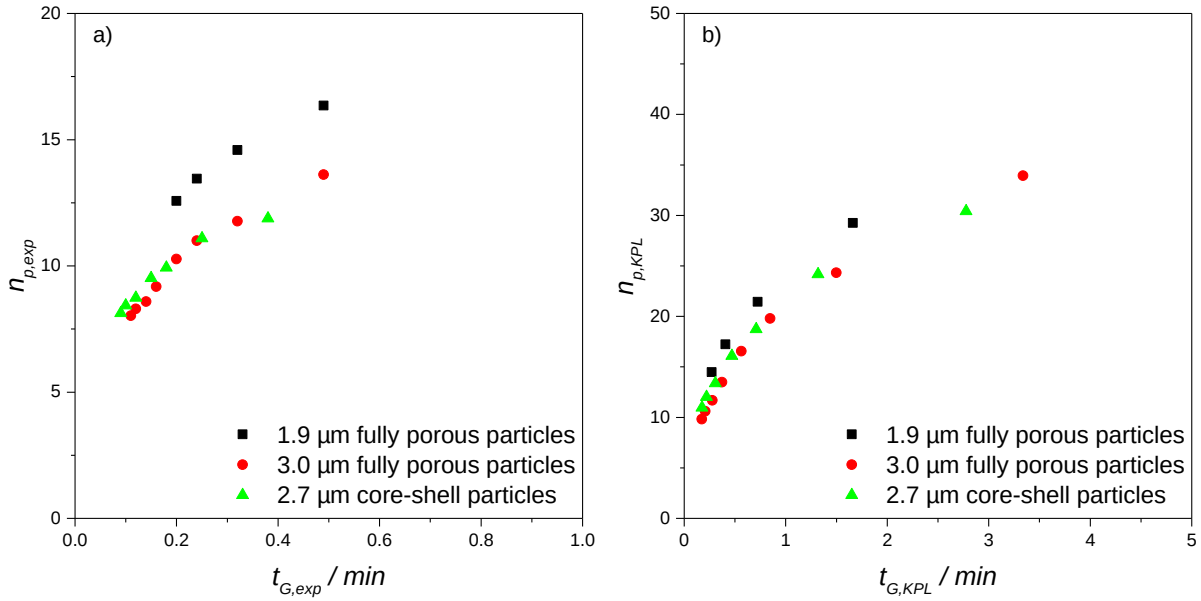

Figure-S 4.4: Comparison of peak capacity for the different chromatographic supports at t_G/t_0 of 2. a) experimentally obtained peak capacities, b) gradient kinetic plots for a maximum pressure of 600 bar (n=3).

Figure-S 4.5 illustrates the comparison of the chromatographic supports for a t_G/t_0 of 4.

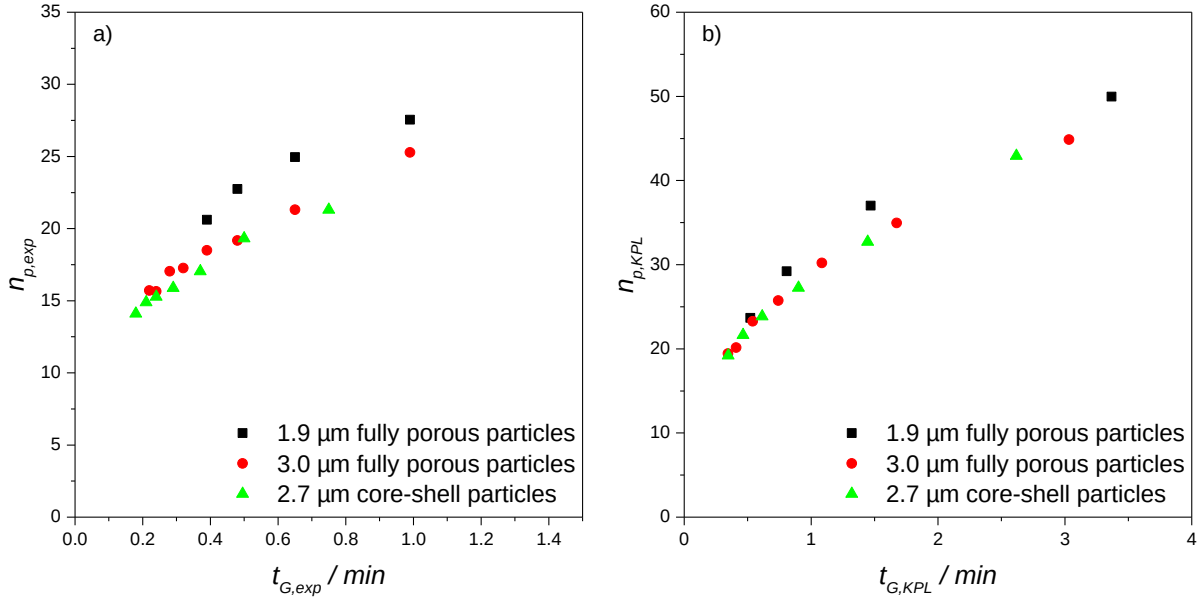

Figure-S 4.5: Comparison of peak capacity for the different chromatographic supports at t_G/t_0 of 4. a) experimentally obtained peak capacities, b) gradient kinetic plots for a maximum pressure of 600 bar (n=3).

In Figure-S 4.6, the results for $n_{p,exp}$ as well as $n_{p,KPL}$ are depicted for a t_G/t_0 of 12.

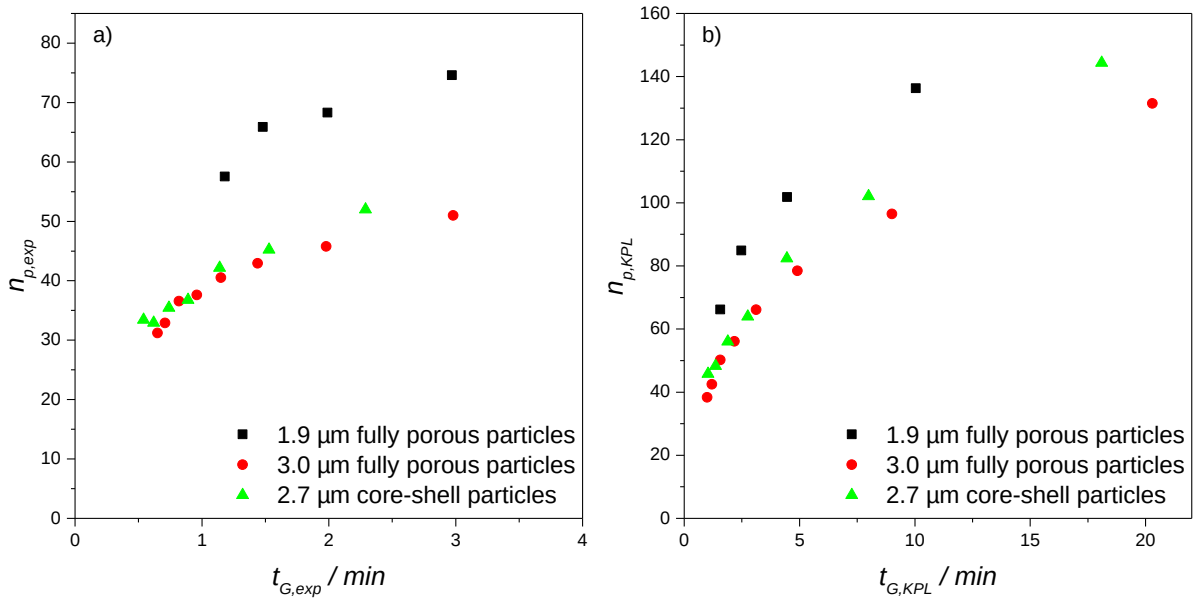

Figure-S 4.6: Comparison of peak capacity for the different chromatographic supports at t_G/t_0 of 12. a) experimentally obtained peak capacities, b) gradient kinetic plots for a maximum pressure of 600 bar (n=3).

4.7.4 Influence of the gradient slope on peak capacity

Figure-S 4.7 illustrates the influence of the gradient slope for the column packed with 3.0 µm fully porous particles.

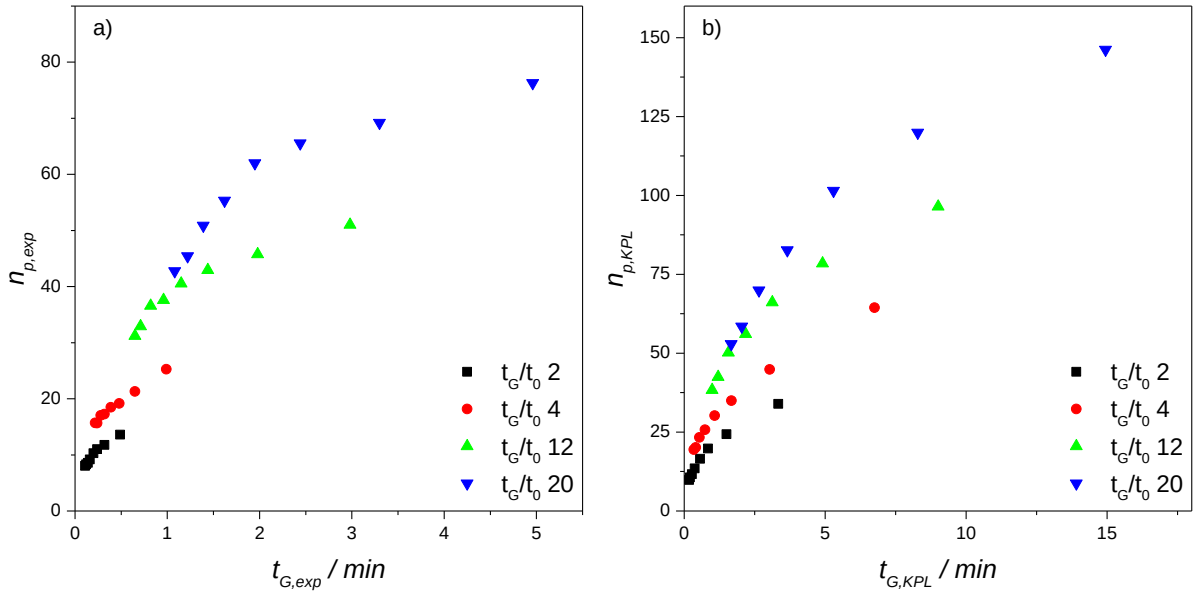

Figure-S 4.7: Influence of the gradient slope on $n_{p,exp}$ as well as $n_{p,KPL}$ for the column packed with 3.0 µm fully porous particles. a) experimentally obtained peak capacity, b) gradient kinetic plots (n=3).

Figure-S 4.8 shows the influence of the gradient slope for the 2.7 µm core-shell particle packed column.

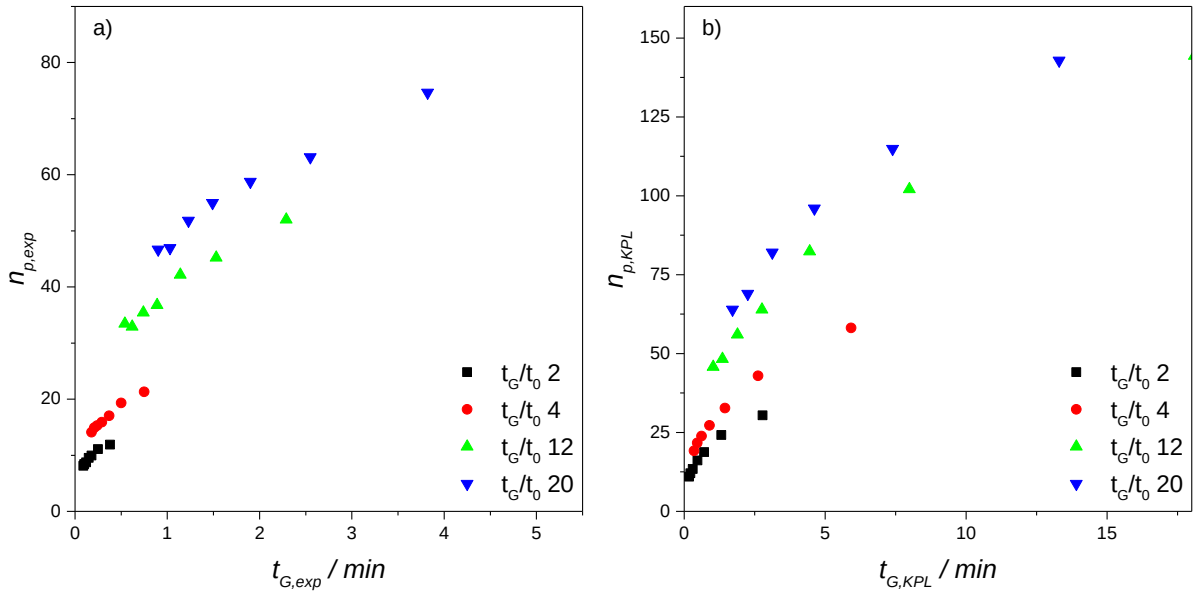

Figure-S 4.8: Influence of the gradient slope on $n_{p,exp}$ as well as $n_{p,KPL}$ for the column packed with 2.7 µm core-shell particles. a) experimentally obtained peak capacity, b) gradient kinetic plots (n=3).

4.7.5 Influence of the detector cell

Figure-S 4.9 illustrates the influence on the obtained $n_{p,exp}$ as well as $n_{p,KPL}$ for the alternative detector cell using the column packed with 1.9 µm fully porous particles for t_G/t_0 of 4.

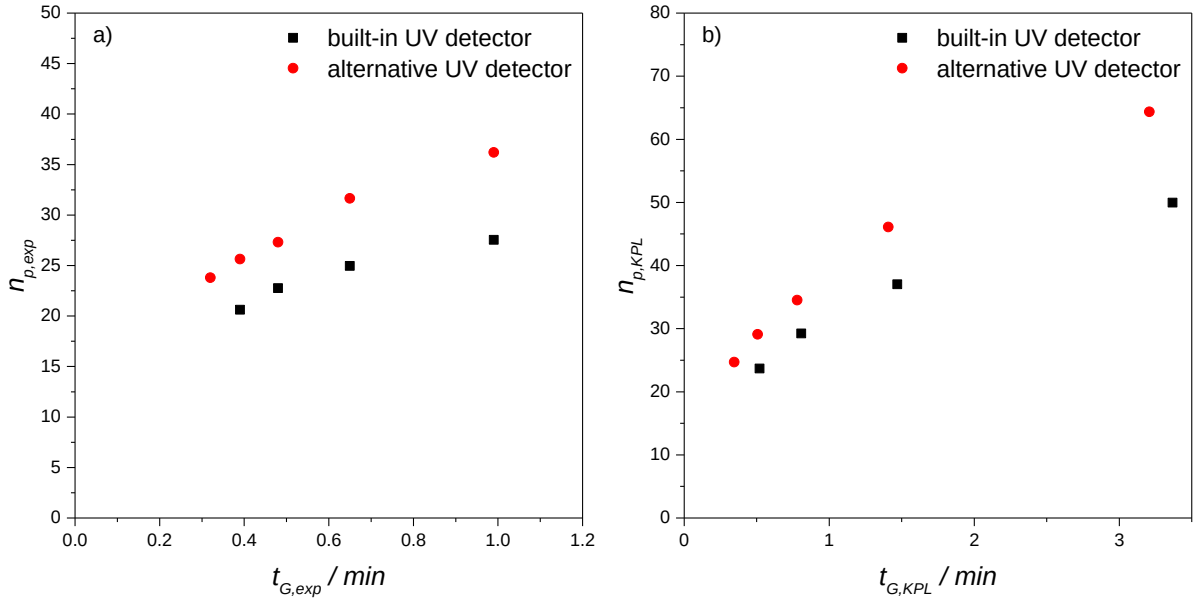

Figure-S 4.9: Comparison of peak capacity for the built-in and alternative UV detector for the column packed with 1.9 µm fully porous particle packed column at a t_G/t_0 of 4. a) experimentally obtained peak capacity, b) gradient kinetic plots (n=3).

Figure-S 4.10 shows the resulting values for t_G/t_0 of 12 on the same stationary phase.

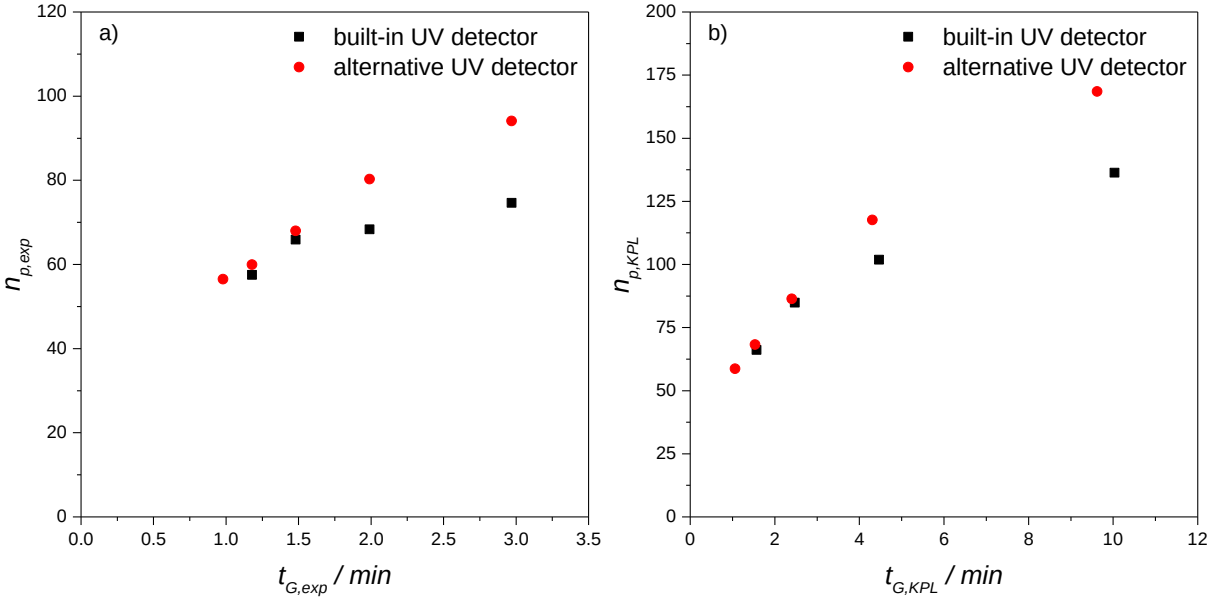

Figure-S 4.10: Comparison of peak capacity for the built-in and alternative UV detector for the column packed with 1.9 µm fully porous particle packed column at a t_G/t_0 of 12. a) experimentally obtained peak capacity, b) gradient kinetic plots (n=3).

Figure-S 4.11 shows the resulting peak capacities for a t_G/t_0 of 20 on the column packed with 1.9 µm fully porous particles.

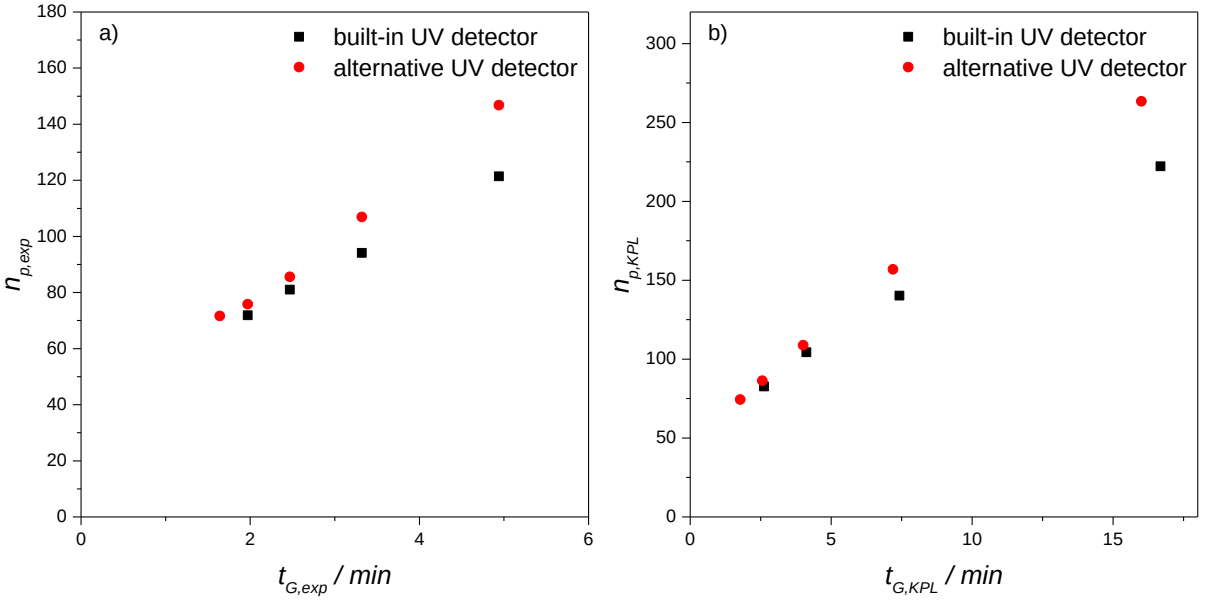

Figure-S 4.11: Comparison of peak capacity for the built-in and alternative UV detector for the column packed with 1.9 µm fully porous particle packed column at a t_G/t_0 of 20. a) experimentally obtained peak capacity, b) gradient kinetic plots (n=3).

4.7.6 References

[1] ChemSpider, http://www.chemspider.com, (accessed 07.08.2016)
[2] U.D. Neue, Theory of peak capacity in gradient elution, J. Chromatogr. A, 1079 (2005) 153-161.

Chapter 5 The influence of temperature on efficiency of microbore liquid chromatography columns

Redrafted from "Hetzel, T., Loeker, D., Blaesing, C., Jaeger, M., Teutenberg, T., Schmidt, T.C., The influence of temperature on efficiency of microbore liquid chromatography columns, submitted to Journal of Separation Science (2017)."

Abstract

The influence of temperature on the performance of micro liquid chromatography columns with an inner diameter of 300 µm has been investigated using a dedicated micro-LC system. Core-shell as well as fully porous particle packed stationary phases are compared on the basis of temperature depending van Deemter and kinetic plot analysis both at isocratic and gradient elution. For isocratic separations the minimum of the van Deemter curve was found to shift to higher linear velocities allowing for faster separations without significant loss of efficiency whereas the absolute minimum remained constant. The results of the kinetic plot analysis indicate higher efficiency with increasing temperature as well as extended pressure capabilities due to the decrease in mobile phase viscosity, which may allow to increase column length. Moreover, the influence of elevated temperature is more pronounced compared to increased pressure capabilities for column void times below 10 s. However, maximum efficiency can be achieved at maximum temperature and pressure in isocratic elution. For gradient elution, the peak capacity can be increased by 25% using a 30 s gradient when rising temperature from 30 to 70 °C. Using a UV detector with less contribution to extra-column variance, the rise in peak capacity is about 40%.

5.1 Introduction

One fundamental aim in liquid chromatography is to achieve more efficient and faster analysis with reduced resource consumption [1, 2]. To that end, particle diameter (d_p) as well as column inner diameter and column length were continuously decreased. Nowadays, core-shell particles with a diameter of 1.3 µm and fully porous particles with a diameter of 1.5 µm are commercially available [3, 4]. However, the decrease in particle diameter inevitably leads to a drastic increase in column back pressure [5]. To overcome this problem, the pressure capabilities of LC systems were enlarged by introducing systems with maximum pressures of 1,500 bar [6]. However, working at such high pressure leads to frictional heating, which can negatively affect column performance due to the formation of temperature gradients within the column [7]. As a consequence, the column inner diameter needs to be decreased for faster heat dissipation [8, 9]. Today, column inner diameters of less than 1.0 mm are available [10]. Moreover, microbore columns with an inner diameter of 300 µm have been introduced for micro liquid chromatography [11, 12]. For such a small column inner diameter, the influence of frictional heating on column performance has been reported to be negligible [13, 14]. Another approach to reduce column back pressure uses elevated temperatures leading to the reduction of mobile phase viscosity [15]. Thereby, the column back pressure is significantly decreased at constant linear velocities [16]. In addition, higher flow rates can be applied leading to faster analysis times [17]. Moreover, molecular diffusion coefficients increase at elevated temperatures [18]. As a consequence, the slope in the mass transfer region of the van Deemter curve can be reduced enabling to work at high linear velocities without compromising separation efficiency [19]. For gradient elution, commonly the peak capacity is considered as a measure of column performance [20, 21]. Several studies reveal the benefit of elevated temperature to increase peak capacity [22-24].

To achieve fast analysis times, high linear velocities are mandatory. Microbore columns with an inner diameter of 300 µm are ideally suited to achieve high linear velocities at flow rates in the low µL min^{-1} range [25]. Thereby, micro-LC allows for high-throughput analysis as well as for very fast second dimension separations in LCxLC [26, 27]. As mentioned above, even faster analysis can be accomplished using elevated temperatures. Therefore, the aim of this study focuses on the investigation of the influence of temperature on the efficiency of micro-LC columns to further increase separation speed. Core-shell as well as fully porous particle packed columns were analyzed using van Deemter as well kinetic plot analysis in case of isocratic experiments. In addition, peak capacity and gradient kinetic plots were examined for gradient

elution. Moreover, the influence of temperature at decreased extra-column variance was determined using a low volume UV detector on the basis of an optical waveguide.

5.2 Materials and methods

All measurements were performed on an Eksigent ExpressLC Ultra system (Sciex, Dublin, CA) with two different standard micro-LC flow modules (flow rate range: 1-10 µL min^{-1}, 5-50 µL min^{-1}). Whereas the first one is specified in the following as "small flow module", the latter is called "large flow module". The pneumatic pumps offer the possibility of generating 690 bar maximum pressure. Flow calibration was carried out at a flow rate of 5 µL min^{-1} for the small flow module whereas the large flow module was calibrated at a flow rate of 25 µL min^{-1}. The applied sample loop is made of fused-silica surrounded by polyetheretherketone (PEEKSil) with an inner diameter of 75 µm and a length of 10 cm. The corresponding loop volume was 442 nL. For sample loop filling, an HTS PAL autosampler (CTC Analytics, Zwingen, Switzerland) was used. The built-in six port valve was used for sample injection using the full loop injection. A static air column oven was used for temperature control of the stationary phase. For data acquisition two different UV detectors were applied. The built-in diode array detector (*DAD*) was employed with a cell volume of 100 nL as well as an alternative detector cell on the basis of optical waveguide technology with a cell volume of 6 nL (KNAUER, Berlin, Germany). Fused-silica capillaries with an inner diameter (*i.d.*) of 50 µm and an outer diameter (*o.d.*) of 360 µm were used for the connection prior to and after the column with a length of 10 cm and 13 cm, respectively. The *o.d.* was expanded to 1/32" using sleeves for the connection to the columns and detectors. For data acquisition and analysis the ClarityChrom (V. 6.1.0) as well as the Eksigent control software (Version 4.2 Patch for ekspert nanoLC 400 and batch acquisition control) were used. Further data processing was performed using Origin Lab V. 9.3 and Microsoft Office Excel 2013. Table 5.1 presents an overview of the investigated columns.

Table 5.1: List of investigated columns including column dimensions, particle and pore diameter, maximum pressure as well as temperature.

description	surface modification	chromatographic support	end capping	L / mm	i. d. / mm	d_p / µm	pore diameter / Å	ΔP_{max}/ bar	maximum temperature / °C
Eksigent HALO	C18	core-shell	fully endcapped	50	0.3	2.7	90	690	60
YMC Triart	C18	fully porous	Multistage endcapped	50	0.3	1.9	120	600	70 (pH 1-7) 50 (pH 7-12)
YMC Triart	C18	fully porous	Multistage endcapped	50	0.3	3.0	120	550	70 (pH 1-7) 50 (pH 7-12)

i.d.: column inner diameter, L: column length, d_p: particle diameter, ΔP_{max}: maximum backpressure

Water (H_2O) and acetonitrile (ACN) were used as mobile phase constituents. Moreover, acetone was used for the determination of the gradient delay volume. All solvents were purchased from Th. Geyer-Chemsolute (Renningen, Germany) with LC-MS grade purity. Formic acid (FA), purchased from Sigma-Aldrich (Seelze, Germany), was used at 0.1% (v/v) as solvent additive to adjust the pH of the mobile phase and analyte mixture.

Table 5.2 shows the selected substances including important physico-chemical properties, while the structural formulas are compiled in Figure-S 5.1.

Table 5.2: List of the selected compounds including CAS number, sum formula, molar mass and log P [28].

number	Compound	CAS	sum formula	purity / %	provider	M / g mol^{-1}	Log P	c / µg mL^{-1}
(1)	5-Fluorouracil**	51-21-8	$C_4H_3FN_2O_2$	≥ 99	Fluka	130.08	0.86	5
(2)	Uracil*,**	66-22-8	$C_4H_4N_2O_2$	≥ 99	Fluka	112.09	0.72	10
(3)	Methotrexate**	59-05-2	$C_{20}H_{22}N_8O_5$	≥ 98	Fluka	454.44	-0.24	20
(4)	Etoposide*,**	33419-42-0	$C_{29}H_{32}O_{13}$	≥ 98	Sigma	588.56	1.16	100*, 50**
(5)	Diclofenac**	15307-86-5	$C_{14}H_{11}Cl_2NO_2$	≥ 98.5	Sigma	296.15	4.26	10
(6)	Naphthalene*	91-20-3	$C_{10}H_8$	≥ 98	Fluka	128.17	2.96	50

* isocratic measurements, ** gradient experiments

5.2.1 Isocratic measurements

For the isocratic measurements, the built-in diode array detector (DAD) was employed with a cell volume of 100 nL having a light path length of 5 mm. Chromatograms were recorded at 254 nm with a data acquisition rate of 10 Hz. For the determination of the van Deemter curves,

the flow rate was varied in a range between 2 and 50 µL min^{-1}. Data fitting was performed via the least square method. All measurements were carried out in triplicate. To investigate the influence of temperature, the column oven temperature was varied between 30, 50 and 70 °C depending on the individual maximum temperature as specified by the column manufacturer. For the isocratic kinetic plots, maximum pressures (ΔP_{max}) of 600 and 1,000 bar were used. The retention factor k was calculated according to Equation 5.1 using the retention time of uracil as column void time (t_0).

$$k = \frac{t_R - t_0}{t_0} \qquad \textbf{Equation 5.1}$$

The mobile phase composition was adjusted for every column and temperature in order to obtain constant retention factors. An overview can be found in the supporting information (Table-S 5.1 - Table-S 5.3).

For the determination of the van Deemter plots, the compounds naphthalene and etoposide were used. Naphthalene was selected because it is often used as model compound [29, 30]. It has a high diffusion coefficient (D_m) due to its low molecular weight. Moreover, it exhibits only hydrophobic interactions with the stationary phase and retention is not influenced by the mobile phase pH. In contrast, etoposide has a higher molecular weight and a lower diffusion coefficient. Furthermore, etoposide is a pharmaceutical of interest in terms of routine analysis. It was also part of a previous study to investigate the selectivity of different stationary phases [31].

For the analyte etoposide, the stock solution was prepared using a mixture of 50/50 H_2O/ACN (v/v). In contrast, naphthalene was dissolved in 100% ACN. For the analysis the single standards were diluted with acidified water in the ratio of 1 to 10. The final concentration for etoposide and naphthalene were 0.1 mg mL^{-1} and 0.05 mg mL^{-1} with a composition of 95/5 and 90/10 H_2O/ACN + 0.1% FA (v/v), respectively.

5.2.2 Gradient experiments

For the gradient experiments, the built-in UV detector with a cell volume of 100 nL as well as the optical-waveguide based UV detector with a cell volume of 6 nL (KNAUER, Berlin, Germany) were used. Detection was carried out at 272 nm with a data acquisition rate of 40 Hz and 50 Hz depending on the applied detector. The gradient experiments were performed in the flow rate range between 10 and 50 µL min^{-1} in 5-µL steps using a linear gradient from 5% to 95% B. For all measurements, the large flow module was used. For the gradient kinetic plots a

ΔP_{max} of 600 bar was considered because increased pressure capabilities showed a limited effect on peak capacity for the range of ultra-fast chromatography with gradient times < 100 s as was demonstrated by Wang et al [24] (see also Figure 4.5).

Uracil is used as column void time marker. All other compounds are pharmaceuticals and have different log P values and therefore different polarity as can be seen from Table 5.2. This is of utmost importance to obtain a uniform distribution over the entire gradient window for an appropriate determination of peak capacity [32]. All stock solutions were prepared at a concentration of 1 mg mL^{-1} using a mixture of 50/50 H_2O/ACN (v/v). For the micro-LC analysis, the single standards were merged and afterwards diluted with acidified water. The final concentrations are given in Table 5.2 with a composition of 96/4 H_2O/ACN + 0.1% FA (v/v). Four different gradient times (t_G) were used to analyze the influence of the gradient slope. Gradient times were set to 0.5, 1.0, 3.0 and 5.0 min at a flow rate of 10 µL min^{-1} for all investigated temperatures. Whereas the first two gradient times were chosen to mimic ultra-fast chromatography, the latter two represent applications requiring higher peak capacity. For an appropriate determination of peak capacity the analytes have to experience the same mobile phase history. Therefore, the ratio between t_G and the column void time (t_0) needed to be kept constant [33, 34]. Therefore, the t_0 values were determined using uracil as column void marker at a mobile phase composition of 10/90 H_2O/ACN + 0.1% FA (v/v). Subsequently, the experimentally obtained t_0 times were corrected for the system void time ($t_{0,sys}$) by replacing the column by a zero-dead volume (*ZDV*) union. The gradient time was adjusted to ensure constant elution volumes resulting in gradient times between 5 s and 5 min depending on the column t_0, flow rate and temperatures (see Table-S 5.4 - Table-S 5.15). Additionally, the ratio between the delay time (t_d) and t_0 had to be kept constant to obtain comparable results. The gradient delay volume was 2 µL ± 4.3% [11]. At the beginning of the analysis, an additional isocratic plateau (t_p) was added to obtain a constant ratio of t_d to t_0 of 2 since t_0 differed for all columns. In the following, t_d will be used as the sum of the gradient delay time (t_{dwell}) and t_p. All measurements were performed in triplicate for each temperature.

5.3 Results and discussion

5.3.1 Temperature depending Deemter analysis

The van Deemter analysis is one of the most common approaches to analyze column performance in isocratic separations [32, 34]. The corresponding van Deemter equation is given in Equation 5.2.

$$H = A \cdot d_p + \frac{B \cdot D_m}{u_0} + C \cdot \frac{d_p^2 \cdot u_0}{D_m}$$ **Equation 5.2**

where H is the plate height, A the eddy diffusion, B the longitudinal diffusion, C the mass transfer, u_0 the linear velocity, D_m the molecular diffusion coefficient and d_p the particle diameter. According to Equation 5.2, the plate height depends on the molecular diffusion coefficient. For the calculation of the temperature dependent diffusion coefficient, the Wilke-Chang equation (Equation 5.3) can be used [35].

$$D_m = 7.4 \cdot 10^{-8} \frac{(\phi_B \cdot M_B)^{1/2} \cdot T}{\eta_B \cdot V_A^{0.6}}$$ **Equation 5.3**

where M_B is the molecular weight of solvent B, T the temperature, ϕ_B the association factor of solvent B, η_B the viscosity of solvent B and V_A the molar volume of solute A. In addition to the direct dependence of diffusion coefficients on temperature, the mobile phase viscosity also changes with temperature. The mobile phase viscosity was calculated according to Equation 5.4 [36].

$$\eta_{\phi,T} = exp\left[\phi\left(-3.476 + \frac{726}{T}\right) + (1-\phi)\left(-5.414 + \frac{1566}{T}\right) + \phi(1-\phi)\left(-1.762 + \frac{929}{T}\right)\right]$$ **Equation 5.4**

where $\eta_{\phi,T}$ is the mobile phase viscosity at the temperature (T) and portion of organic solvent (ϕ) within the mobile phase. To investigate the influence of temperature for miniaturized columns with an *i.d.* of 300 µm, the column oven temperature was varied for the individual columns. Figure 5.1 shows the resulting temperature dependent van Deemter curves for naphthalene on the three investigated columns whereas the corresponding curves for etoposide can be found in the supporting information (Figure-S 5.2).

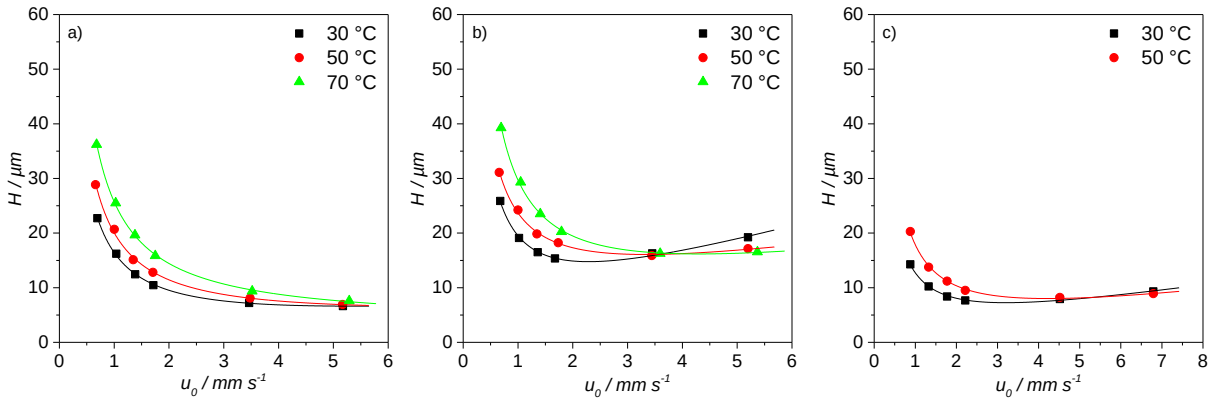

Figure 5.1: Resulting van Deemter curves at 30, 50 and 70 °C for naphthalene for the columns packed with a) 1.9 µm fully porous particles, b) 3.0 µm fully porous particles (1.68, 0.72, 0.16) and c) 2.7 µm core-shell particles (0.62, 0.31, not specified). Data fitting was performed via the least square method. Data were recorded using the small flow module. The numbers in brackets represent the slope of the *C*-term region at the different temperatures (30 °C, 50 °C, 70 °C). For the column packed with 1.9 µm fully porous particles, please refer to Figure 5.2.

As expected from theory, the value for the plate height at constant linear velocity increases in the *B*-term region due to the higher diffusion coefficient at higher temperature [22]. In contrast, the slope in the *C*-term region decreases as can be identified from Figure 5.1 b) and c) according to Equation 5.2. For the column packed with 3.0 µm fully porous particles, the slope decreases by a factor of approximately 10 from 1.68 at 30 °C to 0.16 at 70 °C, whereas a reduction by a factor of 2 from 0.62 to 0.31 can be observed for the 2.7 µm core-shell particle packed column between 30 and 50 °C. As a consequence, the optimum linear velocity (u_{opt}) shifts to higher linear velocities with increasing temperature because of the increased diffusion at higher temperatures [15], whereas the value of H_{min} is almost constant over the entire temperature range. Thereby faster analysis can be performed at increased linear velocities without significant loss of efficiency which is of utmost importance for routine applications and LCxLC [25, 27]. The results clearly show that micro-LC columns can be used at elevated temperatures and behave like conventional LC columns. However, it can be seen from Figure 5.1 a) that the influence of increased temperature cannot be visualized for the minimum plate height as well as the *C*-term region within the applied flow rate range for the 1.9 µm fully porous particle packed column.

5.3.2 Investigation of increased flow rates and temperatures

In order to investigate the efficiency for high linear velocities, the large flow module was installed. After flow calibration, the flow-dependent experiments were performed and compared to the results of the small flow module. Figure 5.2 a) shows the van Deemter curves

obtained for naphthalene at 30 °C on the column packed with 1.9 µm fully porous particles using both flow modules.

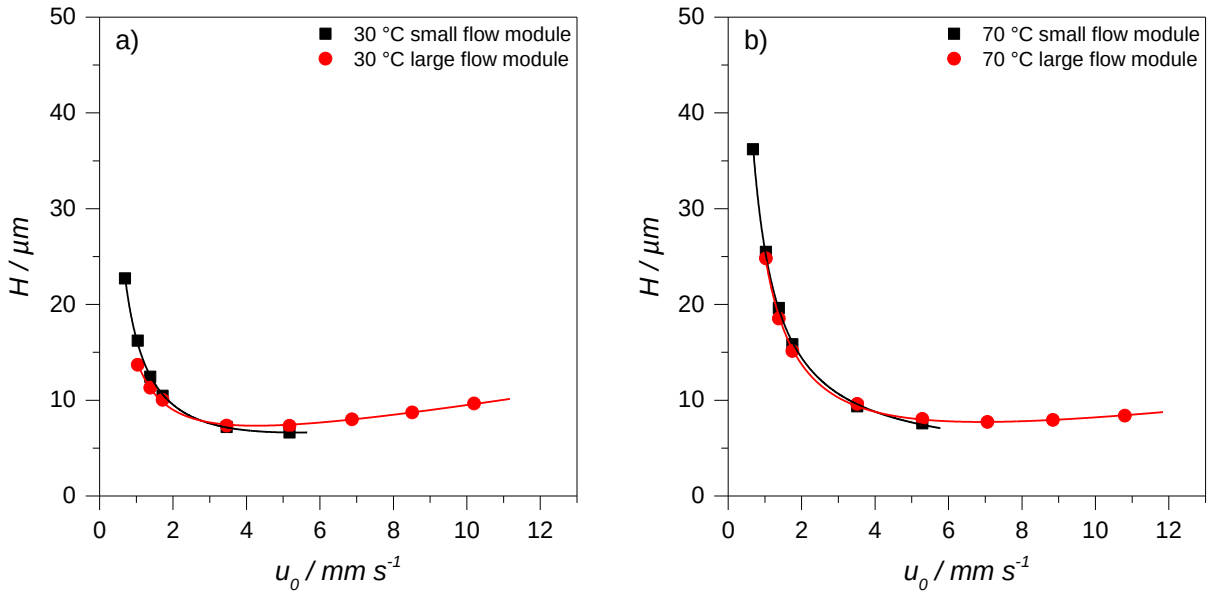

Figure 5.2: Comparison of the resulting van Deemter curves at a) 30 °C (0.46) and b) 70 °C (0.18) using the small (black squares) and large (red circles) flow module for naphthalene on the column packed with 1.9 µm fully porous particles. Data fitting was performed via least square method. The number in brackets represent the slope of the *C*-term region at the corresponding temperature using the curve obtained for the large flow module.

As can be seen the curves almost overlap. For practical purposes, the use of the larger flow module is more favourable since a higher flow rate range can be applied. Mainly, small deviations can be observed in the lower velocity range. This can be explained by the technical characteristics of the large flow module, the use of which should be restricted to the range between 5-50 µL min^{-1} according to manufacturer's specifications. Therefore, larger deviations at low flow rates between 3-5 µL min^{-1} (up to 2 mm s^{-1}) are expected. Nevertheless, the influence of increased linear velocities on *H* can still be evaluated. Even at a linear velocity of 10 mm s^{-1}, *H* is found to be below 10 µm. Figure 5.2 b) illustrates the effect of elevated temperature at increased linear velocities on the plate height. Even at 70 °C, the resulting van Deemter curves appear almost identical between the different flow modules. When comparing the *C*-term regions, the slope decreases from 0.46 at 30 °C (Figure 5.2 a) to 0.18 at 70 °C (Figure 5.2 b). By increasing the temperature to 70 °C a linear velocity of 11 mm s^{-1} and a plate height of 8.4 µm can be achieved at a ΔP_{max} of 280 bar. This corresponds to a flow rate of only 30 µL min^{-1}. When comparing the slopes of the *C*-term region for all applied particle morphologies and diameters, it can be seen that the increase of temperature leads to a

pronounced reduction of the slope within this region. To that end, faster analysis can be performed without significant loss of efficiency.

To investigate the performance at different temperatures at maximum pressure and therefore at maximum efficiency, the results of the van Deemter analysis shall be transformed into kinetic plots.

5.3.3 Temperature depending kinetic plots

In a previous study, it was shown that the sub-2 µm fully porous particles should be used for ultra-fast chromatography with a maximum column void time of 10 s [12]. That is why the following investigations are focussed on this column using naphthalene as reference compound. The data transformation into kinetic plots was achieved according to Equation 5.5 - Equation 5.7 [37].

$$t_0 = \frac{\Delta P_{max}}{\eta} \cdot \left[\frac{K_{v0}}{u_0^2}\right]_{exp} \qquad \textbf{Equation 5.5}$$

$$N = \frac{\Delta P_{max}}{\eta} \cdot \left[\frac{K_{v0}}{u_0 \cdot H}\right]_{exp} \qquad \textbf{Equation 5.6}$$

$$K_{v0} = \frac{u_0 \cdot \eta \cdot L}{\left(\Delta P_{total} - \Delta P_{system}\right)} \qquad \textbf{Equation 5.7}$$

where t_0 is the column void time, N the number of theoretical plates, ΔP_{total} the total backpressure, ΔP_{system} the system backpressure and K_{v0} the permeability. All other symbols are used as above. Mobile phase viscosity was calculated according to Equation 5.4 whereas the permeability was calculated according to Equation 5.7 [37]. In general, the kinetic plot limit (*KPL*) curve illustrates the maximum achievable efficiency at each temperature in a given time at ΔP_{max} [34, 38]. The comparison of the *KPL* curves allows for conclusions about the most efficient combination of temperature and pressure for a given chromatographic support and reveals information about the corresponding column length. At first, the influence of pressure is evaluated at constant temperatures of 30, 50 and 70 °C. The corresponding kinetic plots are depicted in Figure 5.3.

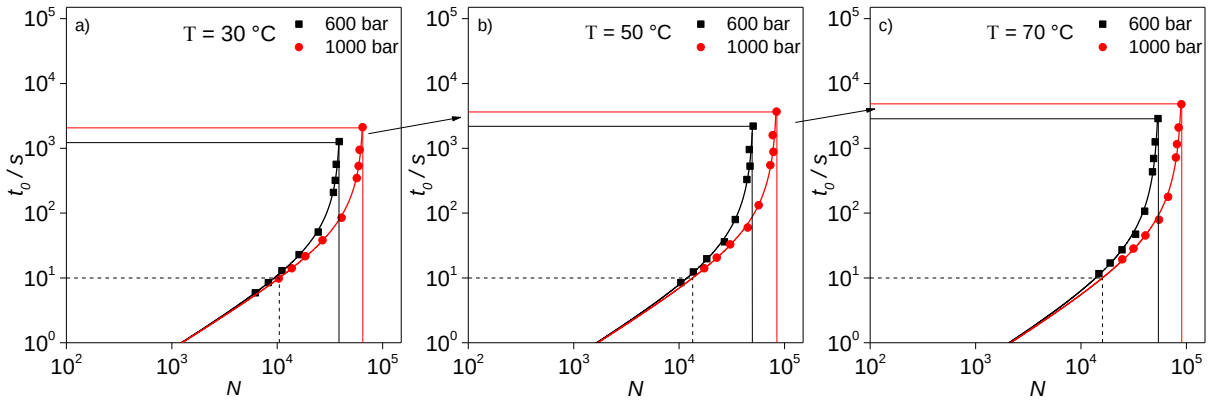

Figure 5.3: Kinetic plots for naphthalene on the column packed with 1.9 µm fully porous particles at a temperature of a) 30, b) 50 and c) 70 °C and varying pressure of 600 (black squares) and 1,000 bar (red circles).

Within the range of ultra-fast chromatography with a column void time between 1 and 10 s which is highlighted by the dashed lines, almost no difference in terms of efficiency can be achieved between 600 and 1,000 bar at each temperature. However, the maximum efficiency rises with increasing temperature between 30 °C and 70 °C from 38,800 to 53,800 theoretical plates for 600 bar and from 64,600 to 89,700 theoretical plates at a ΔP_{max} of 1,000 bar as can be recognized by following the full lines in Figure 5.3. Both effects are attributed to the possibility of using longer column lengths at increased pressure and temperature. As a consequence, high pressure in combination with elevated temperatures is recommended to maximize column efficiency. For a better visualization and to further analyze the range of ultra-fast chromatography the data of Figure 5.3 are rearranged to demonstrate the potential of increased temperature at constant pressure. The resulting kinetic plots are included in Figure 5.4.

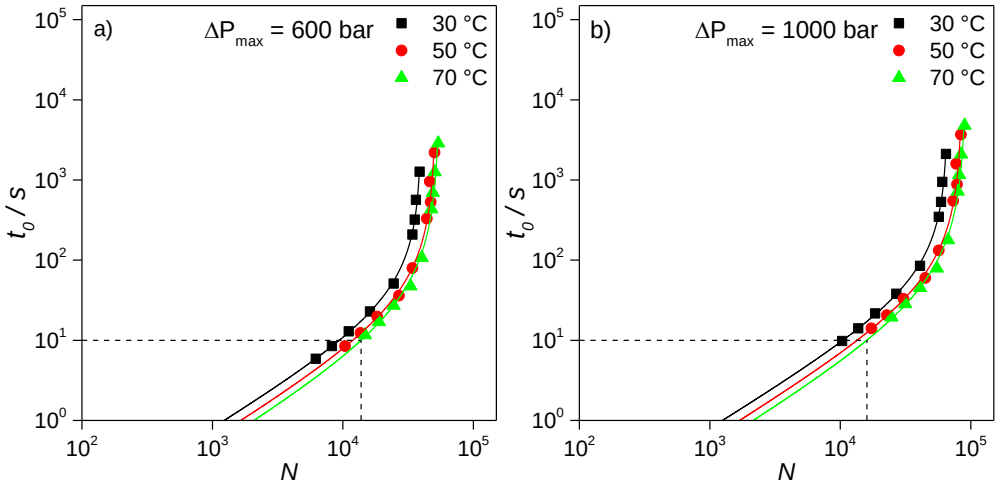

Figure 5.4: Kinetic plots for naphthalene on the column packed with 1.9 µm fully porous particles at constant pressures of a) 600 and b) 1,000 bar at temperatures of 30 (black squares), 50 (red circles) and 70 °C (green triangles).

It can be seen that at constant pressure an increase of temperature leads to higher efficiency even in the range of ultra-fast chromatography. When considering the maximum efficiency, the increase in performance is limited when the column temperature is increased from 50 to 70 °C despite the possibility of using longer column length at 70 °C due to the improved pressure characteristic. Data of the kinetic plot analysis for the three different temperatures used are summarized in Table 5.3.

Table 5.3: Achievable efficiency in the range of ultra-fast chromatography with a column void time of 10^0 and 10^1 s for different temperatures and pressures. In addition, the corresponding column lengths (*L*) as well as efficiency gain are given.

Temperature / °C	**Pressure / bar**			
30	**600**		**1,000**	
Column void time / s	***N***	***L* / cm**	***N***	***L* / cm**
10^0	1231	2.47	1250	3.19
10^1	9393	7.82	10458	10.10
Temperature / °C	**Pressure / bar**			
50	**600**		**1,000**	
Column void time / s	***N***	***L* / cm**	***N***	***L* / cm**
10^0	1651	3.10	1690	4.00
10^1	11901	9.81	13446	12.66
Temperature / °C	**Pressure / bar**			
70	**600**		**1,000**	
Column void time / s	***N***	***L* / cm**	***N***	***L* / cm**
10^0	2078	3.64	2149	4.70
10^1	13788	11.51	15972	14.86

The data of Table 5.3 reveal that it is more efficient to increase the temperature at constant pressure than vice versa. By increasing the temperature from 30 to 70 °C, the decrease in mobile phase viscosity allows for using even longer columns (47%), which cannot be attained through augmenting the pressure from 600 to 1,000 bar at 30 °C (29%). In addition, the slope of the van Deemter curve in the *C*-term region decreases with rising temperature leading to higher efficiency at increased linear velocities using smaller column length. However, the maximum efficiency in the range of ultra-fast chromatography can be achieved at maximum temperature and pressure.

5.3.4 Temperature depending peak capacity and gradient kinetic plots

For gradient elution, the plate height can no longer be taken as the measure of choice for the evaluation of performance. Commonly the peak capacity is considered to evaluate the separation power of a given chromatographic support [20, 21]. The peak capacity ($n_{p,exp}$) can be calculated according to Equation 5.8 assuming a constant peak width across the gradient window [33, 34, 39].

$$n_{p,exp} = 1 + \frac{t_G}{\bar{w}} \qquad \textbf{Equation 5.8}$$

where t_G is the gradient time and $\bar{w}$ the average peak width at the base. For the determination of peak capacity the compounds methotrexate, etoposide and diclofenac were used. As mentioned in Chapter 5.2.2, the analytes have to experience the same relative mobile phase history for an appropriate determination of the peak capacity [33]. Therefore, the ratio of t_G/t_0 as well as t_d/t_0 should be constant for every column and flow rate. Figure 5.5 a) illustrates the peak capacity experimentally determined for the column packed with 3.0 µm fully porous particles for a t_G/t_0 of 2. The t_G/t_0 ratio of 2 is of interest for ultra-fast chromatography and high throughput analysis as well as for online LCxLC [25, 27]. The results for all other chromatographic supports and t_G/t_0 ratios at elevated temperature can be found in the supplementary material (see Figure-S 5.3 to Figure-S 5.6).

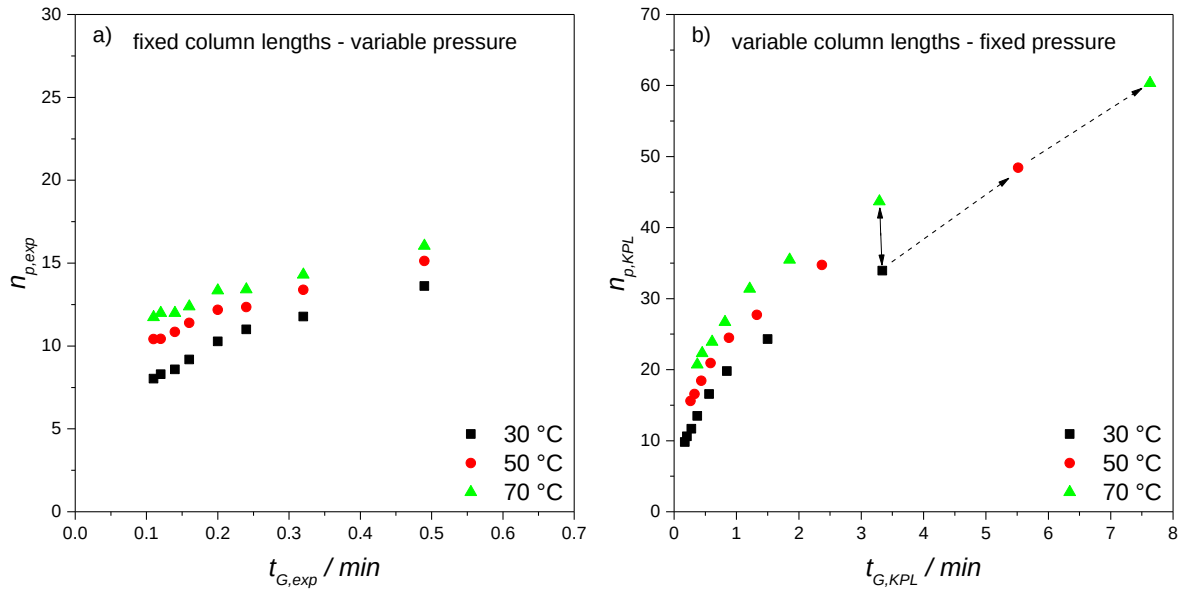

Figure 5.5: Comparison of peak capacity at t_G/t_0 of 2 for the column packed with 3.0 µm fully porous particles at 30 (black squares), 50 (red circles), 70 °C (green triangles). a) experimentally obtained peak capacities, b) gradient kinetic plots for a maximum pressure of 600 bar (n=3). The full line arrow illustrates the difference in peak capacity between 30 and 70 °C at a gradient time of 3.3 min, whereas the dashed arrows demonstrate the increase of maximum peak capacity with rising temperature.

As depicted in Figure 5.5 a), the experimentally determined peak capacity rises with increasing temperature. By changing the temperature from 30 to 70 °C the peak capacity can be increased by 17%. This agrees with data by Guillarme et al. who reported a gain of peak capacity of about 20-30% by increasing the temperature to 90 °C [23]. Petersson et al. also investigated the influence of temperature on peak capacity. They found increased peak capacity for low and well-retained compounds between 40 and 60 °C [22].

The experimentally determined peak capacity can also be transformed into gradient kinetic plots by following Equation 5.9 - Equation 5.11 [34]. Thereby, the different temperatures are compared at maximum efficiency [33].

$$\lambda = \frac{\Delta P_{max}}{\Delta P_{exp} - \Delta P_{ec}} \qquad \textbf{Equation 5.9}$$

$$n_{p,KPL} = 1 + \sqrt{\lambda} \cdot \left(n_{p,exp} - 1\right) \qquad \textbf{Equation 5.10}$$

$$t_{G,KPL} = \lambda \cdot t_{G,exp} \qquad \textbf{Equation 5.11}$$

where ΔP_{exp} is the experimentally obtained backpressure, ΔP_{ec} the extra-column backpressure, λ the length-elongation factor, $n_{p,exp}$ the experimentally obtained peak capacity, $n_{p,KPL}$ the peak capacity and $t_{G,KPL}$ the gradient time of the gradient kinetic plot limits (KPL).

When comparing the $n_{p,KPL}$ in Figure 5.5 b), the peak capacity increases from 34 to 60 by maximizing temperature and column length until the maximum pressure is obtained as indicated by the dashed lined arrows. The gain by the factor of 1.8 is accompanied by an enlargement of the gradient time of about a factor of 2.2. At a constant t_G of approximately 3.3 min, the peak capacity can be increased by 29% when raising temperature from 30 to 70 °C. Considering the peak capacity production rate (ξ) [32, 40], the rise of temperature leads to an increase of ξ from 0.17 s^{-1} to 0.30 s^{-1} according to Equation 5.12.

$$\xi = \frac{n_p}{t_G} \qquad \textbf{Equation 5.12}$$

To increase peak capacity for ultra-fast chromatography smaller particle diameters are explored [11]. Moreover, temperature is assumed to further increase peak capacity as was already shown for the 3.0 µm fully porous particle packed column in Figure 5.5 [18, 22, 23]. In addition, it was demonstrated that an optical waveguide based UV detector with less contribution to extra-column variance is suitable to increase peak capacity even further [11]. To minimize this influence is of particular importance for steep gradients because the generated bands are more vulnerable to extra-column band broadening. In Figure 5.6, the resulting gradient kinetic plot

limits are shown for the detection cell with a volume of 100 nL as well as for the optical waveguide based UV detector with a cell volume of only 6 nL.

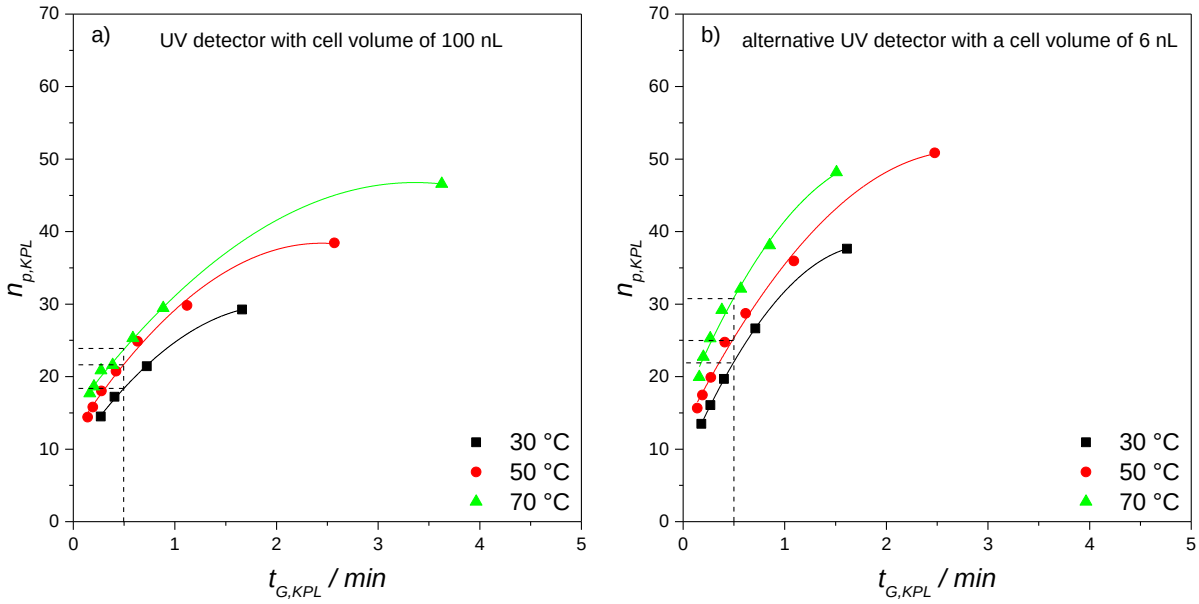

Figure 5.6: Illustration of the resulting $n_{p,KPL}$ at a t_G/t_0 of 2 for the column packed with 1.9 µm fully porous particles at 30 (black squares), 50 (red circles) and 70 °C (green triangles) using a) a UV detector with a cell volume of 100 nL and b) a UV detector on the basis of an optical waveguide with a cell volume of 6 nL (n=3). Best fit lines are displayed as well. The dashed lines illustrate the gain in peak capacity at a gradient time of 30 s for the three different temperatures.

Independent of the detector cell volume, the value for $n_{p,KPL}$ increases with rising temperature. However, for the applicability in LCxLC, the maximum gradient time of 30 s should be evaluated. The dashed lines in Figure 5.6 a) and b) show that for this t_G the peak capacity can be further increased with temperature. Peak capacity increases by 25% from 30 °C to 70 °C for the standard detector cell and the effect is even more pronounced for the low volume detector cell with an increase of 40%. Considering the peak capacity production rate for the UV detector with a cell volume of 100 nL for a t_G of 30 s, a ξ of 0.77 s^{-1} at 70 °C is obtained and therefore comparable to the peak capacity production rate (ξ = 0.73 s^{-1}) derived for the low volume detection cell at 30 °C. The highest ξ of 1.03 s^{-1} can be achieved at 70 °C using the low volume detection cell. Therefore, it can be demonstrated that increased temperature is suitable to maximize peak capacity for ultra-fast chromatography as it was already discussed above for isocratic elution.

5.4 Conclusion

A rise in temperature for isocratic elution is more effective to maximize separation efficiency as compared to increased pressure capabilities at low temperature. However, the maximum

efficiency can be achieved using elevated temperatures in combination with higher ΔP_{max} especially in the range of ultra-fast chromatography with column void times of only 1 to 10 s.

The peak capacity for gradient elution increases with rising temperature as well. Peak capacity production rates up to 1 s^{-1} can be achieved when using a column temperature of 70 °C, 1.9 µm fully porous particles, and a minimized detector cell volume as results from gradient kinetic plot analysis. In further studies the application of even smaller particle diameters will be investigated.

5.5 Acknowledgements

The authors would like to thank all column manufacturers for the donation of information and columns. We would like to especially thank Dr. Friederike Becker (YMC Europe GmbH), Eike Logé and Dr. Peter Fischer (AB Sciex Deutschland GmbH) as well as Dr. Kate Monks (KNAUER Wissenschaftliche Geräte GmbH).

5.6 References

[1] D. Guillarme, J. Ruta, S. Rudaz, J.L. Veuthey, New trends in fast and high-resolution liquid chromatography: a critical comparison of existing approaches, Analytical and Bioanalytical Chemistry, 397 (2010) 1069-1082.
[2] S. Fekete, J. Schappler, J.L. Veuthey, D. Guillarme, Current and future trends in UHPLC, Trac-Trends in Analytical Chemistry, 63 (2014) 2-13.
[3] S. Fekete, J. Fekete, D. Guillarme, Estimation of the effects of longitudinal temperature gradients caused by frictional heating on the solute retention using fully porous and superficially porous sub-2 µm materials, J. Chromatogr. A, 1359 (2014) 124-130.
[4] S. Fekete, K. Ganzler, J. Fekete, Facts and myths about columns packed with sub-3 µm and sub-2 µm particles, J. Pharm. Biomed. Anal., 51 (2010) 56-64.
[5] D. Cabooter, J. Billen, H. Terryn, F. Lynen, P. Sandra, G. Desmet, Detailed characterisation of the flow resistance of commercial sub-2 µm reversed-phase columns, J. Chromatogr. A, 1178 (2008) 108-117.
[6] J. De Vos, M. De Pra, G. Desmet, R. Swart, T. Edge, F. Steiner, S. Eeltink, High-speed isocratic and gradient liquid-chromatography separations at 1500 bar, J. Chromatogr. A, 1409 (2015) 138-145.
[7] A. de Villiers, H. Lauer, R. Szucs, S. Goodall, P. Sandra, Influence of frictional heating on temperature gradients in ultra-high-pressure liquid chromatography on 2.1 mm I.D. columns, J. Chromatogr. A, 1113 (2006) 84-91.
[8] N. Wu, J.A. Lippert, M.L. Lee, Practical aspects of ultrahigh pressure capillary liquid chromatography, J. Chromatogr. A, 911 (2001) 1-12.
[9] G. Desmet, S. Eeltink, Fundamentals for LC Miniaturization, Anal. Chem., 85 (2013) 543-556.
[10] S. Heinisch, G. Desmet, D. Clicq, J.-L. Rocca, Kinetic plot equations for evaluating the real performance of the combined use of high temperature and ultra-high pressure in liquid chromatography: Application to commercial instruments and 2.1 and 1 mm I.D. columns, J. Chromatogr. A, 1203 (2008) 124-136.

[11] T. Hetzel, C. Blaesing, M. Jaeger, T. Teutenberg, T.C. Schmidt, Characterization of peak capacity of microbore liquid chromatography columns using gradient kinetic plots, J. Chromatogr. A, 1485 (2017) 62-69.
[12] T. Hetzel, D. Loeker, T. Teutenberg, T.C. Schmidt, Characterization of the efficiency of microbore liquid chromatography columns by van Deemter and kinetic plot analysis, J. Sep. Sci., 39 (2016) 3889–3897.
[13] S. Fekete, I. Kohler, S. Rudaz, D. Guillarme, Importance of instrumentation for fast liquid chromatography in pharmaceutical analysis, J. Pharm. Biomed. Anal., 87 (2014) 105-119.
[14] F. Gritti, T. McDonald, M. Gilar, Intrinsic advantages of packed capillaries over narrow-bore columns in very high-pressure gradient liquid chromatography, J. Chromatogr. A, 1451 (2016) 107-119.
[15] D. Guillarme, S. Heinisch, J.L. Rocca, Effect of temperature in reversed phase liquid chromatography, J. Chromatogr. A, 1052 (2004) 39-51.
[16] K.J. Fountain, U.D. Neue, E.S. Grumbach, D.M. Diehl, Effects of extra-column band spreading, liquid chromatography system operating pressure, and column temperature on the performance of sub-2-μm porous particles, J. Chromatogr. A, 1216 (2009) 5979-5988.
[17] D.T.T. Nguyen, D. Guillarme, S. Rudaz, J.-L. Veuthey, Fast analysis in liquid chromatography using small particle size and high pressure, J. Sep. Sci., 29 (2006) 1836-1848.
[18] U.D. Neue, J.R. Mazzeo, A theoretical study of the optimization of gradients at elevated temperature, J. Sep. Sci., 24 (2001) 921-929.
[19] A. de Villiers, D. Cabooter, F. Lynen, G. Desmet, P. Sandra, High performance liquid chromatography analysis of wine anthocyanins revisited: Effect of particle size and temperature, J. Chromatogr. A, 1216 (2009) 3270-3279.
[20] U.D. Neue, Theory of peak capacity in gradient elution, J. Chromatogr. A, 1079 (2005) 153-161.
[21] U.D. Neue, Peak capacity in unidimensional chromatography, J. Chromatogr. A, 1184 (2008) 107-130.
[22] P. Petersson, A. Frank, J. Heaton, M.R. Euerby, Maximizing peak capacity and separation speed in liquid chromatography, J. Sep. Sci., 31 (2008) 2346-2357.
[23] D. Guillarme, E. Grata, G. Glauser, J.-L. Wolfender, J.-L. Veuthey, S. Rudaz, Some solutions to obtain very efficient separations in isocratic and gradient modes using small particles size and ultra-high pressure, J. Chromatogr. A, 1216 (2009) 3232-3243.
[24] X.L. Wang, D.R. Stoll, P.W. Carr, P.J. Schoenmakers, A graphical method for understanding the kinetics of peak capacity production in gradient elution liquid chromatography, J. Chromatogr. A, 1125 (2006) 177-181.
[25] T. Hetzel, C. vom Eyser, J. Tuerk, T. Teutenberg, T.C. Schmidt, Micro-liquid chromatography mass spectrometry for the analysis of antineoplastic drugs from wipe samples, Analytical and Bioanalytical Chemistry, 408 (2016) 8221–8229.
[26] J. Leonhardt, T. Teutenberg, G. Buschmann, O. Gassner, T.C. Schmidt, A new method for the determination of peak distribution across a two-dimensional separation space for the identification of optimal column combinations, Analytical and Bioanalytical Chemistry, 408 (2016) 8079–8088.
[27] J. Haun, J. Leonhardt, C. Portner, T. Hetzel, J. Tuerk, T. Teutenberg, T.C. Schmidt, Online and splitless nanoLC x capillaryLC with quadrupole/time-of-flight mass spectrometric detection for comprehensive screening analysis of complex samples, Anal. Chem., 85 (2013) 10083-10090.
[28] ChemSpider, http://www.chemspider.com, (accessed 04.02.2017)
[29] R.W. Brice, X. Zhang, L.A. Colon, Fused-core, sub-2 μm packings, and monolithic HPLC columns: a comparative evaluation, J. Sep. Sci., 32 (2009) 2723-2731.

[30] F. Gritti, G. Guiochon, Kinetic performance of narrow-bore columns on a micro-system for high performance liquid chromatography, J. Chromatogr. A, 1236 (2012) 105-114.
[31] T. Hetzel, T. Teutenberg, T.C. Schmidt, Selectivity screening and subsequent data evaluation strategies in liquid chromatography: the example of 12 antineoplastic drugs, Analytical and Bioanalytical Chemistry, 407 (2015) 8475–8485.
[32] A. Vaast, K. Broeckhoven, S. Dolman, G. Desmet, S. Eeltink, Comparison of the gradient kinetic performance of silica monolithic capillary columns with columns packed with 3 μm porous and 2.7 μm fused-core silica particles, J Chromatogr A, 1228 (2012) 270-275.
[33] K. Broeckhoven, D. Cabooter, F. Lynen, P. Sandra, G. Desmet, The kinetic plot method applied to gradient chromatography: Theoretical framework and experimental validation, J. Chromatogr. A, 1217 (2010) 2787-2795.
[34] G. Desmet, D. Cabooter, K. Broeckhoven, Graphical data representation methods to assess the quality of LC columns, Anal. Chem., 87 (2015) 8593-8602.
[35] S. Heinisch, J.-L. Rocca, Sense and nonsense of high-temperature liquid chromatography, J. Chromatogr. A, 1216 (2009) 642-658.
[36] C.V. McNeff, B. Yan, D.R. Stoll, R.A. Henry, Practice and theory of high temperature liquid chromatography, J. Sep. Sci., 30 (2007) 1672-1685.
[37] D. Cabooter, A. Fanigliulo, G. Bellazzi, B. Allieri, A. Rottigni, G. Desmet, Relationship between the particle size distribution of commercial fully porous and superficially porous high-performance liquid chromatography column packings and their chromatographic performance, J. Chromatogr. A, 1217 (2010) 7074-7081.
[38] G. Desmet, D. Clicq, P. Gzil, Geometry-independent plate height representation methods for the direct comparison of the kinetic performance of LC supports with a different size or morphology, Anal Chem, 77 (2005) 4058-4070.
[39] S. Eeltink, S. Dolman, R. Swart, M. Ursem, P.J. Schoenmakers, Optimizing the peak capacity per unit time in one-dimensional and off-line two-dimensional liquid chromatography for the separation of complex peptide samples, J. Chromatogr. A, 1216 (2009) 7368-7374.
[40] Y. Zhang, X. Wang, P. Mukherjee, P. Petersson, Critical comparison of performances of superficially porous particles and sub-2 μm particles under optimized ultra-high pressure conditions, J. Chromatogr. A, 1216 (2009) 4597-4605.

5.7 Chapter appendix

5.7.1 Structural formula of the investigated analytes

The chemical structures of the analytes are depicted in Figure-S 5.1.

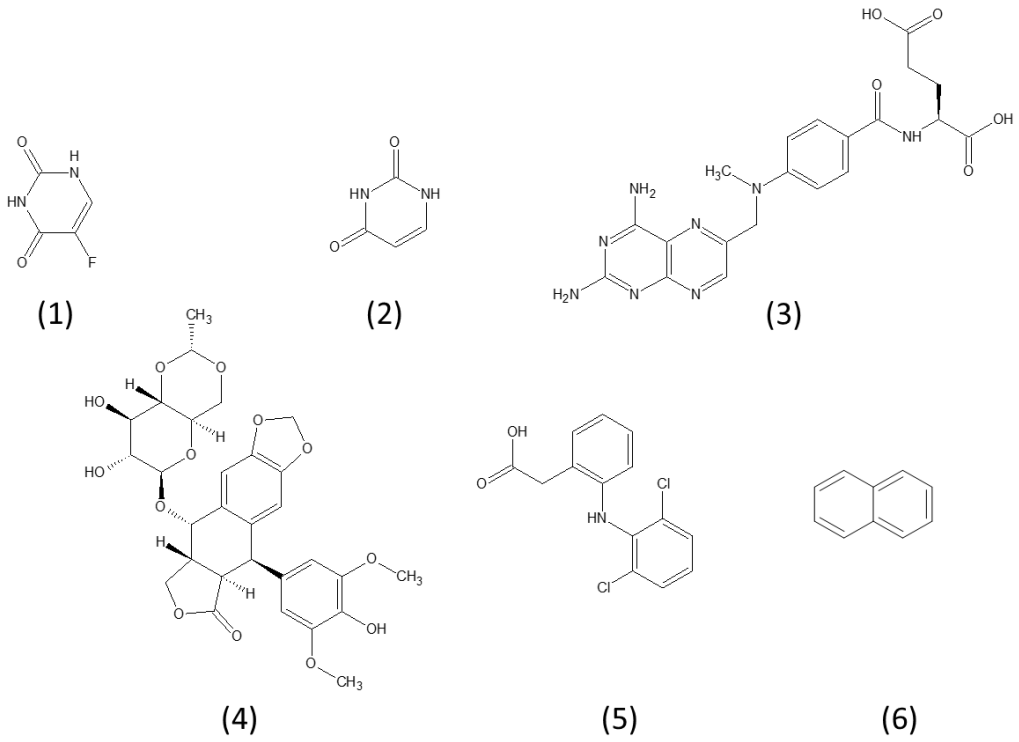

Figure-S 5.1: Chemical structures of the investigated analytes. (1) 5-fluorouracil, (2) uracil, (3) methotrexate, (4) etoposide, (5) diclofenac and (6) naphthalene [1].

Uracil was used for the determination of the column void times. The remaining compounds are pharmaceuticals analyzed within our routine analysis. All analytes differ in polarity which is of utmost importance for the characterization of peak capacity to obtain a uniform distribution across the gradient window. In addition, etoposide and naphthalene were used for the isocratic evaluation.

5.7.2 Mobile phase compositions

For the adjustment of the retention factor (*k*) in isocratic measurements, the mobile phase composition was varied for every column and temperature according to Table-S 5.1 - Table-S 5.3.

Table-S 5.1: Overview of the mobile phase composition at 30 °C for every column.

column	Mobile phase composition: water / acetonitrile (v/v) 30 °C	
	etoposide	naphthalene
Fully porous (50 x 0.3 mm, 1.9 µm)	72.2 / 27.8	58.2 / 41.8
Fully porous (50 x 0.3 mm, 3.0 µm)	72.2 / 27.8	57.4 / 42.6
Core-shell (50 x 0.3 mm, 2.7 µm)	75.0 / 25.0	59.8 / 40.2

Table-S 5.2: Overview of the mobile phase composition at 50 °C for every column.

column	Mobile phase composition: water / acetonitrile (v/v) 50 °C	
	etoposide	naphthalene
Fully porous (50 x 0.3 mm, 1.9 µm)	73.0 / 27.0	61.2 / 38.8
Fully porous (50 x 0.3 mm, 3.0 µm)	73.2 / 26.8	61.6 / 38.4
Core-shell (50 x 0.3 mm, 2.7 µm)	77.0 / 23.0	63.5 / 36.5

Table-S 5.3: Overview of the mobile phase composition at 70 °C for every column.

column	Mobile phase composition: water / acetonitrile (v/v) 70 °C	
	etoposide	naphthalene
Fully porous (50 x 0.3 mm, 1.9 µm)	74.0 / 26.0	64.8 / 35.2
Fully porous (50 x 0.3 mm, 3.0 µm)	74.5 / 25.5	64.7 / 35.3
Core-shell (50 x 0.3 mm, 2.7 µm)	*	*

* not specified for this temperature

5.7.3 Resulting gradient times for the determination of peak capacity depending on temperature

Table-S 5.4 - Table-S 5.15 shows the resulting gradient times (t_G) depending on the flow rate, column and temperature.

Table-S 5.4: Resulting gradient times depending on the flow rate and column for a t_G/t_0 of 2 at 30 °C.

t_G/t_0 = 2	Gradient times (t_G) / min at 30 °C		
Flow rate / µL min^{-1}	1.9 µm fully porous	3.0 µm fully porous	2.7 µm core-shell
10	0.49	0.49	0.38
15	0.32	0.32	0.25
20	0.24	0.24	0.18
25	0.20	0.20	0.15
30		0.16	0.12
35		0.14	0.10
40		0.12	0.09
45		0.11	

Table-S 5.5: Resulting gradient times depending on the flow rate and column for a t_G/t_0 of 2 at 50 °C.

t_G/t_0 = 2	Gradient times (t_G) / min at 50 °C		
Flow rate / µL min^{-1}	1.9 µm fully porous	3.0 µm fully porous	2.7 µm core-shell
10	0.49	0.49	0.38
15	0.32	0.32	0.25
20	0.24	0.24	0.18
25	0.20	0.20	0.15
30	0.16	0.16	0.12
35	0.13	0.14	0.10
40	0.11	0.12	0.09
45		0.11	

Table-S 5.6: Resulting gradient times depending on the flow rate and column for a t_G/t_0 of 2 at 70 °C.

t_G/t_0 = 2	Gradient times (t_G) / min at 70 °C		
Flow rate / µL min^{-1}	1.9 µm fully porous	3.0 µm fully porous	2.7 µm core-shell
10	0.49	0.49	
15	0.32	0.32	
20	0.24	0.24	
25	0.20	0.20	
30	0.16	0.16	
35	0.13	0.14	
40	0.11	0.12	
45	0.10	0.11	

Table-S 5.7: Resulting gradient times depending on the flow rate and column for a t_G/t_0 of 4 at 30 °C.

t_G/t_0 = 4	Gradient times (t_G) / min at 30 °C		
Flow rate / µL min^{-1}	1.9 µm fully porous	3.0 µm fully porous	2.7 µm core-shell
10	0.99	0.99	0.75
15	0.65	0.65	0.50
20	0.48	0.48	0.37
25	0.39	0.39	0.29
30		0.32	0.24
35		0.28	0.21
40		0.24	0.18
45		0.22	

Table-S 5.8: Resulting gradient times depending on the flow rate and column for a t_G/t_0 of 4 at 50 °C.

t_G/t_0 = 4	Gradient times (t_G) / min at 50 °C		
Flow rate / µL min^{-1}	1.9 µm fully porous	3.0 µm fully porous	2.7 µm core-shell
10	0.97	0.99	0.75
15	0.65	0.65	0.50
20	0.48	0.48	0.37
25	0.39	0.39	0.29
30	0.32	0.32	0.24
35	0.26	0.28	0.21
40	0.23	0.24	0.18
45		0.22	

Table-S 5.9: Resulting gradient times depending on the flow rate and column for a t_G/t_0 of 4 at 70 °C.

t_G/t_0 = 4	Gradient times (t_G) / min at 70 °C		
Flow rate / µL min^{-1}	1.9 µm fully porous	3.0 µm fully porous	2.7 µm core-shell
10	0.97	0.99	
15	0.65	0.65	
20	0.48	0.48	
25	0.39	0.39	
30	0.32	0.32	
35	0.26	0.28	
40	0.23	0.24	
45	0.20	0.22	

Table-S 5.10: Resulting gradient times depending on the flow rate and column for a t_G/t_0 of 12 at 30 °C.

t_G/t_0 = 12	Gradient times (t_G) / min at 30 °C		
Flow rate / µL min^{-1}	1.9 µm fully porous	3.0 µm fully porous	2.7 µm core-shell
10	2.97	2.98	2.29
15	1.99	1.98	1.53
20	1.48	1.44	1.14
25	1.18	1.15	0.89
30		0.96	0.74
35		0.82	0.62
40		0.71	0.54
45		0.65	

Table-S 5.11: Resulting gradient times depending on the flow rate and column for a t_G/t_0 of 12 at 50 °C.

t_G/t_0 = 12	Gradient times (t_G) / min at 50 °C		
Flow rate / µL min^{-1}	1.9 µm fully porous	3.0 µm fully porous	2.7 µm core-shell
10	2.92	2.96	2.26
15	1.96	1.94	1.49
20	1.47	1.44	1.10
25	1.17	1.15	0.88
30	0.97	0.96	0.72
35	0.79	0.82	0.62
40	0.68	0.71	0.54
45		0.65	

Table-S 5.12: Resulting gradient times depending on the flow rate and column for a t_G/t_0 of 12 at 70 °C.

t_G/t_0 = 12	Gradient times (t_G) / min at 70 °C		
Flow rate / µL min^{-1}	1.9 µm fully porous	3.0 µm fully porous	2.7 µm core-shell
10	2.92	2.85	
15	1.93	1.90	
20	1.45	1.44	
25	1.15	1.15	
30	0.95	0.96	
35	0.79	0.82	
40	0.68	0.71	
45	0.60	0.65	

Table-S 5.13: Resulting gradient times depending on the flow rate and column for a t_G/t_0 of 20 at 30 °C.

t_G/t_0 = 20	Gradient times (t_G) / min at 30 °C		
Flow rate / µL min^{-1}	1.9 µm fully porous	3.0 µm fully porous	2.7 µm core-shell
10	4.94	4.96	3.82
15	3.32	3.30	2.55
20	2.47	2.44	1.90
25	1.97	1.95	1.49
30		1.62	1.23
35		1.39	1.03
40		1.22	0.90
45		1.08	

Table-S 5.14: Resulting gradient times depending on the flow rate and column for a t_G/t_0 of 20 at 50 °C.

t_G/t_0 = 20	Gradient times (t_G) / min at 50 °C		
Flow rate / µL min^{-1}	1.9 µm fully porous	3.0 µm fully porous	2.7 µm core-shell
10	4.87	4.93	3.77
15	3.26	3.24	2.49
20	2.44	2.42	1.83
25	1.94	1.93	1.46
30	1.61	1.60	1.20
35	1.32	1.38	1.03
40	1.14	1.19	0.90
45		1.05	

Table-S 5.15: Resulting gradient times depending on the flow rate and column for a t_G/t_0 of 20 at 70 °C.

t_G/t_0 = 20	Gradient times (t_G) / min at 70 °C		
Flow rate / µL min^{-1}	1.9 µm fully porous	3.0 µm fully porous	2.7 µm core-shell
10	4.86	4.76	
15	3.21	3.17	
20	2.41	2.36	
25	1.92	1.88	
30	1.59	1.56	
35	1.32	1.33	
40	1.14	1.15	
45	1.01	1.03	

5.7.4 Temperature depending van Deemter curves

Figure-S 5.2 illustrates the resulting temperature depending van Deemter curves for etoposide on the columns packed with 1.9 µm and 3.0 µm fully porous as well as 2.7 µm core-shell particles.

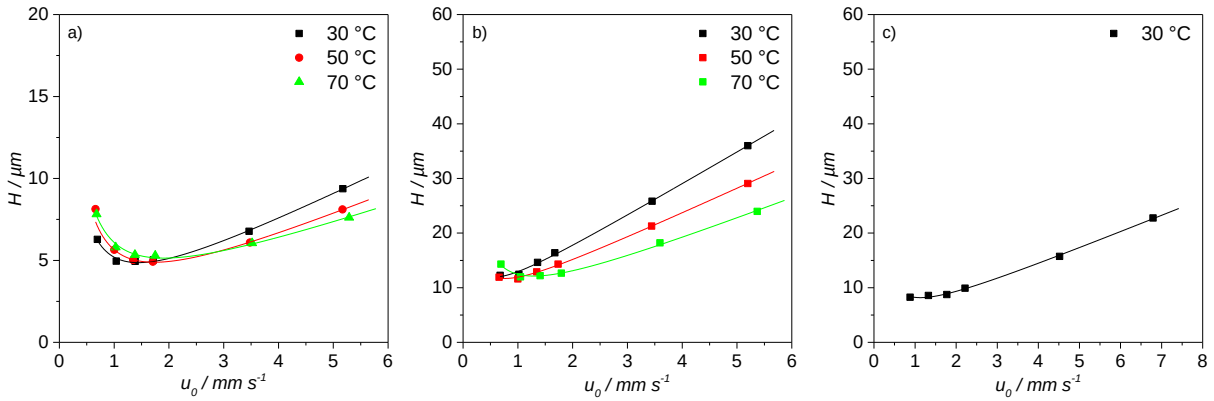

Figure-S 5.2: Resulting van Deemter curves at 30, 50 and 70 °C for etoposide on the column packed with a) 1.9 µm fully porous particles, b) 3.0 µm fully porous particles and c) 2.7 µm core-shell particles.

5.7.5 Temperature depending gradient kinetic plots

The resulting gradient kinetic plots ($n_{p,KPL}$) for the column packed with 3.0 µm fully porous particles for the ratios of the gradient times (t_G) to the column void times (t_0) of 2, 4, 12 and 20 at the three different temperatures of 30, 50 and 70 °C are shown in Figure-S 5.3. For $n_{p,KPL}$ a maximum pressure of 600 bar was used.

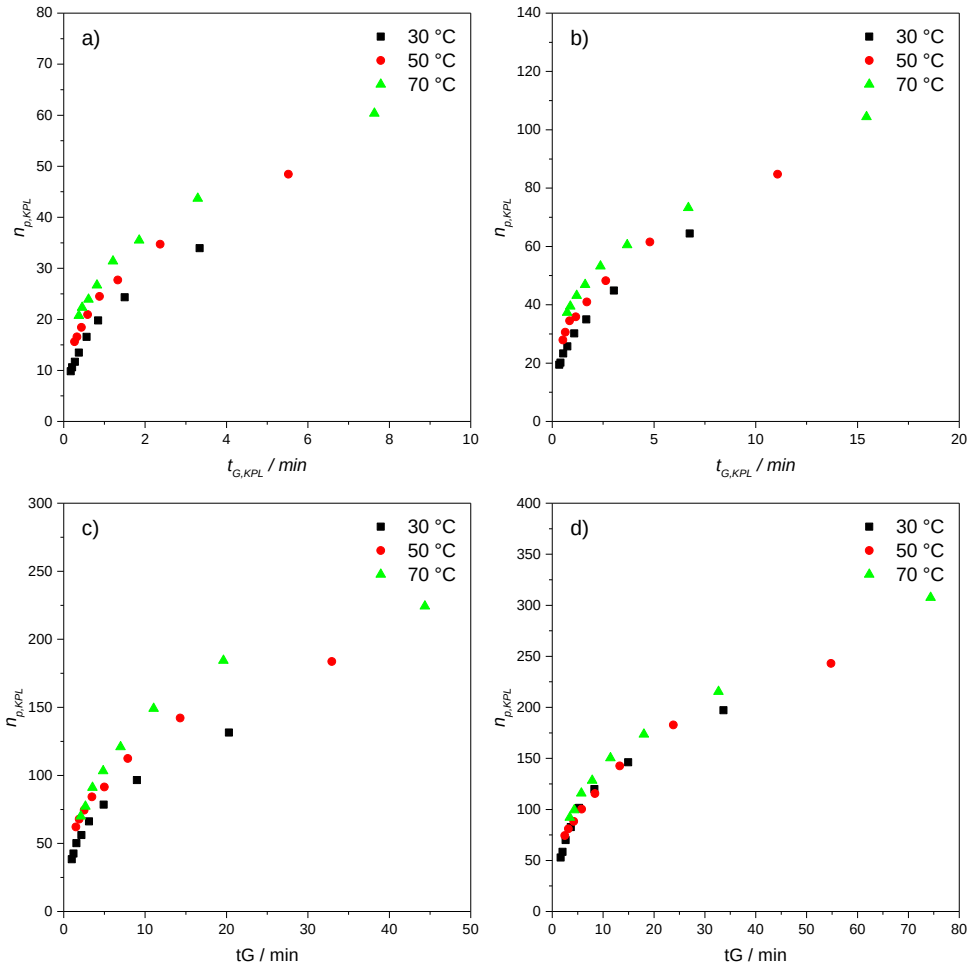

Figure-S 5.3: Comparison of the gradient kinetic plots for the column packed with 3.0 µm fully porous particles at a t_G/t_0 of a) 2, b) 4, c) 12 and d) 20 for the temperatures of 30, 50 and 70 °C. For the calculation of the gradient kinetic plots, a maximum pressure of 600 bar was used (n=3).

Figure-S 5.4 illustrates the comparison of gradient kinetic plots for all t_G/t_0 ratios for the column packed with 2.7 µm core-shell particles at a temperature of 30 and 50 °C.

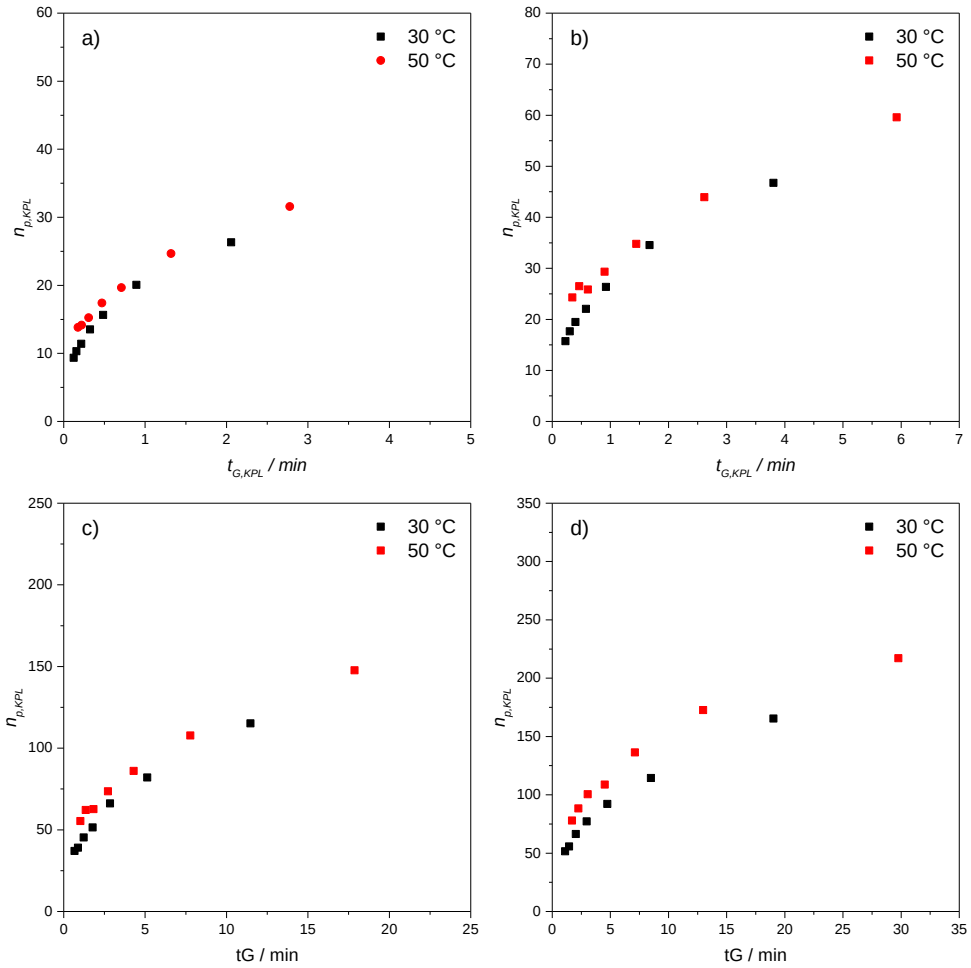

Figure-S 5.4: Comparison of the gradient kinetic plots for the column packed with 2.7 µm fully porous particles at a t_G/t_0 of a) 2, b) 4, c) 12 and d) 20 for the temperatures of 30 and 50 °C. For the calculation of the gradient kinetic plots, a maximum pressure of 600 bar was used (n=3).

In Figure-S 5.5, the results for $n_{p,KPL}$ of all applied t_G/t_0 ratios are depicted for the column packed with 1.9 µm fully porous particles at 30, 50 and 70 °C using the built-in UV detector.

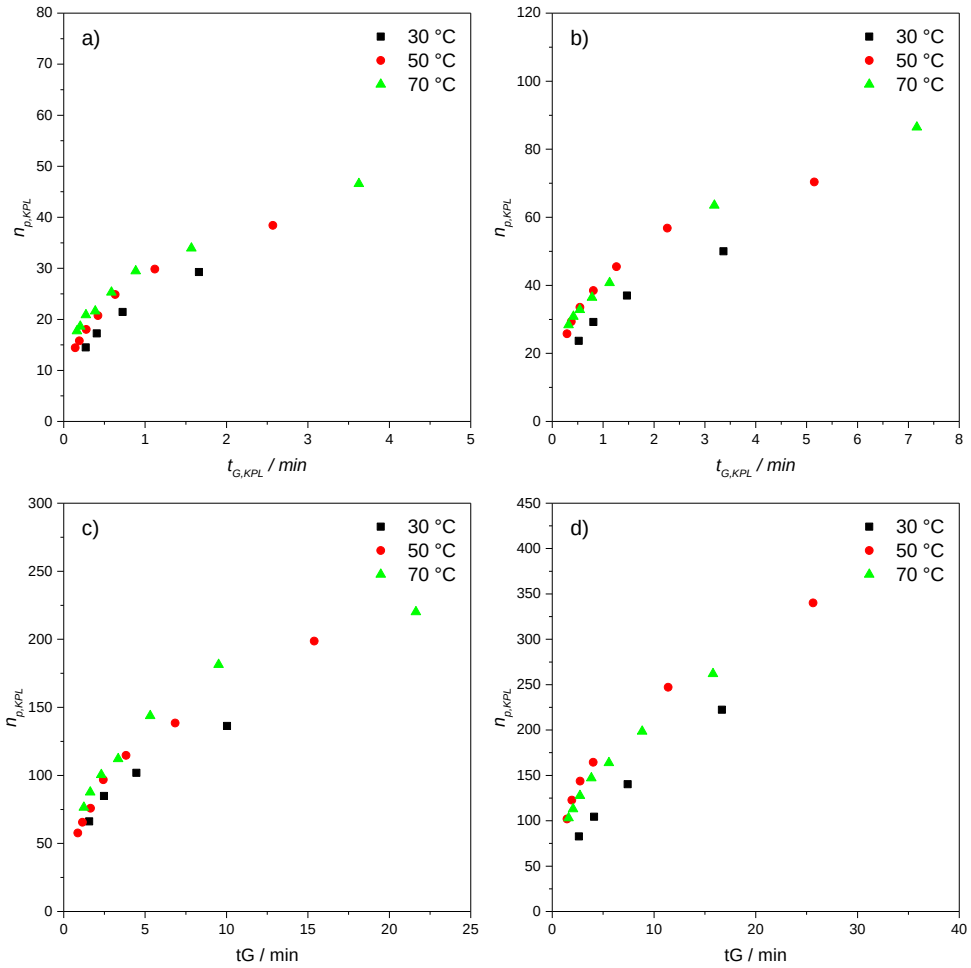

Figure-S 5.5: Comparison of the gradient kinetic plots for the column packed with 1.9 µm fully porous particles at a t_G/t_0 of a) 2, b) 4, c) 12 and d) 20 for the temperatures of 30, 50 and 70 °C using the built-in UV detector. For the calculation of the gradient kinetic plots, a maximum pressure of 600 bar was used (n=3).

The results for $n_{p,KPL}$ of all applied t_G/t_0 ratios are shown in Figure-S 5.6 for the column packed with 1.9 µm fully porous particles at 30, 50 and 70 °C using the alternative UV detector on the basis of an optical waveguide.

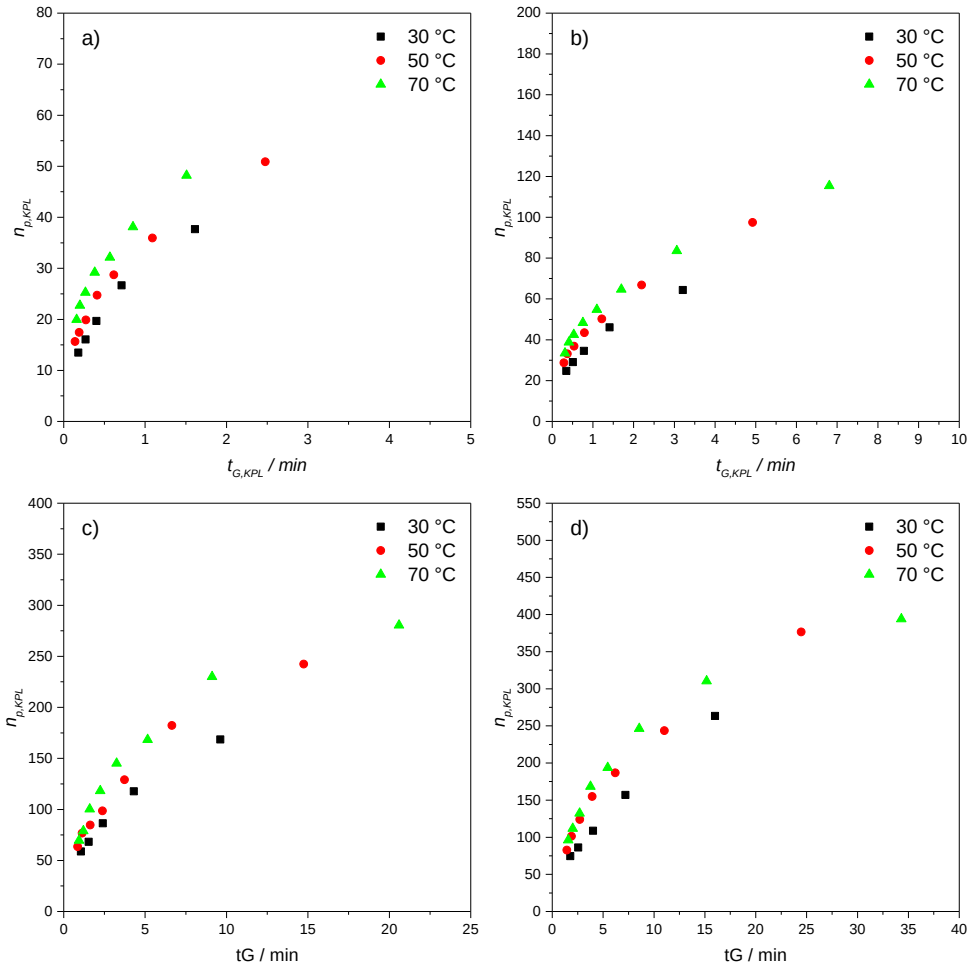

Figure-S 5.6: Comparison of the gradient kinetic plots for the column packed with 1.9 µm fully porous particles at a t_G/t_0 of a) 2, b) 4, c) 12 and d) 20 for the temperatures of 30, 50 and 70 °C using the alternative UV detector on the basis of an optical waveguide. For the calculation of the gradient kinetic plots, a maximum pressure of 600 bar was used (n=3).

5.7.6 References

[1] ChemSpider, http://www.chemspider.com, (accessed 04.02.2017).

Chapter 6 Micro-liquid chromatography mass spectrometry for the analysis of antineoplastic drugs from wipe samples

Redrafted from "Hetzel, T., vom Eyser, C., Tuerk, J., Teutenberg, T., Schmidt, T.C., Micro-liquid chromatography mass spectrometry for the analysis of antineoplastic drugs from wipe samples, Analytical and Bioanalytical Chemistry, 408 (2016) 8221–8229."

Abstract

A fast quantification method for the determination of eleven antineoplastic drugs from wipe samples was developed using micro scale liquid chromatography in combination with tandem mass spectrometry. The extraction efficiency from the wipes has been investigated using different extraction solvents. The results indicate that a mixture of 70/30 water/isopropanol (v/v) acidified with 0.1% formic acid is suitable to desorb the antineoplastic drugs with sufficient recovery between 80-120%. Compared to conventional liquid chromatography, the total analysis time can be reduced to 2.25 min using a 50 x 0.3 mm column at a flow rate of 25 µL min^{-1}. Ion source parameters as well as the injection volume were optimized to ensure the highest sensitivity. The results of method validation showed an instrumental limit of quantification between 0.0068 and 0.0488 ng mL^{-1} using an injection volume of 4.25 µL estimated by the signal to noise ratio. Moreover, the retention time repeatability was determined with a maximum relative standard deviation of 0.4%.

6.1 Introduction

According to the world health organization, cancer is responsible for 13% of all deaths worldwide and current estimations predict an increase of 70% new cases within the next twenty years [1]. The established treatment strategy during cancer therapy is the application of antineoplastic drugs [2, 3]. Apart from patients' wellbeing, the potential health risk for other persons getting in contact with hazardous drugs such as antineoplastics must be considered [4]. Besides pharmacists, nurses, physicians, and other health care workers, staff involved in cleaning, transport, and disposal of hazardous drugs or contaminated material is concerned. Monitoring of occupational exposure has been employed in many healthcare settings and the pharmaceutical industry. Wipe sampling for surface residues of cytostatic drugs is currently the method of choice to determine surface contaminations of the workplace with these drugs as well as the success of cleaning procedures [5-9]. In Germany a substance-independent reference value of 0.1 ng cm^{-2} was established after the Monitoring-Effect Study of Wipe Sampling in Pharmacies (*MEWIP*) [10]. Therefore, reliable and fast analytical methods are needed for routine monitoring to ensure personal safety of health care workers. The common way is the analysis by liquid chromatography (*LC*) mass spectrometry (*MS*) [2, 9, 11]. Whereas in the past compound specific analysis methods were used [6, 12-14], multicomponent analysis approaches are getting of interest [5, 7, 15-17]. This strategy has the advantages of increased information for one sample as well as reducing resources like time, energy and solvents. Nevertheless, these methods are usually based on conventional *LC* characterized by large analysis time, which decreases sample throughput. In order to be able to detect low concentrations in the ng cm^{-2} range of cytostatic drugs, routine laboratories are forced to invest in highly sensitive detection equipment to further optimize routine monitoring of occupational exposure, detection of residual surface contaminations and risk assessment. Besides the primary safety goal, alternative approaches must be found to save resources and costs without compromising sample throughput and data quality to ensure a high return of investment for routine laboratories applying LC-MS/MS. One way to achieve these requirements is the application of miniaturized separation techniques like micro scale liquid chromatography in combination with tandem mass spectrometry (micro-LC-MS/MS) because of the reduced solvent consumption which decreases costs for purchase and disposal of organic solvents. Moreover, the reduced injection volume can significantly contribute to prolong the cleaning intervals of highly sensitive mass spectrometers [18-20]. In general, technological progress must consider all aspects and must not disregard safety issues. In terms of laboratory safety,

toxic organic solvents are a major safety issue. Micro-LC is perfectly suited to reduce the solvent load of a laboratory significantly. In addition, the combination of flow rates in the range of several microliters per minute (µL min^{-1}) and decreased column inner diameter (*i.d.*) between 0.3 to 0.5 mm leads to high linear velocities. In order to achieve similar linear velocities with conventional column *i.d.* (e.g. 4.6 mm), flow rates in the mL min^{-1} range must be applied. Moreover, the reduced gradient delay volumes of dedicated micro-LC systems are a key feature to achieve fast separations and reduced analysis cycle times. As a consequence, the sample throughput can be significantly increased which represents a major advantage for routine analysis. Therefore, micro-LC combines all requirements in terms of green analytical chemistry and covering safety aspects within the laboratory [21].

Although the separation power of micro-LC has been demonstrated in various application areas [18, 20, 22-25] and despite its advantages, the use of micro-LC for routine analysis is often confronted with persistent prejudices like missing robustness and sensitivity [18, 19, 26, 27]. In terms of sensitivity it clearly depends on whether the sample volume is limited, as is often the case for biological applications [19], or the sample volume is not limited. Injecting a sample with a volume of only e.g. 100 nL will always lead to higher sensitivity when using microbore columns instead of analytical columns.

Therefore, the aim of this study is the development and validation of a robust and highly sensitive micro-LC-MS/MS method for regular monitoring and control of the reference value of 0.1 ng cm^{-2} for selected antineoplastic drugs. For this purpose, the extraction and separation of eleven antineoplastic drugs from wipe samples are investigated.

6.2 Material and methods

6.2.1 LC-MS method parameters

All measurements were performed on an Eksigent ExpressLC ultra system coupled to a QTrap 6500 tandem mass spectrometer (Sciex, Dublin, CA). The micro-LC system is based on pneumatic piston pumps with a pressure limit up to 690 bar. Flow calibration was done with a volume of 100 µL at a flow rate of 25 µL min^{-1} using a standard 5-50 µL min^{-1} flow module. Aspirating and dispensing of the sample was done by an HTS PAL autosampler (CTC Analytics, Zwingen, Switzerland), whereas the actual injection was done by the built-in six port valve using the metered injection mode. The installed sample loop has a volume of 10 µL with an inner diameter of 150 µm made of stainless steel. All other system connections were made

of fused silica surrounded by polyetherether ketone (PEEKSil) capillaries with an inner diameter of 50 µm. For temperature control, a column static air oven was used at a temperature of 40 °C. The chromatographic separation was performed on a multistage endcapped YMC Triart C18 (50 x 0.3 mm, 1.9 µm, YMC Europe GmbH, Dinslaken, Germany) column. The flow rate was adjusted to 25 µL min^{-1} to ensure a high linear velocity and to achieve a fast separation. The following gradient program was used: from 10% ACN to 50% in 1.6 min before increasing the organic portion to 99% in 0.9 min. The injection volume was optimized starting from 250 nL.

For MS data acquisition, the multiple reaction monitoring (*MRM*) mode was used. A list of mass transitions is given in Table-S 6.2. The optimization of ion source parameters can be found in the supplementary material (Chapter 6.7.4). For data acquisition and analysis the Eksigent control software (Version 4.1 Patch for ekspert nanoLC 400 and batch acquisition control) and Analyst (Version 1.6.3) were used. Further data processing was done using Origin Lab v. 9.1 and Microsoft Excel 2010.

6.2.2 Sampling protocol

The sampling and subsequent extraction of the antineoplastic drugs is accomplished by the following protocol. For sampling, three wipes from Kimtech Science (Kimberly-Clark Professional, Koblenz, Germany) are moistened with 1 mL wetting solution per wipe. The investigated surface is swept in three different directions using one wipe for each step. The sampling procedure is illustrated in Figure 6.1.

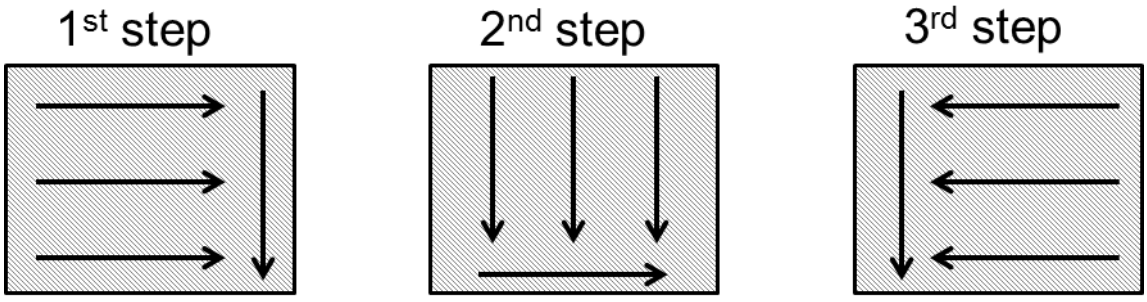

Figure 6.1: Schematic sampling procedure with one wipe for each step. Recommended sampling area: 30 x 30 cm.

Afterwards, the samples are stored in a beaker (Rotilabo, Carl Roth, Karlsruhe, Germany). For sample extraction, 10 mL of extraction solvent per wipe were added and treated in an ultrasonic bath for 15 min. Subsequently, 1 mL of the extract was aspirated and filtered using a 0.45 µm regenerated cellulose filter (Chromafil RC-45/25; Macherey-Nagel, Germany) connected to a

2 mL syringe (B Braun Injekt; B. Braun Melsungen AG; Melsungen, Germany) before transferred into a glass vial which was used for the final analysis.

6.2.3 Wetting solution and evaluation of extraction efficiency by QC samples

At first, the wetting solution for sampling must be specified to ensure a sufficient transfer of each target analyte from the investigated surface into the sampling wipe. Therefore, with respect to the log D values in Table-S 6.1, the wetting solution must be suitable for polar as well as non-polar substances. Since the sampling is done on site by the staff in the pharmacy or ward of the hospitals a non-toxic solution is needed. Several investigations showed sufficient sampling efficiency using a mixture of 30/70 (v/v) water/2-propanol [5, 15], which can be regarded as non-hazardous. For the investigation of sample extraction efficiency, different compositions of dimethyl sulfoxide (DMSO), 2-propanol (IPA), acetonitrile (ACN) with water (H_2O) were used. The latter two were also used as mobile phase constituents with a portion of 0.1% FA (v/v), purchased from Sigma-Aldrich (Seelze, Germany). All other solvents were obtained from Th. Geyer-Chemsolute (Renningen, Germany) and LGC Promochem (Wesel, Germany) with a purity of at least 99.5%.

The three organic extraction agents DMSO, ACN and IPA differ in their properties and elution strength. Whereas DMSO and ACN are aprotic-polar and aprotic-non-polar solvents, IPA has a protic character. The elution strength in reversed phase chromatography increases from ACN over IPA to DMSO. Additionally, the composition of DMSO and ACN was varied between 5-20% (v/v) in 5% steps in combination with H_2O. For IPA five different mixtures were investigated because IPA was identified as suitable wetting solvent [5, 15]. A mixture of 70/30, 80/20, 85/15, 90/10 and 95/5 (v/v) H_2O:IPA was prepared. All solvent compositions used for sample extraction were acidified with 0.1% FA. For the evaluation of the extraction efficiency, four quality control samples (QC) were prepared for each solvent composition. For this purpose, the wipes moistened with the wetting solution were spiked with a solution of a concentration of 5 and 10 ng mL^{-1} to obtain an amount of 165 and 330 ng per sample before extraction solvent was added and the wipes were treated in an ultrasonic bath. Afterwards, 1 mL of the extract was filtered and transferred into the glass vial. The analysis was done with the corresponding matrix calibration as described below.

6.2.4 Stock solutions and matrix calibration

An overview about the investigated substances, analyte properties as well as structural formulae can be found in the supplementary material (Table-S 6.1, Figure-S 6.1). The stock solutions were prepared using a mixture of water/acetonitrile (50/50, v/v) in a concentration of 1 mg mL^{-1} and 0.1 mg mL^{-1}, respectively. The eleven solutions were merged with a final concentration of 10 µg mL^{-1}. For calibration standards an individual sample matrix was made according to the sample preparation procedure and solvent composition. Therefore, three wipes were transferred into the beaker before 3 mL wetting solution and 30 mL extraction solvent were added. After ultrasonic treatment, the solution was filtered and stored in a second beaker. The obtained matrix was used for further dilution of the 10 µg mL^{-1} multicomponent standard to prepare the calibration standards in a range between 0.01 ng mL^{-1} to 100 ng mL^{-1}. Matrix, multicomponent standard and quality control samples were prepared on the same day of measurement.

6.2.5 Method validation protocol

For the final method validation, the following procedure was applied: four QC samples of three different concentrations were prepared according to the procedure described in Chapter 6.2.3 using an independent 1000 ng mL^{-1} multicomponent stock solution to obtain QC samples with a concentration of 1, 10 and 100 ng mL^{-1}. The analysis was performed with the corresponding matrix calibration. Additionally, the limit of detection (LOD) and limit of quantification (LOQ) was determined by the signal-to-noise (S/N) ratio of 3:1 for the LOD and 10:1 for the LOQ. In addition, the method detection limit (MDL) in ng cm^{-2} was calculated on the basis of the recommended sampling area of 900 cm^2. A detailed calculation for the MDL can be found in the supplementary material (Chapter 6.7.5). Furthermore, a tenfold injection of the 1 ng mL^{-1} standard was done to evaluate the system repeatability representing the so-called intra-assay. Moreover, an inter-assay including a four time injection of the 1 ng mL^{-1} standard was performed to investigate the repeatability over three days. At the end, the carry-over was determined using the highest standard in the linear range for the individual target analyte followed by two blank injections.

6.3 Results and discussion

6.3.1 Investigation of extraction efficiency

In order to identify a suitable extraction solution, a recovery between 80-120% was defined although the Occupational Safety & Health Administration (OSAH) recommends a minimum

recovery of 75% [28]. Figure 6.2 shows the recovery for each compound including error bars when using DMSO, ACN and IPA as organic solvent for the 10 ng mL^{-1} QC samples. The resulting recovery for the 5 ng mL^{-1} QC samples showing the same trend can be found in the supplementary material (Figure-S 6.2).

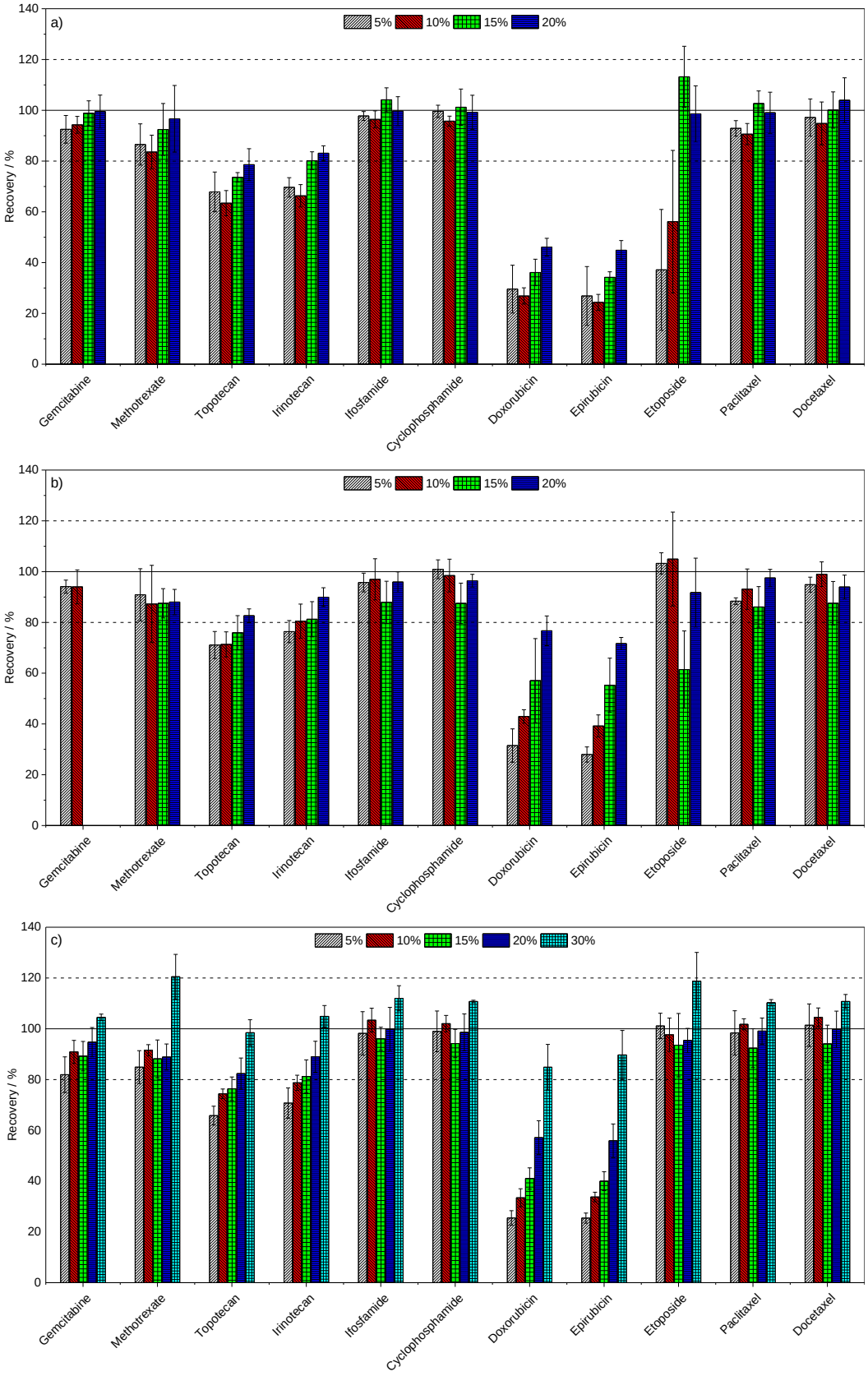

Figure 6.2: Resulting recovery of the eleven antineoplastic drugs for a mixture of a) H_2O:DMSO + 0.1% FA, b) H_2O:ACN + 0.1% FA and c) H_2O:IPA + 0.1% FA in various compositions for a concentration of 10 ng mL^{-1} (see figure legend describing the amount of organic solvent in the extraction solution; number of QC samples = 4).

As can be seen from Figure 6.2 a), the recovery for topotecan, doxorubicin and epirubicin do not fulfill the requirement of 80-120% recovery. All other substances could be extracted sufficiently with a portion of 20% DMSO. This seems surprising because DMSO is often recommended as universal extraction solvent. Next, ACN was investigated as organic solvent because ACN is also used as a mobile phase constituent for chromatography. Figure 6.2 b) illustrates the recovery for ACN as extraction solvent.

Again, the recovery of doxorubicin and epirubicin is below the desired validation criteria. With increasing content of ACN the recovery increases for these two compounds. Therefore, an even higher ACN concentration could lead to sufficient recovery. However, serious chromatographic problems are expected for polar compounds due to the missing focussing at the column head. This is also the reason why no recovery can be estimated for gemcitabine if the ACN content is higher than 10%. At the end, IPA as protic solvent was applied as organic extraction solvent. Finally, it was identified as suitable wetting solution. Figure 6.2 c) shows the obtained recovery rates for IPA.

As illustrated, a mixture of 70/30 H_2O/IPA (v/v) + 0.1% FA represents a suitable solvent composition to obtain sufficient recovery between 80-120% for all substances. Recovery values higher than 100% can be obtained due to matrix effects [29, 30]. The protic solvent property favours the extraction for the epimers doxorubicin and epirubicin due to the possibility of hydrogen bonding and solvation. As expected, the isomers ifosfamide and cyclophosphamide as well as the epimers doxorubicin and epirubicin show comparable behaviour in terms of the extraction efficiency with respect to the solvent composition.

To summarize, a wetting solution of 30/70 H_2O/IPA (v/v) in combination with an extraction agent of 70/30 H_2O/IPA + 0.1% FA (v/v) results in sufficient recovery for all substances. Taking the volume of 3 mL wetting solution and 30 mL extraction solvent into account, the final sample composition is 66.4/33.6 H_2O/IPA (v/v) + 0.1% FA.

6.3.2 Micro-LC-MS/MS analysis

6.3.2.1 Chromatographic requirements and conditions

As can be seen from Table-S 6.2, the epimers doxorubicin and epirubicin have identical mass transitions. Therefore, a chromatographic separation is needed because a differentiation by MS is not possible. In addition, ifosfamide and cyclophosphamide are isomers. Although two different mass transitions are selected, they also must be separated chromatographically due to

cross talk, which is shown more detailed in Chapter 6.7.3.2. The separation of paclitaxel and docetaxel is deemed necessary because of ion suppression. In a previous study, the selectivity of the phase system was investigated [31]. As a result, the YMC Triart C18 (50 x 0.3 mm, 1.9 µm) was identified as a suitable column for the separation of the critical peak pairs. Although it was found that methanol leads generally to an increased selectivity, using H_2O and ACN + 0.1% FA as mobile phase results in a sufficient selectivity for all critical peak pairs in combination with this stationary phase. In addition, ACN is advantageous because of the reduced viscosity leading to a decreased pressure drop. Thereby, higher flow rates can be used to reduce the cycle times and thus increasing sample throughput which is an important factor for routine analysis. Next, the injection volume must be optimized in order to achieve the required LOQ of 0.1 ng mL^{-1}. Usually the injection volume should be 10% maximum of the column void volume. According to Equation 6.1, the geometric column volume is 3.53 µL for a 50 x 0.3 mm column.

$$V_{col} = \left(\frac{d_c}{2}\right)^2 \cdot \pi \cdot L \qquad \textbf{Equation 6.1}$$

Since the accessible column volume is influenced by the stationary phase material, a porosity of 0.7 is considered to calculate the effective column volume (V_{eff}), which is 2.47 µL. Thus the recommended injection volume is approximately 250 nL. Figure-S 6.3 a) shows the resulting chromatogram for the separation of the eleven antineoplastic drugs using an injection volume of 250 nL.

As can be seen, the required LOQ can be achieved for most of the target analytes injecting a mass of only 25 fg. Unfortunately, docetaxel and methotrexate cannot be detected at this concentration. In addition, the S/N ratio for topotecan (S/N: 2.6) is critical. Therefore, a higher injection volume must be chosen to reach the LOQ and to improve the S/N ratio. The resulting chromatogram is illustrated in Figure-S 6.3 b) using an injection volume of 425 nL.

As can be seen a minimum injection volume of 425 nL, which corresponds to an injected mass of 42.5 fg, is needed to achieve the required LOQ. However, peak distortion effects occur for the semi-polar compounds methotrexate and topotecan as becomes clear from magnification in Figure-S 6.3 c) representing the separation for a concentration of 1 ng mL^{-1}. In addition, the peak shape of etoposide shows a peak splitting. The reason for this peak distortion is the missing focussing for the polar and semi-polar compounds at the column head. Due to the increased injection volume and higher elution strength of the injection solvent compared to the initial

mobile phase composition, the chromatographic band of these compounds is broadened. As a consequence, the remaining column volume is not sufficient to compress the band leading to distorted peak shapes. This phenomenon is schematically depicted in Figure-S 6.4. In addition, applying even higher injection volumes leads to an increased pressure drop during the injection when using the 66.4/33.6 H_2O/IPA (v/v) + 0.1% FA solvent composition. For large volume injections (*LVI*) the pressure drop increases to the maximum system pressure. This must also be considered for the final method. Therefore, dilution of the samples was considered as an alternative approach to achieve symmetric peak shapes for all compounds.

6.3.2.2 Sample dilution and large volume injection

In order to compensate the peak distortion phenomena, the number of possible strategies is limited. A lower content of the organic solvent in the extraction solvent is not useful in terms of the required recovery as illustrated in Figure 6.2 c). Another approach is the aqueous dilution of the sample in a ratio of 1/10 (v/v) to decrease the organic portion in the injection solution. The resulting sample composition is 96.6/3.4 H_2O/IPA (v/v) + 0.1% FA. To keep the injected absolute mass of 42.5 fg constant, it is necessary to increase the injection volume by the dilution factor. Therefore, the final injection volume is 4.25 µL. Figure 6.3 shows the resulting chromatogram of the diluted sample for a concentration of 1 ng mL^{-1}.

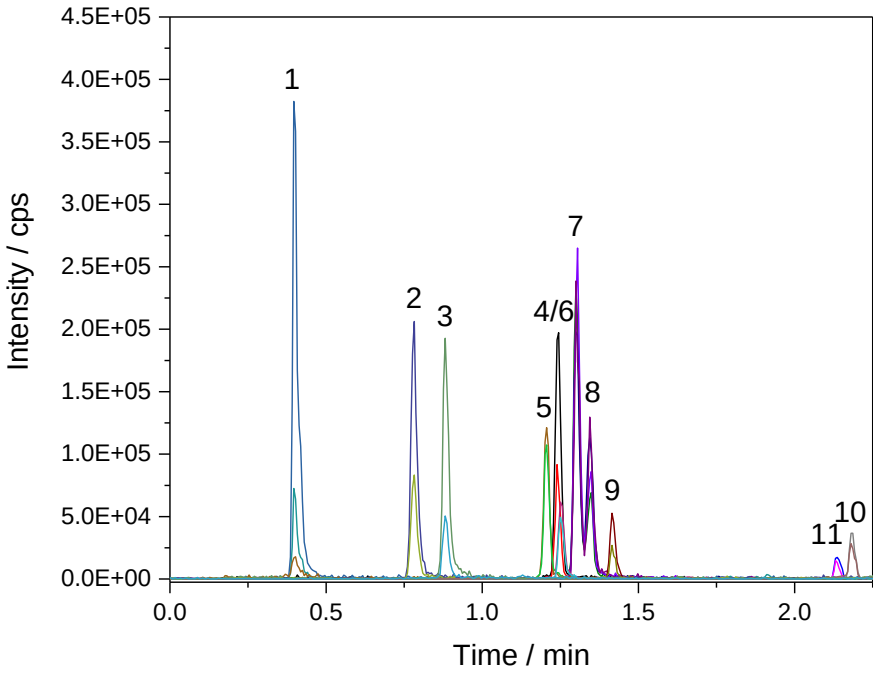

Figure 6.3: Resulting chromatogram for the separation of the eleven antineoplastic drugs for a concentration of 1 ng mL^{-1} using an injection volume of 4250 nL. Analytes: (1) gemcitabine, (2) methotrexate, (3) topotecan, (4) irinotecan, (5) ifosfamide, (6) cyclophosphamide, (7) doxorubicin, (8) epirubicin, (9) etoposide, (10) paclitaxel, (11) docetaxel.

As can be seen, highly symmetric peak shapes are obtained because of the reduced solvent strength of the sample solution. In addition, the separation of the isobaric compounds is still maintained with a critical resolution of 1.2 for ifosfamide (5) and cyclophosphamide (6). Consequently, the dilution factor needs to be considered with respect to the LOQ. Due to the dilution by the factor of 10, the required LOQ is also reduced by the same factor. Therefore, the required LOQ is 0.01 ng mL^{-1}.

6.3.3 Method validation data

Since the method is applied in an accredited environment, method validation data must be recorded. This comprises intra-day and inter-day stability, carry-over as well as LOD and LOQ. The prepared samples are diluted in a ratio of 1/10. Therefore, the final concentrations of the QC samples are 0.1, 1.0 and 10 ng mL^{-1}. For the determination of carry-over, the area of the following blank injection after the highest standard of the linear range for every compound was used.

Table 6.1: Overview of the method validation data including intra-assay, inter-assay, three different level of QC samples, LOD, LOQ, MDL, upper limit as well as Carry-over and retention time repeatability. For the calculation of the MDL in ng cm^{-2}, the recommended sampling area of 900 cm^2 was used. The dilution factor is considered.

Compound	intra-assay 1 ng mL^{-1} / % (n=10)	inter-assay 1 ng mL^{-1} / % (n=12)	QC 0.1 ng mL^{-1} / % (n=4)	QC 1.0 ng mL^{-1} / % (n=4)	QC 10 ng mL^{-1} / % (n=4)	LOD / ng mL^{-1}	LOQ / ng mL^{-1}	MDL / ng cm^{-2}	Upper limit / ng mL^{-1}	Carry-over / %	t_R/ min (n=16)	RSD / %
Gemcitabine	3.4	3.5	119 ± 3.3%	97 ± 6.4%	91 ± 3.2%	0.0020	0.0068	0.0025	25	0.04	0.400	0.4
Methotrexate	4.0	6.8	118 ± 4.8%	104 ± 1.2%	92 ± 3.8%	0.0037	0.0123	0.0045	25	0.19	0.785	0.2
Topotecan	3.0	6.3	110 ± 6.6%	100 ± 4.6%	89 ± 2.0%	0.0018	0.0060	0.0022	25	0.20	0.892	0.2
Irinotecan	5.7	6.1	100 ± 14.8%	100 ± 5.6%	102 ± 3.1%	0.0038	0.0125	0.0046	25	0.19	1.260	0.0
Ifosfamide	4.0	4.8	112 ± 11.5%	117 ± 5.1%	98 ± 3.2%	0.0032	0.0105	0.0039	10	0.34	1.201	0.3
Cyclophosphamide	2.7	3.3	113 ± 8.1%	118 ± 5.8%	102 ± 3.0%	0.0021	0.0069	0.0025	25	0.25	1.239	0.2
Doxorubicin	4.5	4.8	115 ± 6.7%	100 ± 5.2%	85 ± 3.4%	0.0016	0.0052	0.0019	100	0.12	1.304	0.4
Epirubicin	5.4	5.3	115 ± 5.3%	100 ± 4.9%	104 ± 7.2%	0.0029	0.0095	0.0035	25	0.20	1.349	0.3
Etoposide	4.9	11.2	108 ± 24.6%	102 ± 3.0%	93 ± 8.7%	0.0032	0.0108	0.0040	25	0.12	1.420	0.0
Paclitaxel	9.4	12.9	106 ± 13.0%	103 ± 9.5%	111 ± 3.5%	0.0062	0.0207	0.0076	50	0.26	2.172	0.2
Docetaxel	13.5	16.2	107 ± 24.6%	111 ± 19.7%	117 ± 13.1%	0.0146	0.0488	0.0179	25	0.18	2.126	0.2

The data included in Table 6.1 show a sufficient intra- and inter-day stability with a maximum standard deviation below 5% for most of the target compounds. Higher deviations are especially observed for the last eluting analytes paclitaxel and docetaxel. This result is attributed to the low response, as can be seen from the LOD and LOQ, as well as to the elution in the region with an increased gradient slope of 54.4% B min^{-1}. Thereby, the resulting peak width is around 3 to 4 s. As a consequence, with a cycle time of 0.3502 s only 11-12 data points per peak are obtained. This could be the reason why higher deviations are observed for these two compounds. Although it would be possible to decrease the dwell time in order to reduce the MS cycle time, the S/N ratio would be negatively affected due to the increased noise at reduced *MRM* dwell times. Another strategy would be a decreased gradient slope to increase the peak width in order to collect more data points per peak. This approach has several disadvantages. First of all, the sensitivity would decrease because of the increased peak width. Furthermore, higher analysis cycle times are obtained which would impede high sample throughput.

The results for the QC samples for the concentrations of 0.1, 1.0 and 10.0 ng mL^{-1} show sufficient recovery between 80 and 120% for all target analytes. In general, with increasing concentration the standard deviation decreases for almost every substance. This is expected because in particular the QC concentration of 0.1 ng mL^{-1} is near the LOQ.

The LOD and LOQ for an injection of 42.5 fg is around 10 pg mL^{-1} for almost every compound. Again, paclitaxel and docetaxel have an increased LOQ due to the lower response. In order to further decrease the LOQ, the method could be split into two methods, one for the polar and semipolar compounds and one for the nonpolar target analytes. Thereby, a higher injection volume for the nonpolar substances could be used because of the enrichment on the column head. As consequence, two injections for every sample need to be done, which decreases sample throughput. Nevertheless, if higher sensitivity is required, this strategy could be easily applied.

For a valid quantification in the lower ng mL^{-1} range low carry-over and stable retention times are a prerequisite. The data in Table 6.1 show a maximum carry-over of 0.34% for ifosfamide. Therefore, a second blank injection is always done to further decrease the carry-over. The retention time variability with a maximum deviation of 0.4% underlines the stability of the developed method and is below the required limits [32, 33]. To that end, the validation data reveal the applicability of micro-LC separations for routine analysis.

6.3.4 Analysis of real samples

Figure 6.4 shows the separation of three different real samples for the eleven antineoplastic drugs using the micro-LC-MS/MS hyphenation. These real samples were taken from different sampling locations using the described sampling procedure within the hospital pharmacies and application areas at the hospital wards.

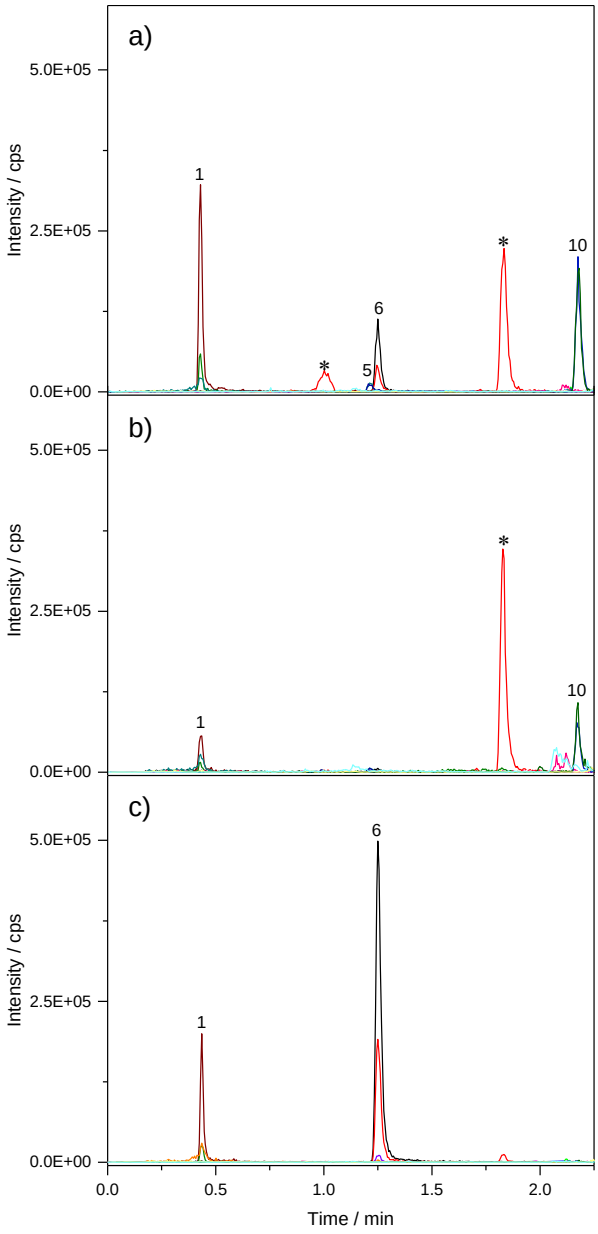

Figure 6.4: Resulting chromatograms for the separation of three different real samples for the eleven antineoplastic drugs using the micro-LC-MS/MS hyphenation. Observed interferences on the selected mass transitions for cyclophosphamide are highlighted by a star.

As can be seen from Figure 6.4, the developed method can be applied for real samples. Mainly, gemcitabine, ifosfamide, cyclophosphamide and paclitaxel were found with a maximum concentration of 28.5 ng mL^{-1} for paclitaxel.

The signals in Figure 6.4 a) and b), highlighted by a star, represent interferences of the second mass transition of cyclophosphamide. If only one *MRM* was recorded, a reliable identification only by this selected *MRM* and resulting retention time would be difficult. Therefore, these examples clearly show the advantages of using the retention time as well as recording two *MRM* transitions for every target analyte as identification criteria.

6.4 Conclusion

The data of method validation clearly show the successful applicability for the analysis of eleven antineoplastic drugs using micro-LC-MS/MS in a routine environment. The common prejudice that this technique can only be used for limited sample volume can be refuted. The instrumental LOQ for an injection of 42.5 fg is sufficient for all target analytes. Because of the dilution factor of 10 the sensitivity of paclitaxel and docetaxel is higher than defined (LOQ = 0.1 ng mL^{-1}) with a maximum instrumental LOQ of 0.49 ng mL^{-1} for docetaxel. However, the reference value depends on the actual sampling area (recommended: 900 cm^2). Therefore, no limitations with respect to the achieved LOQ (MDL_{max} = 0.018 ng cm^{-2}) occurs and thus, the reference value can be achieved when a minimum sampling area of 161 cm^2 is available if small objects like e.g. a telephone handset or a door knob have to be wiped. This equals an area of approximately 13 x 13 cm. Compared to already established conventional LC-MS methods, the obtained instrumental LOQ could be decreased for all substances. In addition, the runtime could be significantly reduced to only 2.25 min per analysis. Thereby, a higher utilization of resources can be ensured leading to higher sample throughput and reduced solvent consumption without compromising sensitivity. As a consequence, the developed method can also be applied for quality control.

6.5 Acknowledgements

The authors would like to especially thank the European Society of Oncology Pharmacy (ESOP) for their support of the MASHA project (Research about Environmental Contamination by Cytotoxics and Management of Safe Handling Procedures). Moreover, we would like to thank Ewelina Korczowska for the organization of sampling and sample shipment.

6.6 References

[1] World Health Organization (WHO), http://www.who.int/cancer/en/, (accessed 26.06.2016)

[2] S. Nussbaumer, P. Bonnabry, J.-L. Veuthey, S. Fleury-Souverain, Analysis of anticancer drugs: A review, Talanta, 85 (2011) 2265-2289.

[3] R. Schierl, A. Boehlandt, D. Nowak, Guidance Values for Surface Monitoring of Antineoplastic Drugs in German Pharmacies, Annals of Occupational Hygiene, 53 (2009) 703-711.

[4] National Institute for Occupational Safety and Health (NIOSH) - List of antineoplastic and other hazardous drugs in healthcare settings 2014. By Connor TH, MacKenzie BA, DeBord DG, Trout DB, O'Callaghan JP. Cincinnati, OH: U.S. Department of Health and Human Services, Centers for Disease Control and Prevention, National Institute for Occupational Safety and Health, DHHS (NIOSH) Publication No. 2014-138 (Supersedes 2012-150). http://www.cdc.gov/niosh/docs/2014-138/pdfs/2014-138.pdf, 2014, (accessed 25.06.2016)

[5] M. Anastasi, S. Rudaz, T.Q. Lamerie, P. Odou, P. Bonnabry, S. Fleury-Souverain, Efficacy of Two Cleaning Solutions for the Decontamination of 10 Antineoplastic Agents in the Biosafety Cabinets of a Hospital Pharmacy, Annals of Occupational Hygiene, 59 (2015) 895-908.

[6] A. Bohlandt, S. Groeneveld, E. Fischer, R. Schierl, Cleaning Efficiencies of Three Cleaning Agents on Four Different Surfaces after Contamination by Gemcitabine and 5-fluorouracile, Journal of occupational and environmental hygiene, 12 (2015) 384-392.

[7] M. Jeronimo, M. Colombo, G. Astrakianakis, C.-Y. Hon, A surface wipe sampling and LC-MS/MS method for the simultaneous detection of six antineoplastic drugs commonly handled by healthcare workers, Analytical and Bioanalytical Chemistry, 407 (2015) 7083-7092.

[8] S. Nussbaumer, L. Geiser, F. Sadeghipour, D. Hochstrasser, P. Bonnabry, J.-L. Veuthey, S. Fleury-Souverain, Wipe sampling procedure coupled to LC-MS/MS analysis for the simultaneous determination of 10 cytotoxic drugs on different surfaces, Analytical and Bioanalytical Chemistry, 402 (2012) 2499-2509.

[9] T.H. Connor, M.D. Zock, A.H. Snow, Surface wipe sampling for antineoplastic (chemotherapy) and other hazardous drug residue in healthcare settings: Methodology and recommendations, Journal of Occupational and Environmental Hygiene, 13 (2016) 658-667.

[10] T.K. Kiffmeyer, J. Tuerk, M. Hahn, H. Stuetzer, C. Hadtstein, A. Heinemann, U. Eickmann, Application and Assessment of a Regular Environmental Monitoring of the Antineoplastic Drug Contamination Level in Pharmacies - The MEWIP Project, Annals of Occupational Hygiene, 57 (2013) 444-455.

[11] R. Turci, C. Sottani, G. Spagnoli, C. Minoia, Biological and environmental monitoring of hospital personnel exposed to antineoplastic agents: a review of analytical methods, Journal of Chromatography B, 789 (2003) 169-209.

[12] D. Merger, C. Tanguay, E. Langlois, M. Lefebvre, J.-F. Bussieres, Multicenter study of environmental contamination with antineoplastic drugs in 33 Canadian hospitals, International Archives of Occupational and Environmental Health, 87 (2014) 307-313.

[13] S. Viegas, M. Padua, A.C. Veiga, E. Carolino, M. Gomes, Antineoplastic drugs contamination of workplace surfaces in two Portuguese hospitals, Environmental Monitoring and Assessment, 186 (2014) 7807-7818.

[14] M. Hedmer, B.A.G. Jonsson, O. Nygren, Development and validation of methods for environmental monitoring of cyclophosphamide in workplaces, Journal of Environmental Monitoring, 6 (2004) 979-984.
[15] T.Q. Lamerie, S. Nussbaumer, B. Decaudin, S. Fleury-Souverain, J.-F. Goossens, P. Bonnabry, P. Odou, Evaluation of Decontamination Efficacy of Cleaning Solutions on Stainless Steel and Glass Surfaces Contaminated by 10 Antineoplastic Agents, Annals of Occupational Hygiene, 57 (2013) 456-469.
[16] S. Nussbaumer, S. Fleury-Souverain, P. Antinori, F. Sadeghipour, D.F. Hochstrasser, P. Bonnabry, J.-L. Veuthey, L. Geiser, Simultaneous quantification of ten cytotoxic drugs by a validated LC-ESI-MS/MS method, Analytical and Bioanalytical Chemistry, 398 (2010) 3033-3042.
[17] J. Tuerk, T.K. Kiffmeyer, C. Hadtstein, A. Heinemann, M. Hahn, H. Stuetzer, H.M. Kuss, U. Eickmann, Development and validation of an LC-MS/MS procedure for environmental monitoring of eight cytostatic drugs in pharmacies, International Journal of Environmental Analytical Chemistry, 91 (2011) 1178-1190.
[18] M. Hilhorst, C. Briscoe, N. van de Merbel, Sense and nonsense of miniaturized LC-MS/MS for bioanalysis, Bioanalysis, 6 (2014) 3263-3265.
[19] S.R. Needham, G.A. Valaskovic, Microspray and microflow LC-MS/MS: the perfect fit for bioanalysis, Bioanalysis, 7 (2015) 1061-1064.
[20] C.C. Christianson, C.J.L. Johnson, S.R. Needham, The advantages of microflow LC-MS/MS compared with conventional HPLC-MS/MS for the analysis of methotrexate from human plasma, Bioanalysis, 5 (2013) 1387-1396.
[21] H. Shaaban, New insights into liquid chromatography for more eco-friendly analysis of pharmaceuticals, Analytical and Bioanalytical Chemistry, (2016) 1-16.
[22] K.D. Patel, A.D. Jerkovich, J.C. Link, J.W. Jorgenson, In-depth characterization of slurry packed capillary columns with 1.0-mu m nonporous particles using reversed-phase isocratic ultrahigh-pressure liquid chromatography, Anal. Chem., 76 (2004) 5777-5786.
[23] S. Hickert, J. Gerding, E. Ncube, F. Huebner, B. Flett, B. Cramer, H.-U. Humpf, A new approach using micro HPLC-MS/MS for multi-mycotoxin analysis in maize samples, Mycotoxin Research, 31 (2015) 109-115.
[24] A. Premstaller, H. Oberacher, W. Walcher, A.M. Timperio, L. Zolla, J.P. Chervet, N. Cavusoglu, A. van Dorsselaer, C.G. Huber, High-performance liquid chromatography-electrospray ionization mass spectrometry using monolithic capillary columns for proteomic studies, Anal. Chem., 73 (2001) 2390-+.
[25] D. Wilffert, A. Asselman, R. Donzelli, J. Hermans, N. Govorukhina, W.J. Quax, N.C. van de Merbel, R. Bischoff, Highly sensitive antibody-free mu LC-MS/MS quantification of rhTRAIL in serum, Bioanalysis, 8 (2016) 881-890.
[26] G. Desmet, S. Eeltink, Fundamentals for LC miniaturization, Anal. Chem., 85 (2013) 543-556.
[27] D.W. Arnold, S.R. Needham, Micro-LC-MS/MS: the future of bioanalysis, Bioanalysis, 5 (2013) 1329-1331.
[28] O.S.H.A. (OSHA), Evaluation Guidelines for Surface Sampling Methods. Salt Lake City, Utah: OSHA Salt Lake Technical Center, (2001).
[29] F. Gosetti, E. Mazzucco, D. Zampieri, M.C. Gennaro, Signal suppression/enhancement in high-performance liquid chromatography tandem mass spectrometry, J. Chromatogr. A, 1217 (2010) 3929-3937.
[30] C. vom Eyser, K. Palmu, R. Otterpohl, T.C. Schmidt, J. Tuerk, Determination of pharmaceuticals in sewage sludge and biochar from hydrothermal carbonization using different quantification approaches and matrix effect studies, Analytical and Bioanalytical Chemistry, 407 (2015) 821-830.

[31] T. Hetzel, T. Teutenberg, T.C. Schmidt, Selectivity screening and subsequent data evaluation strategies in liquid chromatography: the example of 12 antineoplastic drugs, Analytical and Bioanalytical Chemistry, 407 (2015) 8475–8485.
[32] S.J. Lehotay, Y. Sapozhnikova, H.G.J. Mol, Current issues involving screening and identification of chemical contaminants in foods by mass spectrometry, Trends in Analytical Chemistry, 69 (2015) 62-75.
[33] H.G.J. Mol, P. Zomer, M. García López, R.J. Fussell, J. Scholten, A. de Kok, A. Wolheim, M. Anastassiades, A. Lozano, A. Fernandez Alba, Identification in residue analysis based on liquid chromatography with tandem mass spectrometry: Experimental evidence to update performance criteria, Anal Chim Acta, 873 (2015) 1-13.

6.7 Chapter appendix

6.7.1 Structure and analyte properties

Table-S 6.1 shows the selected substances including important physico-chemical properties, while the structural formulas are compiled in Figure-S 6.1. The depicted log D values clearly show that the investigated compounds include polar as well as non-polar substances.

Table-S 6.1: List of the investigated compounds including CAS number, sum formula, pK_a and log D [1-3].

number	compound	CAS	sum formula	Purity / %	provider	pK_a (T=25 °C)	log D (T=25 °C, pH=3)
(1)	gemcitabine	95058-81-4	$C_9H_{11}F_2N_3O_4$	≥ 98	Sigma	3.60 / 11.52	-3.34
(2)	methotrexate	59-05-2	$C_{20}H_{22}N_8O_5$	≥ 98	Fluka	3.41 / 4.70	-2.95
(3)	topotecan	123948-87-8	$C_{23}H_{23}N_3O_5$	≥ 98	Sigma	8.00	-3.36
(4)	irinotecan	97682-44-5	$C_{33}H_{38}N_4O_6$	≥ 97	Sigma	11.71	-0.34
(5)	ifosfamide	3778-73-2	$C_7H_{15}Cl_2N_2O_2P$	≥ 98	Sigma	13.24	0.75
(6)	cyclophosphamide	50-18-0	$C_7H_{15}Cl_2N_2O_2P$	≥97	Sigma	12.78	0.50
(7)	doxorubicin	23214-92-8	$C_{27}H_{29}NO_{11}$	≥ 98	Sigma	9.53	-2.86
(8)	epirubicin	56420-45-2	$C_{27}H_{29}NO_{11}$	≥ 90	Sigma	9.53	-2.86
(9)	etoposide	33419-42-0	$C_{29}H_{32}O_{13}$	≥ 98	Sigma	9.33	0.28
(10)	paclitaxel	33069-62-4	$C_{47}H_{51}NO_{14}$	≥ 95	Sigma	10.36	3.95
(11)	docetaxel	114977-28-5	$C_{43}H_{53}NO_{14}$	≥ 97	Sigma	10.96	2.46

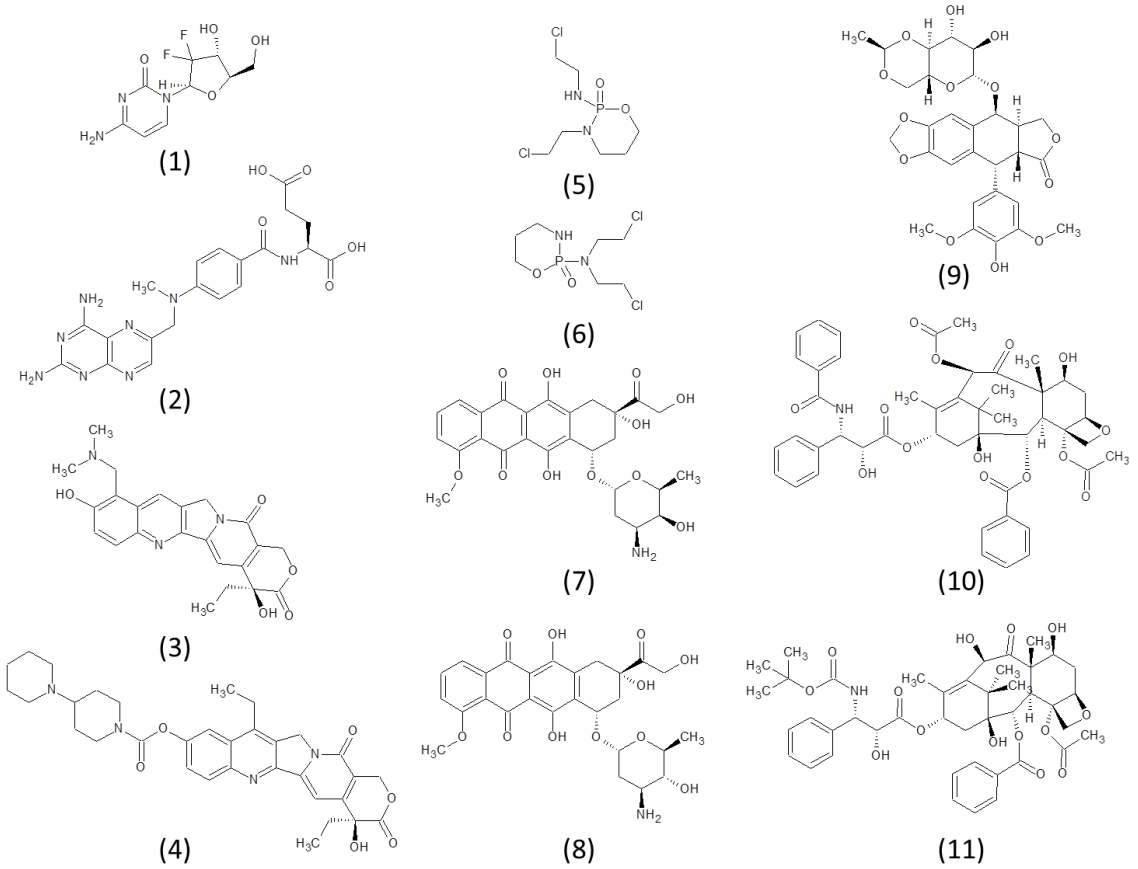

Figure-S 6.1: Structures of the investigated compounds: (1) gemcitabine, (2) methotrexate, (3) topotecan, (4) irinotecan, (5) ifosfamide, (6) cyclophosphamide, (7) doxorubicin, (8) epirubicin, (9) etoposide, (10) paclitaxel, (11) docetaxel [1]. Note: Only the neutral species are shown which are not necessarily present at the applied pH.

A list of the applied *MRM* transitions and MS/MS parameter is given in Table-S 6.2.

Table-S 6.2: Mass transitions and MS/MS parameter of the investigated compounds.

number	compound	Ionization mode	Q_1 *m/z*	Q_3 *m/z*	Dwell time / ms	DP / mV	EP / mV	CE / eV	CXP / mV
1	gemcitabine	ESI pos.	264	112	10	55	10	25	12
				95				61	12
2	methotrexate	ESI pos.	455	308	10	80	10	25	14
				175				47	10
3	topotecan	ESI pos.	422	377	10	56	10	25	22
				46				61	12
4	irinotecan	ESI pos.	587	124	10	196	10	43	12
				167				49	10
5	ifosfamide	ESI pos.	261	154	10	101	10	29	18
				92				33	16
6	cyclophosphamide	ESI pos.	261	140	10	71	10	31	16
				106				25	12
7	doxorubicin	ESI pos.	544	397	10	20	10	15	16
				361				35	14
8	epirubicin	ESI pos.	544	397	10	36	10	17	14
				361				37	10
9	etoposide	ESI pos.	589	229	10	80	10	19	20
				185				53	18
10	paclitaxel	ESI pos.	854	569	10	130	10	13	24
				286				21	20
11	doctaxel	ESI pos.	808	527	10	80	10	13	10
				226				19	24

DP: declustering potential, EP: entrance potential, CE: collision energy, CXP: cell exit potential

6.7.2 Investigation of extraction efficiency

Figure-S 6.2 shows the recovery rates including error bars for DMSO, ACN and IPA as organic solvent for the 5 ng mL^{-1} QC samples.

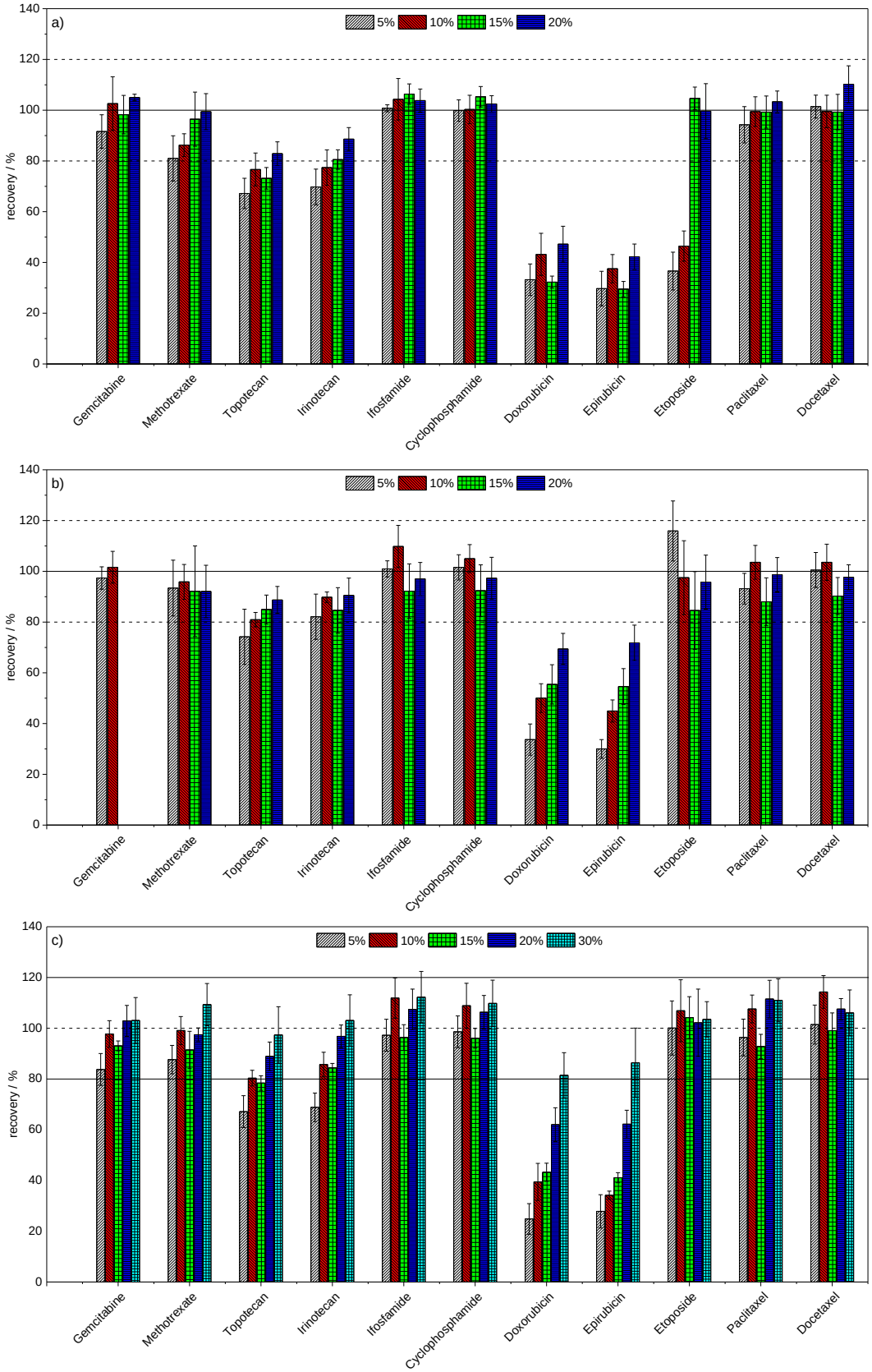

Figure-S 6.2: Resulting recovery rates of the eleven antineoplastic drugs for a mixture of a) H_2O:DMSO + 0.1% FA, b) H_2O:ACN + 0.1% FA and c) H_2O:IPA + 0.1% FA in various compositions for a concentration of 5 ng mL^{-1} (see figure legend describing the amount of organic solvent in the extraction solution; number of QC samples = 4).

6.7.3 Separation of the eleven antineoplastic drugs

6.7.3.1 Investigation and optimization of the injection volume

Whereas Figure-S 6.3 a) illustrates the separation of the eleven antineoplastic drugs using an injection volume of 250 nL for the 0.1 ng mL^{-1} standard, Figure-S 6.3 b) shows the separation for the same concentration using an injection volume of 425 nL. For the separation in Figure-S 6.3 c), an injection of 425 nL was performed analysing a 1.0 ng mL^{-1} standard. The composition of the injection solution is 66.4/33.6 H_2O/IPA (v/v) + 0.1% FA for all chromatograms.

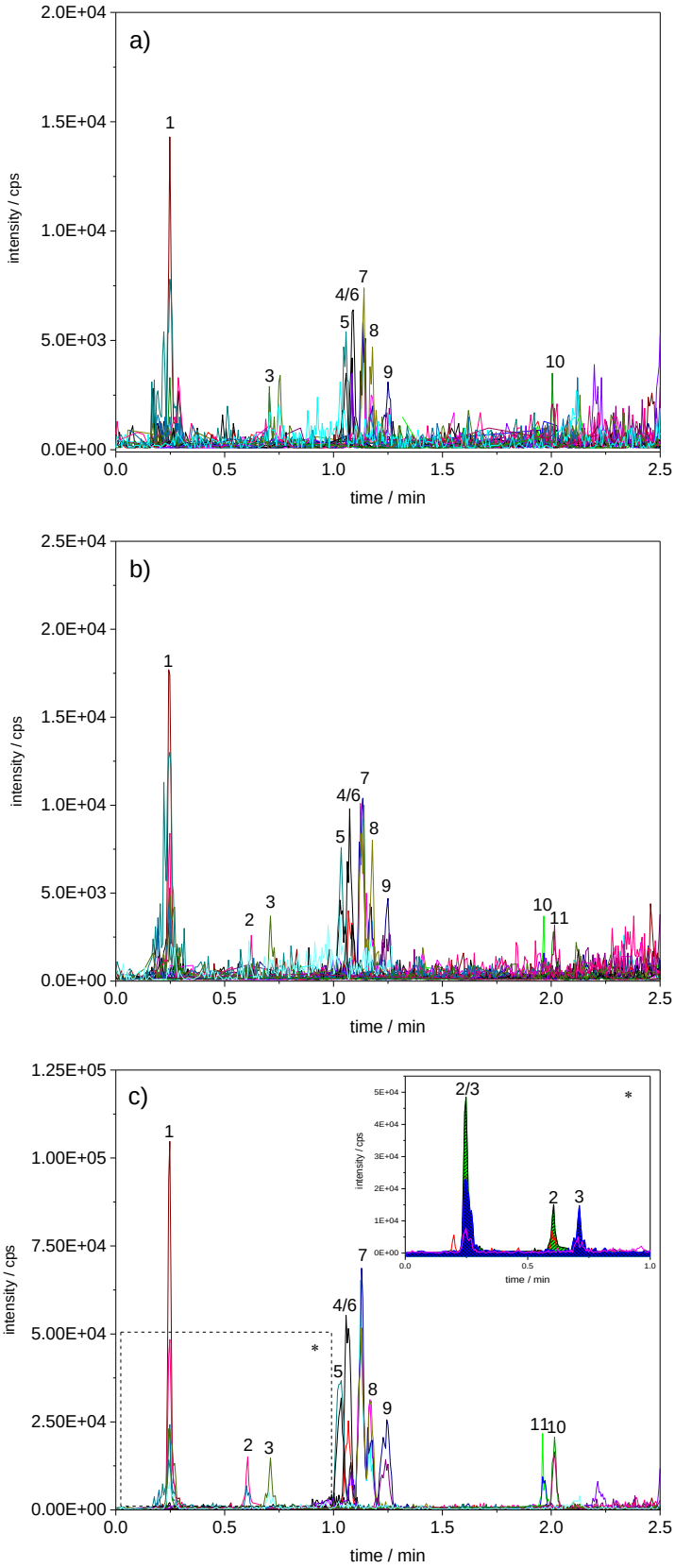

Figure-S 6.3: Resulting chromatogram for the separation of the eleven antineoplastic drugs for a concentration of a) 0.1 ng mL^{-1} using an injection volume of 250 nL, b) 0.1 ng mL^{-1} using an injection volume of 425 nL and c) 1.0 ng mL^{-1} using an injection volume of 425 nL. Analytes: (1) gemcitabine, (2) methotrexate, (3) topotecan, (4) irinotecan, (5) ifosfamide, (6) cyclophosphamide, (7) doxorubicin, (8) epirubicin, (9) etoposide, (10) paclitaxel, (11) docetaxel.

As can be seen in Figure-S 6.3 c), broadened and distorted peak shapes are obtained for an injection volume of 425 nL. The reason is depicted in Figure-S 6.4 illustrating the focussing and missing focussing of polar and non-polar substances depending on the applied injection volume and sample composition.

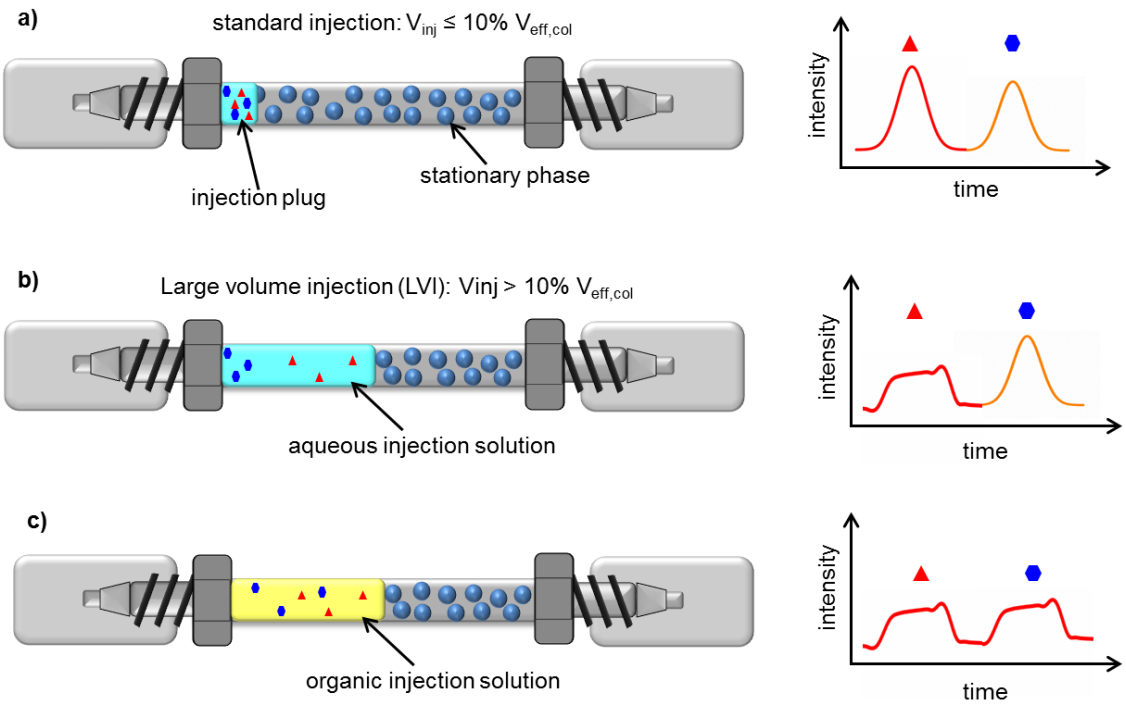

Figure-S 6.4: Schematic illustration of the chromatographic separation and resulting peak shapes for a) the focusing of polar and non-polar compounds using 10% of the column void volume as injection volume, b) the missing focusing of polar substances as well as the focussing of non-polar compounds using an aqueous injection solution with an injection volume higher than 10% of the column void volume and c) the missing focusing of polar substances and non-polar compounds using an organic injection solution with an injection volume higher than 10% of the column void volume.

When the injection volume is chosen below 10% of the column void volume, both polar as well as non-polar substances are focussed at the column head resulting in symmetric peak shapes as depicted in Figure-S 6.4 a). In contrast, if a large volume injection (LVI) is performed asymmetric peak shapes are obtained. These distortion effects are differently pronounced for the polar and semi-polar target analytes depending on the sample composition. When an LVI is applied using an aqueous injection solution, only the polar compounds become broader because of the missing focussing for these substances as illustrated in Figure-S 6.4 b). The remaining column volume is not sufficient to compress the band. Using an organic injection solution, the polar as well as semi-polar substances are affected due to the higher elution

strength of the injection solvent compared to the initial mobile phase composition as shown in Figure-S 6.4 c).

6.7.3.2 Chromatographic separation of cyclophosphamide and ifosfamide

The isomers cyclophosphamide and ifosfamide need to be separated chromatographically due to cross talk. This phenomenon is depicted in Figure-S 6.5.

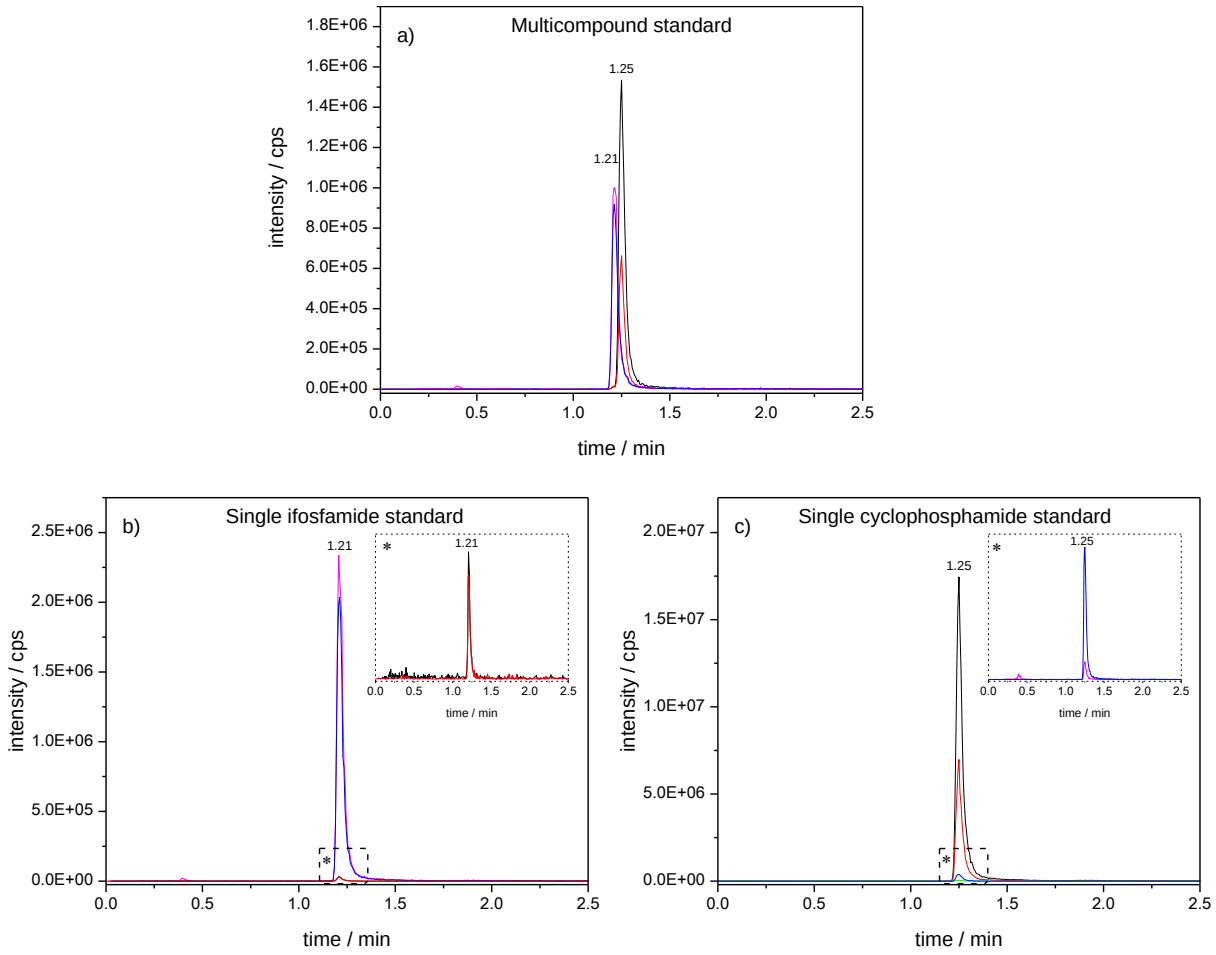

Figure-S 6.5: Resulting *MRM* signals for cyclophosphamide (*m/z* 261 → *m/z* 140, *m/z* 261 → *m/z* 106) and ifosfamide (*m/z* 261 → *m/z* 154, *m/z* 261 → *m/z* 92) using a) a multicompound standard, b) single ifosfamide standard and c) single cyclophosphamide standard.

In Figure-S 6.5 a) the separation of cyclophosphamide and ifosfamide is shown for a 100 ng mL^{-1} standard. In contrast, the chromatograms illustrated in Figure-S 6.5 b) and c) only contain one of these substances. Although only one compound is included a signal can be identified for the other isomer as can be seen from the magnification highlighted by a star. Therefore, if the concentration of one analyte is high and no chromatographic separation is achieved false positive results are the consequence. This can be explained by the MS/MS

spectra of the individual compounds which are depicted in Figure-S 6.6. Whereas Figure-S 6.6 a) shows the MS/MS spectrum for cyclophosphamide at a collision energy of 31 eV, the spectrum for ifosfamide in Figure-S 6.6 b) was recorded using a collision energy of 33 eV. These collision energies equal those values of the selected *MRM* transitions (cyclophosphamide: *m/z* 261 → *m/z* 140, *m/z* 261 → *m/z* 106; ifosfamide: *m/z* 261 → *m/z* 154, *m/z* 261 → *m/z* 92).

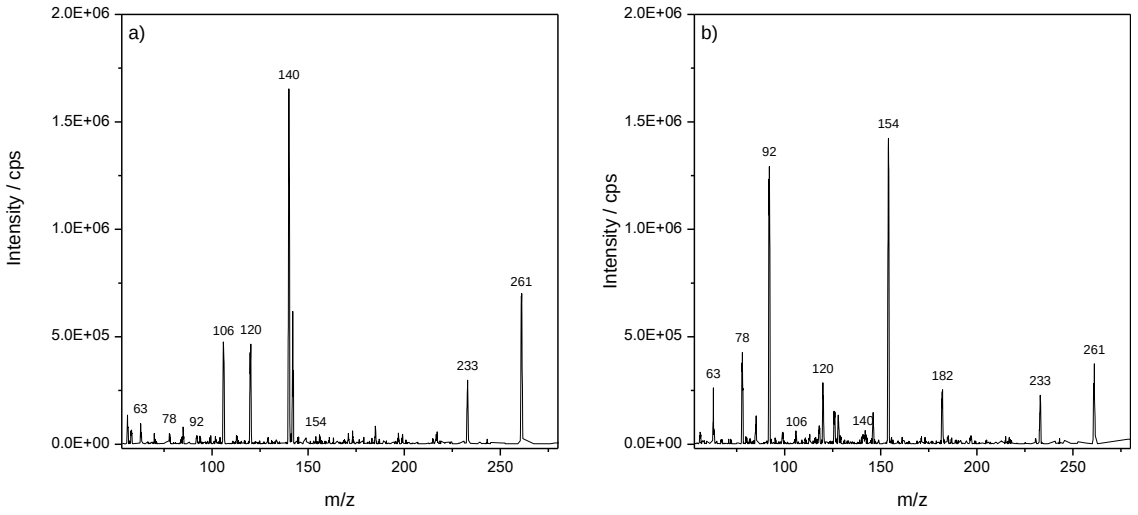

Figure-S 6.6: Resulting MS/MS spectra for a) cyclophosphamide at a collision energy of 31 eV and b) ifosfamide at a collision energy of 33 eV.

As can be seen, the selected product ions for the *MRM* transitions show the highest intensity for the individual compound. Nevertheless, both spectra reveal that cyclophosphamide as well as ifosfamide are capable to form the fragments of the corresponding isomer. That is why the signals are obtained for the individual isomers although only the other is included. As a consequence, a chromatographic separation is mandatory.

6.7.4 Optimization of the ion source parameters

After dilution of the samples by a factor of 10 the MS ion source parameters need to be further optimized to achieve the adapted LOQ of 0.01 ng mL^{-1}. Therefore, flow injection analysis (*FIA*) was performed. During the optimization the influence of the following six different parameters were analysed: Curtain gas (*CUR*), collision activated dissociation gas (*CAD*), ionization voltage (*IS*), ion source temperature (*TEM*), nebulizer gas (*GS1*) and heater gas (*GS2*). At this point it should be noted that the *GS1* depends on the position of the ESI probe and that there is a dependence between *TEM* and *GS2*. Higher temperature can be combined with a low *GS2* and vice versa. Both parameters are critical values because they can cause thermal degradation of certain substances.

During optimization, the predefined values for each parameter are subsequently adjusted and the resulting intensity is recorded automatically by the software. Afterwards, the software creates a report containing all intensity values for each analyte and source parameter value. In addition, the software recommends a method on the basis of the highest number of counts over all analytes. For some cases this approach would yield a sensitive method for all target analytes. But it is also possible that the recommended method is influenced by high signal intensities for certain compounds, which leads to wrong conclusions about the optimal ion source parameters. Therefore, to evaluate the influence of each parameter for each compound the obtained intensity values are normalized to the highest number of counts. Thereby, the loss or gain of intensity can be illustrated when varying the parameter value. Figure-S 6.7 shows the resulting normalized intensities in percent for the ion source temperature between 200 and 450 °C.

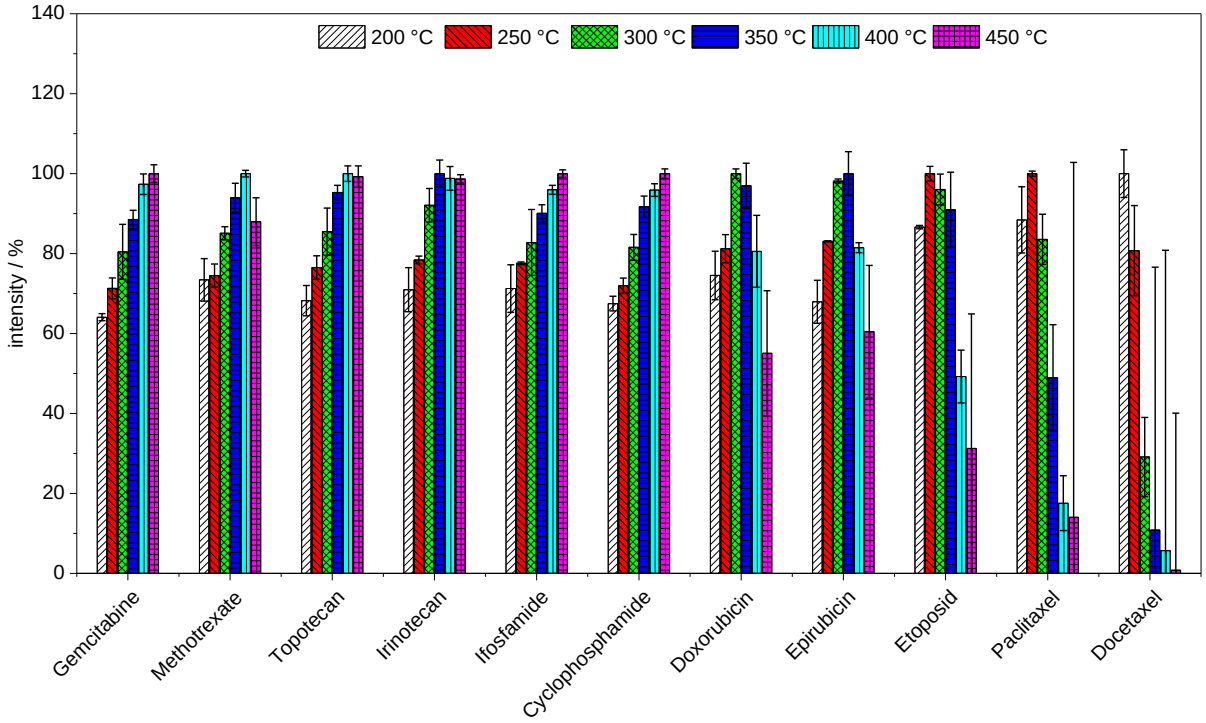

Figure-S 6.7: Resulting intensity for the ion source temperature normalized to the highest number of counts for each analyte and temperature value (n = 3).

As can be seen, for six compounds the intensity increases with increasing temperature. In contrast, for the other substances a loss of intensity can be identified which is very pronounced for etoposide, paclitaxel and docetaxel. Nevertheless the recommended method by the software contains a *TEM* of 400 °C. If this temperature would be chosen, the intensity for the temperature unstable compounds decreases to 10-30%. As a consequence, a target method that achieves the defined LOQs for all substances would not be possible. Therefore, a lower *TEM* is necessary in order to obtain sufficient sensitivity for etoposide, paclitaxel and docetaxel. From Figure-S 6.7

it becomes clear that a temperature of 250 °C favours the intensity for these compounds. For docetaxel a *TEM* of 200 °C would yield even higher intensity but the loss of counts for all other substances is pronounced. Therefore, the ion source temperature was adjusted to 250 °C because it represents the best compromise for all target analytes. As described above, the dependence between the *TEM* and *GS2* must be considered when changing the ion source temperature. That is why the optimization for *GS2* was repeated for a temperature of 250 °C. Figure-S 6.8 shows the comparison of the *GS2* optimization at 450 and 250 °C.

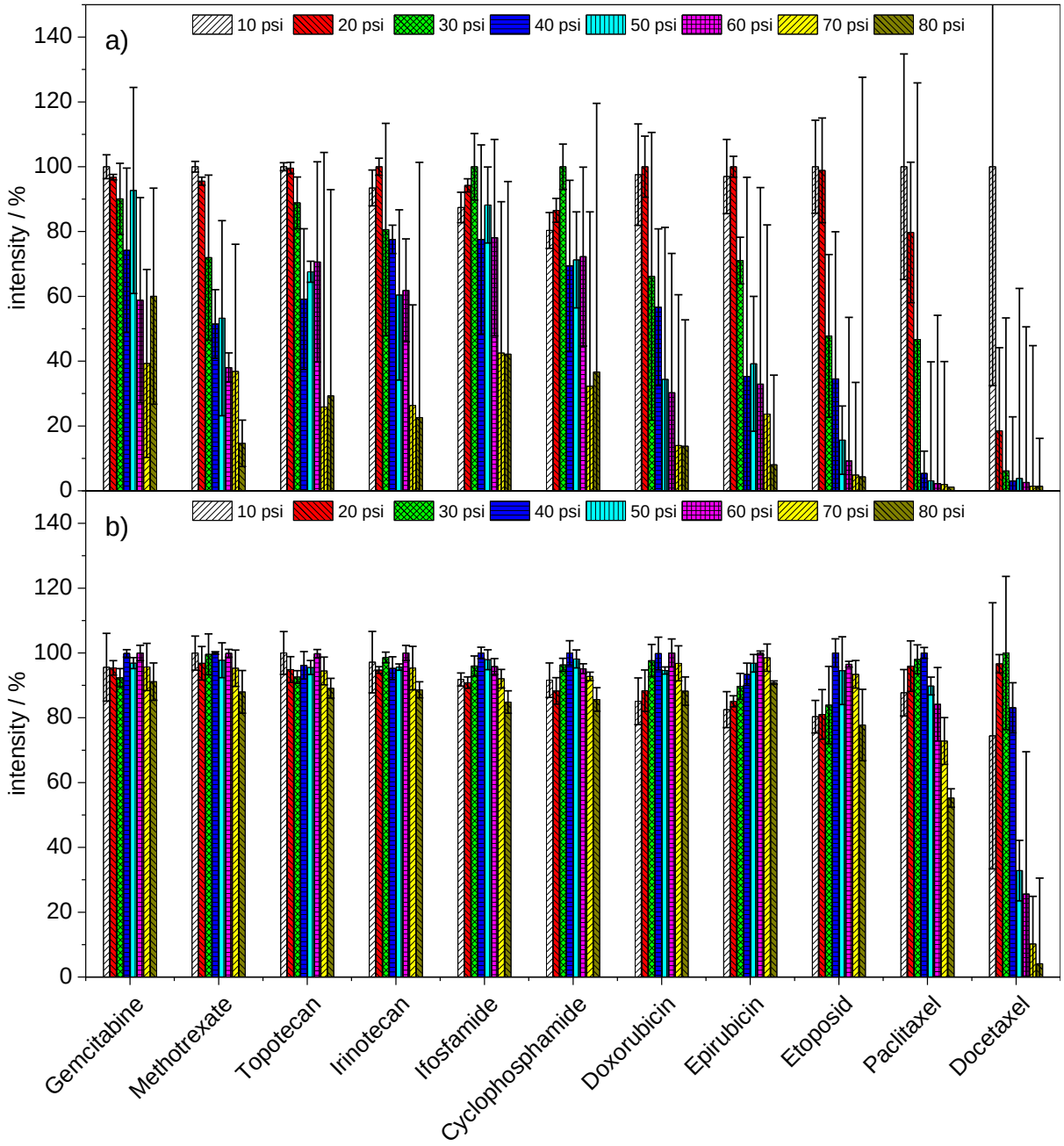

Figure-S 6.8: Comparison of the *GS2* optimization at a) 450 °C and b) 250 °C for the eleven antineoplastic drugs.

As illustrated in Figure-S 6.8 pronounced differences for the optimum *GS2* value are obtained for the individual ion source temperature. This is attributed to the temperature distribution in the ion source as described above. Whereas the optimum setting for *GS2* in Figure-S 6.8 a) is 10 psi at 450 °C, a value of 30 psi should be chosen at 250 °C as depicted in Figure-S 6.8 b). In addition, pronounced differences regarding the error bars can be identified. In general, the error is reduced at 250 °C for almost all substances. The reason is the improved spray stability at the decreased temperature. Again, the MS software recommends a *GS2* value of 60 psi. Therefore, a visual inspection and interpretation of the data is mandatory.

To summarize, Table-S 6.3 gives a comparison of the different ion source parameters as recommended by the MS software and normalization.

Table-S 6.3: Overview of the differences between the ion source parameter for the MS recommended and normalized evaluated values.

Parameter	MS software	Normalization
CUR / psi	20	20
CAD	Medium	Medium
IS / kV	5.5	5.0
TEM / °C	400	250
GS1 / psi	10	10
GS2 / psi	10	30

As can be seen from Table-S 6.3 all other parameters are similar for the MS software and graphically evaluated method. Nevertheless, the normalized intensities can be found in Figure-S 6.10. At this point it must be noted that the ionization voltage is set to 5.0 kV although the resulting intensity is higher for 5.5 kV. The reason is that at 5.5 kV the ESI needle starts to glow leading to unstable spray conditions which is also notable for the peak shapes in the chromatogram. The effect of the ionization voltage at 5.0 kV and 5.5 kV on the ESI needle is illustrated in Figure-S 6.9.

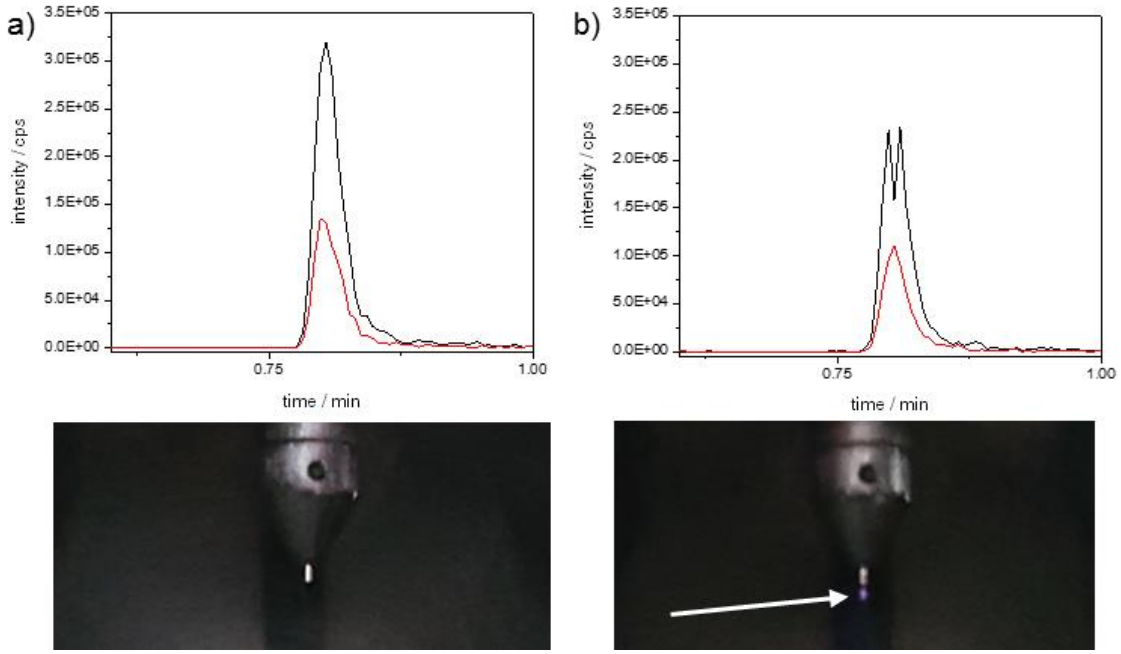

Figure-S 6.9: Illustration of the ESI needle at a) 5.0 kV and b) 5.5 kV.

Figure-S 6.10 shows the resulting normalized intensities in percent for the curtain gas (*CUR*), collision activated dissociation gas (*CAD*) and the ionization voltage (*IS*).

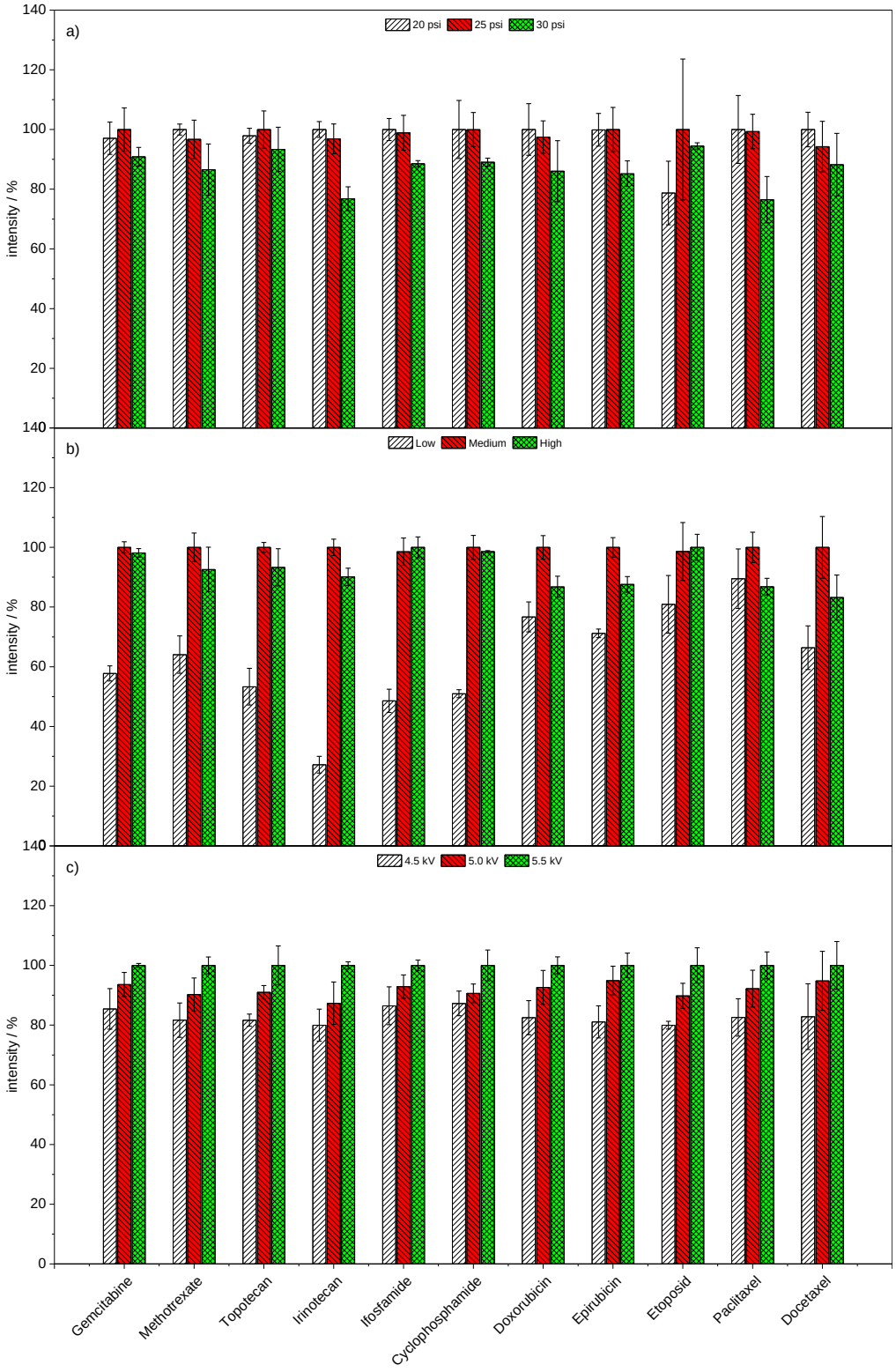

Figure-S 6.10: Resulting intensity for a) the curtain gas (*CUR*), b) the collision activated dissociation gas (*CAD*) and c) ionization voltage (*IS*) normalized to the highest number of counts for each analyte and temperature value (n=3). For further information please refer to the figure legend.

6.7.5 Calculation of the area related results

For the calculation of the area related concentration (*ARC*) the following Equation-S 6.1 can be used. In addition, it can be used to verify whether the estimated concentration is below or above the reference value of 0.1 ng cm^{-2}.

$$ARC = \frac{c \cdot D \cdot V}{A_x}$$ **Equation-S 6.1**

where *c* is the concentration in ng mL^{-1}, *D* the dilution factor of 10, *V* is the volume of wetting and extraction solution in mL and A_x the sampling area in cm^2. To demonstrate that the developed method is suitable for the determination of the reference value the following example from Figure 6.4 a) of the main document is applied. The estimated concentration for ifosfamide (5) was 0.293 ng mL^{-1} under consideration of the dilution factor. The applied volume was 33 mL and the sampling area 900 cm^2. The corresponding area related concentration is 0.011 ng cm^{-2}. Therefore, it can be demonstrated that the developed method is suitable to control the reference value.

6.7.6 References

[1] ChemSpider, http://www.chemspider.com, (accessed 25.06.2016)
[2] Scifinder, https://www.scifinder.cas.org, (accessed 25.06.2016)
[3] DrugBank, http://www.drugbank.ca/, (accessed 25.06.2016)

Chapter 7 Further considerations on selectivity, peak capacity and robustness

The most important parameter during method development is the selectivity of the applied separation technology to obtain a separation between target analytes if needed. In particular the separation of analytes of similar structures like isomers or epimers can only be achieved by sufficient selectivity. Therefore the screening of a suitable phase system is of utmost importance for such analytical problems. Although the choice can be simplified by *PCA* as shown in Chapter 2.3, the screening of a phase system can still be time-consuming and complex. That is why over the last years different separation techniques were developed to achieve higher selectivity. Using specialized detectors like mass spectrometers can help to distinguish between co-eluting analytes on the basis of their mass-to-charge (*m/z*) ratio [1, 2]. However, if isobaric compounds with identical accurate mass and mass transitions are included other approaches need to be considered despite the high selectivity of mass spectrometry. That is why for example two-dimensional liquid chromatography (2D-LC) is of broad interest due to the possibility to combine stationary phases with different retention mechanisms to achieve an orthogonal separation system and thus higher selectivity [3, 4]. One example for a resulting 2D-LC-MS separation for the isomers ifosfamide and cyclophosphamide as well as for the epimers doxorubicin and epirubicin is shown in Figure 7.1 [10].

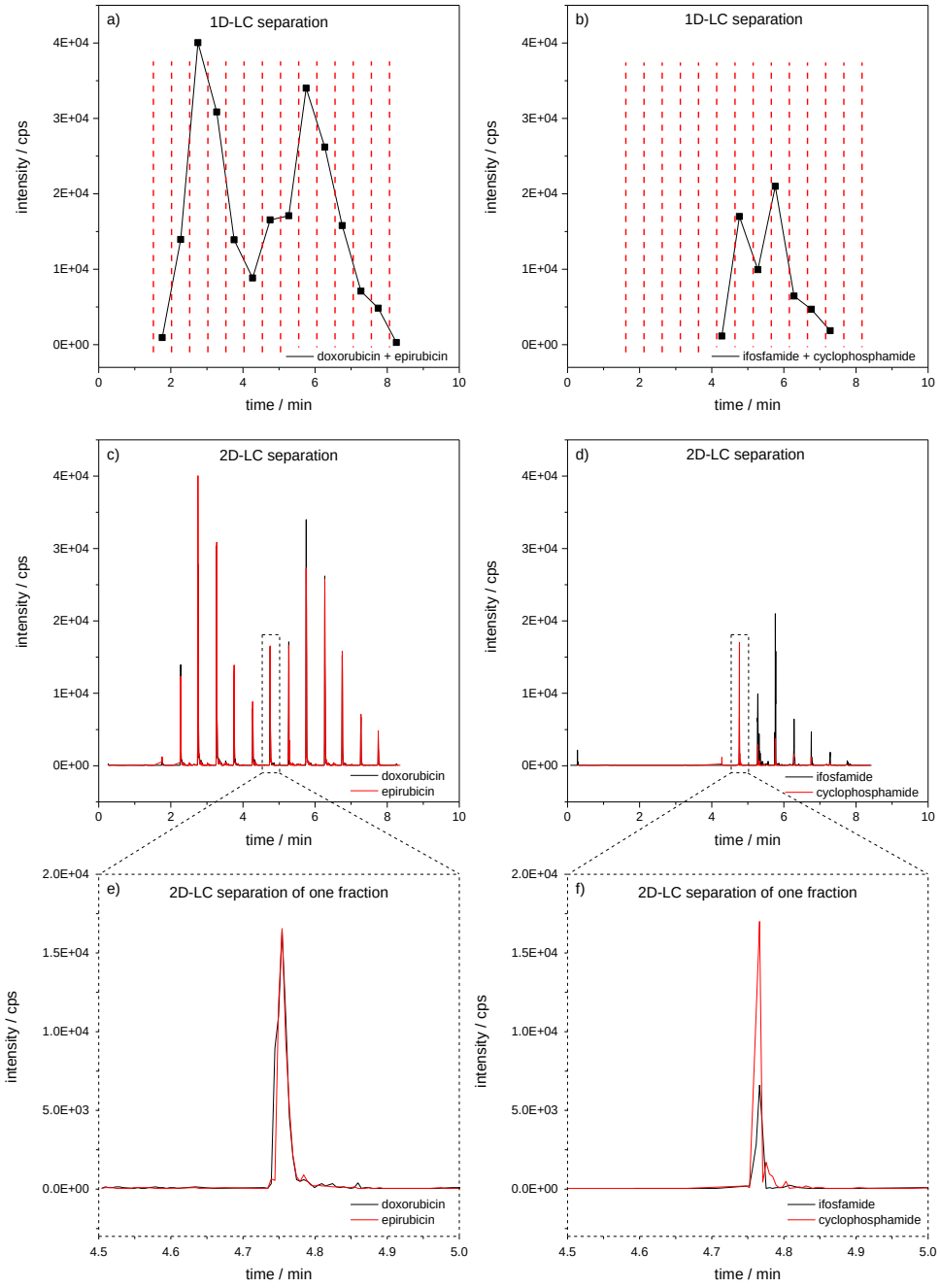

Figure 7.1: Resulting two-dimensional separation of the reconstructed peak shapes within the first dimension for a) the epimers doxorubicin and epirubicin and b) the isomers ifosfamide and cyclophosphamide. The vertical dashed red lines represent the different fractions that are transferred to the second separation dimension. The resulting 2D-LC separations are shown in c) and d) for the individual critical peak pairs. The corresponding separation for one fraction is shown in e) and f) [10].

For both critical peak pairs a partial separation can be obtained as becomes clear from the reconstructed peak shapes of the first dimension in Figure 7.1 a) and b). It can be seen that the resulting resolution is higher for the epimers doxorubicin and epirubicin (Figure 7.1 a) compared to the isomers ifosfamide and cyclophosphamide (Figure 7.1 b). The vertical dashed red lines represent the different fractions that are transferred to the second dimension for further separation as shown in Figure 7.1 c) and d). Unfortunately, a co-elution of both critical peak

pairs occurs in the second dimension as can be identified by the magnification of one fraction analyzed within the second dimension as depicted in Figure 7.1 e) and f) for the individual critical peak pair. The reason is the decreased peak capacity in the second dimension because of a gradient time of only 17 s. Because of this co-elution, the mass spectrometer is not able to distinguish between these compounds. Therefore, the resulting selectivity and peak capacity is not suitable to achieve a separation by 2D-LC-MS for this example. To further increase the selectivity ion mobility spectrometry (*IMS*) has been developed to separate analytes in the gas phase prior to the mass spectrometer or as a stand-alone technique as an alternative approach to chromatography [5]. The separation in *IMS* is based on different drift times of the analyte ions in a drift tube, when the analytes are pushed against a drift gas in an electric field [6, 7]. Target compounds with different mass and/or structure need different times to migrate through the drift tube and thus a separation can be achieved. Nowadays, different techniques of *IMS* are available [8]. It is often being stated that ion mobility can be used to increase selectivity and to separate isobaric substances [9]. Figure 7.2 shows the separation of the critical peak pairs by solely using *IMS*.

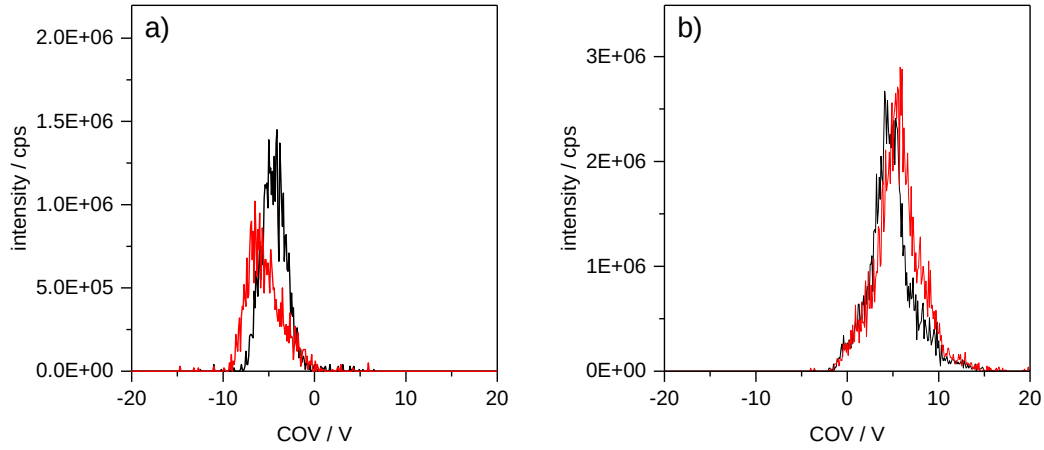

Figure 7.2: Illustration of the resulting separation depending on the applied compensation voltage (COV) of a) the epimers doxorubicin and epirubicin and b) the isomers ifsofamide and cyclophosphamide using solely *IMS* [10].

As can be identified, a separation of the isomers and epimers is not achieved by *IMS* even using isopropanol as modifier to achieve higher selectivity by clustering. In addition, investigations showed that the current potential of *IMS* is often not suitable to achieve a separation of compounds of similar structure because the resolving power is currently not sufficient [8, 10]. Sometimes a separation is only possible if for example adduct formation with sodium takes place as illustrated in Figure 7.3 for ifosfamide and cyclophosphamide.

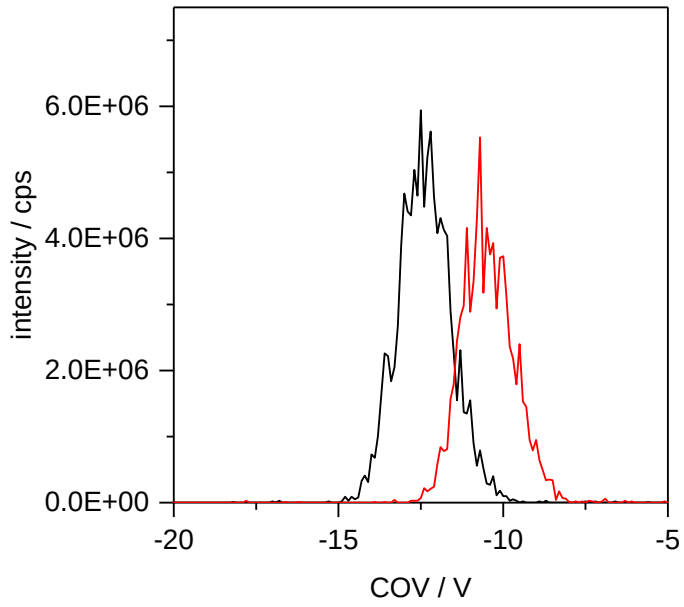

Figure 7.3: Illustration of the resulting separation of ifosfamide and cyclophosphamide as sodium adducts using *IMS* only [10].

As depicted, by adduct formation the structures of the target analytes change in a way that *IMS* can partially separate ifosfamide and cyclophosphamide. However, an adduct formation not always occurs for the investigated analytes. Nevertheless, *IMS* has other advantages such as the separation of matrix ingredients to reduce matrix interferences [6, 9]. In general, the usage of such separation techniques is associated with additional costs for purchase and the complexity of method development and data analysis increases considering LC-IMS-MS [11]. In addition, the applicability with highly efficient *UHPLC* separations can be doubted regarding the sensitivity loss and resulting data acquisition rates whose influence on method robustness will be discussed later. However, it can be demonstrated that *IMS* is currently not suitable to replace chromatography. Therefore, liquid chromatography is still the method of choice and the easiest way to achieve a separation. Figure 7.4 shows the resulting micro-LC-MS/MS separation for the critical peak pairs using the phase system identified by the *PCA*.

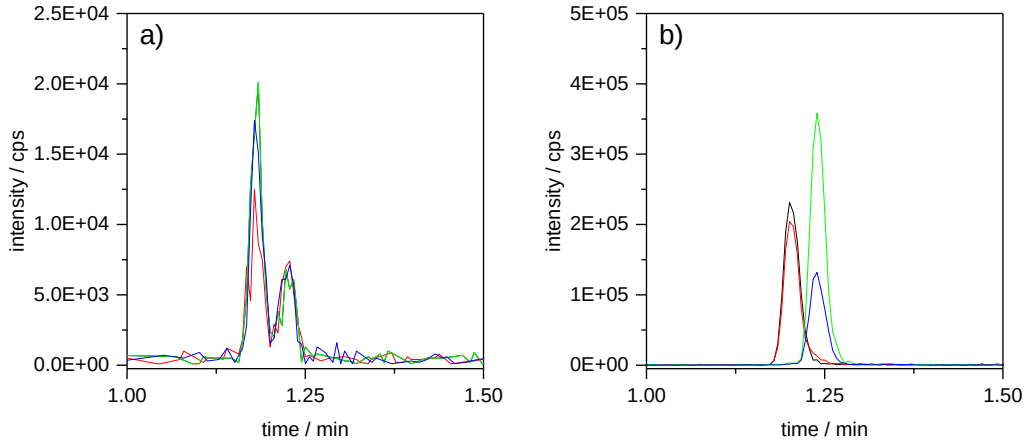

Figure 7.4: Illustration of the resulting separation of a) doxorubicin and epirubicin and b) ifosfamide and cyclophosphamide using micro-LC-MS/MS. For further experimental details please refer to Chapter 6.2.

It is clearly demonstrated that the selectivity as well as the peak capacity of the one dimensional micro liquid chromatography is sufficient to achieve a separation in less than 1.5 min for both critical peak pairs. These examples illustrate that liquid chromatography is still the easiest way to achieve a separation and cannot currently be replaced by *IMS*. Therefore, the development of new stationary phases is the most promising approach to handle the increased requirements in the analytical world until other techniques like *IMS* have been further improved. All manufacturers as well as research groups are working on new surface modifications such as biphenyl or ion exchange to obtain different selectivity [12, 13]. As was shown in Figure 2.4 (*PCA*), the resulting selectivity is totally different compared to conventional C18 columns. However, whether the applied selectivity is helpful or not clearly depends on the analytical problem and therefore on the analytes that need to be resolved.

The same is true for the efficiency or peak capacity when considering gradient elution. It was demonstrated that miniaturized LC columns can provide the same efficiency and peak capacity production rates as their conventional *i.d.* counterparts. However, the question arises whether high peak capacity is needed or not for the analytical problem.

To address this issue for the method of antineoplastic drugs developed in this work, the question can be easily answered when considering the resolution of the critical peak pairs. To demonstrate the potential of higher efficiency at identical selectivity in order to obtain a chromatographic separation for isobaric compounds, the resulting separation of ifosfamide and cyclophosphamide as well as doxorubicin and epirubicin is shown in Figure 7.5. Whereas in Figure 7.5 a) and b) the separation was done on a column packed with 1.9 µm fully porous particles, Figure 7.5 c) and d) illustrate the chromatogram obtained with 3.0 µm fully porous particles.

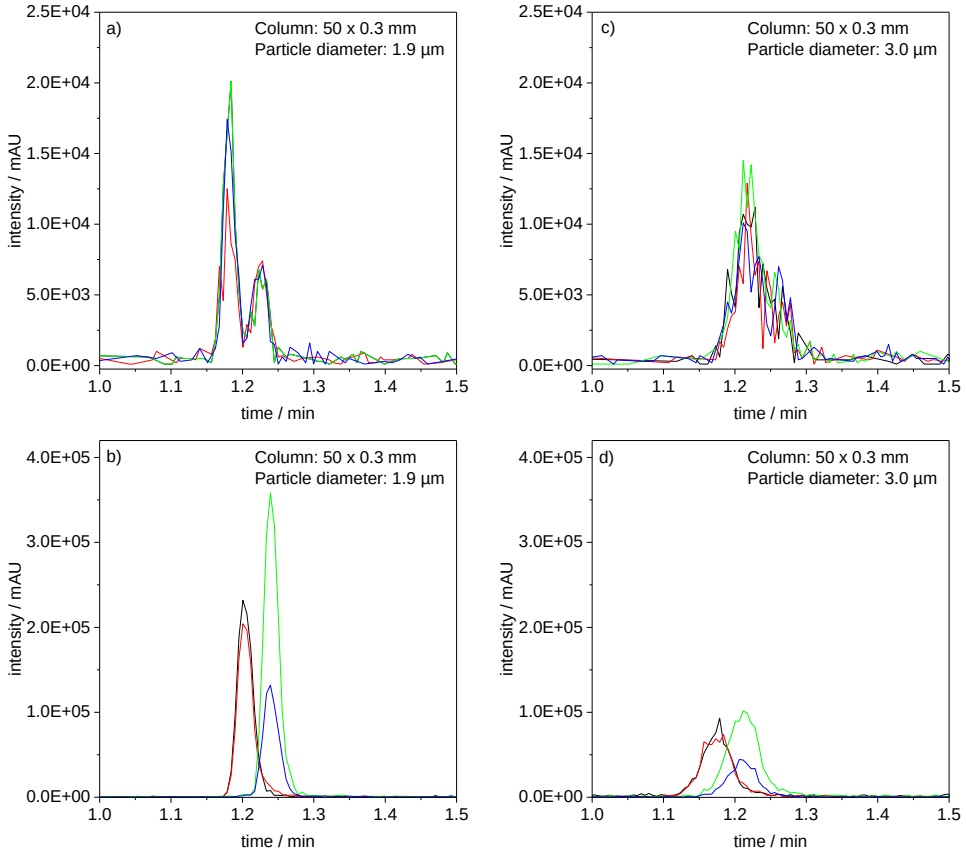

Figure 7.5: Comparison of the separation of the critical peak pairs doxorubicin and epirubicin obtained on a, b) a column packed with 1.9 µm fully porous particles and c, d) a column packed with 3.0 µm fully porous particles. For further experimental details please refer to Chapter 6.2.

A baseline separation can be achieved using the smaller particle diameter whereas the isobaric compounds co-elute when the larger particle diameter is applied. Apparently, by using the smaller particle diameter, higher sensitivity as well as reduced peak widths can be obtained. Thereby the peak capacity increases from 12 which is approximately the peak capacity of the second dimension in the 2D-LC approach of Figure 7.1 to 27 for the reduced particle diameter since the gradient time is constant, which explains approaches of developing and introducing even smaller particles [14-16]. The example clearly demonstrates the potential of smaller particle diameters for fast liquid chromatography although it might be possible to achieve a separation with 3.0 µm particles when using a flatter gradient slope. The consequence are increased analysis times reducing the sample throughput. However, the question arises why sub-2 µm particles have not been established for all applications since higher peak capacity can be achieved in a shorter analysis time. Besides the drastic increase in backpressure, the small resulting peak widths can cause significant limitations especially when a huge number of analytes has to be detected and quantified at low analyte concentrations. In addition, the smaller the particles, the smaller the resulting peak width leading to higher susceptibility in terms of the extra-column band broadening. The same is true for steep solvent gradients. To further

emphasize the appropriate selection of a suitable particle diameter, the probability that a certain number of compounds will be baseline separated depending on the peak capacity can be approximated using Equation 7.1 whereas the relation is graphically shown in Figure 7.6 [17].

$$P' = \left(1 - \frac{m-1}{n-1}\right)^{m-2} \cdot 100\% \qquad \textbf{Equation 7.1}$$

where *P'* is the probability that a baseline separation can be achieved, *m* the number of compounds and *n* the peak capacity.

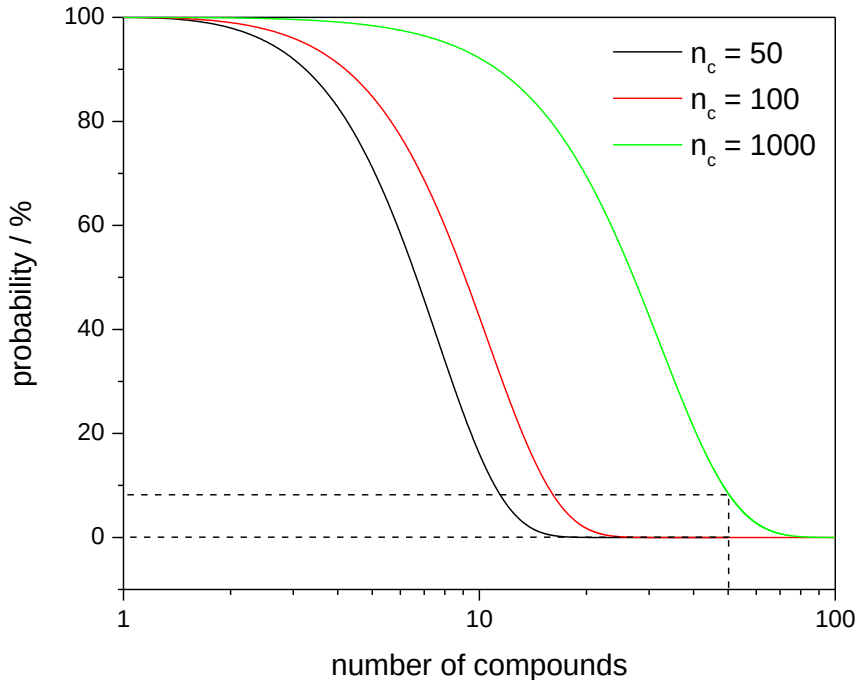

Figure 7.6: Illustration of the probability of baseline separated signals depending on the number of compounds and peak capacity.

As can be identified, the probability drastically decreases with increasing number of compounds and decreasing peak capacity. For example, analyzing 50 compounds with a peak capacity of 50 or 100, the probability is almost zero that all analytes are baseline separated. Even assuming a peak capacity of 1,000, the probability is below 10%. Therefore, when analyzing a high number of compounds, there are regions within the chromatogram where several analytes will co-elute. Usually, mass spectrometry is able to separate co-eluting compounds on the basis of their mass-to-charge ratio. When using triple-quadrupole mass spectrometers the acquisition mode is typically the multiple-reaction-monitoring (*MRM*) mode to ensure high selectivity and sensitivity. Therefore, two mass transitions are recorded, one for quantification and one for substance verification. However, the acquisition of *MRMs* needs time to achieve a sufficient number of data points to accurately represent the peak profile. In mass spectrometry the data acquisition rate depends on the adjusted cycle time which is the sum of the dwell time and pause

time to switch between different *MRMs*. In addition, the cycle time depends on the number of simultaneously detected mass transitions. The higher the number of compounds, the higher the cycle time. Therefore, for multicomponent analysis it is desirable to reduce the cycle time as much as possible to obtain a high data acquisition rate for a high number of simultaneously measured *MRM*. But there are some limitations with common generations of mass spectrometers in terms of useful values for the dwell and pause time. In general, with decreasing dwell time the signal-to-noise ratio decreases leading to higher limits of quantification. Even using sophisticated software algorithms like time-dependent acquisition of mass transitions, the number of compounds that has to be detected simultaneously can be huge for multicomponent analyses. Therefore, it can occur that certain signals cannot be detected with a sufficient number of data points and accuracy especially at low concentrations using sub-2 µm particles. This issue is shown in Figure 7.7 for the separation of antineoplastic drugs separated on the column packed with 1.9 µm fully porous particles.

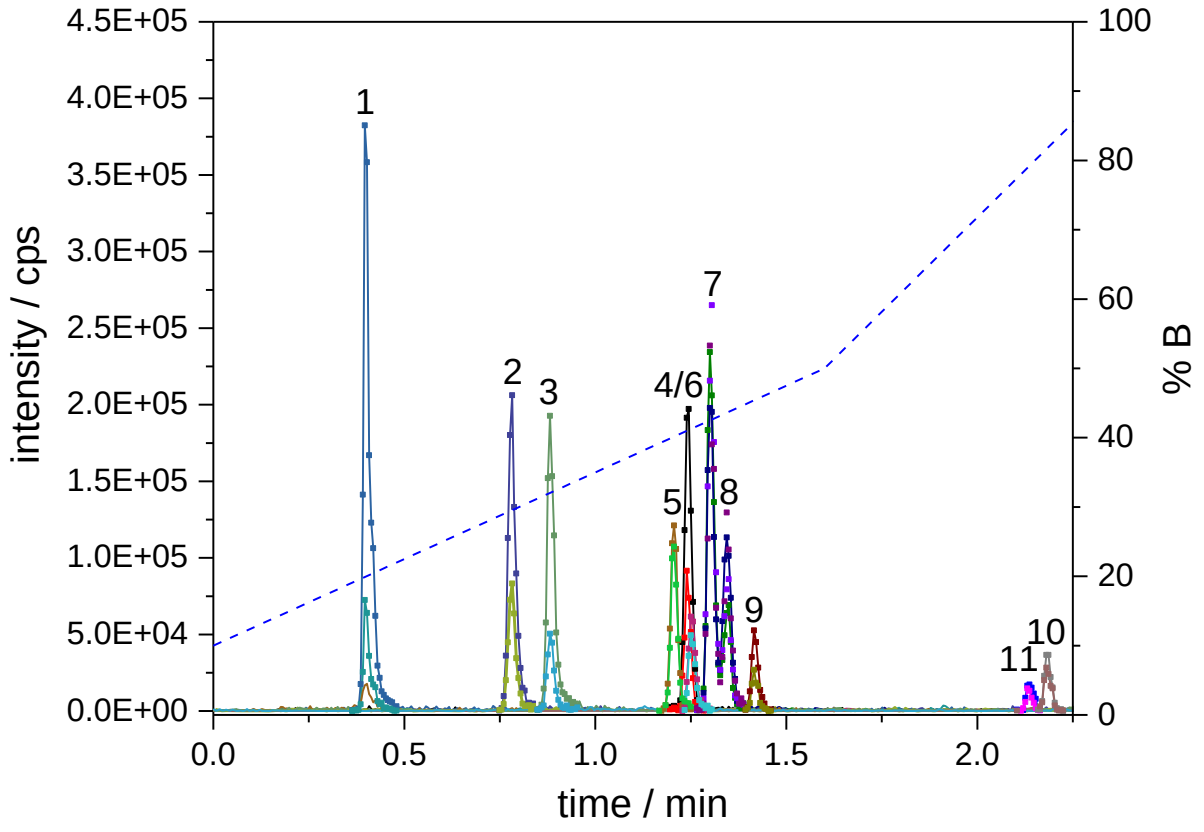

Figure 7.7: Illustration of the peak profiles for the separation of antineoplastic drugs including the number of data points obtained for every compound and selected mass transition. Analytes: 1) gemcitabine (15), 2) methotrexate (13), 3) topotecan (14), 4) irinotecan (12), 5) ifosfamide (12), 6) cyclophosphamide (12), 7) doxorubicin (12), 8) epirubicin (11), 9) etoposide (12), 10) paclitaxel (9) and 11) docetaxel (8). The two lines represent the different mass transitions acquired for the individual target compound whereas the number in brackets refers to the number of data points. The dashed blue line illustrates the applied solvent gradient. For further experimental details please refer to Chapter 6.2.

It becomes clear that all analytes eluting within the first 1.5 min can be represented by a sufficient number of data points due to the lower gradient slope of 25% B min^{-1}. However, the analytes docetaxel (11) and paclitaxel (10) can only be measured by 8 and 9 data points as depicted in Figure 7.8.

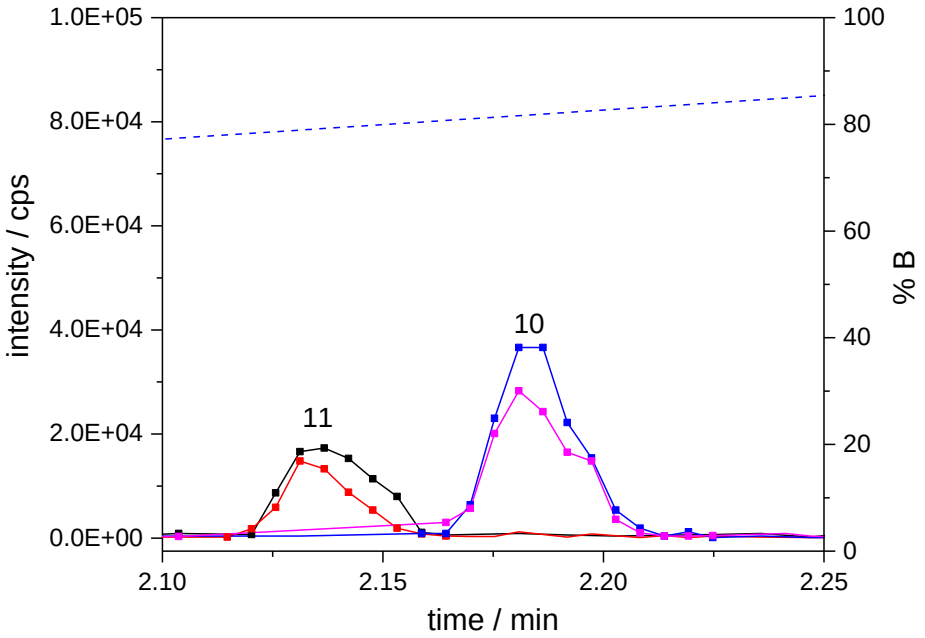

Figure 7.8: Illustration of the peak profile including the number of data points for docetaxel (8) and paclitaxel (9). The two lines represent the different mass transitions acquired for the individual target compound whereas the number in brackets refers to the number of data points. The dashed blue line illustrates the applied solvent gradient. For further experimental details please refer to Chapter 6.2.

Therefore, the applied data acquisition rate is not suitable to represent the peak profile sufficiently because of a resulting peak width below 3 s due to the increased gradient slope of 54% B min^{-1} and the usage of 1.9 µm fully porous particles. For an appropriate quantification, the number of data points should be at least 12 [18]. Otherwise lower method accuracy especially at low concentrations is obtained. Nevertheless, the specifications for method validation regarding the precision are fulfilled as was shown in Chapter 6. For this example, this issue can easily be resolved by increasing the data acquisition rate. However, it must be noted that this example only contains 11 analytes. Therefore, when analyzing a huge number of compounds at low concentrations the effects of an inadequate number of data points will be more pronounced. Moreover, using additional detection techniques like *IMS* will additionally affect the number of data points due to its contribution to the acquisition rate.

Now the question arises why the particle diameter and gradient slope are important parameters for multicomponent analysis. First of all the applied gradient slope defines the resulting peak width. The higher the gradient slope the smaller the resulting peak width as discussed in Chapter

6.3.3 leading to decreased time offered for mass spectrometric detection. In addition, using steep gradients will lead to regions with high number of compounds eluting simultaneously and therefore high peak density. As demonstrated in Figure 7.5, the particle diameter also influences the peak width. Therefore, it can be useful to use larger particles to obtain broader peak shapes in order to provide sufficient time for detection to obtain a sufficient number of data points across a chromatographic peak when a high number of analytes co-elute in multicomponent analysis. Despite the lower peak capacity at constant gradient times, larger particles can be beneficial compared to sub-2 µm particles due to the possibility of increased detection time. Therefore, it must be questioned whether high peak capacity is needed for the analytical problem and which limitations occur due to the resulting peak widths even using fast scanning mass spectrometers in combination with highly efficient UHPLC separations.

In general, if high peak capacity is needed to achieve a separation of e.g. isobaric compounds in fast separations, smaller particle diameters should be used. On the other hand for multicomponent analysis larger particle diameters are favourable with increased gradient times and therefore flat gradient slopes to increase peak capacity with higher peak widths until new generations of mass spectrometers enabling faster acquisition rates and higher sensitivity become available to fully take advantage of the separation power of sub-2 µm particles.

No matter whether a limited number of analytes is investigated or multicomponent analysis is performed, the following conclusions are valid. Decreased gradient slope leads to higher peak capacity regardless which particle diameter is used [19-21]. The application of increased temperature reduces mobile phase viscosity leading to decreased backpressure allowing to apply higher linear velocities [22]. In general, higher flow rates are favourable using constant gradient times to increase k^* [23] and therefore the chromatographic resolution when considering Equation 1.22 (see Chapter 1).

Now, the benefits of micro-LC compared to conventional LC in terms of resource consumption and sample throughput will be discussed to demonstrate the potential of miniaturized separation techniques. Therefore, the developed method obtained on micro-LC-MS/MS is compared to the previously established conventional LC-MS/MS as shown in Figure 7.9.

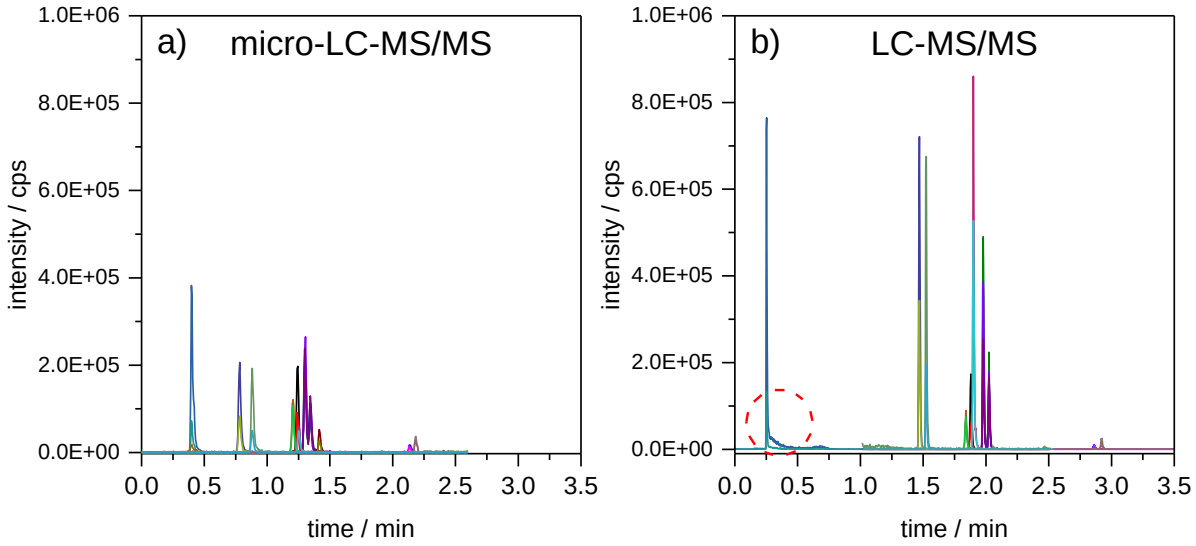

Figure 7.9: Comparison of the separation of antineoplastic drugs obtained on a) a micro-LC system with a 50 x 0.3 mm column packed with 1.9 µm fully porous particles at a flow rate of 25 µL min^{-1} and b) a conventional LC system with a 50 x 2.1 mm column packed with 2.6 µm core-shell particles at a flow rate of 700 µL min^{-1} using an injection volume of 50 µL. The red dashed circle illustrates the column overloading for gemcitabine. For further experimental details please refer to Chapter 6.2.

Whereas Figure 7.9 a) illustrates the separation obtained on a miniaturized LC system using a 50 x 0.3 mm column packed with 1.9 µm fully porous particles, the same separation was done on a conventional HPLC system with a column inner diameter of 2.1 mm and 2.6 µm core-shell particles in Figure 7.9 b). As can be seen, small differences between the resulting chromatograms can be identified due to the fact that different surface modifications were used resulting in different selectivity. However, the separation of the critical peak pairs can be obtained for both approaches. The separation can be achieved using micro-LC in 2.5 min whereas the conventional LC separation takes 3.5 min. To demonstrate the benefit in terms of sample throughput the analysis cycle time needs to be considered. Therefore, the sample preparation by the autosampler is assumed to be 1 min for both LC approaches. During the preparation step the initial mobile phase composition is flushed through the column as part of re-equilibration. To fully re-equilibrate the column to ensure repeatable chromatographic conditions, commonly approximately ten column void volumes are used [24]. Under consideration of the column void volumes of the different columns, the preparation time of the autosampler is sufficient to re-equilibrate the 0.3 mm *i.d.* column. Therefore, the analysis cycle time is 3.5 min. In contrast, for the 2.1 mm *i.d.* column, the preparation time is not adequate to achieve ten column void volumes for re-equilibration. That is why an additional isocratic step needs to be programmed after the gradient to ensure full re-equilibration. As a consequence, the total analysis cycle time increases to approximately 7 min. Comparing the resulting analysis cycle times, an increase in sample throughput by the factor of 2 can be achieved using the

miniaturized column *i.d.* To achieve such cycle times, a flow rate of only 25 µL min^{-1} is used for the 0.3 mm *i.d.* column whereas a flow rate of 700 µL min^{-1} must be applied for the 2.1 mm *i.d.* column due to the fact of increased linear velocity with decreasing column *i.d.* as described in Chapter 1. Consequently the consumption of mobile phase can be reduced by 98% leading to decreased costs for purchase and disposal of LC-MS grade solvents. This is an undisputed benefit of miniaturized separation techniques. To obtain a similar fast separation with a conventional column inner diameter of 2.1 mm the flow rate must be increased to almost 2.0 mL min^{-1} under consideration of the maximum backpressure. Thereby the amount of solvent dramatically increases. In addition, the ionization efficiency of electro-spray ionization (*ESI*) decreases with increasing flow rates although conventional *ESI* sources are specified for flow rates up to 3.0 mL min^{-1} [25]. Regarding the resulting response differences can be identified. However, the limit of quantification is similar for the miniaturized as well as conventional LC-MS approach although the injection volume is decreased for miniaturized column *i.d.* An injection volume of 50 µL was used for the conventional column inner diameter, whereas only 4.25 µL are injected onto the miniaturized column. Thereby, the injected mass is reduced by 92% leading to reduced sample consumption which is of utmost importance for several fields of application. Considering a 0.01 ng mL^{-1} standard, the injected mass is only 42.5 fg for the 0.3 mm *i.d.* column whereas 500 fg are injected on the 2.1 mm *i.d.* column. Nevertheless, the LOQ's are comparable due to the improved signal-to-noise ratio because of the lower amount of matrix ingredients introduced into the mass spectrometer. Of course, it would be possible to choose higher injection volumes for the 2.1 mm *i.d.* column but then even higher amounts of matrix will be transferred into the system and chromatographic issues due to overloading effects can occur as demonstrated by the dashed circle in Figure 7.9 b) for gemcitabine. In addition, the sample consumption as well as the gradient delay volume increases leading to increased analysis time using a fixed-loop autosampler design. Therefore, it could be demonstrated that miniaturized column *i.d.* can offer similar LOQ compared to conventional LC even when the sample volume is not limited. Furthermore, it must be considered that the applied ion source is designed for increased sensitivity at high flow rates. Therefore, it would be necessary to design ion-sources with optimized source geometries for decreased flow rates to further improve the sensitivity because it is possible that the full potential of miniaturized column *i.d.* is currently not being exploited. Regarding the robustness and reproducibility of miniaturized LC columns which is often a point of criticism [26-28], the developed method is compared on two different miniaturized columns as depicted in Figure 7.10. Whereas Figure 7.10 a) illustrates the obtained separation on a new column, Figure 7.10

b) demonstrates the resulting chromatogram achieved on a column of a different batch after 4,000 injections.

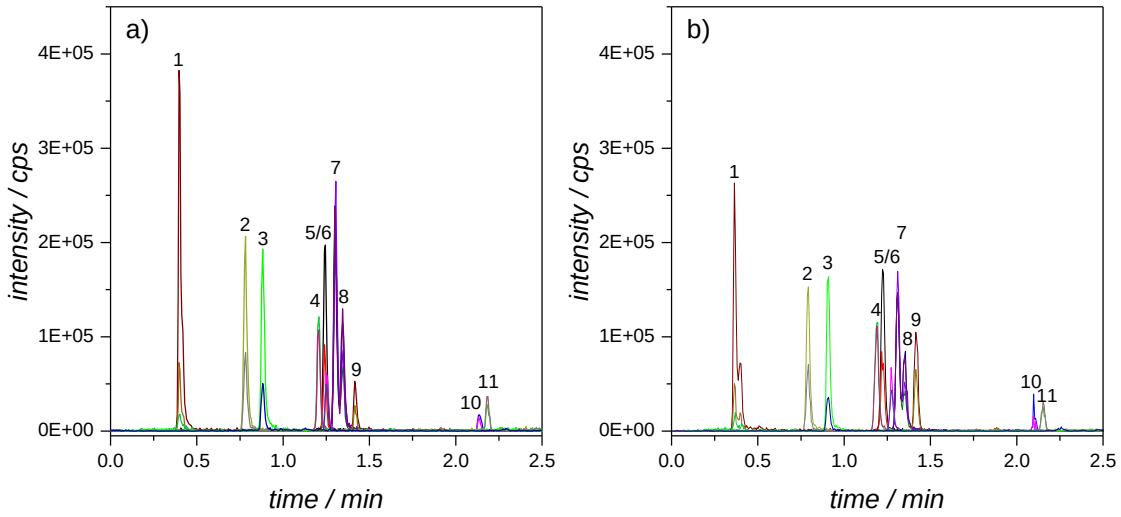

Figure 7.10: Comparison of the separation of antineoplastic drugs obtained on a) new column and b) different batch column after 4,000 injections. For further experimental details please refer to Chapter 6.2.

As can be seen, comparable separations can be achieved on the two different columns although the column used for the separation in Figure 7.10 b) was previously applied for thousands of injections. Only the peak of the polar compound gemcitabine (1) is broadened and little deviations for the semi-polar analytes (4-8) can be identified. In addition, small differences in sensitivity are obtained due to the increased peak width for the intensively stressed column. However, the separation of the critical peak pairs is still sufficient. Therefore, a reliable batch-to-batch column reproducibility can be demonstrated which is important for validated analytical methods [29]. In addition, a sufficient long-term stability is given for miniaturized commercially available LC columns as becomes clear from the total injection number.

7.1 References

[1] J.J. Pitt, Principles and Applications of Liquid Chromatography-Mass Spectrometry in Clinical Biochemistry, The Clinical Biochemist Reviews, 30 (2009) 19-34.

[2] T.M. Annesley, Ion Suppression in Mass Spectrometry, Clinical Chemistry, 49 (2003) 1041-1044.

[3] I. François, K. Sandra, P. Sandra, Comprehensive liquid chromatography: Fundamental aspects and practical considerations—A review, Anal Chim Acta, 641 (2009) 14-31.

[4] P. Dugo, F. Cacciola, T. Kumm, G. Dugo, L. Mondello, Comprehensive multidimensional liquid chromatography: Theory and applications, J. Chromatogr. A, 1184 (2008) 353-368.

[5] B.B. Schneider, T.R. Covey, E.G. Nazarov, DMS-MS separations with different transport gas modifiers, International Journal for Ion Mobility Spectrometry, 16 (2013) 207-216.

[6] E.S. Baker, E.A. Livesay, D.J. Orton, R.J. Moore, W.F. Danielson, D.C. Prior, Y.M. Ibrahim, B.L. LaMarche, A.M. Mayampurath, A.A. Schepmoes, D.F. Hopkins, K. Tang, R.D. Smith, M.E. Belov, An LC-IMS-MS Platform Providing Increased Dynamic Range for High-Throughput Proteomic Studies, Journal of Proteome Research, 9 (2010) 997-1006.

[7] S. Stephan, C. Jakob, J. Hippler, O.J. Schmitz, A novel four-dimensional analytical approach for analysis of complex samples, Analytical and Bioanalytical Chemistry, 408 (2016) 3751-3759.

[8] C. Lapthorn, F. Pullen, B.Z. Chowdhry, Ion mobility spectrometry-mass spectrometry (IMS-MS) of small molecules: Separating and assigning structures to ions, Mass Spectrom. Rev., 32 (2013) 43-71.

[9] B.M. Kolakowski, Z. Mester, Review of applications of high-field asymmetric waveform ion mobility spectrometry (FAIMS) and differential mobility spectrometry (DMS), Analyst, 132 (2007) 842-864.

[10] A. Gold, Vergleich verschiedener Möglichkeiten zur Steigerung der Peakkapazität mittels ein- und zweidimensionaler Flüssigkeitschromatographie und Untersuchung der angewandten Methoden hinsichtlich ihrer Eignung zur Trennung von Isobaren, Masterthesis Fachbereich Chemie, Hochschule Niederrhein / University of Applied Sciences: Krefeld, Germany, (2016).

[11] E. Szymanska, A.N. Davies, L.M.C. Buydens, Chemometrics for ion mobility spectrometry data: recent advances and future prospects, Analyst, 141 (2016) 5689-5708.

[12] S. Di Palma, P.J. Boersema, A.J.R. Heck, S. Mohammed, Zwitterionic Hydrophilic Interaction Liquid Chromatography (ZIC-HILIC and ZIC-cHILIC) Provide High Resolution Separation and Increase Sensitivity in Proteome Analysis, Anal. Chem., 83 (2011) 3440-3447.

[13] S. Lupo, T. Kahler, P. Connolly, Accurate Pain Management Analysis in Under 5 Min on Raptor Biphenyl Superficially Porous Particle LC Columns, LCGC, (2015).

[14] L.E. Blue, J.W. Jorgenson, 1.1 μm superficially porous particles for liquid chromatography. Part I: Synthesis and particle structure characterization, J. Chromatogr. A, 1218 (2011) 7989-7995.

[15] L.E. Blue, J.W. Jorgenson, 1.1 μm Superficially porous particles for liquid chromatography: Part II: Column packing and chromatographic performance, J. Chromatogr. A, 1380 (2015) 71-80.

[16] S. Fekete, J. Fekete, D. Guillarme, Estimation of the effects of longitudinal temperature gradients caused by frictional heating on the solute retention using fully porous and superficially porous sub-2 μm materials, J. Chromatogr. A, 1359 (2014) 124-130.

[17] J.M. Davis, J.C. Giddings, Statistical theory of component overlap in multicomponent chromatograms, Anal. Chem., 55 (1983) 418-424.

[18] DIN, Deutsche Einheitsverfahren zur Wasser-, Abwasser- und Schlammuntersuchung - Gemeinsam erfassbare Stoffgruppen (Gruppe F) - Teil 47: Bestimmung ausgewählter Arzneimittelwirkstoffe und weiterer organischer Stoffe in Wasser und Abwasser - Verfahren mittels Hochleistungs-Flüssigkeitschromatographie und massenspektrometrischer Detektion (HPLC-MS/MS oder -HRMS) nach Direktinjektion (F 47). (2015).
[19] A. Vaast, K. Broeckhoven, S. Dolman, G. Desmet, S. Eeltink, Comparison of the gradient kinetic performance of silica monolithic capillary columns with columns packed with 3 μm porous and 2.7 μm fused-core silica particles, J. Chromatogr. A, 1228 (2012) 270-275.
[20] T. Hetzel, C. Blaesing, M. Jaeger, T. Teutenberg, T.C. Schmidt, Characterization of peak capacity of microbore liquid chromatography columns using gradient kinetic plots, J. Chromatogr. A, 1485 (2017) 62-69.
[21] U.D. Neue, Theory of peak capacity in gradient elution, J. Chromatogr. A, 1079 (2005) 153-161.
[22] D. Guillarme, S. Heinisch, J.L. Rocca, Effect of temperature in reversed phase liquid chromatography, J. Chromatogr. A, 1052 (2004) 39-51.
[23] P. Petersson, A. Frank, J. Heaton, M.R. Euerby, Maximizing peak capacity and separation speed in liquid chromatography, J. Sep. Sci., 31 (2008) 2346-2357.
[24] J.W. Dolan, How Much Is Enough?, LCGC North America, 21 (2003) 968-972.
[25] IonDrive™ Turbo V Ion Source - Operator Guide, https://sciex.com/Documents/manuals/iondrive-turbo-v-operator-guide-en.pdf, 2015, (accessed 02.02.2017)
[26] C.C. Christianson, C.J.L. Johnson, S.R. Needham, The advantages of microflow LC-MS/MS compared with conventional HPLC-MS/MS for the analysis of methotrexate from human plasma, Bioanalysis, 5 (2013) 1387-1396.
[27] D.W. Arnold, S.R. Needham, Micro-LC-MS/MS: the future of bioanalysis, Bioanalysis, 5 (2013) 1329-1331.
[28] K.A. Oudhoff, T. Sangster, E. Thomas, I.D. Wilson, Application of microbore HPLC in combination with tandem MS for the quantification of rosuvastatin in human plasma, Journal of Chromatography B, 832 (2006) 191-196.
[29] ICH - International Council for Harmonisation - Validation of Analytical Procedures: Text and Methodology, http://www.ich.org/fileadmin/Public_Web_Site/ICH_Products/Guidelines/Quality/Q2_R1/Step4/Q2_R1__Guideline.pdf, 1996, (accessed 04.02.2017)

Chapter 8 General conclusions and outlook

In general, it could be demonstrated that miniaturized LC systems exhibit the same robustness and sensitivity compared to conventional LC separations as was presented in Chapter 6. Fast, reliable and efficient separations can be achieved with less resource consumption qualifying micro-LC-MS/MS as a future technology in terms of green analytical chemistry for routine application and high throughput separations. Therefore, this technique is ideally suited in the field of quality control within the pharmaceutical industry due to the need of increased productivity at reduced costs without compromising quality [1]. Multivariate data analysis like the principal component analysis (*PCA)* is suitable to simplify the identification of a chromatographic phase system for the separation of the critical peak pairs. This approach has the advantage of taking into account the properties of the compounds of interest. Conventional column classification methods are usually applied to compare different stationary phases with respect to their retention mechanisms using model analytes [2]. Therefore, for real applications, the obtained information are often not suitable to directly identify a suitable phase chemistry and can therefore only suggest a possible stationary phase due to the provided interactions. Performance characterization procedures like the van Deemter analysis or the kinetic plot theory can be performed to evaluate the quality of LC columns and their time-based potential to provide efficiency for practical purposes. Although the efficiency of miniaturized columns is often being questioned, it was shown that a sub-2 µm fully porous particle packed column with an inner diameter of 300 µm achieves similar packing quality compared to their conventional counterparts [3, 4]. Moreover, comparable peak capacity production rates in gradient elution can be obtained [5]. Therefore, no compromise in terms of efficiency due to the usage of micro-LC columns with an inner diameter of 300 µm must be made. Nevertheless, the influence of the extra-column volume needs to be further decreased to take full advantage of the separation efficiency as discussed in Chapter 1 [1, 6, 7]. By using such tools it can be ensured that optimum conditions are chosen for the developed liquid chromatography method in terms of selectivity, efficiency and analysis time [8, 9].

To further improve the separation different strategies can be applied. First of all, the system design needs to be improved to reduce extra-column band broadening. After reducing the extra-column variance, the possibility of using even smaller particles in the lower sub-2 µm range packed in shorter columns ($L \leq 3$ cm) should be evaluated to accelerate the separation to further increase sample throughput at reduced resource consumption. After implementing optimized

system and column designs, the sample throughput can be further increased by using sophisticated valve technology. So-called multiplexing systems can be used to interlace the workflow of sample preparation steps and subsequent analysis to minimize the downtime of mass spectrometers leading to an increased return of invest. If this succeeds, micro-LC-MS/MS can further change the field of high-throughput analysis to replace conventional liquid chromatography.

Moreover, different types of particle morphologies such as non-porous particles or core-shell particles obtained by pseudomorphic transformation to obtain uniform pore-channels should be applied at higher system pressure capabilities [10-12]. The benefit of increased heat dissipation favours the applicability of miniaturized column *i.d.* at increased pressure due to the decreased impact of frictional heating [13]. Furthermore, sample enrichment techniques as well as approaches to increase the injection volume need to be further developed to increase detection sensitivity to take full advantage of decreased dilution by the column volume. In general, this topic is of huge interest as can be identified by previously published approaches like online solid phase extraction hyphenated to nano-LC as well as temperature-assisted on column solute focusing [14-16]. In addition, the development of even more sensitive and micro-LC compatible detection techniques is mandatory to obtain a diverse repertoire of different detection capabilities and to ensure higher acceptance of these miniaturized chromatographic systems.

8.1 References

[1] S. Fekete, I. Kohler, S. Rudaz, D. Guillarme, Importance of instrumentation for fast liquid chromatography in pharmaceutical analysis, J. Pharm. Biomed. Anal., 87 (2014) 105-119.
[2] M.R. Euerby, M. James, B.O. Axelsson, O. Rosen, P. Petersson, Validation of the extended Tanaka column characterization protocol by multivariate analysis of chromatographic retention of low-molecular-weight analytes on reversed phase columns using methanol and acetonitrile as organic modifiers, J. Sep. Sci., 35 (2012) 2592-2598.
[3] T. Hetzel, D. Loeker, T. Teutenberg, T.C. Schmidt, Characterization of the efficiency of microbore liquid chromatography columns by van Deemter and kinetic plot analysis, J. Sep. Sci., 39 (2016) 3889–3897.
[4] G. Desmet, S. Eeltink, Fundamentals for LC Miniaturization, Anal. Chem., 85 (2013) 543-556.
[5] T. Hetzel, C. Blaesing, M. Jaeger, T. Teutenberg, T.C. Schmidt, Characterization of peak capacity of microbore liquid chromatography columns using gradient kinetic plots, J. Chromatogr. A, 1485 (2017) 62-69.
[6] S. Fekete, J. Fekete, The impact of extra-column band broadening on the chromatographic efficiency of 5 cm long narrow-bore very efficient columns, J. Chromatogr. A, 1218 (2011) 5286-5291.
[7] S. Buckenmaier, C.A. Miller, T. van de Goor, M.M. Dittmann, Instrument contributions to resolution and sensitivity in ultra high performance liquid chromatography using small bore columns: Comparison of diode array and triple quadrupole mass spectrometry detection, J. Chromatogr. A, 1377 (2015) 64-74.
[8] G. Desmet, D. Cabooter, K. Broeckhoven, Graphical data representation methods to assess the quality of LC columns, Anal. Chem., 87 (2015) 8593-8602.
[9] G. Desmet, D. Clicq, P. Gzil, Geometry-independent plate height representation methods for the direct comparison of the kinetic performance of LC supports with a different size or morphology, Anal Chem, 77 (2005) 4058-4070.
[10] J. De Vos, M. De Pra, G. Desmet, R. Swart, T. Edge, F. Steiner, S. Eeltink, High-speed isocratic and gradient liquid-chromatography separations at 1500 bar, J. Chromatogr. A, 1409 (2015) 138-145.
[11] F. Gritti, Impact of straight, unconnected, radially-oriented, and tapered mesopores on column efficiency: A theoretical investigation, J. Chromatogr. A, 1485 (2017) 70-81.
[12] T.-C. Wei, A. Mack, W. Chen, J. Liu, M. Dittmann, X. Wang, W.E. Barber, Synthesis, characterization, and evaluation of a superficially porous particle with unique, elongated pore channels normal to the surface, J. Chromatogr. A, 1440 (2016) 55-65.
[13] J. De Vos, K. Broeckhoven, S. Eeltink, Advances in ultrahigh-pressure liquid chromatography technology and system design, Anal. Chem., 88 (2016) 262-278.
[14] R.E. Wilson, S.R. Groskreutz, S.G. Weber, Improving the Sensitivity, Resolution, and Peak Capacity of Gradient Elution in Capillary Liquid Chromatography with Large-Volume Injections by Using Temperature-Assisted On-Column Solute Focusing, Anal. Chem., 88 (2016) 5112-5121.
[15] M.A. Stravs, J. Mechelke, P.L. Ferguson, H. Singer, J. Hollender, Microvolume trace environmental analysis using peak-focusing online solid-phase extraction-nano-liquid chromatography-high-resolution mass spectrometry, Analytical and Bioanalytical Chemistry, 408 (2016) 1879-1890.
[16] S.R. Groskreutz, S.G. Weber, Temperature-assisted on-column solute focusing: A general method to reduce pre-column dispersion in capillary high performance liquid chromatography, J. Chromatogr. A, 1354 (2014) 65-74.

List of abbreviations and symbols

%	percent	CXP	cell exit potential
%B	percent of organic solvent	D	dilution factor
(v/v)	volume percent	d_{10}	cumulative 10% point of diameter
<	less-than	d_{90}	cumulative 90% point of diameter
>	greater-than	DAD	diode array detector
°C	degree Celsius	d_c	column diameter
µL	microliter	d_d	domain size
µm	micrometer	D_m	molecular diffusion coefficient
2D-LC	two-dimensional liquid chromatography	DMSO	dimethyl sulfoxide
2D-LC-MS	two-dimensional liquid chromatography mass spectrometry	Doc	docetaxel
A	Eddy diffusion	Doxo	doxorubicin
A_x	sampling area	d_p	particle diameter
Å	angstrom	DP	declustering potential
a, b ,c	dimensionless Knox coeffcients	e. g.	exempli gratia
A_1, A_2	cross sectional area	E_0	separation impedance
ACN	acetonitrile	EP	entrance potential
AFC	automatic flow control	EPG	embedded polar group
ARC	area related concentration	Epi	epirubicin
B	longitudinal diffusion	ESI	electrospray ionization
BEH	Ethylene Bridged Hybrid	ESOP	European Society of Oncology Pharmacy
C	mass transfer	etc.	et cetera
c	concentration	eV	electronvolt
C18	octadecylsilane	F	flow rate
CAD	collision activated dissociation gas	FA	formic acid
CAS	Chemical Abstracts Service	fg	femtogram
CE	collision energy	GS1	nebulizer gas
CFD	computational fluid dynamic	GS2	heater gas
Chip-LC	chip liquid chromatography	H	plate height
cm	centimeter	h	reduced plate height
CP	cyclophosphamide	H_2O	water
cps	counts per second	H_{min}	minimum plate height
CUR	curtain gas	h_{min}	minimum reduced plate height

HPLC	high performance liquid chromatography
HSS	High Strength Silica
Hz	hertz
i.d.	inner diameter
ID	inner diameter
IF	ifosfamide
IMS	ion mobility spectrometry
IPA	2-propanol
IS	ionization voltage
k	retention factor
k*	gradient retention factor
k_e	retention factor at the point of elution
KPL	kinetic plot limit
kV	kilovolt
K_{v0}	column permeability
L	column length
LC	liquid chromatography
LC-MS	liquid chromatography mass spectrometry
LC-MS/MS	liquid chromatography tandem mass spectrometry
LCxLC	comprehensive two-dimensional chromatography
L_{exp}	experimental column length
L_{KPL}	gradient kinetic plot column length
LOD	limit of detection
log D	octanol-water distribution coefficient
log P	logarithmic octanol-water partition coefficient
LOQ	limit of quantification
LVI	large volume injection
m	number of compounds
m/z	mass-to-charge ratio
mAU	milli absorbance units
MDL	method detection limit
MEWIP	Monitoring-Effect Study of Wipe Sampling in Pharmacies
MFC	microfluidic flow control
mg	milligram
micro-LC	micro-liquid chromatography
micro-LC-MS/MS	micro liquid chromatography tandem mass spectrometry
min	minutes
mL	milliliter
mm	millimeter
MRM	multiple reaction monitoring
MS	mass spectrometry
ms	milliseconds
MS/MS	tandem mass spectrometry
N	number of theoretical plates
n	number of replicates
N*	gradient number of plates
nano-LC	nano liquid chromatography
ng	nanogram
nL	nanoliter
nm	nanometer
n_p	peak capacity
$n_{p,exp}$	experimentally obtained peak capacity
$n_{p,KPL}$	gradient kinetic plot limits
o.d.	outer diameter
ODS	octadecylsilane

OSAH	Occupational Safety & Health Administration	s_x	variance of x-data
P’	probability	s_{xy}	covariance
Pac	paclitaxel	s_y	variance of y-data
PC	principal component	T	temperature
PCA	Principal component analysis	t_0	column void time
PEEK	polyetheretherketone	$t_{0,ec}$	system void time
PEEKSil	fused silica surrounded by polyetheretherketone	t_D	critical diffusion time
PFP	pentafluorophenyl	t_{dwell}	gradient delay time
pg	picogram	TEM	ion source temperature
pH	potentia Hydrogenii – negative decimal logarithm of the hydrogen ion activity	t_G	gradient time
pK_a	logarithmic acid dissociation constant	$t_{G,exp}$	experimental gradient time
psd	particle size distribution	$t_{G,KPL}$	gradient kinetic plot gradient time
psi	pound-force per square inch	$t_{intersection}$	time of intersection
Q	volume based velocity	t_p	time of an isocratic plateau
Q1	precursor-ion mass	$t_{plateau}$	time of plateau
Q3	product-ion mass	t_R	retention time
QC	quality control	$t_{R,obs}$	observed retention time
r	column radius	u_0	linear velocity
R	resolution	UHPLC	ultra-high performance liquid chromatography
R^2	coefficient of determination	u_{opt}	optimum linear velocity
r_c	column radius	UV	ultraviolet
RP	reversed phase	ν	reduced velocity
RSD	relative standard deviation	V	volume of the wetting solution
s	seconds	v_1, v_2	flow velocity
S	constant of the linear solvent strength model	V_{cap}	capillary volume
S/N	signal-to-noise ratio	V_{col}	column volume
s^2	unexplained variance	$V_{col,eff}$	effective column volume
SAX	strong anion exchange	$V_{d,cor}$	corrected gradient delay volume
SB	StableBond	$V_{d,exp}$	experimentally determined gradient delay volume
SS	stainless steel		

V_{delay}	gradient delay volume
V_{det}	detector volume
V_{dwell}	gradient dwell volume
V_{eff}	effective column volume
V_{inj}	injection volume
V_m	mobile phase volume
$\bar{w}$	average peak width
$w_{4\sigma,ec}$	extra-column peak width
$w_{4\sigma,obs}$	observed peak width
ZDV	zero-dead volume
α	selectivity factor
α^*	gradient selectivity factor
γ	tortuosity factor
Δ	delta
$\Delta(k_{last}-k_{first})$	difference of the retention factor between the first and last eluting compound
Δk_{total}	available chromatographic space
ΔP	backpressure
ΔP_{ec}	extra-column backpressure
ΔP_{exp}	experimental pressure drop
ΔP_{max}	maximum backpressure
ΔP_{system}	system backpressure
ΔP_{total}	total backpressure
$\Delta\phi$	change in mobile phase composition
ε	porosity
η	mobile phase viscosity
λ	length-elongation factor
ξ	peak capacity production rate
σ	standard deviation
σ^2	peak variance
σ^2_{ec}	extra-column variance
$\sigma^2_{v,cap}$	variance of the capillaries
$\sigma^2_{v,col}$	variance of the column
$\sigma^2_{v,det}$	variance of the detector
$\sigma^2_{v,ec}$	extra-column variance
$\sigma^2_{v,ec,cap}$	variance of the capillaries
$\sigma^2_{v,ec,det}$	variance of the detector
$\sigma^2_{v,ec,inj}$	variance of the injector
$\sigma^2_{v,inj}$	variance of the injector
$\sigma^2_{v,total}$	total system variance
Φ	flow resistance

List of figures

List of tables

Appendix

List of publications

Publications in peer-reviewed journals

1. **Hetzel, T.**, Loeker, D., Blaesing, C., Jaeger, M., Teutenberg, T., Schmidt, T.C., The influence of temperature on efficiency of microbore liquid chromatography columns, submitted: Journal of Separation Science, (2017).
2. **Hetzel, T.**, Blaesing, C., Jaeger, M., Teutenberg, T., Schmidt, T.C., Characterization of peak capacity of microbore liquid chromatography columns using gradient kinetic plots, Journal of Chromatography A, 1485 (2017) 62-69.
3. **Hetzel, T.**, C. vom Eyser, J. Tuerk, T. Teutenberg, T.C. Schmidt, Micro-liquid chromatography mass spectrometry for the analysis of antineoplastic drugs from wipe samples, Analytical and Bioanalytical Chemistry, 408 (2016) 8221-8229.
4. **Hetzel, T.**, Loeker, D., Teutenberg, T., Schmidt, T.C., Characterization of efficiency of micro liquid chromatography columns by van Deemter and Kinetic plot analysis, Journal of Separation Science, 39 (2016) 3889-3897.
5. **Hetzel, T.**, Teutenberg, T., Schmidt, T.C., Selectivity screening and subsequent data evaluation strategies in liquid chromatography: the example of 12 antineoplastic drugs, Analytical and Bioanalytical Chemistry, 407 (2015) 8475-8485.
6. Leonhardt, J., **Hetzel, T.**, Teutenberg, T., Schmidt, T.C., Large volume injection of aqueous samples in nano liquid chromatography using serially coupled columns, Chromatographia, 78 (2015) 31-38.
7. Haun, J., Leonhardt, J., **Hetzel, T.**, Portner, C., Tuerk, J., Teutenberg, T., Schmidt, T.C., On-line and splitless nanoLC x capillaryLC with quadrupole/time-of-flight mass spectrometric detection for comprehensive screening analysis of complex samples, Analytical Chemistry, 85 (2013) 10083-10090.

Other articles

1. Teutenberg, T., **Hetzel, T.**, Leonhardt, J., Loeker, D., Basics of 2D-LC - When it's getting really complex, G.I.T. Laboratory Journal, (2017).
2. Teutenberg, T., **Hetzel, T.**, Leonhardt, J., Loeker, D., Micro-LC The Basics - For Those Times When We're in a Hurry, G.I.T. Laboratory Journal, (2017).
3. Teutenberg, T., **Hetzel, T.**, Leonhardt, J., Loeker, D., Basics of chromatography - Selectivity versus efficiency, G.I.T. Laboratory Journal, (2017).

4. Teutenberg, T., **Hetzel, T.**, Leonhardt, J., Loeker, D., The project “From Tswett’s “Farbschreibung” to Modern Chromatography. A Historical Overview”, G.I.T. Laboratory Journal, 11-12 (2016) 31-33.
5. Teutenberg, T., **Hetzel, T.**, Leonhardt, J., Loeker, D., The project “Advanced Liquid Chromatography”, G.I.T. Laboratory Journal, 11-12 (2016) 29-30.
6. Teutenberg, T., **Hetzel, T.**, Leonhardt, J., Loeker, D., Schulze, P., Are the Lights on Green? Micro-LC’s Road to Routine Analysis, G.I.T. Laboratory Journal, 5-6 (2016) 18-21.
7. Teutenberg, T., **Hetzel, T.**, Optimization of Ionization Efficiency - Using a Design of Experiments Approach in Liquid Chromatography Mass Spectrometry, GIT Separation, 2 (2015) 26-29.
8. **Hetzel, T.**, Teutenberg, T. Giegold, S., Automatisierte Methodenentwicklung - Multikomponentenanalytik für 12 ausgewählte Zytostatika, GIT Labor-Fachzeitschrift, 3 (2014) 32-35.
9. Teutenberg, T., **Hetzel, T.**, Wiese, S., Die Verbindung macht's - Evaluierung eines Säulenschaltkonzepts für die Mikro-LC-MS, Laborpraxis, 9 (2014) 72-74.
10. Wiese, S., **Hetzel, T.**, Teutenberg, T., Giegold, S., Liedschulte, A. V., So ist es effizienter - Lösungsmittelersparnis durch UHPLC mit 1-mm-ID-Trennsäule, Laborpraxis, 3 (2014) 22-24.
11. Teutenberg, T., Freihoff, S.-D., **Hetzel, T.**, Leonhardt, J., Waiting for the future? Nano-, micro-, and two-dimensional HPLC are already proving their worth, q&more, 1 (2014) 36-40.
12. Teutenberg, T., Leonhardt, J., **Hetzel, T.**, Freihoff, S.-D., Tuerk, J. Bettermann, H., Fischer, B., Do we really need chromatography? The role of chromatography and different detection techniques in the context of mass spectrometry, G.I.T. Laboratory Journal, 1 (2013) 8-12.

Book chapters

1. **Hetzel, T.**, Teutenberg, T., Portner, C., Türk, J., Requirements for the (U)HPLC hyphenation with different mass spectrometers, in: S. Kromidas (Ed.) The HPLC-Expert II: Optimizing the Benefits of HPLC/UHPLC, Wiley-CH (2017) 171-192.
2. Wiese, S., **Hetzel, T.**, The modern HPLC-/UHPLC-System, in: S. Kromidas (Ed.) The HPLC-Expert II: Optimizing the Benefits of HPLC/UHPLC, Wiley-CH (2017) 29-51.

3. Wiese, S., **Hetzel, T.**, Aspects of modern UHPLC - Experiences of a user, in: S. Kromidas (Ed.) The HPLC-Expert II: Optimizing the Benefits of HPLC/UHPLC, Wiley-CH (2017) 281-300.
4. **Hetzel, T.**, Portner, C., Wiese, S., vom Eyser, C., Türk, J., Teutenberg, T., Aspects of the development of methods in LC-MS-Coupling, in: S. Kromidas (Ed.) The HPLC-MS Handbook for Practitioners, Wiley-CH (2017).
5. Teutenberg, T., **Hetzel, T.**, Portner, C., Wiese, S., vom Eyser, C., Türk, J., Aspekte der Methodenentwicklung in der LC-MS-Kopplung, in: S. Kromidas (Ed.) Das HPLC-MS-Buch für Anwender, Wiley-CH (2017).
6. Teutenberg, T., **Hetzel, T.**, Portner, C., Türk, J., Anforderungen bei der (U)HPLC-Kopplung mit unterschiedlichen Massenspektrometern in: S. Kromidas (Ed.) Der HPLC-Experte II - so nutze ich meine HPLC/UHPLC optimal, Wiley-CH (2015) 175-201.

Oral presentations

Only contributions as lead author are considered.

1. **Hetzel, T.**, Blaesing C., Teutenberg T., Schmidt T.C., Charakterisierung der Trennleistung miniaturisierter Trennsäulen, ANAKON 2017, Tübingen 03.04.2017.
2. **Hetzel, T.**, Teutenberg. T., Schmidt T.C., Development of a fast method for the analysis of cytotoxic drugs using micro-LC-MS/MS, 27th Doktorandenseminar AK Separation Science, Hohenroda 10.01.2017. **Prize for the best oral presentation.**
3. **Hetzel, T.**, Teutenberg. T., Entwicklung und Validierung einer schnellen Mikro-LC-MS/MS Methode am Beispiel von Zytostatika, NOVIA Analytiktage 2016, Bad Soden 22.11.2016.
4. **Hetzel, T.**, Teutenberg. T., Grundlagenschulung der HPLC, UCB Pharma, Monheim 27.10.2016.
5. **Hetzel, T.**, Teutenberg. T., Methodenentwicklung und Validierung in der HPLC - Beispiel Zytostatika. Klinkner & Partner HPLC Schulung, Potsdam 07.10.2016.
6. **Hetzel, T.**, Loeker, D., Teutenberg, T., Schmidt, T.C., Characterization of efficiency of micro liquid chromatography columns by van Deemter and Kinetic plot analysis, 31st International Symposium on Chromatography (ISC 2016), Cork, Ireland 31.08.2016.
7. **Hetzel, T.**, Tuerk. J., Modern Trends in LC-MS/MS. 6th Berlin LC-MS/MS Symposium, Berlin 13.04.2015.

8. **Hetzel, T.**, Teutenberg. T., Methodenentwicklung in der HPLC - Beispiel Zytostatika, Klinkner & Partner HPLC Schulung, Saarbrücken 15.10.2015.
9. **Hetzel, T.**, Teutenberg. T., Ist die Mikro-LC wirklich fit für die Routine? NOVIA Analytiktage 2015, Bad Soden 18.11.2015.
10. **Hetzel, T.**, Teutenberg. T., MicroLC-MS/MS - Ready for Routine analysis? 10th Diskussionstreffen der LC/MS-Fachgruppe der Deutschen Gesellschaft für Massenspektrometrie (DGMS), Wuppertal 10.11.2014.

Poster presentations

1. **Hetzel, T.**, vom Eyser, C., Schmidt, T.C., Tuerk, J., Teutenberg, T., Analysis of selected antineoplastic drugs from wipe samples using micro-liquid chromatography tandem mass spectrometry, 31st International Symposium on Chromatography (ISC 2016), Cork, Ireland 2016.
2. **Hetzel, T.**, Leonhardt, J., Loeker, D., Teutenberg, T., Bohrisch, J., Analytical chracterization of stationary phases packed with pearl cellulose particles, 31st International Symposium on Chromatography (ISC 2016), Cork, Ireland 2016.
3. **Hetzel, T.**, Loeker, D., Schmidt, T.C., Becker, F., Teutenberg, T., Characterization of efficiency of micro liquid chromatography columns by van Deemter analysis, 32nd International Symposium on Microscale Separations and Bioanalysis (MSB 2016), Queen's Landing in Niagara-on-the-Lake, Canada 2016.
4. **Hetzel, T.**, Tuerk, J., Schmidt, T.C., Teutenberg, T., Analysis of hormones and pharmaceuticals using µLC-MS/MS hyphenation in combination with column switching, 42nd International symposium on high performance liquid phase separations and related techniques (HPLC 2015), Geneva, Switzerland 2015.
5. **Hetzel, T.**, Schmidt, T.C., Teutenberg, T., Selectivity screening and subsequent data evaluation strategies in HPLC: the example of twelve antineoplastic drugs, 42nd International symposium on high performance liquid phase separations and related techniques (HPLC 2015), Geneva, Switzerland 2015.
6. **Hetzel, T.**, Tuerk, J., Schmidt, T.C., Teutenberg, T., Analysis of hormones and pharmaceuticals using µLC-MS/MS hyphenation in combination with column switching, Analytical Forum Water Contaminants (AFWC 2015), Koblenz 2015.
7. **Hetzel, T.**, Teutenberg, T., Implementation of column switching on the basis of µLC-MS/MS hyphenation for routine analysis, 38th International Symposium on Capillary Chromatography (ISCC 2014), Riva del Garda, Italy 2014.

8. Wiese, S., Gassner, O., **Hetzel, T.**, Teutenberg, T., Evaluation of a concept coupling flame ionization detection with nano-liquid chromatography, 38th International Symposium on Capillary Chromatography (ISCC 2014), Riva del Garda, Italy 2014.
9. Wenkel, N. Hetzel, T., Freihoff, S., Gehrmann, L., Portner, C., Teutenberg, T., Tuerk, J., Development of methods on the basis of large-volume-injection solid-phase extraction hyphenated to tandem mass spectrometry for the determination of hormones, 61st ASMS Conference on Mass Spectrometry and Allied Topics (ASMS 2013), Minneapolis, United States of America 2013.

Curriculum vitae

Der Lebenslauf ist in der Online-Version aus Gründen des Datenschutzes nicht enthalten.

For reasons of data protection, the curriculum vitae is not included in this online document.

Erklärung (Declaration)

Hiermit versichere ich, dass ich die vorliegende Arbeit mit dem Titel

„Characterization of micro liquid chromatography - theoretical performance limits and practical aspects for routine analysis on the example of cytotoxic drugs"

selbst verfasst und keine außer den angegebenen Hilfsmitteln und Quellen benutzt habe, und dass die Arbeit in dieser oder ähnlicher Form noch bei keiner anderen Universität eingereicht wurde.

Krefeld, 13.02.2017

Terence Hetzel

Acknowledgements

I want to express my deepest gratitude to my research supervisors Prof. Dr. Torsten C. Schmidt and Dr. Thorsten Teutenberg for their professional support as well as endless encouragement and commitment during my work. In addition, I would like to thank Dr. Steffen Wiese for his useful advices and constructive discussions.

Furthermore, I would like to thank all my further co-authors, namely Dr. Claudia vom Eyser, Denise Loeker, Christina Bläsing, Dr. Jochen Türk and Prof. Dr. Martin Jäger for their cooperation and fruitful discussions.

Moreover, I would like to thank all my colleagues at the Institute of Energy and Environmental Technology for the excellent collaboration and help during my work.

Especially, I would like to express my graditude to my whole family for their support and most importantly to my fiancé Anne for her endless patience, support and encouragement.